Heinrich Heine Universität Düsseldorf

MOI III
MOLEKÜLE DER INFEKTION
MANCHOT GRADUIERTENSCHULE

Characterisation of interactions between the cGAS-STING pathway for type I IFN production and autophagy during vaccinia virus infection

Inaugural dissertation

for the attainment of the title of doctor
in the Faculty of Mathematics and Natural Sciences
at the Heinrich Heine University Düsseldorf

presented by

Noémi Vágó

from Budapest, Hungary

Leverkusen, March 2023

from the Institute of Molecular Virology
at the Heinrich-Heine-University Düsseldorf

Published by permission of the
Faculty of Mathematics and Natural Sciences at
Heinrich Heine University Düsseldorf

Supervisor: Prof. Dr. Ingo Drexler
Co-supervisor: Prof. Dr. Dieter Willbold

Date of the oral examination: 28.08.2023

Table of Contents

List of abbreviations

3MA	3-methyladenine
AD	anno domini
Ambra1	activating molecule in Beclin1-regulated autophagy
AMP	adenosine monophosphate
APS	ammonium persulfate
AraC	cytosine arabinoside
ATG	autophagy-related genes
BAC	bacterial artificial chromosome
BC	before Christ
BMDCs	bone marrow derived dendritic cells
BSA	bovine serum albumin
CAI	Center of Advanced Imaging
CAM	chloramphenicol
Cas9	CRISPR-associated protein 9
CEB	crude extraction buffer
CEB-PK	CEB + Proteinase K
cGAMP	cyclic guanosine monophosphate-adenosine monophosphate
cGAS	cyclic GMP-AMP synthase
CLSM	confocal laser scanning microscopy
CPE	cytopathic effect
CRISPR	clustered regularly interspaced short palindromic repeats
CQ	chloroquine
CVA	chorioallantois vaccinia virus Ankara
dd H_2O	distilled water
DAPI	4´,6-diamidino-2-phenylindole
DMEM	Dulbecco´s Modified Eagle´s Medium
DMSO	dimethyl sulfoxide
DMXAA	dimethylxanthone acetic acid
dsDNA	double stranded DNA
dsRed	Discosoma Red
EBV	Epstein-barr virus
ECL	enhanced chemiluminescence
eGFP	enhanced form of green fluorescent protein
EFC	entry-fusion complex
ELISA	enzyme-linked immunosorbent assay
ENPP1	Ecto-nucleotide pyrophosphatase phosphodiesterase 1
Epox	epoxomicin
ERGIC	endoplasmic reticulum-Golgi intermediate compartment
EVs	extracellular virions
FACS	fluorescence-activated cells sorting
FBS	fetal bovine serum

FIP200	focal adhesion kinase family-interacting protein of 200 kDa
GABARAPs	γ-aminobutyric acid receptor-associated proteins
GAGs	glycosaminoglycans
GCA	golgicide A
GM-CSF	granulocyte-macrophage colony-stimulating factor
GMP	guanosine monophosphate
H-DLG	HeLa DsRed-LC3-eGFP
HCMV	human cytomegalovirus
HCV	hepatitis C virus
HIV-1	human immunodeficiency virus 1
hpi	hours post-infection
HRP	horse radish peroxidase
HSV-1	herpes simplex type 1
IFN	interferon
IRF3	interferon regulatory factor 3
IVs	immature virions
Kana	I-SceI-kanamycin cassette
kbp	kilo-base pairs
KO	knockout
KSHV	Kaposi´s sarcoma-associated herpesvirus
LAP	LC3 associated phagocytosis
LB	lysogeny broth
LC3	microtubule-associated protein 1A/1B-light chain 3
LIR	LC3-interacting region
LPS	lipopolysaccharide
M	molar
mA	milliampere
MEF	mouse embryonic fibroblast cells
MHC	major histocompatibility complex
MHV68	murine gammaherpesvirus 68
MOI	multiplicity of infection
mTOR	mammalian target of rapamycin
MVs	mature virions
MVA	modified vaccinia virus Ankara
NDP52	nuclear domain 10 protein 52
NEB	New England Biolabs
NP	nucleoprotein
O/N	overnight infected
OD600	optical density at wavelength 600 nm
OVA	ovalbumin
P-	phosphorylated form
PA	polyallomer
PAGE	polyacrylamide gel electrophoresis

PAMPs	pathogen-associated molecular patterns
PBS	phosphate buffered saline
PCR	polymerase chain reaction
PFA	paraformaldehyde
PE	phosphatidylethanolamine
PEI	polyethyleneimine
PI3K	phosphatidylinositol 3-kinase
PI3K-III	class III phosphatidylinositol 3-kinase
PI3P	phosphatidylinositol 3-phosphate
PKA	cAMP-dependent kinase
poly(I:C)	polyinosinic:polycytidylic acid
poxins	poxvirus immune nucleases
PRRs	pattern-recognition receptors
PUVA	psoralen and ultraviolet A radiation
Rapa	rapamycin
RB1CC1	retinoblastoma 1-inducible coiled-coil 1
recMVA	recombinant MVA
RFV	rabbit fibroma virus
RIG-I	retinoic-acid-inducible gene-I
RLRs	RIG-I-like receptors
rpm	round per minute
RPMI	Roswell Park Memorial Institute medium
RT	room temperature
SARS-CoV-2	severe acute respiratory syndrome coronavirus 2
SDS	sodium dodecyl sulphate
siRNA	silencing RNA
SQSTM1	sequestosome-1
SSC	single cell clone
SsR	scrambled siRNA
STING	stimulator of interferon genes
T182,5	182,5 cm^2 culturing flask
TBE	Tris-borate EDTA buffer
TBK1	TANK-binding kinase 1
TBST	tris-buffered saline with Tween 20
$TCID_{50}$/ml	tissue culture infection dose 50 per millilitre
TEMED	N,N,N′,N′-Tetramethylethylenediamine
TLRs	Toll-like receptors
TRIM	tripartite motif protein
UBL	ubiquitin-like
ULK	uncoordinated 51-like kinase
VACV	vaccinia virus
VPS	vacuolar protein sorting
WHO	World Health Organization

WIPI	WD-repeat protein interacting with phosphoinositides
WIPI2	WIPI isoform 2
WR	Western Reserve
WT	wild type
WVs	wrapped virions

Summary

Poxviruses are large dsDNA viruses whose replication occurs inside the cytoplasm in special compartments, which are called viral factories. There are several virulent strains (e.g., Western Reserve [WR] and Lister) expressing immunomodulatory genes, which inhibit type I and II interferon (IFN) production during infection. In addition to virulent viruses, there are also highly attenuated strains, an example of which is modified vaccinia virus Ankara (MVA). MVA is unable to complete a full replication cycle in most mammalian cells, but it induces a type I IFN response and autophagy upon infection. The dsDNA-induced cGAS-STING pathway has been established to play a crucial role in inducing type I IFN expression upon viral infection, while autophagy is responsible for cleaning infectious materials from cells. Notably, only a limited amount of information is available regarding how these two major pathways are affected during vaccinia virus (VACV) infection; therefore, the present study aimed to gain a deeper understanding of how MVA induces and WR inhibits these important innate immune effector mechanisms. The findings could lead to further improvements of MVA as a vaccine vector for fighting against tumour development and infectious diseases.

Several knockout (KO) cell lines specifically affecting the autophagy and/or cGAS-STING pathways for type I IFN production were generated and tested during VACV infection. Immunoblotting revealed that MVA induced and WR inhibited STING-dependent non-canonical autophagy, in which the presence of Beclin1 and the downstream members of the canonical autophagy pathway are essential, contrary to previously documented cGAMP-induced autophagy. Furthermore, the absence of TBK1 negatively affected the phosphorylation of STING in MEF cells; however, it had no impact on elevated LC3 lipidation, suggesting an accelerated degradation of P-STING. Moreover, p62 was proven to be critical for the removal of the P-STING:P-TBK1 complex after MVA infection, but it was not essential for STING-dependent non-canonical autophagy activation. In addition, different early- and late-stage inducers or inhibitory reagents for canonical autophagy and cGAS-STING pathways for type I IFN production, or even strategies for inactivating VACV strains chemically or non-chemically, were introduced. These approaches revealed that WR-induced inhibition of the activation of the autophagy and cGAS-STING pathways for type I IFN production were heavily dependent on uncoating and early viral gene expression, while MVA likely requires only binding to induce activation for both mechanisms.

To identify the gene(s) responsible for inhibiting the activation of autophagy and cGAS-STING pathways for type I IFN production during infection with the virulent strain, a siRNA screen of 80 conserved WR genes was conducted using high-content confocal microscopy and flow cytometry. Once the results of both approaches had been analysed and summarised, five virulent virus genes (A10L, A18R, B5R, B13R, and C10L) were selected according to their levels of mismatch (presence of mutated, truncated, or deleted genes) between MVA and WR genome sequences. One additional candidate was included (B2R) in the target list due to a recent publication describing the effect of this specific poxin gene. Then, the selected genes were used to generate recombinant MVA viruses, which were reconstituted with and expressed the previously selected WR genes in their natural locus. The preliminary results indicated that recombinant MVA (recMVA) expressing the WR gene B2R (MVA-VV-B2) was able to interfere with the autophagy and cGAS-STING pathways both in the early and late phases of infection. In addition, cells infected with MVA-VV-A10 and -A18 for 4 h displayed reduced autophagy activation without influencing the cGAS-STING pathway for type I IFN production. However, cells previously infected for 24 hours with MVA-VV-A18 exhibited an even more decreased P-STING level upon AraC treatment, which was contrary to the expected results. Since A18R is an early/late gene, while A10L is a late gene, these findings could suggest that the early expressed precursor forms of late viral genes in the infected cells could have different effects on the cellular pathways compared with their actual late-expressed forms. This should be investigated further in future studies.

1 Introduction

1.1 Poxviruses

1.1.1 A short history of smallpox

1.1.1.1 Smallpox in ancient times

While it is almost impossible to pinpoint the exact time and place of origin of the infectious disease smallpox (caused by a species of the variola virus) in human history, there are indications that it already existed in ancient times. The earliest clues include the documentation of three mummified corpses that displayed the typical lesions caused by smallpox infection from as early as Egypt´s Eighteenth (1580 – 1350 BC) and Twentieth Dynasties (1200 – 1100 BC). One of them was Pharaoh Ramses V, who in died 1157 BC and whose body was displayed in Cairo at the time of documentation. The upper body exhibited a rash of elevated pustules as well as raised pimples, which were considered evidence of a smallpox infection (1–4). Since this time, documented smallpox cases have been found in several countries over the centuries. For instance, a few early cases from Asia were documented in the notes of an imperial dermatologist of the Han dynasty of ancient China, who described a new disease brought from outside by invaders (the Huns) to China between the 2nd and 4th century AD; moreover, an ancient Sanskrit text from India from the 7th century AD that mentioned the disease '*masūrikā*', while the Persian physician al-Razi wrote about the treatment of smallpox and measles from Baghdad in 910 (3–5). There have also been several outbreaks of mysterious diseases since ancient times in Europe. The earliest could be the Plague of Athens, described by Thucydides, which occurred immediately after the Peloponnesian War (431 – 404 BC) when an unknown disease was brought back by returning soldiers. Thucydides mentioned several clinical symptoms that could have been caused by variola virus (6); however, they also fit with other diseases, including typhus (7). Another early smallpox epidemic could be the Antonine Plague, which struck the Roman Empire in 165 AD and was described by Galen (8). Notably, the complete list of outbreaks could fill several books (3–5).

1.1.1.2 First steps towards eradication

Not only is the origin of this deadly disease a mystery, but also it is difficult to pinpoint when and where the first attempts to eradicate smallpox occurred. An early form of preventive inoculation called variolation was based on materials extracted from smallpox pustules, which were then transferred to healthy individuals to grant them protection against the actual disease.

An unknown and mystical procedure appeared in the 10th century AD in China, but it was considered taboo at the time. The first written method appeared in medical texts around 1500 and discussed the intranasal insufflation of powdered scab material (4, 9). Another method of inoculation was described in the early 18th century in the Ottoman Empire, in which pustules were pricked using a needle to collect the infectious material, which was then stored; next, a healthy patient's skin was scratched until it bled and the collected substance was introduced into the wound, preferably at several points on the body (10, 11). In addition, another method of inoculation had already existed for years already in India (12). This type of variolation spread to Europe, mainly thanks to the efforts of Lady Mary Wortley Montague (1689 – 1762), the wife of a British diplomat in Constantinople, after she witnessed and underwent the inoculation procedure together with her son in the Ottoman Empire. When she returned to England in 1721, she ordered her daughter to be inoculated as well (13, 14). Once the safety and efficacy of this method had been demonstrated, it quickly spread throughout Europe as well as the New World (15).

1.1.1.3 Birth of the first vaccine

After observing several cases and listening to tales in and around Gloucester, England, on 14th May 1796, Edward Jenner (1749 – 1823) inoculated the 8-year-old James Phipps with cowpox material from the lesions of a milkmaid named Sarah Nelmes. The boy was monitored, and on 1st July Jenner inoculated him with smallpox material, but no disease developed afterwards. Based on this successful inoculation, Jenner decided to call this new form of treatment 'vaccination', based on the Latin words *vacca* ('cow') and *vaccinia* ('cowpox') (4, 13, 16–19). Slowly but steadily, the constantly improving method of vaccination replaced variolation throughout the world, and by the beginning of the 19th century, it had become mandatory by law in several countries. Simultaneously, however, due to recurring smallpox pandemics, it became painfully obvious that a single vaccination did not provide lifelong protection. In 1847, Germany was among the first countries to introduce a law requiring the vaccination of every child at the age of 2 years and then again at the age of 12 unless he or she had caught the disease within the past 5 years (4, 13). Over the following decades, increasingly fewer people died due to smallpox, but it persisted in many countries as an endemic disease. In 1966, the World Health Organization (WHO) enhanced the efforts to eliminate smallpox in every country by launching its smallpox eradication programme. The programme was completed in 1980, when the WHO officially declared smallpox to have been eradicated worldwide (20).

At this point, it is crucial to mention that the virus used by the WHO to eradicate smallpox was not cowpox but mostly vaccinia virus (VACV), and the origin of this strain is unclear even today (21–23). As a safer substitute during the 1970s, an attenuated vaccinia strain known as modified vaccinia virus Ankara (MVA) was used for vaccination in Germany on more than 120 000 individuals without any major side effects (24, 25).

1.1.2 VACV

The *Poxviridae* family consists of the *Entomopoxvirinae* (poxviruses that infect insects) and *Chordopoxvirinae* subfamilies (poxviruses that infect vertebrates, including humans). Within the second subfamily, there are 18 genera, though only the *Orthopoxvirus* genus is important for this thesis. Among others, the smallpox-causing variola virus as well as vaccinia and cowpox viruses belong to this group (26).

Poxviruses are large, linear dsDNA viruses with genomes that can vary from 150 to 300 kbp and can be translated into more than 200 proteins (27). These viruses are unique since they replicate within the cytoplasmic compartment of infected cells instead of in the nucleus (28). The mechanism of entry of VACV into the cytoplasm has been intensively studied because it can depend on the target cell, the strain of the infecting virus, and even the morphological type of the virion (29–33). There are two antigenically distinct infectious forms of the virus, namely mature virions (MVs), which only have one outer membrane bilayer (34), and extracellular virions (EVs), which have an additional membrane layer originating from the early endosome or trans-Golgi network (35). MVs are considered more stable and abundant, which makes them ideal for host-to-host transmission of the virus, while EVs are more delicate but play a crucial role in the dissemination of virus particles within the infected host (36, 37).

1.1.2.1 Replication cycle of VACV

The first step of entry occurs when the virus attaches to the cell surface. MVs utilise viral proteins [A27 and H3 to bind heparan (38, 39), D8 to bind chondroitin (40) and A26 to bind laminin (41)] to interact with host cell glycosaminoglycans (GAGs) for binding (42). Most entry studies have focused on purified MVs, which has led to a limited understanding of the EV binding mechanism. It seems the EV proteins A34 and B5 are required to interact with GAGs (43). Following successful attachment, the virus is internalised either through the plasma membrane or through macropinocytosis (44, 45) (**Figure 1**). Fusion is mediated for both infectious forms by the entry-fusion complex (EFC) of VACV, which consists of 11 essential

proteins (A28, A21, A16, F9, G9, G3, H2, J5, L1, L5, and O3) to transport the virus core into the cytoplasm (46–56).

At this point, several mechanisms are activated in sequence: early viral gene expression, which is promoted by previously encoded transcription machinery inside the viral core after virion assembly (28, 57–59); genome uncoating (60); and the formation of viral factories (61). Approximately half of the VACV gene products are expressed early (62, 63). As an effect of the early genes in the special aforementioned compartments, DNA replication is initiated and followed by intermediate and late gene expression (64). The newly transcribed proteins are required for virion morphogenesis and used during the assembly of new virions. This process starts with the formation of crescent-shaped membranes, which expand and integrate viral DNA to form spherical immature virions (IVs). These particles then develop into brick-shaped MVs (65). For crescent-shaped and further membrane formation, the structural proteins D13 (66), A14 (67) and A17 (68) as well as the regulatory proteins A6 (69), A11 (70), F10 (71), H7 (72), L2 (73), and A30.5 (74) are essential. Next, the MVs leave the viral factories and are transported to the Golgi network and endoplasmic reticulum (ER) by the microtubules of the infected cell. The MVs are then wrapped with two additional membrane layers derived from these organelles (75, 76). For this process, the viral proteins A27 (77), B5, A34 (78, 79), and F13 (80) are required. The triple membrane-encased particles are called wrapped virions (WVs), which can be transported to the cell surface to undergo exocytosis and leave the cell. During exiting, the outermost membrane layer of the virion fuses with the cell membrane; thus, the particles that appear outside of the cell are EVs wrapped in a double membrane. They are responsible for spreading the infection from cell to cell and for disseminating the virus within the infected host (81–83).

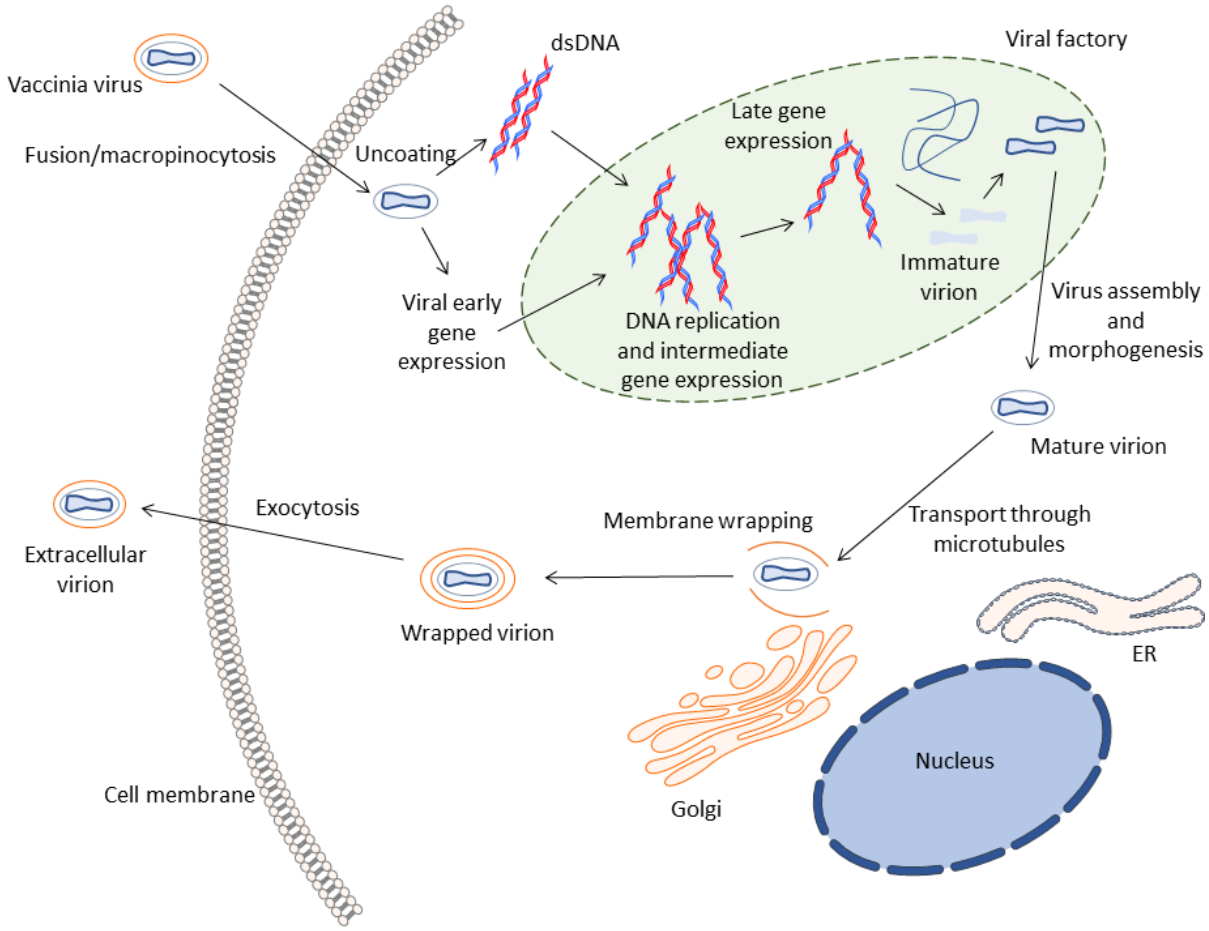

Figure 1. Vaccinia virus replication cycle. This process is considered unique among DNA viruses since poxviruses replicate in the cytoplasm instead of the nucleus.

1.1.3 MVA

MVA is an attenuated vaccinia virus strain that was created by the serial passage of the virulent chorioallantois vaccinia virus Ankara (CVA) strain in chicken embryonic fibroblast cells (84, 85). MVA lost approximately 31 kbp of its parental viral genome, resulting in six large deletion regions, which prevent virus assembly after DNA replication and late gene expression in most mammalian cells (86–89). Moreover, as a result of this loss, MVA lacks several immunomodulatory genes that would normally hamper any immune responses upon infection when they are present in virulent strains (84, 85, 90). Consequently, MVA is able to trigger potent innate immune reactions through type I interferon (IFN) expression (91–93) as well as adaptive immune response through major histocompatibility complex (MHC) -I and -II antigen presentation (94, 95). However, these mechanisms still require further investigation.

1.2 Innate immune responses

During everyday life, it is essential for all living organisms to be able to defend themselves when, for example, they are attacked by predators. It is the same at the cellular level, only in this case the host is fighting pathogens, such as viruses. The first line of defence in this fight is the innate immune system, where pattern-recognition receptors (PRRs) recognise conserved pathogen-associated molecular patterns (PAMPs) to trigger efficient immune responses for fighting the invading viruses (96). Several types of PRRs can recognise viral nucleic acids and initiate anti-viral responses, including toll-like receptors (TLRs), RIG-I-like receptors (RLRs) and cytosolic DNA sensors (97). Amid the possible mechanisms that neutralise viruses, one of the most critical is the type I IFN response, which involves several IFN-α isoforms, IFN-β and cytokine production. The expression of type I IFN genes is strictly regulated by several intracellular signalling pathways (98), one of which is known to be the cGAS-STING pathway.

1.2.1 cGAS-STING pathway for type I IFN production

1.2.1.1 Activation and mechanism of the cGAS-STING pathway

The cGAS-STING pathway is activated when free nucleic acid appears in the cytoplasm (from bacteria, viruses or self-DNA) and is bound by the dsDNA sensor cyclic GMP-AMP synthase (cGAS) (99). cGAS binds the sugar-phosphate backbone of dsDNA regardless of the sequence. The protein then undergoes a conformational change which enables it to bind ATP and GTP to synthesise the second messenger 2′3′ cyclic AMP-GMP (cGAMP) (100–103), thereby activating the protein known as the stimulator of interferon genes (STING). Noteworthily, cGAMP can be transferred to uninfected cells through gap junctions, where it can initiate STING-dependent type I IFN expression (104). STING (also known as Transmembrane protein 173, ERIS and MITA) (105–107) is a transmembrane dimer protein anchored to the ER by four transmembrane domains in its amino-terminal (or N-terminal) domain; this is followed by the dimerisation domain and carboxy-terminal (or C-terminal) tail, which reaches into the cytoplasm (108–110) (**Figure 2**). STING can be activated by other cyclic dinucleotides (e.g., cyclic di-GMP or cyclic di-AMP), which are not produced by cGAS (111). Upon stimulation through its dimerisation domain, STING binds and phosphorylates TANK-binding kinase 1 (TBK1) via its conformationally changed C-terminal tail. Together, they translocate towards the Golgi apparatus to bind and phosphorylate IFN regulatory factor 3 (IRF3), the transcription factor for type I IFN signalling. The phosphorylated IRF3 dimerises and undergoes

autophosphorylation before translocating into the nucleus and initiating type I IFN expression (112–116).

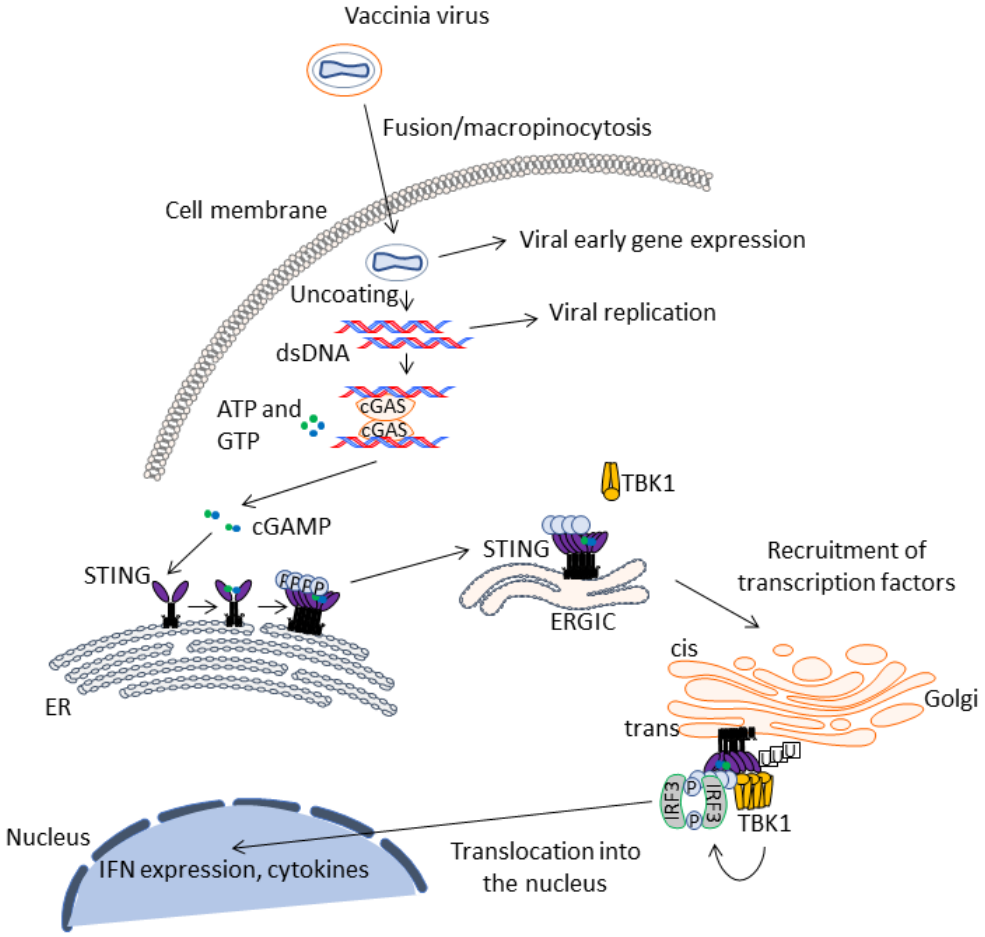

Figure 2. The cGAS-STING pathway of cytosolic DNA sensing. Vaccinia virus is used here as an example to illustrate how dsDNA appears in the cytoplasm**.**

Furthermore, this signalling pathway is strictly regulated to circumvent unnecessary activation or extensive type I IFN production, which would harm the host cell itself. As an example, research demonstrated that autophagy-related protein Beclin1 negatively regulates cGAMP production by directly interacting with cGAS to initiate DNA removal from the cytosol by inducing autophagy (117). The enzyme ecto-nucleotide pyrophosphatase phosphodiesterase 1 (ENPP1), a type II transmembrane glycoprotein, is a negative regulator of the cGAS-STING pathway and controls the hydrolysis of cGAS-produced 2′3′-cGAMP but not that of 3′3′-cGAMP (118, 119). One of the many examples of STING regulation occurs through ubiquitination: the E3 Ubiquitin ligase tripartite motif proteins 32 and 56 (TRIM32 and TRIM56) positively regulate cGAS and STING activation by promoting K63 polyubiquitination of the protein upon activation (120–122). Furthermore, TRIM30α promotes

the K48 polyubiquitination of STING, targeting the protein for proteasomal degradation, thus acting as a negative regulator (123). The autophagy protein uncoordinated 51-like kinase (ULK) 1 was reported to have a negative regulatory effect on STING to prevent expanded proinflammatory gene transcription (124). Even the members of the cGAS-STING pathway have regulatory functions: when the amount of 2′3′-cGAMP exceeds a certain level within the cell, the STING phase-separator is formed to prevent the overactivation of the protein by condensating the overflowing cGAMP, STING, and TBK1 molecules, before facilitating their degradation (125). TBK1 can be negatively regulated by the cooperation of ABIN1, TAX1BP1, and A20 proteins to reduce the anti-viral response of cells infected with vesicular stomatitis virus (126). Additionally, TRIM21 promotes the proteasomal degradation of IRF3 through the K48-linked ubiquitination of the protein (127).

1.2.1.2 Viral interference in the cGAS-STING pathway

The cGAS-STING pathway is considered an important IFN and proinflammatory cytokine that senses and responds to DNA in the cytoplasm (128–132); therefore, DNA viruses have developed several ways to interfere with different parts of the signalling route (133). For example, herpes simplex virus 1 (HSV-1) VP22 protein and Kaposi's sarcoma-associated herpesvirus (KSHV) ORF52 protein can interfere with the enzymatic activity of cGAS (134, 135) . Human cytomegalovirus (HCMV) US9 protein is able to block STING dimerisation and activation (136), and murine gammaherpesvirus 68 (MHV68) ORF11 protein binds directly to TBK1 to inhibit type I IFN production (137). In the case of poxviruses, virulent VACV strains can prevent STING activation through various approaches (138). For instance, the VACV protein F17 destabilises cGAS through mTOR dysregulation (139). Research has also demonstrated that poxvirus immune nucleases (poxins), encoded by the VACV B2R gene, can cleave cGAMP to evade innate immunity (140). Furthermore, virulence factor VACV C6 and K7 proteins directly interact with TBK1 to inhibit IRF3 and IRF7 activation (141, 142), while VACV N2 protein inhibits IRF3 activity inside the nucleus (143). Moreover, although SARS-CoV-2 is a positive-sense single-stranded RNA virus, it seems capable of blocking the STING pathway, among others, to prevent type I IFN expression (144). However, studies have demonstrated that external activation of STING signalling can limit SARS-CoV-2 replication, making this mechanism a potential therapeutic target for overcoming future coronavirus outbreaks (145, 146).

Additionally, an increasing number of studies have found evidence that STING is centrally involved in another fundamental cellular process – namely macroautophagy (hereinafter simply referred to as 'autophagy') (147–149).

1.2.2 Autophagy

Autophagy is a highly conserved process from yeast to mammals that maintains cellular homeostasis after any stress stimuli by degrading organelles and large protein aggregates (150–152). In mammalian canonical autophagy, the components of this pathway can be grouped according to the function and hierarchy of the participating gene products as follows: the uncoordinated 51-like kinase 1 complex, autophagy-related gene (ATG) 9 together with the ATG2-18 complex, the class III phosphatidylinositol 3-kinase (PI3K-III) complex, and two types of ubiquitin-like (UBL) binding reaction systems, the ATG12 conjugation complex, and the ATG8 complex (153, 154).

1.2.2.1 Formation of the autophagosome

The initiators of autophagy are negatively controlled by the mammalian target of rapamycin (mTOR) and cAMP-dependent kinase (PKA) pathways in a nutrient-rich environment and initiated upon starvation or infection (155–158). Following these conditions, the ULK1 initiation complex is activated. This complex consists of ULK1 (159); ULK2; ATG13; the focal adhesion kinase family-interacting protein of 200 kDa (FIP200, the mammalian orthologue of Atg17), also called retinoblastoma 1-inducible coiled-coil 1 (RB1CC1) (160, 161); and ATG101 (162) (**Figure 3**). ULK1 undergoes autophosphorylation and phosphorylates ATG13 and FIP200. ATG13 also interacts with each member of this complex directly upon activation (161). Following the release of inhibition, the triggered ULK1 complex activates the PI3K-III or membrane nucleation complex, which includes Beclin1 (the mammalian orthologue of Atg6) (163), vacuolar protein sorting (VPS) 34 (164, 165), VPS15 (166), ATG14L (167–170), and the activating molecule in Beclin1-regulated autophagy (Ambra1), a positive regulator of autophagy (171). After ULK1 phosphorylates Beclin1 and Ambra1, VPS34 is responsible for generating phosphatidylinositol 3-phosphate (PI3P), a molecule that marks the location of phagosome formation (172, 173).

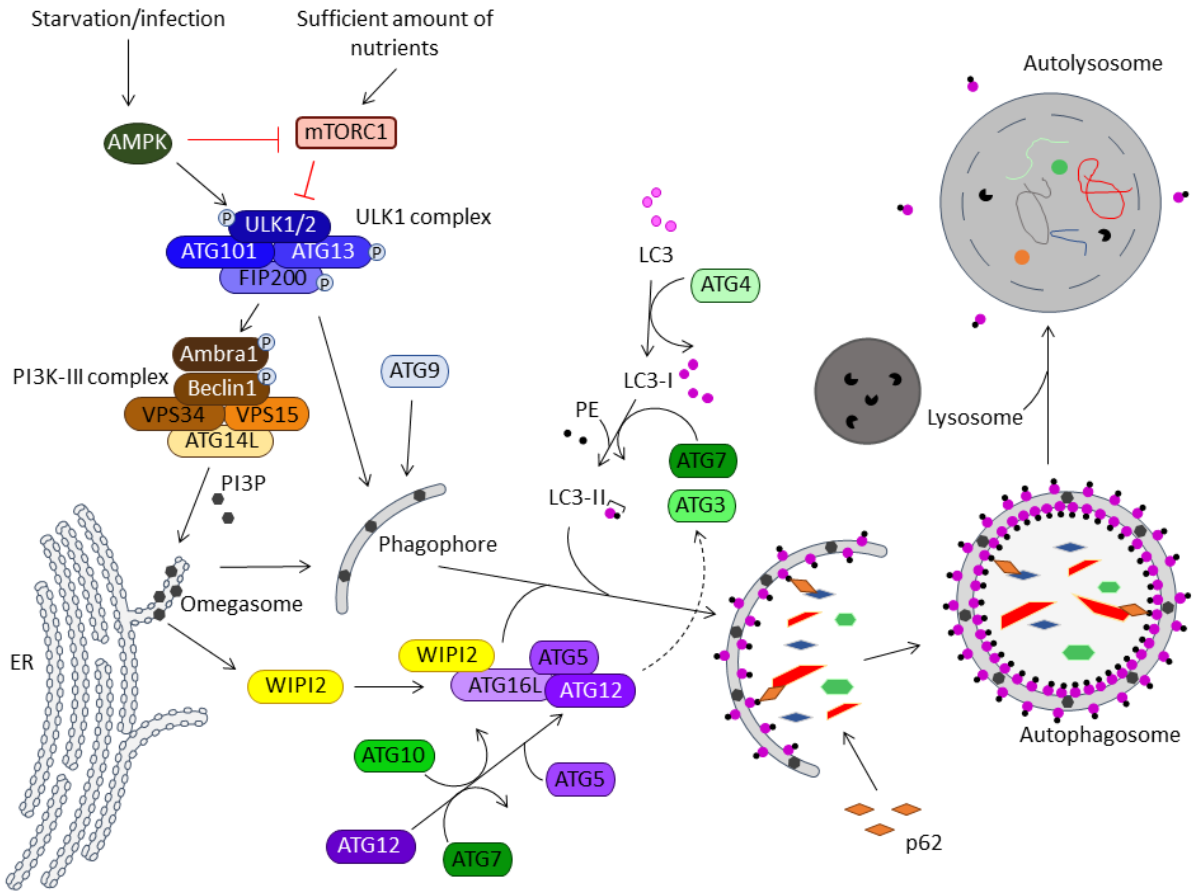

Figure 3. Canonical autophagy pathway. This pathway is initiated by stress signals (e.g., starvation or infection), whereas it is blocked in an environment with a sufficient amount of nutrients. Upon activation the cascade-like system starts with the initiation or ULK1 complex, followed by the membrane nucleation or PI3K-III complex and phagophore formation originating from omegasome regions. This triggers the recruitment of WIPI proteins, which aids the elongation of phagophore formation by attracting the ATG16L1-ATG12-ATG5 complex, ATG9 and ATG2. Then, LC3 formation and lipidation are triggered during the expansion phase, while LC3-II attracts molecules with cargo to be destroyed before the autophagosome is ready to be sealed. After closure, the sealed vesicles fuse with lysosomes to destroy the previously delivered cargo.

While the origin of the autophagosomal membrane is still under extensive investigation, studies have revealed several possible sources, including the ER (174), ER-mitochondria contact sites (175), mitochondria (176), and ERGIC (the ER-Golgi intermediate compartment) (177). These regions, called omegasomes, are rich in PI3P (174). The stimulation of the nucleation complex leads to the recruitment of WIPI (WD-repeat protein interacting with phosphoinositides) proteins (WIPI has several isoforms in humans), and WIPI isoform 2 (WIPI2) is the mammalian orthologue of Atg18 (178). WIPI2 interacts directly with ATG16L1 (179, 180), which in return recruits the ATG12-ATG5 complex (179, 181). Simultaneously, ATG2 (182) interacts with ATG9 (183) to expand and elongate the autophagosome (184). To mobilise the

ATG12-ATG5 complex, ATG12 is first activated by an E1-like enzyme called ATG7. This process is followed by the conjugation of ATG5 by the E2-like enzyme ATG10, causing the already bound ATG12-ATG5 conjugate to bind to ATG16L1 (185). The resulting ATG16L1-ATG12-ATG5 complex acts as an E3 ligase and stimulates the ATG8 family, which includes the mammalian homologue microtubule-associated protein 1A/1B-light chain 3 (LC3, which hereinafter is used as a representative of the ATG8 family) and γ-aminobutyric acid receptor-associated proteins (GABARAPs). First, the protease ATG4 must process LC3 to LC3-I in preparation for phosphatidylethanolamine (PE) binding (186). Next, LC3-I is activated by the E1-like enzyme ATG7 and conjugated to membrane-associated PE by the E3-like enzyme ATG3, resulting in a membrane-bound, lipidated form called LC3-II, which is incorporated into the expanding autophagosome (175). As the phagophore prepares to seal, LC3-II attracts components of the autophagic machinery that contain the LC3-interacting region (LIR) to deliver cargo for degradation and achieve completion. During selective autophagy, the cargo is labelled (usually with ubiquitin chains) and transported by specific autophagy receptors, including optineurin, nuclear domain 10 protein 52 (NDP52) (187), and p62/sequestosome-1 (SQSTM1, hereinafter 'p62') (188). After the phagophore closes, it becomes a double membrane vesicle that is ready to fuse with a lysosome. This process leads to autolysosome formation and the degradation of the previously delivered cargo (189–194).

1.2.2.2 Crosstalk between autophagy and other signalling pathways

In addition to clearing the cytoplasm from aggravated proteins, a form of selective autophagy called xenophagy provides measures to eliminate intracellular pathogens. This process involves the activation and participation of other signalling pathways [e.g., RLR signalling (195), TLR signalling (196) and cGAS-STING signalling (197)], followed by a robust immune response [e.g., type I IFN expression or inflammasome formation (198, 199)]. Focusing on the interactions of autophagy and the cGAS-STING pathway, ATG9a functions as a negative regulator for the translocation of STING and TBK1 upon dsDNA treatment (200). As previously mentioned, Beclin1 interacts with cGAS, while ULK1 interferes with STING to downregulate type I IFN expression (117, 124). Prabakaran *et al.* demonstrated that the selective autophagy receptor p62 is responsible for delivering the activated and phosphorylated STING-TBK1-IRF3 complex into the autophagosome for degradation to prevent continuous type I IFN expression (197). In addition, studies have demonstrated the influence of the STING pathway on autophagy. Increasing evidence suggests that TBK1 interacts with mTOR to regulate autophagy by directly associating with mTORC1 and mTORC2 (201–204). Research

also revealed that STING can induce non-canonical autophagy, which is dependent on the presence of ATG5 by directly interacting with LC3 but is independent of ULK1 or Beclin1 upon poly(dA:dT) treatment or HSV-1 infection (147). This non-canonical autophagy induction is independent of TBK1 or IRF3 and seems to be an ancient function of the cGAS-STING pathway that is dependent on WIPI2 upon cGAMP treatment (148).

1.2.2.3 Autophagy and viruses

As mentioned earlier, autophagy plays an essential role in the clearance of different viruses (205). For example, the Sindbis virus capsid is targeted by p62 and the E3 ubiquitin-protein ligase SMURF1 for autophagosomal degradation through ubiquitination (206). The depletion of p62 or KO of ATG5 during Sindbis virus infection led to the accumulation of the toxic viral capsid which resulted in higher mortality during *in vivo* experiments (207). Furthermore, HSV-1 replication is controlled by autophagy rather than type I IFN expression in dorsal root ganglionic neurons (208). During human immunodeficiency virus 1 (HIV-1) infection, viral particles are taken up and processed in autolysosomes to be presented on MHC-II molecules, which are responsible for extracellular antigen presentation, to initiate the adaptive immune response (209, 210). This mechanism is also essential during MVA infection to stimulate $CD4^+$ T cells *in vitro* (94).

Since autophagy plays a critical role in the innate defence line during viral infection, viruses have evolved to counteract or even hijack this mechanism (211–213). The hepatitis C virus (HCV) protein NS5B, an RNA-dependent RNA polymerase, was demonstrated to interact with ATG5 to promote viral replication (214). HCV also induces the expression of two autophagy regulatory proteins (UVRAG and Rubicon) to enhance and then block autophagosomal maturation. This process enhances HCV replication since the accumulating autophagosomes are unable to fuse with lysosomes (215). Moreover, SARS-CoV-2 seems to promote autophagy through direct interaction with its M protein and LC3, which leads to enhanced autophagic activity and reduced type I IFN expression (216). Moreover, SARS-CoV-2 ORF3a protein interferes with lysosomal fusion, resulting in the accumulation of autophagosomes containing viral particles (217). Studies have also found that the HSV-1 protein ICP34.5 and US11 bind to Beclin1 to inhibit autophagy cell-type dependently (218, 219). Additionally, Epstein–Barr virus (EBV) is able to block lysosomal fusion and uses the autophagosomes as a form of transportation to the plasma membrane to enhance viral replication (220). In the case of VACV, autophagy is not used during the replication process (221); however, the virus induces a novel ATG12-ATG3 conjugation that leads to massive LC3 lipidation. Interestingly, these infected

cells lack autophagosome formation and autophagy flux, a clear sign that autophagy is selectively blocked (222, 223). Moreover, as mentioned earlier, the VACV protein F17 interferes with mTOR to enhance viral late protein production (139). According to a recent study, VACV phosphorylates p62 as well as other selective autophagy receptors to increase the movement of the proteins into the nucleus, thus avoiding being targeted by them (224).

1.3 Aim of the PhD thesis

Several studies have aimed to elucidate the mechanisms by which the autophagy and cGAS-STING pathways can hinder the replication of different viruses in the hope of exploiting these mechanisms for therapeutic purposes. On the virus side, VACV is a crucial viral vaccine vector that has received much research attention in the hope of using it to fight existing and upcoming diseases. Remarkably, however, barely any studies have investigated how the cGAS-STING pathway for type I IFN production, a major dsDNA sensing system together with autophagy (the 'cleaner of the cell'), handle VACV, a dsDNA virus that replicates in the cytoplasm. Recently, an increasing number of studies have provided evidence of a link between these two mechanisms (147, 148, 197, 225).

Previous findings from our group have revealed that the attenuated VACV strain MVA is able to induce LC3 lipidation as well as the importance of autophagy for $CD4^+$ T cell activation during the course of infection (94). Moreover, MVA was demonstrated to generate type I IFN expression through the cGAS-STING pathway (92). Follow-up experiments then confirmed that MVA, already during the early phase of infection, activates the cGAS-STING pathway for type I IFN production and autophagy. In addition, infection with the virulent VACV strain Western Reserve (WR) did not induce these two pathways during this time period; however, activation seemed to appear after a minimum of 8 h post-infection (hpi) (226). Moreover, MVA-induced autophagy seemed to be independent of the presence of ULK1/2 and ATG13, which are two essential members of the initiation complex for canonical autophagosome formation (227).

To follow up on the aforementioned results, in the first part of the thesis, I aimed to investigate the relationship between a plausible non-canonical autophagy pathway and the cGAS-STING pathway for type I IFN production during the early phase of infection with MVA and WR. I generated and tested several KO cell lines that specifically affect the canonical autophagy and cGAS-STING pathways for type I IFN production to investigate the mechanism behind MVA-induced activation and WR-induced inhibition of both pathways.

In the second part of the thesis, I aimed to identify WR early genes that are potentially involved in the inhibition of the two aforementioned cellular defence mechanisms. For my investigation, I generated recombinant MVA (recMVA) strains expressing WR genes previously selected through flow cytometry and/or high-content confocal microscopy. Then, I used these recMVA to investigate the impact of WR gene products in infected cells on the previously seen STING-dependent activation of the autophagy and cGAS-STING pathways for type I IFN production during the early and late phases of infection.

2 Materials

2.1 Cell lines

Name	Description	Source/Reference
BMDC	Bone marrow-derived dendritic cells	C57/BL6 mice
DF-1	Chicken embryonic fibroblasts	ATCC (CRL-12203)
HeLa	Human cervical carcinoma cells	ATCC (CCL-2)
HeLa DsRed-LC3-eGFP	Human cervical carcinoma cells, stably expressing DsRed-LC3-eGFP	Houda Khatif (227)
MEF	Murine embryonic fibroblasts	Dr. Björn Storck
MEF ATG3-KO	MEF CRISPR-Cas9	Dr. Björn Storck
MEF ATG7-KO	MEF CRISPR-Cas9 knocked out for ATG7	This study
MEF ATG12-KO	MEF CRISPR-Cas9 knocked out for ATG12	This study
MEF ATG13-KO	MEF CRISPR-Cas9 knocked out for ATG13	Dr. Björn Storck
MEF Beclin1-KO	MEF CRISPR-Cas9 knocked out for Beclin1	This study
MEF cGAS-KO	MEF knocked out for cGAS	Prof. Dr. Veit Hornung
MEF IRF3-KO	MEF CRISPR-Cas9 knocked out for IRF3	This study
MEF p62-KO	MEF CRISPR-Cas9 knocked out for p62	This study
MEF STING-KO	MEF CRISPR-Cas9 knocked out for STING	This study
MEF TBK1-KO	MEF CRISPR-Cas9 knocked out for TBK1	This study

2.2 Viruses

MVA (cloned isolate F6) at 582nd passage on CEF and recombinant MVA were generated by homologous recombination as described previously (228).

Name	Description	Source/Reference
MVA-P7.5-eGFP	Recombinant MVA (recMVA) virus expressing an enhanced form of green fluorescent protein (eGFP) under early and late promoter P7.5	(229)
MVA-P7.5-NP-SIIN-eGFP	recMVA virus expressing a fusion protein consisting of the nucleoprotein (NP) from influenza A virus (type Puerto Rico 68), the SIINFEEKL peptide (OVA257-264) from the protein ovalbumin (OVA) and eGFP under early and late promoter P7.5	(229)
MVA-P11-eGFP	recMVA virus expressing eGFP under late promoter P11	Ronny Tao
Rabbit fibroma virus (RFV)	Helper virus for recMVA generation	(230)
WR WT	Wild type Western Reserve strain	Prof. Dr. Ingo Drexler
WR-P7.5-NP-SIIN-mCherry	Recombinant WR virus expressing a fusion protein consisting of the NP from influenza A virus (type Puerto Rico 68), the SIINFEEKL peptide (OVA257-264) from the protein OVA and mCherry under early and late promoter P7.5	Dr. Jonathan Wilson Yewdell
WR-P7.5-NP-SIIN-eGFP	Recombinant WR virus expressing a fusion protein consisting of the NP from influenza A virus (type Puerto Rico 68), the SIINFEEKL peptide (OVA257-264) from the protein OVA and eGFP under early and late promoter P7.5	Dr. Jonathan Wilson Yewdell

The following viruses were generated during this study. The WR genes were selected according to the results of confocal microscope and FACS analysis of siRNA silencing screening of 80 conservative WR genes during early infection. The genes below showed noticeable

resemblance to MVA-infected cells and had the most mismatches and/or deletions on the amino-acid level between MVA and WR genomes.

Name	Description
MVA-VV-A10	recMVA virus expressing WR-A10L gene with its promoter-like upstream DNA sequences at its orthotopic position (12 mismatches in MVA on the amino-acid level compared with WR)
MVA-VV-A18	recMVA virus expressing WR-A18R gene with its promoter-like upstream DNA sequences at its orthotopic position (8 mismatches in MVA on the amino-acid level compared with WR)
MVA-VV-B2	recMVA virus expressing WR-B2R gene with its promoter-like upstream DNA sequences at its orthotopic position (B2R is absent in MVA)
MVA-VV-B5	recMVA virus expressing WR-B5R gene with its promoter-like upstream DNA sequences at its orthotopic position (B5R is expressed only late in MVA, but early and late in WR)

2.3 Bacteria

Name	Description	Growth temperature	Source/reference
E.coli XL-1-Blue	Chemical-competent cells	37 °C	Stratagene
E.coli GS1783 #22	Carrying MVA-BAC clone: pMVAF-DX, BAC self-excising	32 °C	Dr. Matthew G. Cottingham

2.4 Plasmids

Name	Description	Source/Reference
pcDNA3.1D V5-His-Topo	Vector plasmid used during cloning of recMVA viruses	Addgene
pEP-MVA-dVI-PK1L	Template plasmid for BAC selection or I-SceI-kanamycin cassette (Kana)	(231)
pMK-RQ-KanR-A10L	pMK-RQ-KanR plasmid containing synthetic WR-A10L gene used for cloning recMVA virus	Invitrogen
pMK-RQ-KanR-B5R	pMK-RQ-KanR plasmid containing synthetic WR-B5R gene used for cloning recMVA virus	Invitrogen
pMK-RQ-KanR-	pMK-RQ-KanR plasmid containing synthetic	Invitrogen

B13R	WR-B13R gene used for cloning recMVA virus	
pMA-AmpR-C10L	pMA-AmpR-C10L plasmid containing synthetic WR-C10L gene used for cloning recMVA virus	Invitrogen

2.5 Gene strands

Name	Description	Source
*Not*I-MVA128L-promoterWRA18R-MVA130L-*Age*I	Synthesised gene strand containing synthetic WR-A18R gene used for cloning recMVA virus	Eurofins Genomics
*Not*I-MVA167-promoterWRB2R-MVA169/170R-*Age*I	Synthesised gene strand containing synthetic WR-B2R gene used for cloning recMVA virus	Eurofins Genomics

2.6 Primers

All primers were purchased from Eurofins Genomics, and sequencing primers were also designed by using the online-available software of the company.

Name	Sequence (5´ to 3´)	Purpose
NotI-iMVAA11_fwd	GGGGGCGGCCGCATAGACATTTGACGAAGAGTTAT	Cloning PCR
AgeI-iMVAA9_rev	GGGGACCGGTATGAATTTGGTCGTAGCTTTTG	Cloning PCR
BAC-EcoRI-A10_fwd	GGGGGAATTCAAGGCAAAAATTGTTAACGGTG TATTAAGCAGACAAGATTTAGGGATAACAGGGTAA TCGATTTATTC	Cloning PCR
BAC-EcoRI-aph_rev	GGGGGAATTCCCAGTGTTACAACCAATTAACC	Cloning PCR
pcDNA-fw_1	TAATACGACTCACTATAGGGAGAC	Sequencing
A10-fw_2	GATTGACGGATACAGAATACAGAG	Sequencing
A10-fw_3	TAACCTGTTGGCGAAGGAAC	Sequencing
A10-fw_4	TACTTCAGCGTTTGATCTTCTC	Sequencing
A10-fw_5	TTCAATGCTAAAGTAGGCGATG	Sequencing
pcDNA-rv_1	GGCAAACAACAGATGGCTGGCAAC	Sequencing
A10-rv_2	GAACATCCATTGAGTCGGAG	Sequencing
A10-electro_F1	CATTTGACGAAGAGTTATTTCAT	Cloning PCR, Sequencing

A10-electro_R1	ATGAATTTGGTCGTAGCTTTTG	Cloning PCR, Sequencing
NotI-MVAA17_fwd	GGGGGCGGCCGCGGCATAAACGATTGCTGCTGTTCC	Cloning PCR
AgeI-MVAA19_rev	GGGGACCGGTCATGACGTGTTCTGCCTGTCAG	Cloning PCR
BAC-EcoRI-A18_fwd	GGGGGAATTCAAGTCAGGAACTATTAATCGCATTTT AGTTATTACTAAACTACGTAGGGATAACAGGGTAATC GATTATTC	Cloning PCR
A18-fw_2	CCTCTTCAACGCAAAGTCGTATC	Sequencing
A18-fw_3	TTTGAGCCATATTCCACAGAC	Sequencing
A18-fw_4	TCGGAAACATCAAGAATCCGATCC	Sequencing
A18-rv_2	TGTTCCAATCCGACTGCCTC	Sequencing
A18-electro_F1	TAAACGATTGCTGCTGTTCC	Cloning PCR Sequencing
A18-electro_R1	GGTTAAGATTTCCGACATCAC	Cloning PCR, Sequencing
NotI-MVAB1_fwd	GGGGGCGGCCGCATGCACCTAGAGAATTGCTGC	Cloning PCR
AgeI-MVAB3_rev	GGGGACCGGTCAGTGTCTTCCACTCCATCTGG	Cloning PCR
BAC-BmgBI-B2_fwd	GGGGCACGTCTGGATAGGAGATTGTATCTGTCAAGT TACTGCTGTGGACGTATAGGGATAACAGGGTAATC GATTTATTC	Cloning PCR
BAC-BmgBI-aph_rev	GGGGGACGTGCCAGTGTTACAACCAATTAACC	Cloning PCR
B2-fw_2	TGGTGTTACAGTCAGGTGAAC	Sequencing
B2-fw_3	ATCTTTCTTCTACTATATCGGCGG	Sequencing
B2-rv_2	GTTTCCTGTTTCAAGTACGTGATG	Sequencing
B2-electro_F1	GAATTGCTGCAATATATTACCA	Cloning PCR, Sequencing
B2-electro_R1	CCATTCACAATATCAAAATGAT	Cloning PCR, Sequencing
NotI-MVAB4_sh_fwd	GGGGGCGGCCGCGAAGTCGTGTACGTAATATC	Cloning PCR
AgeI-MVAB6_sh_rev	GGGGACCGGTTGCCTGAGTAAAAATGCTCTAAC	Cloning PCR
BAC-EcoRI-B5-aph_fwd	GGGGGAATTCCACCATGACACTAAGTTGCAACGGCG AAACAAAATATTTTCGTTGCTAGGGATAACAGGGTAA TCGATTATTC	Cloning PCR
B5-fw_2	GATCAGGGATATCATTCTTCGG	Sequencing

B5-fw_3	TGGAATCCCGTACTCCCAATATG	Sequencing
B5-pcDNA-rv_1	CCCAGAATAGAATGACACCTACTC	Sequencing
B5-rv_2	CAGAGATGTAATCAGAAACTGTGC	Sequencing
B5-electro_F1	GTCTATTATCCAAGAAGCTGG	Cloning PCR, Sequencing
B5-electro_R1	GAAGACATCTCAATTGATTCTAGC	Cloning PCR, Sequencing
NotI-MVAB12_fwd	GGGGGCGGCCGCTGAGTTCTGTGTAGATCATCCGTTC	Cloning PCR
AgeI-MVAB15_rev	GGGGACCGGTTGCGGTATGCATAGGACGACC	Cloning PCR
BAC-BstBI-B13-aph_fwd	GGGGTTCGAATACGTATCTCCGACGGAAATGGTAG ATGTAAGTATGATGTCTATGTAGGGATAACAGGGTA ATCGATTTATTC	Cloning PCR
BAC-BstBI-aph_rev	GGGGTTCGAACCAGTGTTACAACCAATTAACC	Cloning PCR
B13-fw_2	CGATATTCTGCCGTGTTTAAAG	Sequencing
B13-fw_3	CTCTAGTAAAGTCAGGACTGACAG	Sequencing
B13-rv_2	AAGTATACGGCACTAATTGCTAGG	Sequencing
B13-electro_F1	TGAGTTCTGTGTAGATCATCCGTTC	Cloning PCR, Sequencing
B13-electro_R1	TGCGGTATGCATAGGACGACC	Cloning PCR, Sequencing
NotI-iMVAC11_fwd	GGGGGCGGCCGCTGTGATAATGCATACTGTTAGTC	Cloning PCR
AgeI-iMVAC9_rev	GGGGACCGGTCTATACAAGATATGGTTGTGCC	Cloning PCR
BAC-BglII-iC10-aph_fwd	GGGGAGATCTATGTCTGTTAGTAAATAACCATCT AGGTATAGGTATCGTTAAAGTAGGGATAACAGGG TAATCGATTTATTC	Cloning PCR
BAC-BglII-aph_rev	GGGGAGATCTCCAGTGTTACAACCAATTAACC	Cloning PCR
BAC-MfeI-iC10-aph_F	GGGGCAATTGCCGTTCTAGACATATCCGTTTCATATA ATAGATCAATGACTACTATAGGGATAACAGGGTAATC GATTTATTC	Cloning PCR
BAC-MfeI-aph_R	GGGGCAATTGCCAGTGTTACAACCAATTAACC	Cloning PCR
C10-fw_2	GTCCTCTTTCCTCTTATAACATCG	Sequencing
C10-fw_3	ATTTGGAAACACCGATATGTGGAG	Sequencing
C10-fw_4	CGATGATACAGATATATGGACTCC	Sequencing
C10-rv_2	TGATTGTTTGACGAATCACGAG	Sequencing

S1aph_rev_in	ATTCGTGATTGCGCCTGAGC	Sequencing
S2aph_fwd_in	CGTACTCCTGATGATGCATG	Sequencing
S4aph_fwd_out	TGGTATTGATAATCCTGATATG	Sequencing
GFP_fwd	TTGTACAGCTCGTCCATGCCGAG	Control PCR
GFP_rev	GCAAGGCCGGATCTGGGAATTC	Control PCR
RFV_fwd	AAAGATGCGTACATTGGACCC	Control PCR
RFV_rev	GTTCGAGACTAGAAAAGCGCC	Control PCR

2.7 siRNA sequences

The siRNA library to silence 80 conserved genes of WR was described before by Kilcher and colleagues (232). Only the list of the top selected targets is shown below, the full list is under section 6.2.1.2 Supplementary materials of recMVA generation. All sequences have 3′ dTdT overhangs.

Name	Sequence (sense)
A10L oligo1	CAAUUAACAUUAGUUCGGA
A10L oligo2	CUCAAUGGAUGUUCUAGCA
A10L oligo3	GACUUGAGGCAAUCAUCGU
A18R oligo1	CGUCAUUUGCGUACCCAAU
A18R oligo2	GUCGUAUCUGAAGUAGUUU
A18R oligo3	CUAUUAGAUAGGACGGUAU
B5R oligo1	GGAAUGUCAACCUCUUCAA
B5R oligo2	GUUAUACAUCUUAGUUGUA
B5R oligo3	GAAUGUUAUUCCAUCAUGU
B13R oligo1	CACUGAUUGUCGCACUAUA
B13R oligo2	GUCUAUGUACGGCAAGGCA
B13R oligo3	GGCAUUUAAUCACGCAUCU
C10L oligo1	GUUCUAAUUGGGUACCCUU
C10L oligo2	CGUUAAAGAUAAACGUAUA
C10L oligo3	CGGAUAAGGAUAUUAUGUU

2.8 Antibodies

2.8.1 Primary antibodies

Antigen	Species	Application	Source/reference
ATG3 (#3415)	Rabbit	WB	Cell Signaling
ATG7 (D12B11)	Rabbit	WB	Cell Signaling
ATG12 (D88H11)	Rabbit	WB	Cell Signaling
ATG13 (SAB4200100)	Rabbit	WB	Sigma-Aldrich
β-actin (A2228)	Mouse	WB	Sigma-Aldrich
Beclin1 (D40C5)	Rabbit	WB	Cell Signaling
cGAS (D3O8O)	Rabbit	WB	Cell Signaling
GFP (11814460001)	Mouse	WB	Roche
IRF3 (D83B9)	Rabbit	WB	Cell Signaling
LC3B (L7543)	Rabbit	WB	Sigma-Aldrich
mCherry (5993)	Rabbit	WB	BioVision
p62/SQSTM1 (P0067)	Rabbit	WB	Sigma-Aldrich
Phospho-IRF3 (4D4G)	Rabbit	WB	Cell Signaling
Phospho-STING (mouse specific D8F4W)	Rabbit	WB	Cell Signaling
Phospho-TBK1/NAK (D52C2)	Rabbit	WB	Cell Signaling
STING (D2P2F)	Rabbit	WB	Cell Signaling
TBK1/NAK (D1B4)	Rabbit	WB	Cell Signaling
VACV (9503-2057)	Rabbit	WB	BioRad

2.8.2 Secondary antibodies

Antigen	Conjugate	Species	Application	Source/reference
Anti-rabbit (111-035-144)	HRP	Goat	WB	Jackson
Anti-mouse (115-035-146)	HRP	Goat	WB	Jackson

2.9 Chemicals and reagents

2.9.1 Antibiotics

Name	Used for	Concentration	Source/reference
Ampicillin	Bacteria colony selection	100 µg/ml	Roth
Chloramphenicol	Bacteria colony selection	30 µg/ml	Roth
Kanamycin	Bacteria colony selection	30 µg/ml	Roth
Puromycin dihydrochloride	Selection of transduced cells	10 µg/ml	Sigma-Aldrich

2.9.2 Reagents

Name	Description	Concentration	Source/reference
3MA	Autophagy inhibitor	5 mM	Sigma-Aldrich
AraC	DNA replication and late gene expression inhibitor	40 µg/ml	Sigma-Aldrich
cGAMP	Second messenger of STING	20 µg/ml	Invivogen
Chloroquine	Autophagy inhibitor	40 µg/ml	Sigma-Aldrich
DMXAA	Mouse-STING activator	5 µg/ml	Invivogen
Epoxomicin	Proteasomal inhibitor	10 µg/ml	Sigma-Aldrich
Golgicide A	Inhibitor of assembly and transport of Golgi	10 µg/ml	Merck
Psoralen	dsDNA crosslinker	1 µg/ml	Sigma-Aldrich
Rapamycin	Autophagy inducer	30 µg/ml	Cayman Chemical
Saponin	Cell membrane permeabilization	0.05 %	Sigma-Aldrich

2.9.3 Other reagents and chemicals

Amersham Protran nitrocellulose WB membrane	Roth
Agarose	Biozym
Albumine fraction V	Roth
β-mercaptoethanol	Roth
Bromophenol blue	Merck

D(+)-Saccharose	VWR
DAPI	Vector
DMSO	Sigma-Aldrich
DreamTaq Green PCR Master Mix (2X)	ThermoFisher
eBioscience Fixable Viability dye eFlour 660	ThermoFisher
Endonucleases (restriction enzymes)	New England Biolabs
Enzyme buffers (10X)	New England Biolabs
Ethanol absolute	Merck
EZ-Vision in gel	VWR
Gel loading dye purple (6X)	New England Biolabs
Glycerol	Roth
Glycine	Roth
Hoechst (33342)	Invitrogen
Hydrochloric acid (32%)	Roth
Hyper ladder 1kb	Bioline
Isoflurane	Piramal
Isopropanol	Merck
Methanol	Merck
LB-Broth (Lennox)	Roth
LE Agarose	Biozym
Lipofectamin	Thermo Scientific
P1, P2 and P3 buffers for DNA isolation	Qiagen
PageRuler Prestained protein ladder	Thermo Scientific
Paraformaldehyde	Merck
Pierce ECL Western blotting substrate	Thermo Scientific
Pharm-Lyse	BD
Phenol-chloroform	Roth
Polybrene	Sigma-Aldrich
PEI	Sigma-Aldrich
ProteinaseK	AGS GmbH
Quick Ligase	New England Biolabs
Quick Ligase Reaction Buffer (2X)	New England Biolabs
Rotiphorese Gel 30	Roth

SDS, ultrapure	Roth
Skimmed milk powder	Sufocin
Sodium azide	Merck
Sodium chloride	Sigma-Aldrich
TEMED	VWR
Tris-base	Roth
TBE (10X)	VWR
Triton X-100	Sigma-Aldrich
Trypan blue stain (0.4%)	Gibco
Turbofect	ThermoFisher
Tween 20	Merck
Ultrapure Distilled Water DNase/RNase free	Invitrogen

2.10 Media and buffers

2.10.1 Cell culture medium

DMEM	Gibco
FBS Superior	Biotech
PBS (1X)	Gibco
RPMI	Gibco
Trypsin-EDTA (0.05%)	Gibco

Growth medium	DMEM/RPMI + 10 % FBS
Freezing medium	FBS + 10 % DMSO
M2 medium	RPMI + 10% FBS + 28 µl 80% (v/v) β-mercaptoethanol

2.10.2 Bacteria medium

LB-agar	35 g on 1 L H_2O (1.5 % w/v agar content)
LB-medium	20 g on 1 L H_2O

2.10.3 SDS polyacrylamide gel electrophoresis (SDS-PAGE) buffers

10X Laemmli running buffer	250 mM Tris-base
	2 M Glycine
	1 % (w/v) SDS

5X sample loading buffer	250 mM Tris pH 6.8 10 % SDS 30 % Glycerol (100 %) 12.5 % β-mercaptoethanol 0.05 % Bromophenol blue
12 % separating gel (big)	19.8 ml Acrylamide 10.5 ml 2 M Tris/HCl pH 8.8 249 µl 20 % SDS 18.7 ml H_2O 99.5 µl TEMED 597 µl 10 % APS
Stacking gel (big)	3 ml Acrylamide 2.4 ml 0,5 M Tris/HCl pH 6.8 90 µl 20 % SDS 12.6 ml H_2O 24 µl TEMED 240 µl 10 % APS
10X TBST	0.1 M Tris/HCl pH 8.0 1.5 M NaCl 0.5 % (v/v) Tween 20
10X transfer buffer	0.5 M Tris-base 0.4 M Glycine
1X transfer buffer	100 ml 10X transfer buffer 200 ml Methanol 700 ml dd H_2O
Tyr-lysis buffer	50 mM Tris/HCl pH 8.0 150 mM NaCl 0.02 % NaN_3 1 % Triton X-100

2.10.4 Other buffers

Blocking buffer (ELISA)	3 % BSA

	0.05 % Tween 20 in PBS
Blocking buffer (WB)	5 % milk powder/BSA in TBST
Coating buffer (ELISA)	0.2 M carbonate/bicarbonate pH 9.4 in PBS
FACS buffer	5 % BSA 0.02 % NaN_3 in PBS
Fixing buffer (IF)	2 % PFA
Wash buffer (ELISA)	0.05 % Tween 20 in PBS
Crude extraction buffer (CEB)	750 mM Tris 200 mM (NH4)2SO4 12 mM MgCl2 pH 8.8
CEB-Proteinase K (PK) (1 ml)	100 µl CEB 100 µl PK 25 µl 20 % Tween 20 775 µl ddH_2O

2.11 Kits

LumiKine Xpress mIFN-β 2.0	Invivogen
Nucleospin Gel and PCR Clean-up	Macherey-Nagel
Phusion High-fidelity PCR kit	New England Biolabs
QIAprep Spin Miniprep Kit	Qiagen
QIAquick Gel extraction Kit	Qiagen

2.12 Equipment

Benchtop orbital shaker MaxQ 4000	Thermo Scientific
Blotting machine	Neolab
Centrifuge 5424R	Eppendorf
Centrifuge Heraeus Pico 21	Thermo Scientific
ChemoStar Touch ECL Imager	Intas
Cross-linker	Peqlab

Electrophoresis chambers	Neolab
Eporator	Eppendorf
FACS Canto II Diva	BD Biosciences
Heating plate MR Hei-Tec	Neolab
Heracell 240i CO_2 incubators	Thermo Scientific
LSM 710 confocal microscope	Zeiss
Magnetic shaker St. 5	Neolab
Mars safety sterile benches	Labogene
Multiskan GO	Thermo Scientific
NanoDrop 2000	Thermo Scientific
Opera LX high-throughput microscope	PerkinElmer
Professional Trio Thermocycler	Biometra
Rocking shaker ST 5	CAT
Sonopuls HD 200	Bandelin
Sorvall ST 16R centrifuge	Thermo Scientific
Sorwall WX+ Ultra Series centrifuge	Thermo Scientific
ThemoMixer C	Eppendorf
UV-transilluminator (UVsolo TS)	Biometra
Vortex Genie 2	Scientific Industries

3 Methods

3.1 Cell biology and virology methods

3.1.1 Cell culture and cell counting

All cells were incubated in an incubator containing 5 % CO_2 at 37 °C. For cell cultivation, DMEM with 10 % heat inactivated FBS for MEF cells, RPMI with 10 % FBS for HeLa and DF-1 cells and M2 medium for BMDCs was used. After cell-confluency reached 80 – 90 %, cells were passaged in the following way. First, old culturing medium was discarded, cells were washed with PBS and then detached from surface using 0.05 % trypsin-EDTA. After detachment, trypsin was neutralised with fresh culturing medium, cells were split into 1:10 and transferred into a new culture flask containing fresh medium.

When cell-numbers needed to be determined, cell suspension was mixed with trypan blue in 1:5 ratio and living cells were counted using a Neubauer chamber.

3.1.2 Freezing and thawing of cells

For freezing, after detachment and trypsin inactivation, cells were pelleted by centrifugation at 1500 rpm (ST 16R) for 5 min at room temperature (RT). Supernatant was discarded and pellet was resuspended in an appropriate volume of 4 °C cold freezing medium and aliquoted to 1.5 ml cryotubes. Tubes were kept at -80 °C for short-term and transferred to the liquid nitrogen tank for long-term storage.

For thawing, cells from cryotubes were resuspended in pre-warmed medium and pelleted by centrifugation at 1500 rpm (ST 16R) for 5 min at RT. Supernatant was discarded and cells were resuspended in fresh culture medium, then transferred into cell culture flask and cultivated as described in the previous section.

3.1.3 Preparation of BMDCs

BMDCs were derived from femurs and tibiae of C57/BL6 mice after animals were killed by cervical dislocation. Hind limbs were cut off from the body and cleaned with 70 % ethanol. Bones were cleaned from fur and muscle tissue, disinfected with ethanol one more time and placed into 6 cm dish containing M2 medium. Ends of each bone were cut and bone marrow was flushed out with M2 medium using a sterile syringe. Bones were washed three times with the culture medium and cells were transferred into 50 ml falcon tube, then centrifuged at 1500 rpm (ST 16R) for 5 min at RT. Supernatant was discarded and pellet was resuspended in lysis-

buffer (diluted 1:10 with dd H_2O) for 1 min at RT to remove erythrocytes. Afterwards, PBS was added to neutralise the lysis-buffer and cells were centrifuged at 1500 rpm (ST 16R) for 5 min at RT. After discarding the supernatant, pellet was resuspended with M2 medium, then filtered through a 0.75 µm cell strainer. Cells were counted as described in section 3.1.1 and adjusted to a density of 5 x 10^6 cells/ml/plate and seeded into 10 cm petri dishes with 10 ml of M2 medium containing 10 % GM-CSF. On the third day after the preparation, another 10 ml of M2 medium containing 10 % GM-CSF was added to the cultured cells. On the sixth day, 10 ml of supernatant was discarded and fresh culturing medium with 10 % GM-CSF was added to the cells. On the seventh day, BMDCs were used for *in vitro* experiments.

3.1.4 Positive clone selection and single cell clone-picking of CRISPR-Cas9 knocked out cells

Generation of lentiviral virus (transfection and virus isolation) and transduction of MEF cells was done by Cornelia Barnowski and these protocols are shown in Appendix section 6.1.2.

Successfully transduced MEF cells were selected with puromycin three days post-transduction. Cells were given fresh culturing medium with puromycin (10 µg/ml), put back into 37 °C incubator for three days then supernatant was exchanged to fresh medium supplemented with puromycin for another two days. Afterwards, supernatant was discarded and puromycin free culturing medium was given on top. The confluency of the cell layer was monitored to expand the surviving cells. From expanded cell populations (from now on called bulk population), protein was isolated and checked for being knocked out for the gene of interest by immunoblotting. Parts of bulk populations were frozen as back-up for future experiments. If the bulk population was confirmed as mixture of WT and KO cells, then single cell clones were picked.

In case of single cell clone-picking, cells were counted as described in section 3.1.1 and diluted to obtain 10 cells/ml concentration. The 100 µl of the diluted cell-suspension was plated into 96-well-plates for each desired KO cell line, then cultured and expanded until cells reached sufficient confluency to isolate protein to confirm the KO and freeze them away.

3.1.5 recMVA BAC-rescue with the help of rabbit fibroma virus (RFV)

DF-1 cells were seeded in 6-well-plates a day prior to transfection in order to reach 70 % confluency on the day of transfection. During the whole procedure cut-end tips were used. Transfection mix was prepared: 6 µl Turbofect, 5 µg BAC DNA which was then filled up to

400 µl with pure RPMI, then incubated for 20 min at RT. Next, 600 µl pure RPMI was added to mixture and culturing medium was removed from DF-1 cells. The previously prepared 1 ml transfection mix was added to cells dropwise, then cells were incubated for 3 h at 37 °C. Afterwards, RFV as helper virus was diluted to get MOI 1 in 100 µl RPMI containing 5 % FBS for each well and the mixture was pipetted into culture medium of the DF-1 cells directly. Plates were put back into 37 °C incubator and were shaken in every 15 min for 1 h. Then supernatant was exchanged to 2 ml of fresh culturing medium and plates were put back into 37 °C incubator. After 48 h up to 96 h, cells were monitored for plaques showing GFP expression, then wells with the highest number of GFP positive cells were harvested by scraping and centrifugation at 4000 rpm (5424R) at 4 °C for 10 min. Supernatant was discarded and pellet was resuspended in 800 µl culturing medium. After three cycles of freeze-thawing, samples were sonicated three times for 1 min and 50 µl of sample with 450 µl culturing media was pipetted on top of previously seeded 70 % confluent DF-1 cells in 6-well-plates in serial dilutions (10^{-1} to 10^{-5}). This was considered as first passage of the recMVA viruses. After adding 1.5 ml culturing media to cells, plates were put into 37 °C incubator and after 3 – 4 days, cells were monitored for GFP expression. Wells from the highest dilution with most infected cells were harvested by scraping, and the previously described protocol was repeated two more times to have at least three blind passages. Virus containing samples were kept at -80 °C for the time being.

3.1.6 Selection of GFP (-) and cytopathic effect (CPE) (+) cells

DF-1 cells were seeded in 96-well-plates a day prior with 100 µl RPMI containing 2 % FBS to reach 75 – 80 % confluency on the day of infection, while one 96-well-plate was calculated for each dilution. Virus-dilutions were prepared from samples of the 3rd passage from 10^{-1} to 10^{-8} and 100 µl of each virus dilution was added to corresponding wells. After 5 – 7 days, cells were monitored for GFP (-) expression and CPE (+). Wells without GFP expression but with CPE were harvested by scraping (minimum 1 – 2 positive wells from 10). To check for the presence of GFP, RFV, and genes of interest via PCR, 100 µl of the harvested samples were taken. Another 50 µl of the samples were used for amplification of the positive clones and the rest was kept at -80 °C as back-up. To amplify positive clones, previously seeded DF-1 cells were infected with the above mentioned 50 µl with 450 µl culturing medium and cultured in 37 °C incubator for 2 - 3 days.

3.1.7 recMVA amplification and generation of crude stock

To harvest, positive virus clones in 6-well-plates were scraped into supernatant and centrifuged at 4000 rpm (5424R) for 10 min at 4 °C. Supernatant was discarded and pellet was resuspended in 1 ml culturing medium. After samples went through three cycles of freeze-thawing, they were sonicated three times for 1 min. For amplification, 300 µl of samples were added to previously seeded DF-1 cells in one 182.5 cm^2 culturing flask (T182.5) with 25 ml culturing medium and was put into 37 °C incubator for 2 – 4 days. When cells were highly infected, above-described protocol was repeated (harvesting into 50 ml falcon tubes instead of 1.5 ml tubes) and 300 µl of samples were then distributed into ten T182.5 with previously seeded DF-1 cells and 25 ml of culturing media for each to generate crude stock of the recMVA viruses. After 3 – 4 days, highly infected cells were harvested as previously described with the exception that after the 4000 rpm (ST 16R) centrifugation step, pellets were resuspended with 4 ml ice cold 10 mM Tris pH 9 and all pellets of the same recMVA virus were pooled together. With another 2 ml 10 mM Tris the pellet-containing tubes were washed and transferred into crude stock-containing tube. Samples went through three cycles of freeze-thawing and were sonicated three times for 1 min on ice and kept at -80 °C. Then, crude stock was titrated before generation of purified virus stocks.

3.1.8 Titration of recMVA containing solutions

DF-1 cells were seeded with 100 µl RPMI containing 5 % FBS in 96-well-plates a day prior to reach 70 % confluency on the day of infection. For titration, 10-fold serial dilutions were prepared from 10^{-5} to 10^{-10} by taking 50 µl of the previously prepared virus stock and added to 450 µl fresh culturing medium (RPMI + 2 % FBS) (10^{-1}). Tube was briefly vortexed and 200 µl of suspension was taken form 10^{-1} and added to 800 µl fresh medium (10^{-2}). Vortexing and transfer of dilutions was repeated two more times (10^{-3} and 10^{-4}), then from the 10^{-4} dilution 500 µl was taken and added to 4,5 ml fresh medium (10^{-5}). After briefly vortexing, 1 ml was taken from 10^{-5} and was added to 9 ml fresh medium (10^{-6}). This protocol was repeated until reaching 10^{-10}. When preparation for titration was finished, 100 µl of 10^{-5} virus dilution was added to the first column of the 96-well-plate, 100 µl of 10^{-6} virus dilution was added to the second and third columns and was continued like this with all the prepared dilutions finishing with mixture of 10^{-10}. To the last column normal culturing medium was added as negative control. Plates were put into 37 °C incubator and plaque formation were monitored 7 days after titration, then $TCID_{50}$ was calculated according to the following equation:

$$virus\ paricles\ per\ ml = 10^{a+0,5+\Sigma(\frac{b}{n})}\ x\ 10$$

Where “a” means the last dilution with 100 % CPE, “b” means the number of wells with CPE in further dilutions and “n” means the number of wells per dilution.

3.1.9 Generation of purified recMVA stocks

For purified virus stocks, twenty T182.5 flasks of previously seeded DF-1 cells were infected with MOI 1 of the titrated crude stock for 3 – 4 days. To harvest, cells were scraped into supernatant and transferred into ultracentrifuge buckets. Buckets were balanced by using ice cold 10 mM Tris pH 9 and centrifuged by using pre-chilled ultracentrifuge rotor (A-621) at 16000 rpm for 1.5 h at 4 °C. Supernatant was discarded and pellets were resuspended three times with 10 ml 10 mM Tris. Virus containing material was then pooled and stored at -80 °C. After samples went through three cycles of freeze-thawing and ultrasonic needle was disinfected with the combination of 80 % ethanol and 10 min UV light, the 50 ml virus material containing falcon tube was transferred into beaker filled with ice and sonicated three times for 15 sec at 76 % power. Tube was centrifuged at 4000 rpm (ST 16R) for 5 min at 4 °C and supernatant was transferred into a new 50 ml tube. Pellet was mobilised and resuspended in 15 ml 10 mM Tris and was sonicated again three times for 15 sec. Tube was centrifuged at 4000 rpm

(ST 16R) for 5 min at 4 °C and supernatant was pooled with the material from the previous round, then virus material was kept on ice. Ultracentrifuge buckets for rotors AH 626-36 and -17 were chilled at 4 °C since the day before of purification and irradiated before usage. Six 36 ml polyallomer (PA) vials (previously autoclaved) were filled each with 25 ml of 36 % sucrose solution and virus supernatant was distributed equally over the six sucrose cushions, then balanced with 10 mM Tris. PA vials were placed into buckets for AH 626-36 rotor and centrifuged at 13500 rpm for 1 h at 4 °C. Supernatant was removed by pipetting and remaining residual fluid was decanted by placing PA vials mouth-down on paper towels soaked with 80 % EtOH. Pellets were resuspended with 6 + 6 ml of 10 mM Tris and transferred into a 50 ml falcon tube. Six 17 ml PA vials were filled each with 12 ml of 36 % sucrose solution and virus-containing material was equally distributed over the six sucrose cushions, then balanced with 10 mM Tris. PA vials were placed into buckets for AH 626-17 rotor and centrifuged at 13500 rpm for 1 h at 4 °C. Supernatant was removed as described before and pellets were resuspended with 0.5 + 0.5 ml 1 mM Tris pH 9. Purified virus stock was titrated and kept at -80 °C.

3.2 Molecular biology methods

3.2.1 En passant bacterial artificial chromosome (BAC) mutagenesis

This method was described by Karsten Tischer and colleagues as an efficient combination of several pre-existing methods to modify large DNA molecules in *E. coli;* in short: as a first step, positive selection markers are introduced into the target of modification. During the second step, by the combination of I-*SceI* cleavage and intramolecular Red recombination (also called homologous recombination-based technique) with the introduced sequence duplications from the previous step, the positive selection markers are removed (233–235). This procedure was altered by Lianpan Dai by using competent cells containing MVA-BAC instead of the previously described infectious herpes virus system (231).

3.2.2 Isolation of DNA from bacteria

Plasmid and BAC DNA were both isolated with the same method but during the procedure for the latter, cut-end tips were used. All steps were performed on ice. DNA was isolated from 3 ml bacteria cultured overnight, and the remaining 1 ml was used to prepare glycerol stock (mixed with 1 ml of autoclaved 80 % [v/v] glycerol) which was then kept at -80 °C. Bacteria culture was centrifuged at 8000 rpm (5424R) for 4 min at 4 °C and supernatant was discarded by pipetting out. 250 µl P1 resuspension buffer from Qiagen was used to resuspend pellet, then 350 µl P2 lysis buffer was added. Samples were inverted three times and were incubated on ice for 3 min. Then, 350 µl P3 neutralisation buffer was added to samples and tubes were inverted five times, then incubated on ice for 13 min. Samples were centrifuged at 14500 rpm (5424R) at 4 °C for 5 min and 500 µl supernatant was transferred into new 2 ml tubes. 500 µl chloroform-isoamyl alcohol was added to samples, then vortexed briefly and tubes were centrifuged at 14500 rpm (5424R) for 2 min at 4 °C. Separated 500 µl DNA was transferred into new 2 ml tubes and 500 µl isopropanol was added to samples, then tubes were inverted seven times and incubated 1h at 4 °C. Tubes were then centrifuged at 14500 rpm (5424R) at 4 °C for 20 min to precipitate DNA. Supernatant was discarded and 500 µl 70 % EtOH was added to samples, then centrifuged at 14500 rpm (5424R) for 10 min at 4 °C to remove residual isopropanol. Supernatant was discarded and pellet was dried on top of paper towels. Pellet was resuspended in 50 µl dd H_2O and incubated for at least 1 h at 4 °C to assure complete dissolution. Afterwards, DNA concentration was determined by using NanoDrop 2000 photometer.

3.2.3 Polymerase Chain Reaction (PCR)

PCRs were performed using either Phusion high-fidelity PCR kit or DreamTaq Green PCR master mix according to the manufacturers´ guidelines. DreamTaq was only used for analytical PCRs while Phusion was used for all other cloning purposes.

3.2.4 Restriction digestion of DNA

DNA was digested using New England Biolabs (NEB) restriction enzymes according to the manufacturer´s guidelines. For cloning purposes, 5 µg DNA was used from the selected insert and 10 µg DNA from the plasmid vector. The final volume of mixture was 50 µl when one, and 100 µl when two enzymes were used during restriction digestion.

3.2.5 Agarose gel electrophoresis

PCR products and digested plasmid fragments were loaded on 1 % (w/v) agarose TBE gels and run for 1 h at 130 V. Gels contained EZ-Vision in-gel solution for visualisation, and 1 kb HyperLadder was used as a size marker. DNA fragments were visualised by using UV-transilluminator or Chemostar Touch ECL Imager.

3.2.6 Purification of DNA fragments

DNA fragments of interest were cut out from agarose gels on UV-transilluminator using a clean scalpel. DNA containing gel-piece was measured and DNA was purified by using Nucleospin Gel and PCR clean-up kit according to the manufacturer´s guidelines. The same kit was used for direct purification of PCR products. DNA concentration was measured by using NanoDrop 2000 photometer. DNA was stored at 4 °C for short-term periods or at -20 °C for long-term periods.

3.2.7 DNA ligation

Ligations were performed using Quick Ligation kit, vector and insert (90 µg) were mixed in a molecular ratio of 1:3 or 1:7 in a total volume of 20 µl. Ligation mixture was incubated for 10 min at RT and used directly for transformation.

3.2.8 Transformation

For general cloning purposes, chemically competent XL-1 Blue *E. coli* bacteria was used for transformation. A 50 µl bacteria aliquot was thawed on ice for 15 min, then previously prepared ligation mixture was added to bacteria and mixed carefully. Tube was incubated on ice for 30 min, then mixture was exposed to “heat-shock” for 1 min 15 sec at 42 °C and immediately

cooled down on ice for 2 min. Afterwards, 900 µl pre-warmed empty LB medium was added to bacteria mixture and tube was incubated for 1 h at 37 °C at 800 rpm on ThermoMixer shaker. Tube was centrifuged at 3000 rpm (5424R) for 3 min at RT and pellet was resuspended in 100 µl empty LB medium before plated on pre-warmed LB agar plates supplemented with antibiotic(s) for positive selection and for overnight incubation in a bacteria incubator at 37 °C. Each picked colony (usually 4) was cultured with 4 ml LB medium supplemented with antibiotic(s) for positive selection overnight at 37 °C in a bacteria incubator at 200 rpm for plasmid DNA isolation.

For 1st recombination, electrocompetent GS1783 #22 *E. coli* bacteria were used for transformation. A 50 µl bacteria aliquot was thawed on ice for 15 min and by using cut-end tips, 100 ng purified single stranded DNA of genes of interest including I-*Sce*I-kanamycin cassette from PCR amplification was added to it and mixed carefully. Mixture was then transferred into pre-cooled 1 mm cuvette and pulsed at 1500 V, 200 Ω, 25 µF. Afterwards, with 1 ml of pre-warmed LB medium, bacteria mixture was transferred into 1.5 ml tube and was incubated for 2 h at 32 °C at 800 rpm on ThermoMixer shaker. Tube was centrifuged at 3000 rpm (5424R) for 3 min at RT and pellet was resuspended in 100 µl empty LB medium before 20 and 80 µl of the resuspensions were plated on pre-warmed LB agar plates supplemented with kanamycin and chloramphenicol (CAM) for 2 days in a bacteria incubator at 32 °C. Twelve to sixteen colonies were picked and dissolved in 50 µl PCR grade water, then 2 µl of each colony-mixture was dotted on a pre-warmed LB agar plate supplemented with kanamycin and CAM for overnight in a bacteria incubator at 32 °C to prepare a "back-up" plate. The rest of the resuspended colony-mixture was incubated at 95 °C for 10 min to prepare DNA for colony PCR.

For 2nd recombination, one colony PCR-confirmed positive colony from the 1st recombination was used from the back-up plate and was incubated in 1 ml LB medium supplemented with CAM for 4 h at 32 °C at 200 rpm (MaxQ 4000). Afterwards, 1 ml LB medium supplemented with CAM and 2 % L-arabinose was added to culture and was incubated 1 h at 32 °C at 200 rpm (MaxQ 4000) to induce I-*Sce*I mediated cleavage to remove positive selection marker from genes of interest. For 30 min, culture was incubated at 42 °C at 200 rpm (MaxQ 4000) to induce homologous recombination of the DNA at the site of duplications of nucleotides present in the sequence of interest. Bacteria culture was incubated for 2 h at 32 °C, then optical density at wavelength 600 nm (OD600) was measured by Multiskan GO and 10 µl of a 1:100 (OD600 $\leq$ 0.5) or a 1:1000 (OD600 > 0.5) dilution was plated on pre-warmed LB agar plates

supplemented with CAM and 1 % L-arabinose for 2 days in a bacteria incubator at 32 °C. Colonies were picked and treated as described during 1st recombination section, except this time the back-up plate was propagated on an LB agar plate supplemented with CAM and 1 % L-arabinose. Four colony PCR confirmed positive clones were picked and cultured with 4 ml LB medium supplemented with CAM for 1 – 2 days at 32 °C in a bacteria incubator at 200 rpm for BAC-DNA isolation.

3.2.9 Isolation of viral DNA

For DNA extraction, crude extraction buffer with proteinase K (CEB-PK) was prepared. 100 µl of samples from section 3.1.7 were centrifuged at 1400 rpm (5424R) for 2 min at RT. Supernatant was discarded and pellet was resuspended in 20 µl CEB-PK. Samples were incubated at 56 °C for 3 h, then PK was inactivated at 96 °C for 12 min.

3.2.10 DNA sequencing

All DNA sequencing samples were sent to Eurofins Genomics Germany GmbH, using their TubeSeq service. Plasmid DNA and purified PCR products were also sent here for sequencing.

3.3 Immunological methods

3.3.1 Western blot (WB)

3.3.1.1 Infection, cell lysis and protein extraction

HeLa and all MEF cell lines were seeded in 6-well-plates with 2 ml culturing medium one day prior to reach 80 – 90 % confluency on the day of infection. Right before infection, supernatant was exchanged to 900 µl fresh culturing medium. MVA and/or WR stock was diluted in 100 µl medium and added directly to the cells, then put back to 37 °C incubator until harvesting time. During the first hour of infection, plates were shaken in every 15 minutes. BMDCs were harvested by scraping, counted, and infected on the same day. Two million cells were infected in approximately 200 µl medium in a 15 ml falcon tube and for the first hour of infection, tubes were shaken in every 10 minutes. Cells were then transferred to 6-well-plates and medium was adjusted to 1 ml. Plates were put back into 37 °C incubator until harvesting time.

At the time of harvesting, virus containing supernatant was exchanged to 500 µl ice cold PBS, then cells were scraped from wells and transferred into 1,5 ml tubes. Samples were centrifuged at 5000 rpm (5424R) for 7 min at 4 °C. Supernatant was discarded and pellets were resuspended in 80 µl Tyr-lysis buffer, then stored at -80 °C until usage. After three cycles of freeze-thawing,

samples were subjected to sonication three times for 1 min to open cellular material, then centrifuged at 15000 rpm (5424R) for 10 min at 4 °C to pellet out cellular debris. Supernatant was then transferred into fresh tubes and stored at -80 °C.

3.3.1.2 Sodium dodecyl sulphate-polyacrylamide gel electrophoresis (SDS-PAGE) and immunoblotting

SDS-PAGE was carried out according to the method described Laemmli, where proteins are separated on the basis of their molecular masses (236). Protein samples were mixed with 5X sample loading buffer and incubated at 95 °C for 5 min for denaturation. Samples were then loaded onto polyacrylamide gels (4 % stacking and 12 % separating gel) together with a pre-stained protein ladder as a marker. Separation was performed for small gels (10 pockets) at 130 V for 1 h, for big gels (20 pockets) 230 V for 2.5 h.

After separation, proteins were transferred to a nitrocellulose membrane by semi-dry blotting (16 V for 1 h), then membranes were blocked with either 5 % (w/v) BSA or 2 % (w/v) milk powder dissolved in 1X TBST for 1 h at RT on a shaker to prevent unspecific antibody binding. Membranes were then incubated in primary antibodies diluted in blocking solution and incubated overnight at 4 °C on a shaker. The following day, membranes were washed three times for 5 min with 1X TBST and incubated with horseradish peroxidase (HRP)-coupled secondary antibodies diluted in blocking solution for 1 h at RT on a shaker. Next, membranes were washed three times 5 min with 1X TBST and covered with enhanced chemiluminescence (ECL) substrate. Stained protein markers were detected through chemiluminescence by using ChemoStar Touch ECL Imager from Intas and they were quantified by using ImageJ software.

3.3.2 Confocal microscopy imaging

For confocal microscopy imaging analysis, HeLa DsRed-LC3-eGFP cells were seeded onto microscope cover slips in 12-well-plates to reach 80 % confluency on the day of infection. Cells were infected with MVA-P7.5-NP-SIIN-eGFP with MOI 10 or WR-P7.5-NP-SIIN-eGFP with MOI 5 and plates were carefully shaken every 10 min for the first hour of infection, then cells were fixed at given time points. Next, supernatant containing medium was discarded and cells were washed with PBS carefully, then incubated with 0.05 % saponin solution for 5 min at RT to remove free eGFP from the cytoplasm. Cells were washed two times with PBS and fixed with 2 % PFA for 20 min at RT. After this, PFA was removed, and cells were washed two times with PBS, then incubated with 0.05 % saponin solution for another 5 min at RT. Microscopy slides were prepared by adding one drop of DAPI containing mounting medium

and carefully dried cover slips were placed on top of mounting medium. Cover slips were sealed with nail polish on top of slides and were detected by using LSM 710 confocal microscope at the Center of Advanced Imaging (CAI) facility and visualised by ZEISS ZEN blue edition software.

3.3.3 siRNA silencing screen of 80 conserved WR genes for high-content confocal microscopy

This protocol was adjusted from a previously published one (237) with the help of Melanie Krause (238). The siRNA 96-well-plates were thawed on ice and centrifuged at 1200 rpm (ST 16R) for 5 min at RT. Transfection mix consisting of 0.15 µl Lipofectamin with 15 µl empty DMEM per well was prepared and incubated at RT for at least 5 min, then mixture was added to previously administered 15 µl siRNA into wells of specific PhenoPlate 96-well-plates from PerkinElmer, and was incubated for 1 h at RT. Then, 1 x 10^4 HeLa DsRed-LC3-eGFP cells per well were seeded with 70 µl culture medium on top of the siRNA-Lipofectamin mixture and put into 37 °C incubator for overnight (minimum 20 h). The following day, cells were infected with MVA-P7.5-eGFP MOI 10 and/or WR MOI 5 containing 50 µl culture medium and put back into 37 °C incubator. Plates were shaken in every 10 min for the first hour of infection and after a 6-h-infection period, virus containing supernatant was removed and cells were washed with PBS, then incubated with 0.05 % saponin solution for 5 min at RT to remove free eGFP from the cytoplasm. Afterwards, cells were washed carefully two times with PBS and were fixed with 4 % PFA for 15 min. Next, wells were washed three times for 5 min with PBS, then permeabilised with ice cold methanol at -20 °C for 20 min. Afterwards, cells were blocked with 3 % BSA for 1 hour at RT and washed again three times for 5 min with PBS. Next, nuclei of blocked cells were stained with Hoechst (1:10000) in 40 µl final volume for 1 h at RT on a shaker. Until imaging with Opera LX high-throughput microscope, plates were stored at 4 °C covered with aluminium foil.

3.3.4 Flow cytometry and fluorescence-activated cell sorting (FACS)

The preparation and infection of cells were done as described in section 3.3.3 until the end of the 6-h-infection period. Then, cells were trypsinised (30 µl/well) and transferred with 70 µl/well culture medium into V-bottom 96-well-plates. Plates were centrifuged at 1500 rpm (ST 16R) for 3 min at 4 °C, then supernatant was discarded, and pellets were washed with PBS. Live/dead staining was performed by resuspending the cells in 100 µl viability dye (Viability Dye eFluor 660 – APC)/well and incubated for 20 min on ice in dark. Then, plates were

centrifuged at 1500 rpm (ST 16R) for 3 min at 4 °C and washed once with PBS. For permeabilization, cells were resuspended and incubated with 0.05 % saponin solution for 2 min on ice, then volume was filled up to 200 µl with PBS. Plates were centrifuged at 1500 rpm (ST 16R) for 3 min at 4 °C and washed one more time with PBS. Afterwards, cells were fixed with 100 µl/well 2 % PFA and transferred into 100 µl FACS buffer-containing FACS tubes. Fluorescent signal was measured by using FACS Canto II Diva and measurements were analysed by using FlowJo software.

3.4 Statistics

Statistical values were calculated in GraphPad Prism software using 1-way ANOVA or student t-test with $p < 0.05$ considered as significant: one star * indicates $p \leq 0.05$, two stars ** indicate $p \leq 0.01$ and three stars *** indicate $p \leq 0.001$.

4 Results

4.1 Analysis of interactions between the STING-dependent autophagy and type I IFN production during the early phase of VACV infection

4.1.1 Dependencies of MVA-induced activation and WR-induced inhibition of the autophagy and cGAS-STING pathways

First, different cell lines were examined (MEF, HeLa and BMDCs) after 4 h of infection with MVA and/or WR. For MVA infection, multiplicity of infection (MOI) 10 and a specifically modified strain expressing eGFP under the early and late promoter P7.5 (MVA-P7.5-eGFP) was used. To reach a similar level of infectivity for the virulent strain WR, MOI 5 of WR expressing a fusion protein that consisted of the nucleoprotein (NP) from influenza A virus (type Puerto Rico 68), the SIINFEEKL peptide (OVA257-264) from the protein ovalbumin (OVA), and mCherry under the early and late promoter P7.5 (WR-P7.5-NP-SIIN-mCherry) was distributed on 70 - 80 % confluent cells, independently of cell types. With immunoblotting, different proteins for autophagy activation and for the cGAS-STING pathway for type I IFN production were visualised simultaneously (**Figure 4**). The described conditions were used for all experiments unless stated otherwise. Western blot analysis revealed a strong increase in the protein level of LC3-II during MVA infection in all cell types, a clear manifestation of enhanced autophagic activity. In addition, MVA-infected cells exhibited obvious markers of activation of the cGAS-STING pathway for type I IFN production, as phosphorylated forms (P-) of STING, TBK1, and IRF3 were clearly detected. For HeLa cells, P-STING was not visible, but the total level of STING was decreased due to activation and likely degradation to avoid the drastic induction of type I IFN upon infection. On the other hand, all WR-infected cells exhibited LC3-II protein levels comparable to the non-infected (mock) controls, and no increase in size appeared for phosphorylated proteins of members of the other pathway. When cells were simultaneously co-infected with MVA and WR, the results indicated a similar outcome compared to WR-infected cells. This provides strong evidence that WR actively inhibits the activation of the pathways normally induced by MVA. Regarding the BMDCs, rapamycin was used as a positive control for activating autophagy and inducing LC3 lipidation without activating the cGAS-STING pathway for type I IFN production. Cells infected with WR exhibited a slightly different size for STING compared with the mock controls, although

the reason for this was unclear (**Figure 4A**). All MVA-infected cells exhibited a significant increase in LC3-II protein levels (normalised to β-actin) compared with the mock controls independently of cell type (**Figure 4B**). These results clearly indicated that the induction by MVA and inhibition by WR were present in mouse as well as human cells.

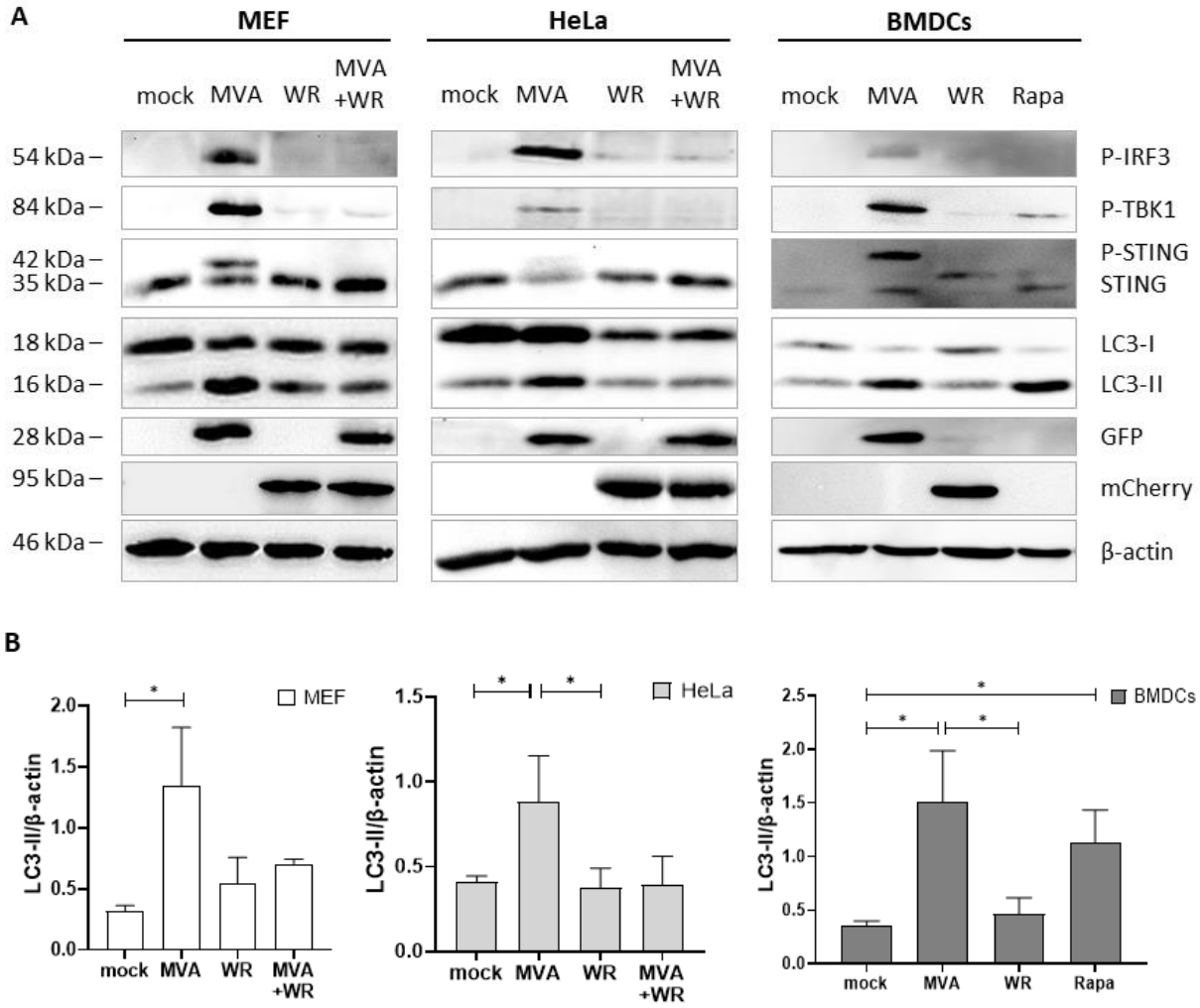

Figure 4. MVA activates autophagy and cGAS-STING pathway for type I IFN production cell type independently. (A) Induction of activation of autophagy and the cGAS-STING pathway for type I IFN production was observed in wild type (WT) MEF, HeLa and BMDC cells under non-infected (mock), MVA- or WR-infected, MVA and WR co-infected, or rapamycin (Rapa)-treated conditions. First, 70 – 80 % confluent cells were infected for 4 h with MOI 10 for MVA expressing eGFP under control of the vaccinia virus early/late promoter P7.5 (MVA), MOI 5 for WR expressing a fusion gene coding for the influenza A nucleoprotein, ovalbumin-derived peptide SIINFEEKL and fluorescent protein mCherry under control of the vaccinia virus early/late promoter P7.5 (WR), or MOI 10 of MVA together with MOI 5 of WR (MVA+WR). After infection, cells were harvested and lysed and protein levels were determined by Western blot analysis. For Rapa treatment, 30 µg/ml of reagent was added to cells for the duration of infection. (B) Quantification of LC3-II protein levels normalised to β-actin in WT MEF, HeLa and BMDC cells (n = 3). Data are depicted as the mean ± SD of three independent experiments. * = $p < 0.05$; ns = not significant; two-tailed Student's t-test.

Next, I investigated how MVA-induced activation of the pathways relates to the amount of virus used during the infection process. MEF cells were infected with MOI 1, 5, 10 and 20 of MVA (**Figure 5**). Western blot analysis revealed that increasing amounts of virus triggered a similar rise in protein levels for LC3-II as well as the activated forms of the cGAS-STING pathway for type I IFN production. This result demonstrates the importance of the viral dose during infection with MVA and also elucidates the sensitivity of these critical cellular pathways. Since infections with MOI 5, 10, and 20 of MVA all triggered a significant increase in LC3 lipidation, I used MOI 10 of MVA for the rest of my experiments.

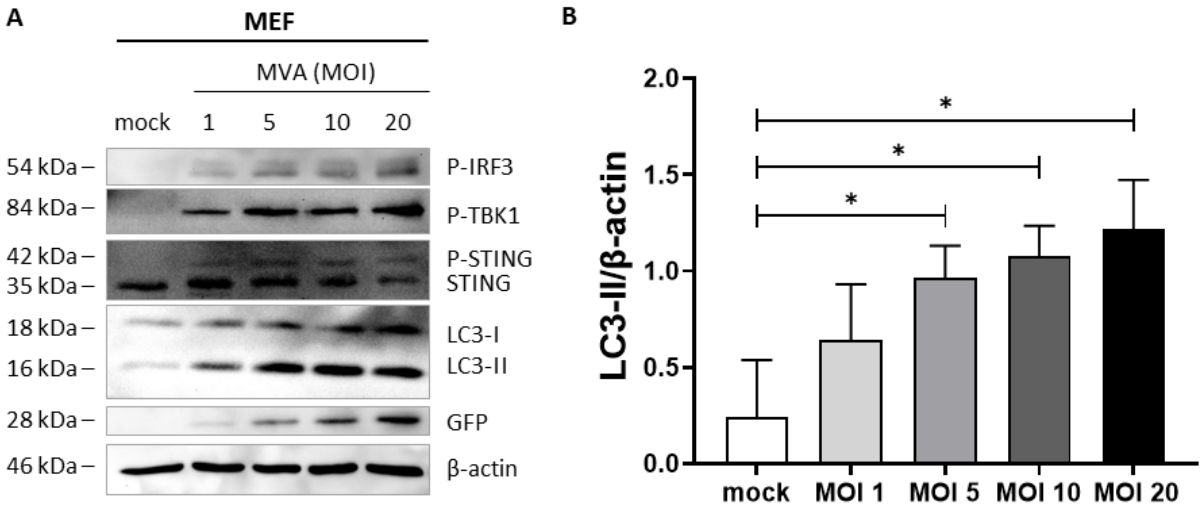

Figure 5. MVA activates the autophagy and cGAS-STING pathway for type I IFN production dose-dependently. (A) Induction of activation of autophagy and the cGAS-STING pathway for type I IFN production was observed in MEF wild type (WT) cells under mock control or MVA-infected conditions using MOI 1, 5, 10 or 20 of MVA expressing eGFP under control of the vaccinia virus early/late promoter P7.5 (MVA) to infect 70 – 80 % confluent cells for 4 h. After infection, cells were harvested and lysed and protein levels were determined by Western blot analysis. (B) Quantification of LC3-II protein levels normalised to β-actin in MEF WT cells (n = 3). Data are depicted as the mean ± SD of three independent experiments. * = $p < 0.05$; ns = not significant; two-tailed Student's t-test.

In regard to WR, Moloughney *et al.* (222) reported that VACV infection leads to an aberrant ATG12-ATG3 conjugation, which results in the accumulation of LC3 but simultaneously prevents LC3 attaching to the autophagosomal membrane, thus causing a decrease in functional autophagosomes. However, they conducted their experiments with 24-h infection periods, when VACV requires approximately 8 h to complete a full replication cycle. Based on these findings, a detailed kinetic study determining the LC3 accumulation during WR infection was performed. For these experiments, HeLa DsRed-LC3-eGFP (H-DLG) cells were used which were created by Houda Khatif, a former member of the laboratory. The importance of these

cells stems from the fact that upon autophagy induction, the C-terminus-located eGFP is cleaved from LC3 to enable the formation of LC3-II. Through this, LC3-II only retains the DsRed signal, while the free eGFP in the cytoplasm can be removed through gentle washing (227). The 70 % confluent H-DLG cells seeded on microscope cover slips were infected with MOI 10 of MVA-P7.5-NP-SIIN-eGFP or MOI 5 of WR-P7.5-NP-SIIN-eGFP for a different number of hours. The cells were then washed with 0.05 % saponin to remove free eGFP and then finally fixed with 2 % PFA. For these experiments, recombinant strains of MVA and WR were used, expressing a fusion gene coding for the influenza A nucleoprotein, ovalbumin-derived SIINFEEKL, and fluorescent protein eGFP under control of the vaccinia virus early/late promoter P7.5. This was done to ensure that, during the saponin wash, only insoluble and membrane attached proteins would remain within the cells. MVA (green nuclear signal) already induced LC3 lipidation (red signal) 1 h post-infection, and the LC3-II signal increased with time (**Figure 6A**). Interestingly, cells that were not infected but were close to infected ones also exhibited high autophagy activity, which is commonly called the bystander effect. In this context, uninfected cells started to display the induction of autophagy when they were in close proximity to infected cells. During the first hours of WR infection (green nuclear signal), there was no sign of LC3 lipidation. The first autophagy marker appeared in cells infected for at least 6 h (**Figure 6B**). From that point on, an increasing number of LC3-II were detected, which is in line with previous studies' findings (222, 238). These results indicated that MVA is able to induce autophagy from the moment that gene expression is detectable within the cells as well as triggers similar behaviour in non-infected bystander cells. In the case of WR, the delay in LC3 lipidation was a clear sign of autophagy inhibition, which then led to the probably aberrant increase of LC3-II within the infected cells, as previously mentioned. Moreover, there was no sign of the bystander effect during the course of infection with WR.

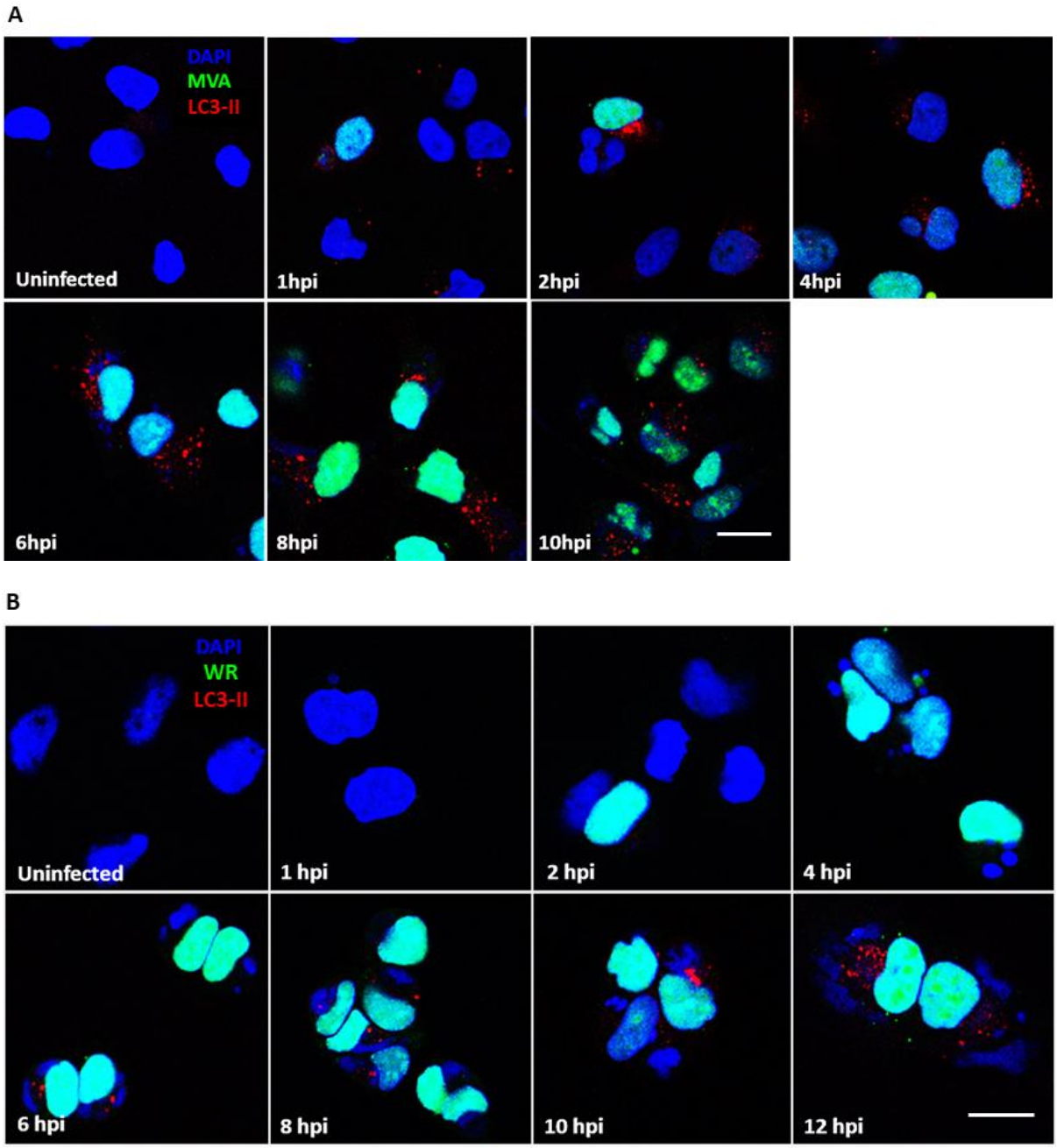

Figure 6. Confirmation of LC3-II lipidation using confocal microscopy imaging at different time points upon infection with MVA or WR. HeLa DsRed-LC3-eGFP (H-DLG) cells were infected for the time indicated. Organelles stained with DAPI (stained nucleus) but not expressing eGFP were assumed to be viral DNA-containing factories. Scale bars represent 10 µm (n = 3). (A) MOI 10 of MVA expressing a fusion gene coding for the influenza A nucleoprotein, ovalbumin-derived peptide SIINFEEKL, and fluorescent protein eGFP under vaccinia virus early/late promoter P7.5 (MVA) was used to infect 70 % confluent cells. At the time of harvest, cells were washed with 0.05 % saponin to remove free eGFP and fixed with 2 % PFA. (B) MOI 5 of WR expressing a fusion gene coding for the influenza A nucleoprotein, ovalbumin-derived peptide SIINFEEKL and fluorescent protein eGFP under vaccinia virus early/late promoter P7.5 (WR) was used as described for (A).

Taken together, these results indicate that MVA activated autophagy and the cGAS-STING pathway for type I IFN production cell type independently soon after infection, and that the induction of these mechanisms also depended on the dose of the virus used. WR actively inhibited these pathways cell type independently, which became clear during co-infection with the inducer MVA. This blockage seemed to be resolved for both pathways at 6 – 8 hpi, which aligns with the findings of the aforementioned studies.

4.1.2 MVA-induced autophagy is independent of type I IFN expression

Since the results demonstrated that the activation of autophagy and the cGAS-STING pathway for type I IFN production seemingly occurs simultaneously upon MVA-induced infection, my next question was whether these mechanisms are dependent upon one another. To clarify this, MEF cell lines were created and important participants of the cGAS-STING pathway were knocked out using the CRISPR-Cas9 technique (**Supplementary figure 1A**). First, autophagy and cGAS-STING pathway activation were investigated in WT, cGAS-KO, and STING-KO MEF cells during infection with MVA or WR (**Figure 7**). As positive controls, cGAMP was used to activate the cGAS-STING pathway for type I IFN production and rapamycin was used to activate canonical autophagy.

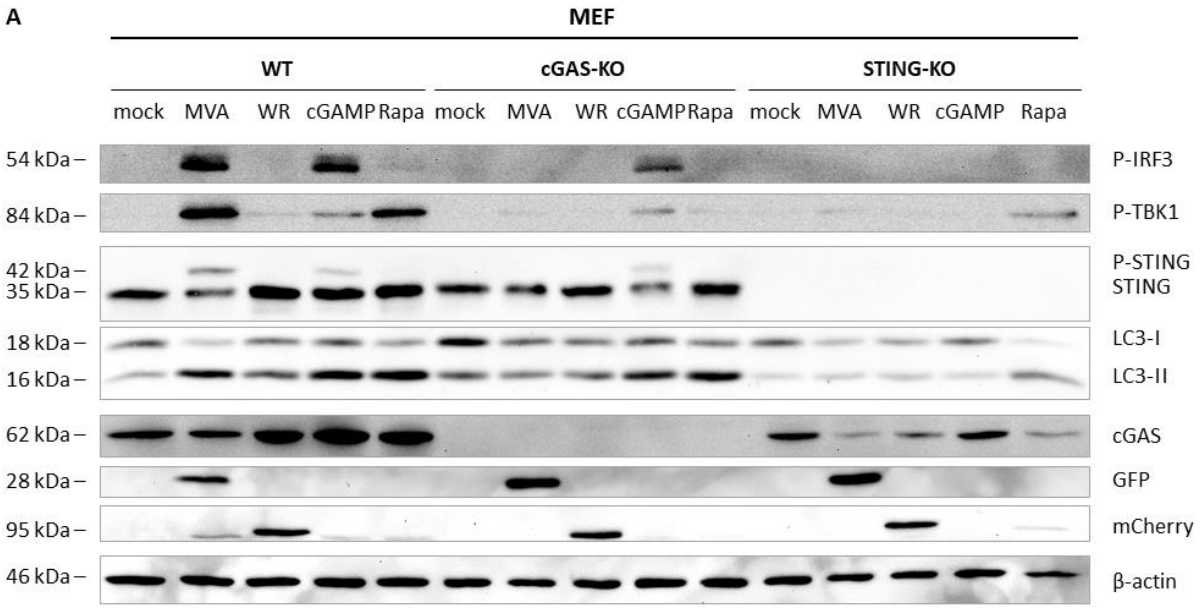

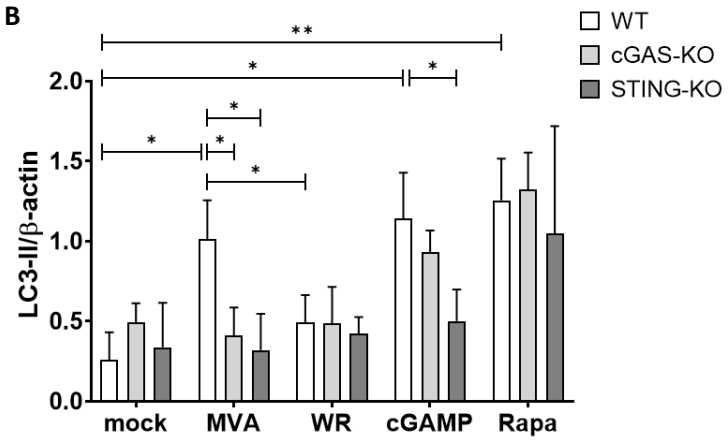

Figure 7. MVA-induced autophagy is cGAS- and STING-dependent, which may be considered a non-canonical autophagy pathway. (A) Induction of activation of autophagy and the cGAS-STING pathway for type I IFN production was observed in wild type (WT), cGAS-KO, and STING-KO MEF cells under non-infected (mock), MVA- or WR-infected, or cGAMP- or rapamycin-treated (Rapa) conditions. First, 70 – 80 % confluent cells were infected for 4 h with MOI 10 for MVA expressing eGFP under control of the vaccinia virus early/late promoter P7.5 (MVA) and MOI 5 of WR expressing a fusion gene coding for the influenza A nucleoprotein, ovalbumin-derived peptide SIINFEEKL and fluorescent protein mCherry under control of the vaccinia virus early/late promoter P7.5 (WR). For cGAMP treatment 20 µg/ml and for Rapa treatment 30 µg/ml of reagent was added to cells for the duration of infection. After infection, cells were harvested and lysed and protein levels were determined by Western blot analysis. (B) Quantification of LC3-II protein levels normalised to β-actin in MEF WT, cGAS-KO and STING-KO cells (n = 3). Data are depicted as the mean ± SD of three independent experiments. * = $p < 0.05$; ** = $p < 0.01$; ns = not significant; two-tailed Student's t-test.

In the WT MEF cells, cGAMP treatment induced the activation of the autophagy and cGAS-STING pathways (**Figure 7A**), which were comparable to the level of MVA-infected cells (**Figure 7B**). Furthermore, rapamycin induced both the phosphorylation of TBK1 as well as LC3 lipidation, as demonstrated by Bodur *et al.* (202). In cGAS-KO MEF cells, MVA infection was unable to induce as strong phosphorylation of TBK1 as it did in WT cells, and and furthermore, no visible P-IRF3 was detected. In addition, LC3 lipidation upon MVA infection was completely missing compared with the WT MVA-infected cells; however, the cGAMP-treated cells exhibited enhanced LC3-II protein levels and phosphorylation of the investigated members of the cGAS-STING pathway compared with the uninfected controls. In addition, rapamycin-treated cGAS-KO cells exhibited similarly non-activated states of proteins compared with the WT rapamycin-treated cells except for the lack of P-TBK1. In STING-KO cells, MVA was similarly unable to activate both pathways, as in cGAS-KO cells. Moreover, cGAMP treatment did not initiate the phosphorylation of TBK and IRF3, while enhanced LC3 lipidation was also missing. On the other hand, rapamycin treatment acted as a positive control

for canonical autophagy activation and again, P-TBK1 was clearly detectable. Crucial to mention here is that the protein level of cGAS in STING-KO cells varied according to different stimuli. MVA and WR infections, and even rapamycin treatment, seemingly reduced the cGAS protein level, while cGAMP treatment had no effect on it and was more comparable to the phenotype of the mock-infected cells. These findings suggested that during MVA infection, the presence of cGAS and STING is essential for achieving type I IFN expression, but these proteins are also necessary for MVA-induced autophagy activation. Noteworthily, in cGAS-KO cells, those with cGAMP treatment displayed a similar phenotype to the WT cGAMP-treated cells; however, in STING-KO cells, this rescue effect was absent during the activation of autophagy and the cGAS-STING pathway for type I IFN production. This finding confirms that the presence of STING is essential for non-canonical autophagy to function properly in MEF cells. Additionally, MVA and WR infections also seemed to achieve similarly reduced cGAS protein levels in STING-KO cells but in different ways and for different purposes. During MVA infection, cGAS is depleted to induce type I IFN expression, while WR more likely interferes with the stability of the same protein to inhibit the activation of the pathway.

Next, the effector proteins downstream of STING activation were investigated. Using the same set-up as that for the cGAS-KO and STING-KO cells, the activation abilities of TBK1- and IRF3-KO MEF cells during MVA or WR infection and cGAMP or rapamycin treatment were compared (**Figure 8**). In TBK1-KO cells, P-STING during MVA infection and cGAMP treatment were completely missing (**Figure 8A**), but LC3 lipidation were comparable to the similarly treated WT cells (**Figure 8B**). In IRF3-KO cells, except for the missing P-IRF3 marker, the phenotypes of P-TBK1, P-STING and LC3-II were comparable to the WT cells. Here, it is important to mention that, on average, the cGAMP-treated IRF3-KO cells displayed a similar protein level for P-STING as the MVA-infected IRF3-KO cells, but this blot was selected due to the overall quality. These results confirmed that LC3 lipidation can occur during MVA infection and cGAMP or rapamycin treatment, even if known effector proteins downstream of STING are not present in the cell.

According to these results, the presence of cGAS and STING is essential for MVA-induced autophagy activation, which exhibits a non-canonical mechanism. Additionally, the presence of TBK1 seems crucial for phosphorylating STING upon stimulation in MEF cells. To summarise, MVA-induced LC3 lipidation is completely independent of the expression of type I IFN in MEF cells.

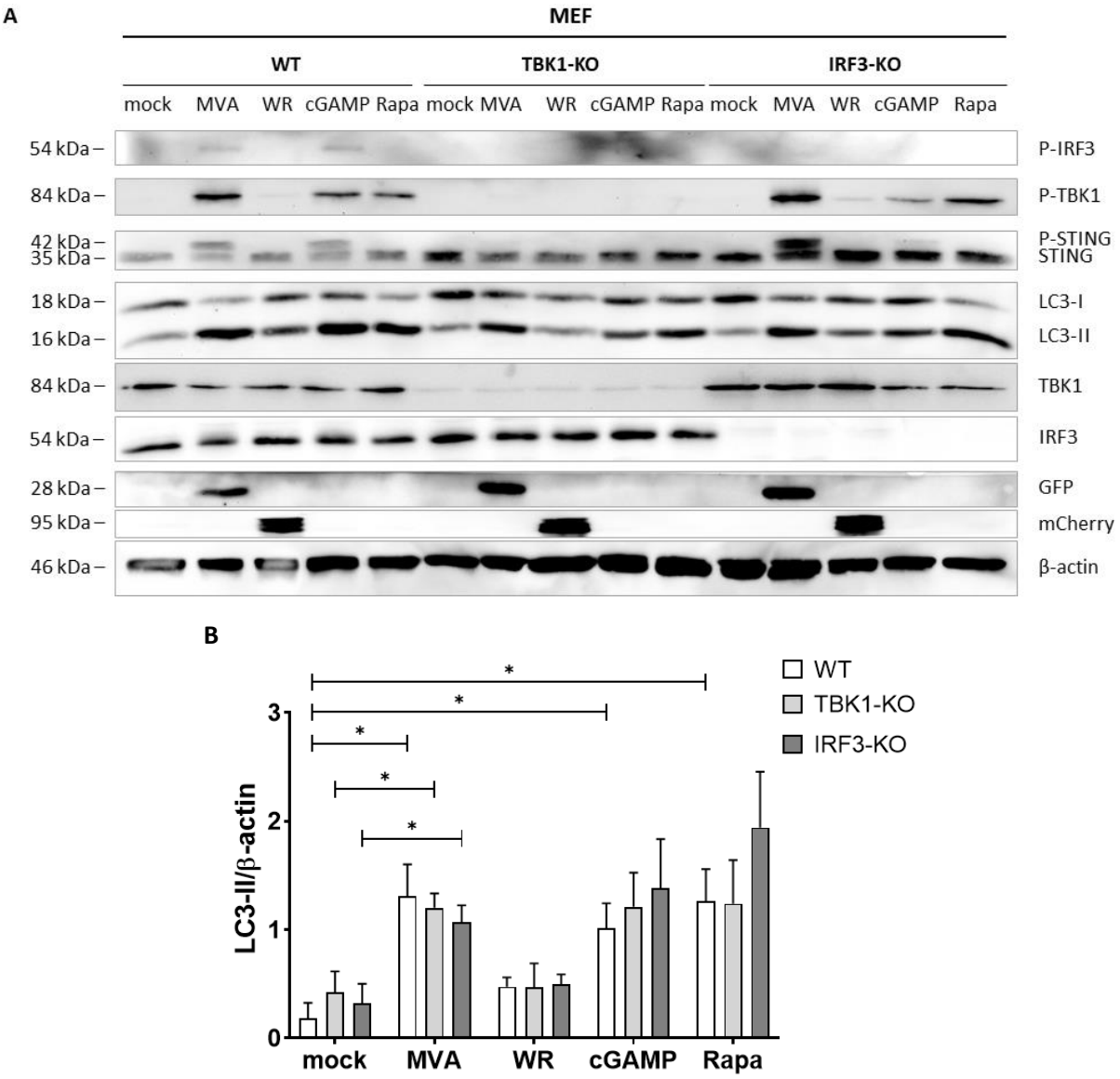

Figure 8. LC3-II lipidation is TBK1- and IRF3-independent, indicating that type I IFN expression is not required for MVA-induced autophagy. (A) Induction of activation of autophagy and cGAS-STING pathway for type I IFN production was observed in wild type (WT), TBK1-KO, and IRF3-KO MEF cells under non-infected (mock), MVA- or WR-infected, or cGAMP- or rapamycin-treated (Rapa) conditions. First, 70 - 80 % confluent cells were infected for 4 h with MOI 10 for MVA expressing eGFP under control of the vaccinia virus early/late promoter P7.5 (MVA) and MOI 5 of WR expressing a fusion gene coding for the influenza A nucleoprotein, ovalbumin-derived peptide SIINFEEKL and fluorescent protein mCherry under control of the vaccinia virus early/late promoter P7.5 (WR). After infection, cells were harvested and lysed and protein levels were determined by Western blot analysis. For cGAMP treatment, 20 µg/ml and for Rapa treatment 30 µg/ml of reagent was added to cells for the duration of infection. (B) Quantification of LC3-II protein levels normalised to β-actin in MEF WT, TBK1-KO, and IRF3-KO cells (n = 3). Data are depicted as the mean ± SD of three independent experiments. * = $p < 0.05$; ns = not significant; two-tailed Student's t-test.

4.1.3 MVA induces non-canonical autophagy

4.1.3.1 Initiation complex

After examining the cGAS-STING pathway for type I IFN production, I also investigated autophagy. To do so, MEF cell lines were used, which were supplied by Dr. Björn Stork's group, or they were created using gene editing by CRISPR/Cas9 as previously mentioned (**Supplementary figure 1B-D**). First, the initiation complex was examined using ATG13-KO MEF cells (from Dr. Björn Stork). Research demonstrated that cells lacking ATG13 display a reduction in LC3 lipidation after starvation (239). Based on the P-STING, P-TBK1 and P-IRF3 protein markers of the ATG13-KO MEF cells infected with MVA or treated with cGAMP, the mechanism that induces type I IFN was not influenced by the lack of ATG13 (**Figure 9A**). It was not clear why the amount of STING protein was lower in these KO cells, but the initiation of type I IFN expression was not affected (**Supplementary figure 2**). Interestingly, ATG13-KO MEF cells exhibited an undisrupted formation of LC3-II upon MVA infection and cGAMP treatment. Moreover, the observed LC3 lipidation was significantly upregulated, as in the similarly treated WT cells (**Figure 9B**). In addition, the WR-infected cells did not exhibit significant upregulation of LC3-II, which was comparable with the WT WR-infected cells. Treatment with cGAMP also induced autophagosome formation, which suggests that MVA and the second messenger cGAMP both induced an autophagy pathway that deviated from the canonical or starvation-induced pathway. However, treatment with rapamycin did not induce LC3 lipidation, suggesting that the canonical autophagosome formation pathway is not functional in ATG13-KO MEF cells was expected.

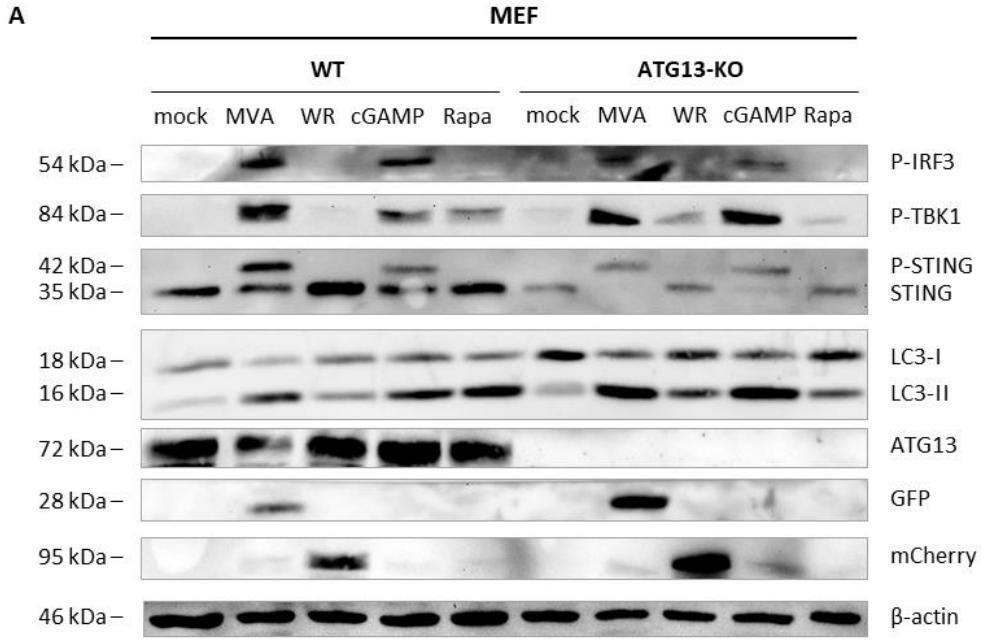

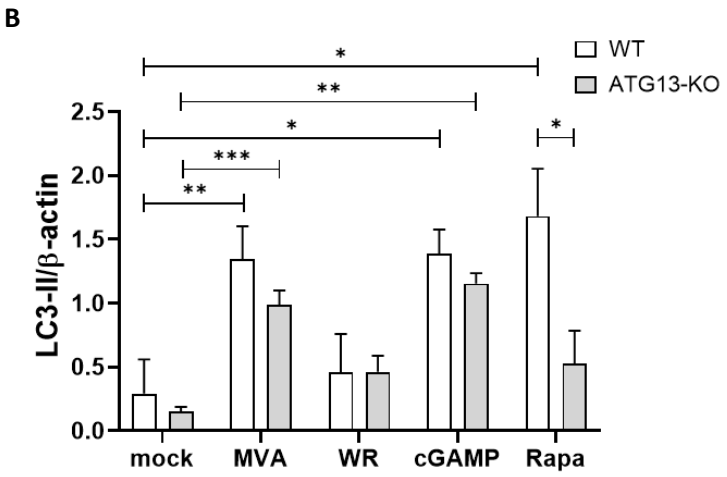

Figure 9. MVA-induced autophagosome formation is independent of ATG13. (A) Induction of activation of autophagy and the cGAS-STING pathway for type I IFN production was observed in wild type (WT) and ATG13-KO MEF cells under non-infected (mock) controls, MVA- or WR-infected, or cGAMP- or rapamycin-treated (Rapa) conditions. First, 70 – 80 % confluent cells were infected for 4 h with MOI 10 for MVA expressing eGFP under control of the vaccinia virus early/late promoter P7.5 (MVA) and MOI 5 of WR expressing a fusion gene coding for the influenza A nucleoprotein, ovalbumin-derived peptide SIINFEEKL and fluorescent protein mCherry under control of the vaccinia virus early/late promoter P7.5 (WR). After infection, cells were harvested and lysed and protein levels were determined by Western blot analysis. For cGAMP treatment, 20 µg/ml and for Rapa treatment 30 µg/ml of reagent was added to cells for the duration of infection. (B) Quantification of LC3-II protein levels normalised to β-actin in MEF WT and ATG13-KO cells (n = 3). Data are depicted as the mean ± SD of three independent experiments. * = $p < 0.05$; ** = $p < 0.01$; *** = $p < 0.001$; ns = not significant; two-tailed Student's t-test.

The effects of MVA infection in ULK1/2-KO MEF cells (contributed by Dr. Björn Stork's group) were also investigated under similar conditions; however further experiments were stopped due to the fact that rapamycin treatment induced LC3 lipidation in these cells (**Supplementary figure 3**). Still, this result demonstrated that the presence of ATG13 during MVA infection is not essential for achieving significant LC3 lipidation, although it has an impact on STING protein levels.

4.1.3.2 Nucleation complex

Next, the nucleation complex was investigated. Beclin1-KO MEF cells were generated using the CRISPR-Cas9 technique (**Supplementary figure 1B**). Gui *et al.* demonstrated that autophagosome formation was significantly upregulated in HEK293T cells lacking Beclin1 after cGAMP treatment but not after Torin1 treatment (148). Unexpectedly, no P-STING protein could be detected in Beclin1-KO MEF cells during MVA infection, which was

accompanied with faint P-TBK1 and missing P-IRF3 signals (**Figure 10A**). In addition, LC3 lipidation was already upregulated in the mock-infected cells, and only moderately upregulated after infecting Beclin1-KO cells with MVA (**Figure 10B**). Furthermore, autophagosome formation was not significantly upregulated upon WR infection compared with the KO mock-infected cells. However, the protein expression levels of LC3-II in Beclin1-KO cells were significantly higher than those in the WT WR-infected cells. cGAMP treatment also induced the phosphorylation of proteins involved in the cGAS-STING pathway for type I IFN production and moderately upregulated autophagosome formation. Rapamycin treatment induced a similar outcome in both pathways in Beclin1-KO cells, as occurred in WT cells. As it was uncertain whether Beclin1-KO MEF cells should be used due to the observed effect of rapamycin treatment on autophagosome formation, Torin1 was used to determine whether LC3 lipidation occurs after treatment with a different autophagy inducer (**Supplementary figure 4**). Torin1 treatment resulted in similar levels of LC3 lipidation as MVA infection which appeared less than rapamycin treatment in WT and Beclin1-KO MEF cells.

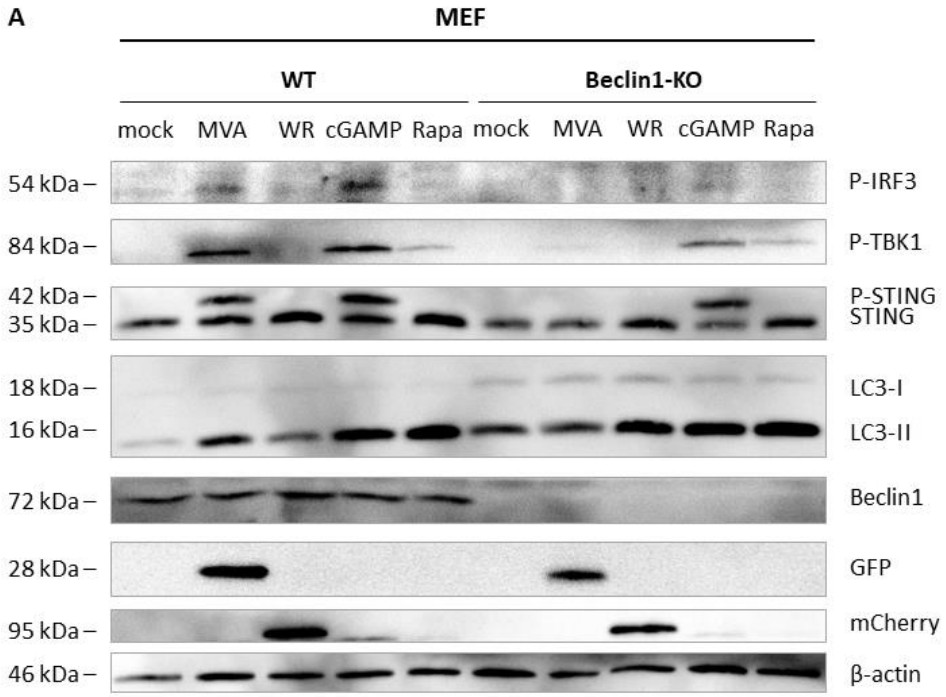

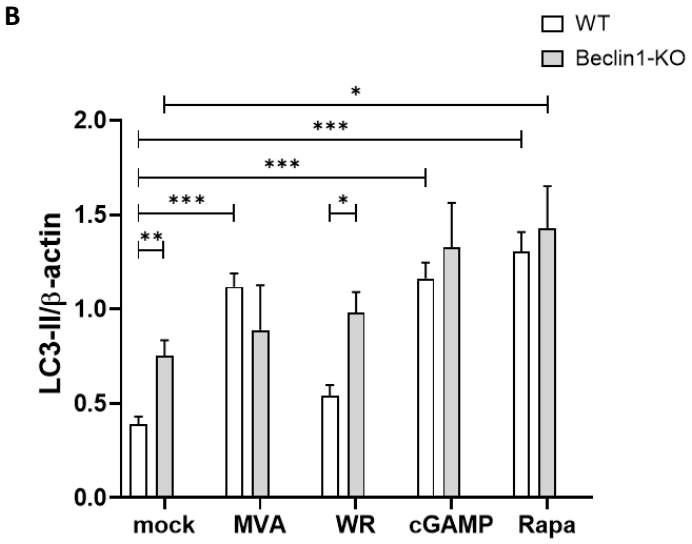

Figure 10. MVA-induced autophagosome formation and activation of the cGAS-STING pathway for type I IFN production seem dependent on the presence of Beclin1. (A) Induction of activation of autophagy and the cGAS-STING pathway for type I IFN production was observed in wild type (WT) and Beclin1-KO MEF cells under non-infected (mock), MVA- or WR-infected, or cGAMP- or rapamycin-treated (Rapa) conditions. First, 70 – 80 % confluent cells were infected for 4 h with MOI 10 for MVA expressing eGFP under control of the vaccinia virus early/late promoter P7.5 (MVA) and MOI 5 of WR expressing a fusion gene coding for the influenza A nucleoprotein, ovalbumin-derived peptide SIINFEEKL and fluorescent protein mCherry under control of the vaccinia virus early/late promoter P7.5 (WR). After infection, cells were harvested and lysed and protein levels were determined by Western blot analysis. For cGAMP treatment, 20 µg/ml and for Rapa treatment 30 µg/ml of reagent was added to cells for the duration of infection. (B) Quantification of LC3-II protein levels normalised to β-actin in MEF WT and Beclin1-KO cells (n = 3). Data are depicted as the mean ± SD of three independent experiments. * = $p < 0.05$; ** = $p < 0.01$; *** = $p < 0.001$; ns = not significant; two-tailed Student's t-test.

Moreover, I sought to investigate the effects of MVA infection on VPS34-KO MEF cells as another member of the nucleation complex under similar conditions, yet the experiments had to be stopped. Although the cells went through single-cell selection and a single clone was selected to be expanded and used for experiments, VPS34-KO clones reverted to the WT phenotype for VPS34 protein expression after a certain number of passages (**Supplementary figure 1B**). Unfortunately, my attempt to create and examine WIPI2-KO MEF cells also resulted in a similar outcome (**Supplementary figure 1C**). However, the aforementioned result confirms that the MVA-induced cGAS-STING pathway for type I IFN production and for autophagy is dependent on the presence of Beclin1; furthermore it demonstrates that MVA activates these pathways differently than cGAMP or rapamycin.

4.1.3.3 Expansion and elongation complex

ATG12-KO MEF cells were generated through CRISPR-Cas9 gene editing (**Supplementary figure 1C**) and used to investigate the relevance of the proteins for autophagosome expansion and elongation. This study also confirmed that the unspecific protein detected at 100 kDa in an immunoblot analysis had no influence on the function of the target protein (**Supplementary figure 5**). Upon MVA infection, there was no sign of P-STING, P-TBK1 or P-IRF3 in KO cells. Moreover, LC3-II appeared more similar to the mock-infected cells of ATG12-KO MEF cells (**Figure 11A**) than the WT cells, being barely visible upon infection. In addition, cGAMP-treated cells exhibited primarily weak markers of autophagy (LC3-II) and only slightly more visible markers for cGAS-STING pathway activation for type I IFN production (P-IRF3, P-TBK1 and P-STING). On the other hand, rapamycin induced significant LC3 lipidation in ATG12-KO cells (**Figure 11B**). At this point, it seemed that rapamycin induces a type of autophagy that is dependent only on the initiation complex – not on other downstream members of the canonical pathway. Additionally, ATG12 was demonstrated to be essential for MVA-induced activation of the cGAS-STING pathway for type I IFN production and for autophagy, which seems to differ from the manner in which cGAMP and rapamycin activate these pathways.

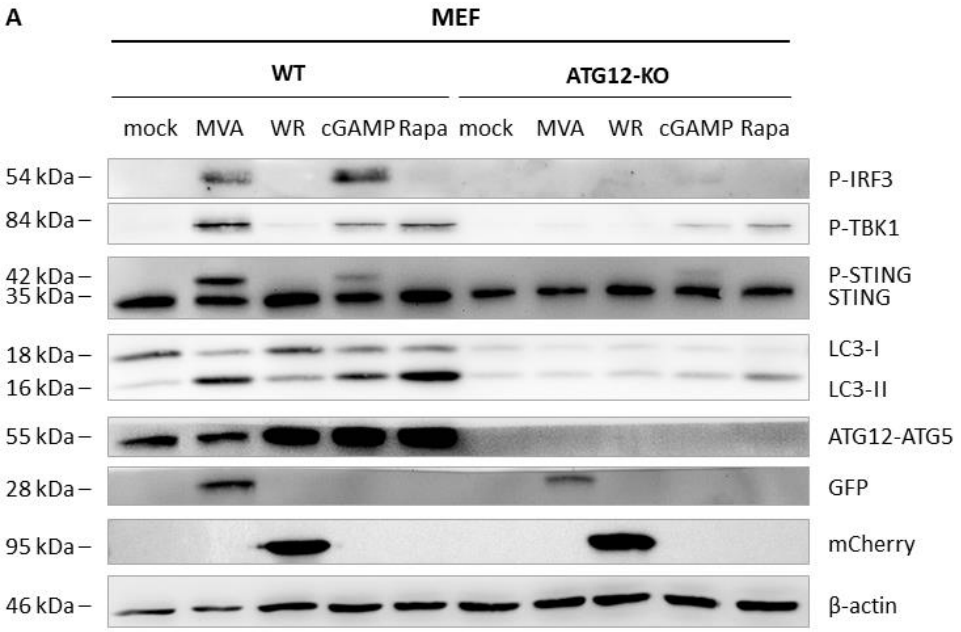

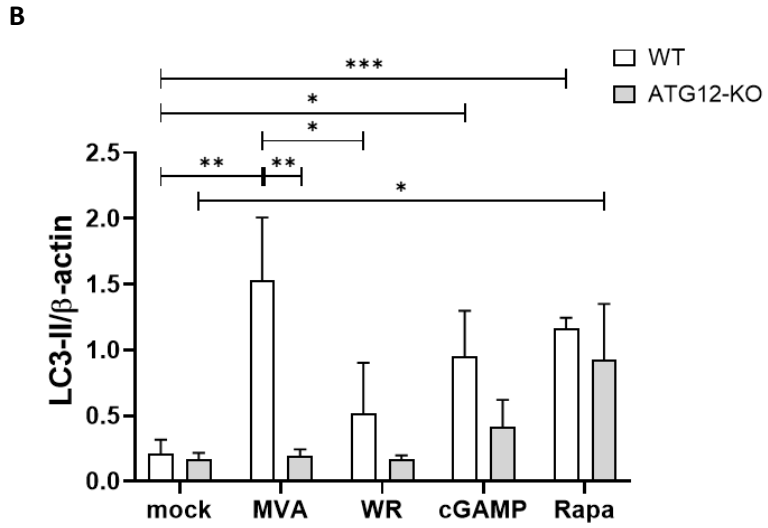

Figure 11. MVA-induced activation of autophagosome formation and the cGAS-STING pathway for type I IFN production is dependent on the presence of ATG12. (A) Induction of activation of autophagy and cGAS-STING pathway for type I IFN production was observed in wild type (WT) and ATG12-KO MEF cells under non-infected (mock), MVA- or WR-infected, or cGAMP- or rapamycin-treated (Rapa) conditions. First, 70 – 80 % confluent cells were infected for 4 h with MOI 10 for MVA expressing eGFP under control of the vaccinia virus early/late promoter P7.5 (MVA) and MOI 5 of WR expressing a fusion gene coding for the influenza A nucleoprotein, ovalbumin-derived peptide SIINFEEKL and fluorescent protein mCherry under control of the vaccinia virus early/late promoter P7.5 (WR). After infection, cells were harvested and lysed and protein levels were determined by Western blot analysis. For cGAMP treatment, 20 µg/ml and for Rapa treatment 30 µg/ml of reagent was added to cells for the duration of infection. (B) Quantification of LC3-II protein levels normalised to β-actin in MEF WT and ATG12-KO cells (n = 3). Data are depicted as the mean ± SD of three independent experiments. * = $p < 0.05$; ** = $p < 0.01$; *** = $p < 0.001$; ns = not significant; two-tailed Student's t-test.

4.1.3.4 Before autophagosome sealing

As the last step of autophagy includes the period before closing the autophagosome and the recruitment and processing of LC3, ATG7-KO (created by CRISPR-Cas9 gene editing; **Supplementary figure 1D**) and ATG3-KO (provided by Dr. Björn Stork) MEF cells were used to investigate the requirement of ATG7 or ATG3 for the activation of autophagy and/or the cGAS-STING pathway for type I IFN production during VACV infection (**Figure 12**). As expected, the lack of ATG7 and ATG3 had no effect on the activation of the cGAS-STING pathway upon MVA infection or cGAMP treatment, since the level of P-STING, P-TBK1, and P-IRF3 in the KO cell lines were comparable to those of the similarly treated WT cells. However, why ATG3-KO cells seemed to have a lower amount of unphosphorylated STING with and without stimuli is unknown. Moreover, LC3 lipidation was completely disrupted and

uninducible upon MVA infection or rapamycin treatment in ATG7-KO and ATG3-KO cells. The faint mCherry signal in all MVA-infected and cGAMP-treated cells represented the leftover primary antibody staining from P-TBK1 after intensive washing, as the membrane was stained by using primary antibody for mCherry after it had already been stained for P-TBK1. There was no stripping step between the detection of P-TBK1 and the addition of primary antibody for mCherry staining – only extensive washing. The lack of ATG3 also seemed to decrease the protein level of ATG7 in ATG3-KO cells, although the reason for this finding has yet to be clarified. This result demonstrates that ATG7 and ATG3 are both essential for autophagosome formation upon MVA infection and cGAMP or rapamycin treatment. However, while ATG7 is dispensable, ATG3 has an impact on the protein level of STING in MEF cells.

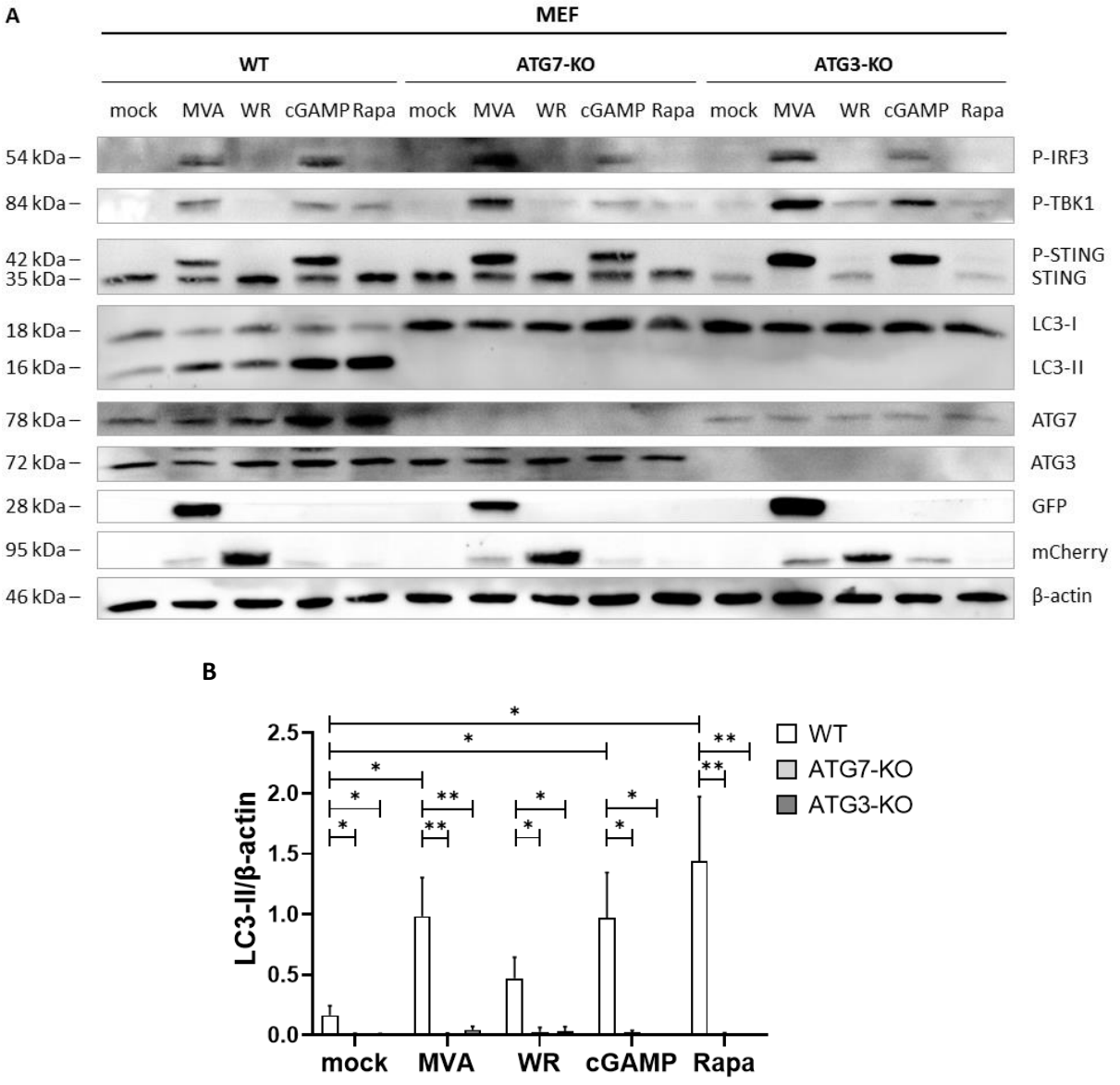

Figure 12. MVA-induced autophagosome formation is dependent on ATG7 and ATG3, but activation of the cGAS-STING pathway for type I IFN production is largely independent of ATG7 and ATG3. (A) Induction of activation of autophagy and cGAS-STING pathway for type I IFN production was observed in wild type (WT), ATG7-KO, and ATG3-KO MEF cells under non-infected (mock), MVA- or WR-infected, or cGAMP- or rapamycin-treated (Rapa) conditions. First, 70 – 80 % confluent cells were infected for 4 h with MOI 10 for MVA expressing eGFP under control of the vaccinia virus early/late promoter P7.5 (MVA) and MOI 5 of WR expressing a fusion gene coding for the influenza A nucleoprotein, ovalbumin-derived peptide SIINFEEKL and fluorescent protein mCherry under control of the vaccinia virus early/late promoter P7.5 (WR). After infection, cells were harvested and lysed and protein levels were determined by Western blot analysis. For cGAMP treatment, 20 µg/ml and for Rapa treatment 30 µg/ml of reagent was added to cells for the duration of infection. (B) Quantification of LC3-II protein levels normalised to β-actin in MEF WT, ATG7-KO and ATG3-KO cells (n = 3). Data are depicted as the mean ± SD of three independent experiments. * = $p < 0.05$; ** = $p < 0.01$; ns = not significant; two-tailed Student's t-test.

4.1.3.5 Selective autophagy receptor

A study demonstrated that p62, a specific autophagy receptor, plays a crucial role in controlling cGAS-STING signalling upon dsDNA stimulation (197). The present study further investigated this process using p62-KO MEF cells (created using CRISPR-Cas9 gene editing), examining whether the presence of this receptor is necessary for the MVA-induced activation of the cGAS-STING pathway for type I IFN production and for autophagy (**Figure 13**). Interestingly, p62-KO MEF cells displayed a more intensely phosphorylated state of proteins involved in signalling in the cGAS-STING pathway (**Figure 13A**) during MVA infection. By contrast, the cells treated with cGAMP or rapamycin were more comparable to the similarly stimulated WT cells. WR-infected cells were also unaffected by the lack of p62. On the other hand, LC3 lipidation was significantly higher in p62-KO cells upon MVA or even WR infection (**Figure 13B**). The differences in the cGAMP- or rapamycin-treated cells were not significant. As a confirmation of this result, I previously observed that the bulk population of p62-KO MEF cells, which were infected overnight (O/N, circa 20 h) with MVA, displayed noticeable protein levels for P-STING, P-TBK1, and P-IRF3 as well as a strong marker for LC3-II compared with WT MVA O/N-infected cells (**Supplementary figure 6**). For the WT MVA O/N-infected cells, the markers for phosphorylated protein levels were mostly absent, and LC3 lipidation was comparable to the normal MVA-infected cells. This result indicated that p62 also plays a crucial role in cGAS-STING pathway activation upon MVA infection in addition to contributing to selective autophagy.

Taken together, these observations suggest that ATG13 from the initiation complex is not necessary for MVA-induced autophagy but has an effect on the protein level of STING, which is not yet understood. Second, the absence of Beclin1 had no effect on cells treated with cGAMP and rapamycin, but the baseline protein level of LC3-II was already so high in the mock-infected cells that MVA lost its ability to induce the activation of the cGAS-STING pathway for type I IFN production and for autophagy. Next, the absence of ATG12 had visible effects during MVA-infection for the initiation of both pathways, while again, the cGAMP- and rapamycin-treated cells were comparable to the similarly treated WT cells. Furthermore, the absence of ATG7 had no effect on the activation of the cGAS-STING pathway, which was mostly also the case for the ATG3-KO cells, although why the STING protein level seemed lower than in the WT cells is unknown. Finally, p62 was found to be critical in regulating the degree to which the autophagy and cGAS-STING pathways are activated in response to VACV infection. Also important to note is that rapamycin-induced autophagy was only dependent on the initiation complex and was not disrupted when other downstream members of the canonical autophagy process were missing. These results indicate how little is known about the connection between the two major innate immune mechanisms during MVA and WR infection since none of these results have previously been reported for these experimental circumstances.

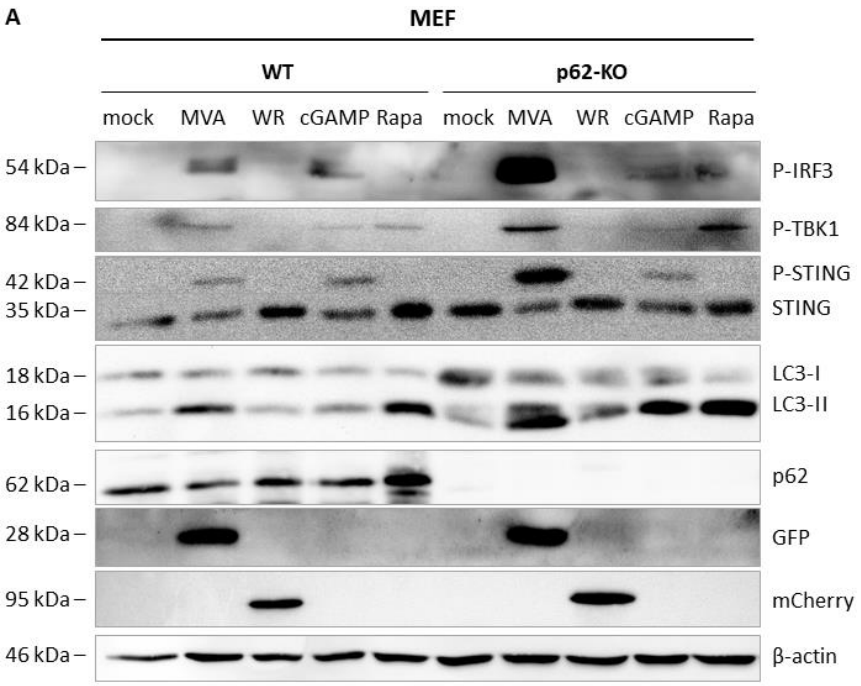

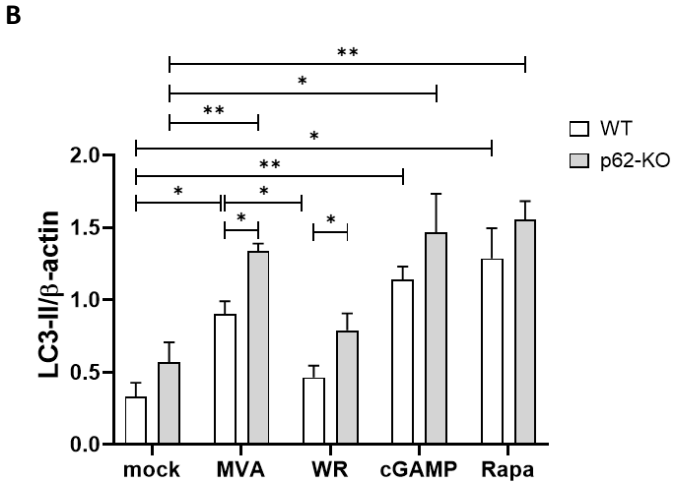

Figure 13. MVA-induced activations of autophagosome formation and cGAS-STING pathway for type I IFN production are upregulated in p62-KO MEF cells. (A) Induction of activation of autophagy and cGAS-STING pathway for type I IFN production was observed in WT and p62-KO MEF cells under non-infected (mock), MVA- or WR-infected, or cGAMP- or rapamycin (Rapa)-treated conditions. First, 70 – 80 % confluent cells were infected for 4 h with MOI 10 for MVA expressing eGFP under control of the vaccinia virus early/late promoter P7.5 (MVA) and MOI 5 of WR expressing a fusion gene coding for the influenza A nucleoprotein, ovalbumin-derived peptide SIINFEEKL and fluorescent protein mCherry under control of the vaccinia virus early/late promoter P7.5 (WR). After infection, cells were harvested and lysed and protein levels were determined by Western blot analysis. For cGAMP treatment, 20 µg/ml and for Rapa treatment 30 µg/ml of reagent was added to cells for the duration of infection. (B) Quantification of LC3-II protein levels normalised to β-actin in MEF WT and p62-KO cells (n = 3). Data are depicted as the mean ± SD of three independent experiments. * = $p < 0.05$; ** = $p < 0.01$; ns = not significant; two-tailed Student's t-test.

4.1.4 Influence of chemical agonists and antagonists of autophagy and/or cGAS-STING pathways during MVA or WR infection

Until this point, all cells had been examined after single MVA or WR infection, without any inducers or inhibitors added to them. During the next stage of my research, I focused on what occurs when the cells are additionally stimulated with specific chemicals during VACV infection.

4.1.4.1 Inducers

First, different reagents were tested for their ability to induce autophagy and/or to activate the cGAS-STING pathway when added to the cells at the time of infection (**Figure 14**). Autophagosome formation was stimulated with rapamycin, which influenced mTOR and the early stages of autophagy. Chloroquine (CQ) was applied to prevent the degradation of cargo inside the already sealed autophagosomes. For the cGAS-STING pathway, cGAMP served as the natural second messenger for activating STING, while dimethylxantone acetic acid

(DMXAA) functioned as a murine-restricted STING-activating ligand. Until this point, the effects of rapamycin and cGAMP treatment on uninfected cells had been revealed using immunoblotting. In the mock-infected but CQ-treated cells, the cGAS-STING pathway was completely unaffected, as determined based on the absence of phosphorylated protein markers (**Figure 14A**). As expected, the degradation of LC3-II was inhibited, which led to a significant upregulation of the protein level of LC3-II in infected cells compared with mock-infected or untreated cells (**Figure 14B**). The mock-infected and DMXAA-treated cells mimicked the effects of cGAMP in both pathways. Mock-infected cells with or without reagent treatment served as controls for MVA- and WR-infected cells.

In MVA-infected cells, none of the treatments seemed to negate the effect of MVA infection on the activation of the cGAS-STING pathway for type I IFN production and for autophagy. However, according to the visibility of P-TBK1 and P-IRF3 of MVA-infected and rapamycin- or CQ-treated cells, there appeared to be some interference with the induction of the cGAS-STING pathway. In addition, the protein level of GFP, which served to monitor MVA infection, was lower in rapamycin- and CQ-treated cells than in cells infected only with MVA or infected with MVA in combination with cGAMP or DMXAA treatment. While the reason for this result is unclear, perhaps the used chemical agonists were able to activate the cGAS-STING and autophagy pathways earlier than the course of MVA-induced infection, leading to a reduced level of GFP marker. Furthermore, cGAMP or DMXAA treatment during MVA infection exhibited no change in the LC3-II protein levels, which could indicate that infection with MOI 10 MVA triggers the maximum degree of activation for both pathways.

In WR-infected cells, treatment with rapamycin or CQ both significantly induced the activation of autophagy in MEF WT cells even though they were infected with a virus that has been demonstrated to inhibit autophagy. Moreover, the protein level of mCherry, which was used as a marker to monitor WR infection, was reduced in WR-infected and rapamycin-treated cells compared with cells only infected with WR. The cause of the reduction of the viral marker is yet to be clarified, but it may follow a similar process observed during MVA infection. Interestingly, for WR-infected and cGAMP-treated cells, the cGAS-STING pathway for type I IFN production was hindered, as demonstrated by the P-STING, P-TBK1 and P-IRF3; moreover, LC3 lipidation was also more comparable to the cells only infected with WR. By contrast, DMXAA treatment during WR infection seemed to overcome the inhibitory effect of the virus for both mechanisms. This result indicated that rapamycin, CQ and DMXAA all

function in a manner that is unaffected by the inhibitory ability of WR, but that cGAMP is actively rendered ineffective or even destroyed by the same virus.

Overall, the aforementioned results indicated that MOI 10 of MVA significantly induces the autophagy and cGAS-STING pathways and cannot be improved by adding further activator reagents during infection. In case of the virulent strain, the canonical early- and late-stage autophagy agonists could overcome the inhibitory effect of WR for LC3 lipidation, which means that the canonical activation of autophagy can surpass the inhibition of the hypothetical non-canonical pathway. On the other hand, WR can actively interfere with cGAMP to prevent the activation of the investigated immune responses, while the binding of DMXAA to STING is unhindered.

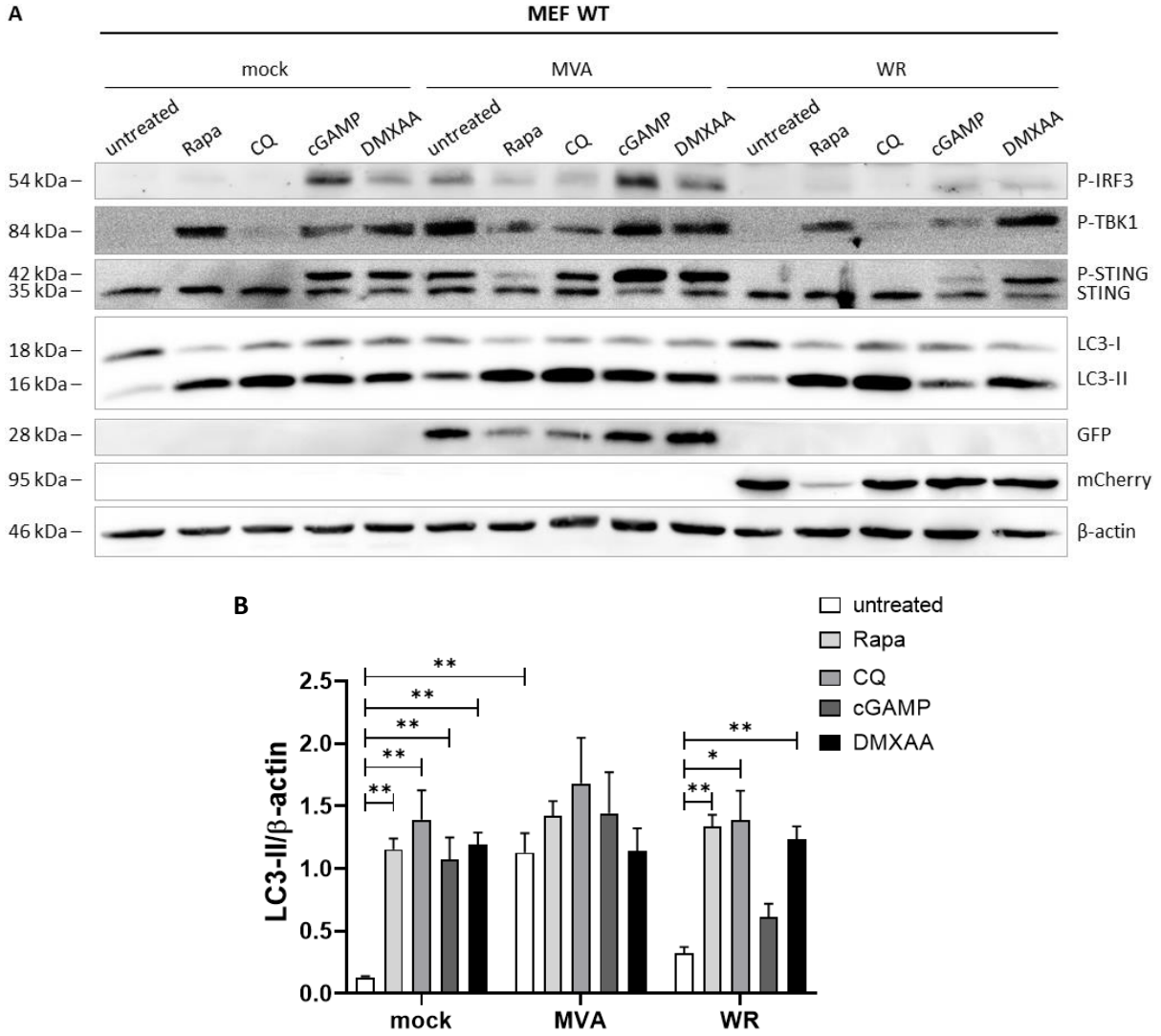

Figure 14. WR can actively interfere with the second messenger of STING. (A) Induction of activation of autophagy and cGAS-STING pathway for type I IFN production was observed in WT MEF cells under non-infected (mock), MVA- or WR-infected conditions without any treatment, with rapamycin (Rapa), chloroquine

(CQ), cGAMP or DMXAA treatment at the same time. First, 70 – 80 % confluent cells were infected for 4 h with MOI 10 for MVA expressing eGFP under control of the vaccinia virus early/late promoter P7.5 (MVA) and MOI 5 of WR expressing a fusion gene coding for the influenza A nucleoprotein, ovalbumin-derived peptide SIINFEEKL and fluorescent protein mCherry under control of the vaccinia virus early/late promoter P7.5 (WR). After infection, cells were harvested and lysed and protein levels were determined by Western blot analysis. For Rapa treatment, 30 µg/ml, for CQ treatment 40 µM, for cGAMP treatment 20 µg/ml and for DMXAA treatment 5 µg/ml of reagent was added to cells for the duration of infection. (B) Quantification of LC3-II protein levels normalised to β-actin in MEF WT cells (n = 3). Data are depicted as the mean ± SD of three independent experiments. * = $p < 0.05$; ** = $p < 0.01$; ns = not significant; two-tailed Student's t-test.

4.1.4.2 Inhibitors and antagonists

In the next stage, specific inhibitors were applied to interfere with the autophagy and cGAS-STING pathways for the same amount of time as the VACV infection (**Figure 15**). For autophagy inhibition, 3-methyladenin (3MA) was used as a specific inhibitor of the class III PI-3K complex and for canonical autophagy. Furthermore, epoxomicin (Epox) was used to inhibit proteasomal degradation and rule out the possibility that any aspect of the observed MVA-induced activation of WR-induced inhibition relies on this function. Moreover, the ability of Epox to impair DNA replication and gene expression, which leads to no intermediate and late gene expression but prolonged early gene expression, was also exploited. To interfere with the cGAS-STING pathway for type I IFN production, golgicide A (GCA) was applied to cells as a reversible inhibitor of soluble and membrane-associated protein secretion at the ERGIC, which led to the disassembly of the trans-Golgi and Golgi network as well as disrupted the cGAS-STING pathway for type I IFN production. In cells only treated with the inhibitors without additional VACV infection, none of the treatments seemed to trigger any kind of unexpected effect on MEF WT cells compared with mock-infected and untreated cells (**Figure 15A**). This finding indicated that these cells are suitable controls for cells infected with MVA or WR and additionally treated with reagents.

In addition, during MVA infection, 3MA and Epox were unable to prevent MVA-induced activation of autophagy and STING-, TBK1-, and IRF3 phosphorylation. Even though the protein levels of the phosphorylated members of the cGAS-STING pathway for type I IFN production and LC3-II were slightly lower upon MVA infection with 3MA treatment, they were not significantly lower than the MVA-infected cells without 3MA treatment (**Figure 15B**). On the other hand, treating MVA-infected cells with GCA completely prevented the activation of both major pathways. This finding could indicate that without traffic between the

ER and the Golgi, MVA cannot induce the cGAS-STING pathway for type I IFN production and for autophagy simultaneously.

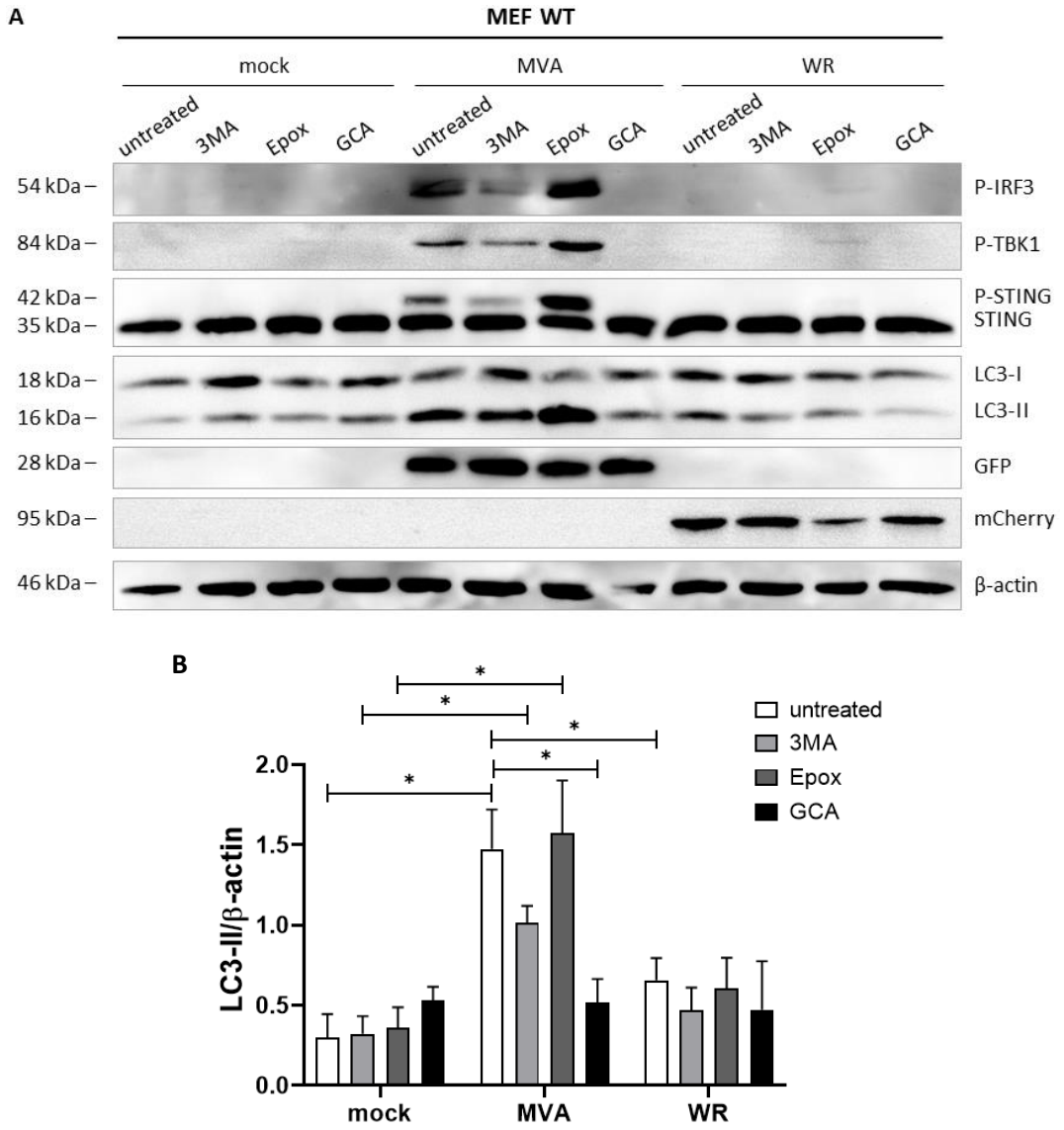

Figure 15. MVA-induced activation of the cGAS-STING pathway for type I IFN production and for autophagy is dependent on traffic between the ER and the ERGIC. (A) Induction of activation of autophagy and cGAS-STING pathway for type I IFN production was observed in wild type (WT) MEF cells under non-infected (mock), MVA- or WR-infected conditions without any treatment, or with 3-methyladeni (3MA), epoxomicin (Epox) or golgicide A (GCA) treatment at the same time. First, 70 – 80 % confluent cells were infected for 4 h with MOI 10 for MVA expressing eGFP under control of the vaccinia virus early/late promoter P7.5 (MVA) and MOI 5 of WR expressing a fusion gene coding for the influenza A nucleoprotein, ovalbumin-derived peptide SIINFEEKL and fluorescent protein mCherry under control of the vaccinia virus early/late promoter P7.5 (WR). After infection, cells were harvested and lysed and protein levels were determined by Western blot analysis. For GCA treatment 10 µM of reagent was added to cells for the duration of infection. For

3MA treatment 5 mM and for Epox treatment 10 µM of reagents was added to the cells 1 h prior to infection and then left on until harvesting time together with the designated VACV strain. (B) Quantification of LC3-II protein levels normalised to β-actin in MEF WT cells (n = 3). Data are depicted as the mean ± SD of three independent experiments. * = $p < 0.05$; ns = not significant; two-tailed Student's t-test.

In WR-infected cells, no treatment could overwrite the inhibitory effect of WR upon infection. This result reveals that WR achieved inhibition of the cGAS-STING pathway for type I IFN production and for autophagy independently of these specifically targeted processes.

Since none of the inhibitors could interfere with the inhibition induced by WR infection, a reagent for blocking DNA replication and late gene expression, cytosine arabinoside (AraC), was used next (**Figure 16**).

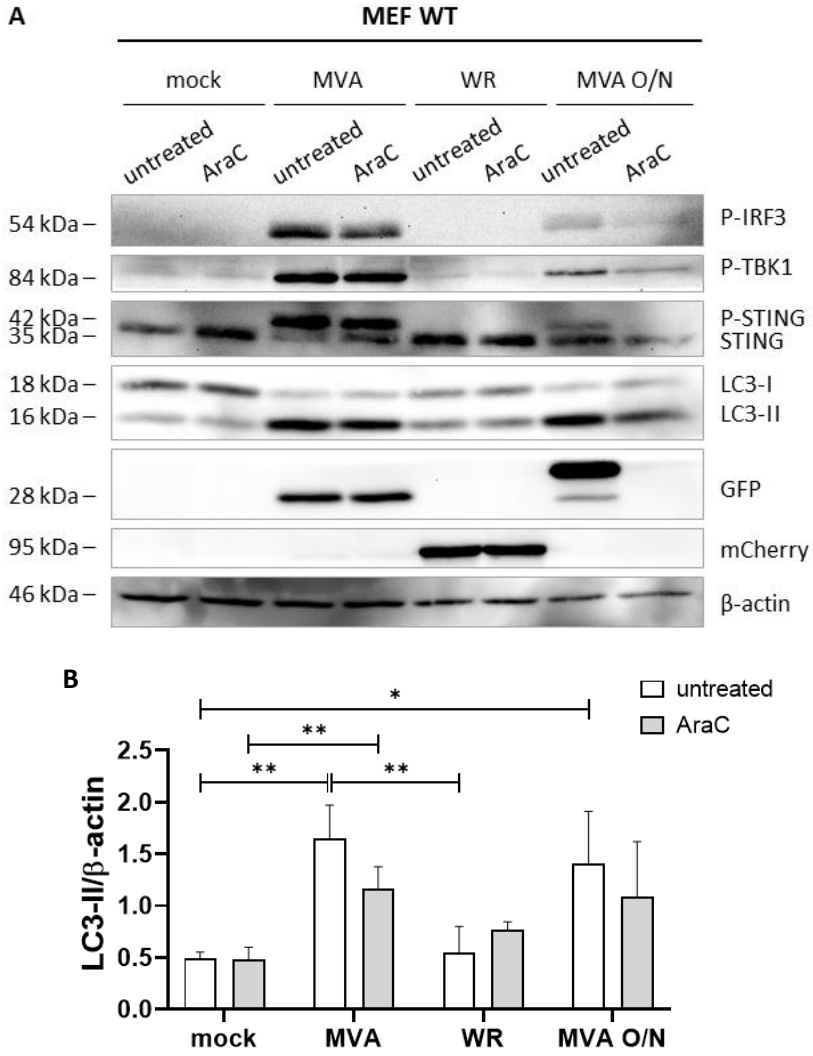

Figure 16. Viral DNA replication and late gene expression are dispensable for MVA-induced and WR-inhibited activation of the cGAS-STING pathway for type I IFN production and for autophagy. (A) Induction of activation of autophagy and cGAS-STING pathway for type I IFN production was observed in wild type (WT) MEF cells under non-infected (mock), MVA- or WR-infected conditions with or without AraC

treatment at the same time. First, 70 – 80 % confluent cells were infected for 4 h with MOI 10 for MVA expressing eGFP under control of the vaccinia virus early/late promoter P7.5 (MVA) and MOI 5 of WR expressing a fusion gene coding for the influenza A nucleoprotein, ovalbumin-derived peptide SIINFEEKL and fluorescent protein mChery under control of the vaccinia virus early/later promoter P7.5 (WR) or overnight with MOI 10 for MVA expressing eGFP under control of the vaccinia virus late promoter P11 (MVA O/N). After infection, cells were harvested and lysed and protein levels were determined by Western blot analysis. For AraC treatment, 40 µg/ml of reagent was added to cells for the duration of infection. (B) Quantification of LC3-II protein levels normalised to β-actin in MEF WT cells (n = 3). Data are depicted as the mean ± SD of three independent experiments. * = $p < 0.05$; ** = $p < 0.01$; ns = not significant; two-tailed Student's t-test.

Mock-infected and AraC-treated cells exhibited no differences compared with mock-infected but untreated cells, indicating that AraC alone is not enough to trigger either of the two pathways (**Figure 16A**). Moreover, the treatment had no significant effect in MVA-infected cells with regard to the protein levels of the phosphorylated forms of the cGAS-STING pathway for type I IFN production or LC3-II (**Figure 16B**). In addition, WR-infected cells did not exhibit any difference upon AraC treatment. AraC only seemed to affect cells infected with MVA overnight. These cells were included to demonstrate the effect of AraC treatment since they cells were infected with MVA-P11-eGFP, in which GFP is expressed under the vaccinia virus late P11 promoter and thus only becomes visible at approximately 6 hpi. Since AraC blocks DNA replication and late gene expression, AraC-treated and MVA-P11-eGFP infected cells were unable to express GFP. The protein levels of the examined members of the two pathways were lower for the untreated and mock-infected cells compared with cells infected with MVA overnight or with AraC-treated and overnight infected cells. This result demonstrates that neither MVA nor WR requires viral DNA replication or late gene expression to execute MVA-induced activation or WR-induced inhibition of the cGAS-STING pathway for type I IFN production and for autophagy.

To further investigate the mechanisms behind MVA-induced and WR-inhibited activation of the cGAS-STING pathway for type I IFN production and for autophagy, a combination of psoralen and ultraviolet A radiation (PUVA) was used to simultaneously inhibit early gene expression and DNA replication through the formation of interstrand cross-links upon PUVA treatment (**Figure 17**). Mock-infected but PUVA-treated cells exhibited no differences compared with untreated and mock-infected cells, which demonstrated that PUVA treatment alone did not trigger any kind of immune response in MEF WT cells (**Figure 17A**). In MVA-infected cells, a negligible difference existed between treated and untreated cells for both pathways. However, in WR-infected and MVA-WR-co-infected cells, PUVA treatment

seemed to negate the inhibitory effect of WR. All phosphorylated forms of the members of the cGAS-STING pathway for type I IFN production appeared on the membrane, as did significantly upregulated LC3-II (**Figure 17B**). Furthermore, PUVA treatment significantly increased the LC3-II protein level in PUVA-treated and WR-infected or PUVA-treated and MVA-WR-co-infected cells compared with mock-infected and PUVA-treated cells, as well as compared with untreated WR-infected or untreated MVA-WR-coinfected cells. This result indicates that, while MVA-induced activation of STING-mediated autophagy and IFN I production was not dependent on early viral gene expression, this type of gene expression was essential for the WR-induced inhibition of both pathways.

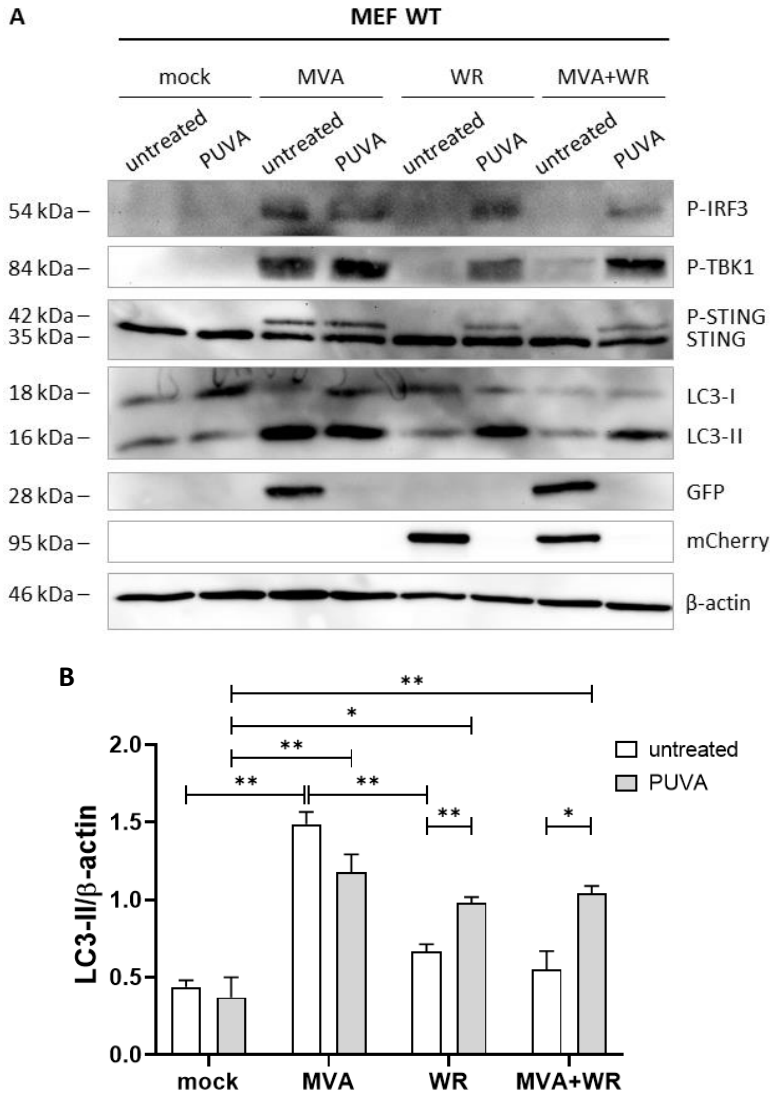

Figure 17. WR-induced inhibition of activation of the cGAS-STING pathway for type I IFN production and for autophagy is significantly dependent on viral early gene expression. (A) Induction of activation of autophagy and cGAS-STING pathway for type I IFN production was observed in wild type (WT) MEF cells under non-infected (mock), MVA- or WR-infected or MVA and WR co-infected conditions with or without the combination of psoralen and ultraviolet A radiation (PUVA) treatment at the same time. First, 70 – 80 %

confluent cells were infected for 4 hours with MOI 10 for MVA expressing eGFP under control of the vaccinia virus early/late promoter P7.5 (MVA) and MOI 5 of WR expressing a fusion gene coding for the influenza A nucleoprotein, ovalbumin-derived peptide SIINFEEKL and fluorescent protein mCherry under control of the vaccinia virus early/late promoter P7.5 (WR), or MOI 10 of MVA together with MOI 5 of WR (MVA+WR). For PUVA treatment, 1 µg/ml of psoralen was added to virus-containing medium and incubated for 15 min on ice. Afterwards, the psoralen-treated virus-containing medium was placed under direct UV light for 15 min and added to the cells for the duration of infection. After infection, cells were harvested and lysed and protein levels were determined by Western blot analysis. (B) Quantification of LC3-II protein levels normalised to β-actin in MEF WT cells (n = 3). Data are depicted as the mean ± SD of three independent experiments. * = $p < 0.05$; ** = $p < 0.01$; ns = not significant; two-tailed Student's t-test.

As an additional approach and to corroborate the outcome of the PUVA experiment, VACV was heat-inactivated at various temperatures prior to infection. By incubating VACV strains at 56 °C for 1 h prior to infection, the secondary structures of viral proteins are denaturated (240), which leads to the impaired initiation of cell entry from the virus side as well as limited or no viral early gene expression. VACV strains were incubated at 42 °C for 1 h prior to infection to investigate whether this temperature had already had an impact on viral entry and early gene expression (**Figure 18**).

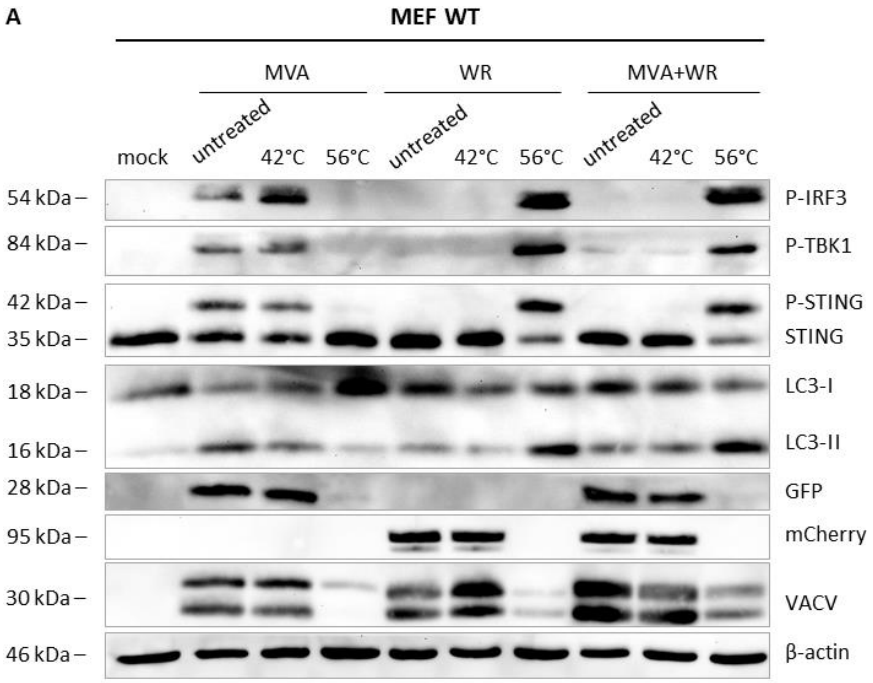

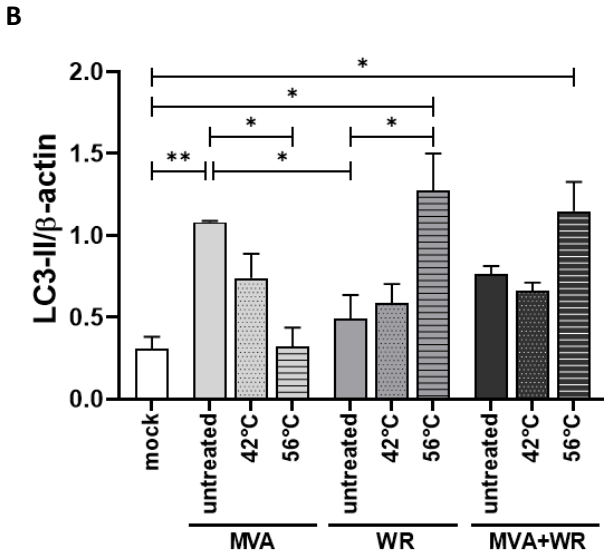

Figure 18. While MVA loses, WR gains ability to induce activation of autophagy and cGAS-STING pathway for type I IFN production after inactivating the viruses at 56 °C. (A) Induction of activation of autophagy and cGAS-STING pathway for type I IFN production was observed in wild type (WT) MEF cells under non-infected (mock), MVA- or WR-infected or MVA and WR co-infected conditions. MVA and WR were inactivated for 1 h at 42 °C or 56 °C before being added to cells or left on ice for the duration of the inactivation period. Then, 70 – 80 % confluent cells were infected for 4 h with MOI 10 for MVA expressing eGFP under control of the vaccinia virus early/late promoter P7.5 (MVA) and MOI 5 of WR expressing a fusion gene coding for the influenza A nucleoprotein, ovalbumin-derived peptide SIINFEEKL and fluorescent protein mCherry under control of the vaccinia virus early/late promoter P7.5 (WR), or MOI 10 of MVA together with MOI 5 of WR (MVA+WR). After infection, cells were harvested and lysed and protein levels were determined by Western blot analysis. (B) Quantification of LC3-II protein levels normalised to β-actin in MEF WT cells (n = 3). Data are depicted as the mean ± SD of three independent experiments. * = $p < 0.05$; ** = $p < 0.01$; ns = not significant; two-tailed Student´s t-test.

When MVA was incubated at 42 °C for 1 h before infection, the results indicated no disturbance in the activation of the cGAS-STING pathway for type I IFN production (**Figure 18A**), but there was a slight decrease in the protein level of LC3-II (**Figure 18B**). However, cells infected with MVA inactivated at 56 °C for 1 h before infection exhibited protein levels more similar to mock-infected cells without any sign of the phosphorylated forms of STING, TBK1, or IRF3 proteins. There was also a significant decrease in LC3 lipidation for these cells. In WR-infected cells, incubation at 42 °C for 1 h did not appear to have an effect compared with the untreated WR-infected cells. However, when WR was inactivated at 56 °C for 1 h, the observed outcome for proteins was more comparable to the untreated MVA-infected cells regarding the activation of the cGAS-STING pathway for type I IFN production and for autophagy. The LC3 lipidation level was also significantly higher compared with mock-infected or untreated WR-infected

cells. The MVA-WR-co-infected cells exhibited a similar result as there was no visible change occurred in markers for autophagy or cGAS-STING pathway for type I IFN production after viruses were incubated at 42 °C, but changes in marker proteins of both pathways were noticeable after inactivation at 56 °C. Although MVA seemingly lost its ability to induce activation of autophagy and cGAS-STING pathway for type I IFN production, the fact that WR could no longer inhibit the induction of said pathways was obvious when WR was incubated at 56 °C prior to infection. A weak marker for VACV proteins also appeared in the infected cells inactivated at 56 °C. This result seemed to verify that MVA induces at least one essential mechanism after viral entry but before early gene expression, and similarly, WR interferes with at least one activator of the cGAS-STING pathway for type I IFN production and for autophagy immediately after its entry into cells. In addition, considering the weak marker for VACV inactivated at 56 °C, it is possible that viral entry was successful, but due to the high temperature, the viral capsid was partly de-naturated, thus preventing uncoating.

To further investigate whether uncoating is interrupted, I treated MVA and WR with 2 % paraformaldehyde (PFA) to fix and inactivate the viruses but leave them structurally intact, unable to actively initiate viral cell entry, or perform any other essential mechanisms for viral replication. Unfortunately, the mock control treated with 2 % PFA induced LC3 lipidation, which appeared more comparable to MVA infection than the untreated mock control (**Supplementary figure 7**). Consequently, I could not use PFA treatment in my experiments.

Overall, MVA infection at MOI 10 seemed to be able to strongly induce the activation of the autophagy and cGAS-STING pathways, while WR could directly interfere with exogenous cGAMP but not with DMXAA treatment to hamper endogenous type I IFN expression. Furthermore, the MVA-induced activation of both autophagy and IFN I production was seemingly independent of the classical type III PI-3K complex involved in canonical autophagy and proteasomal degradation, although the induced activation of both pathways observed in this study was prevented when MVA-infected cells were simultaneously treated with GCA. Moreover, WR-induced inhibition of the activation of autophagy and cGAS-STING pathways were heavily dependent on uncoating and early viral gene expression, while MVA likely requires only binding to cells to induce activation for both mechanisms.

4.2 Generation of recombinant MVA (recMVA) viruses containing specific WR genes relevant for inhibiting the induction of autophagy

4.2.1 Identification of possible inhibitory genes for autophagy during WR infection

To identify WR genes that could be responsible for the inhibitory activity of this virus strain on autophagy, and perhaps simultaneously on cGAS-STING activation, an autophagy-reporter cell line (HeLa DsRed-LC3-eGFP; H-DLG) was used, which was originally created by Houda Khatif (227). I also cooperated with Dr. Jason Mercer's laboratory at UCL to perform a siRNA screen during VACV infection based on two methods – namely high-content confocal laser scanning microscopy (CLSM) and fluorescence-activated cells sorting (FACS). Melanie Krause, a member of Dr. Jason Mercer's laboratory helped to adjust the protocol when I travelled there to perform the experiments. Dr. János Kriston-Vizi, a leader of bioinformatics at UCL, supported us by performing the high-throughput imaging and initial quantification of DsRed-positive H-DLG cells using an Opera LX high-throughput microscope. Moreover, Dr. Artur Yakimovich, also from the Mercer lab, was kind enough to conduct further bioinformatic analysis on the previously processed data.

H-DLG cells were generated to stably express LC3 fused with DsRed at the N-terminus and eGFP at the C-terminus, as described previously (227). Upon autophagy induction, eGFP was removed from its position to enable LC3-II formation and integration in the autophagosomal membrane. To reduce the background, free eGFP and unbound DsRed-LC3-eGFP were removed from the cytoplasm with a gentle saponin wash. Thus, cells that were DsRed-positive and eGFP-negative could be monitored for autophagosome formation and autophagy activation (**Supplementary figure 8**). The siRNA screen contained 80 conserved WR genes, including three different siRNA sequences per gene, and was used to treat H-DLG cells for approximately 16 h prior to a 6-h infection period with MVA, WR or coinfection with MVA and WR. First, cells were analysed through high-content CLSM with the help of the people listed above (**Supplementary figure 9**) or through FACS in our lab (**Figure 19**). A complete list of WR genes can be found in Kilcher *et al.*'s publication (232). The results from the FACS read-out are included in **Figure 19A** and **B** (without statistics), and the top candidates of both read-outs are depicted in **Figure 20**. It is unclear why MVA-WR co-infected cells exhibited such a high percentage of DsRed only-positive cells, but this may be due to the different sensitivity of the

FACS read-out system compared with immunoblotting. Since I performed both of these protocols, pipetting error as a disturbance factor can be excluded.

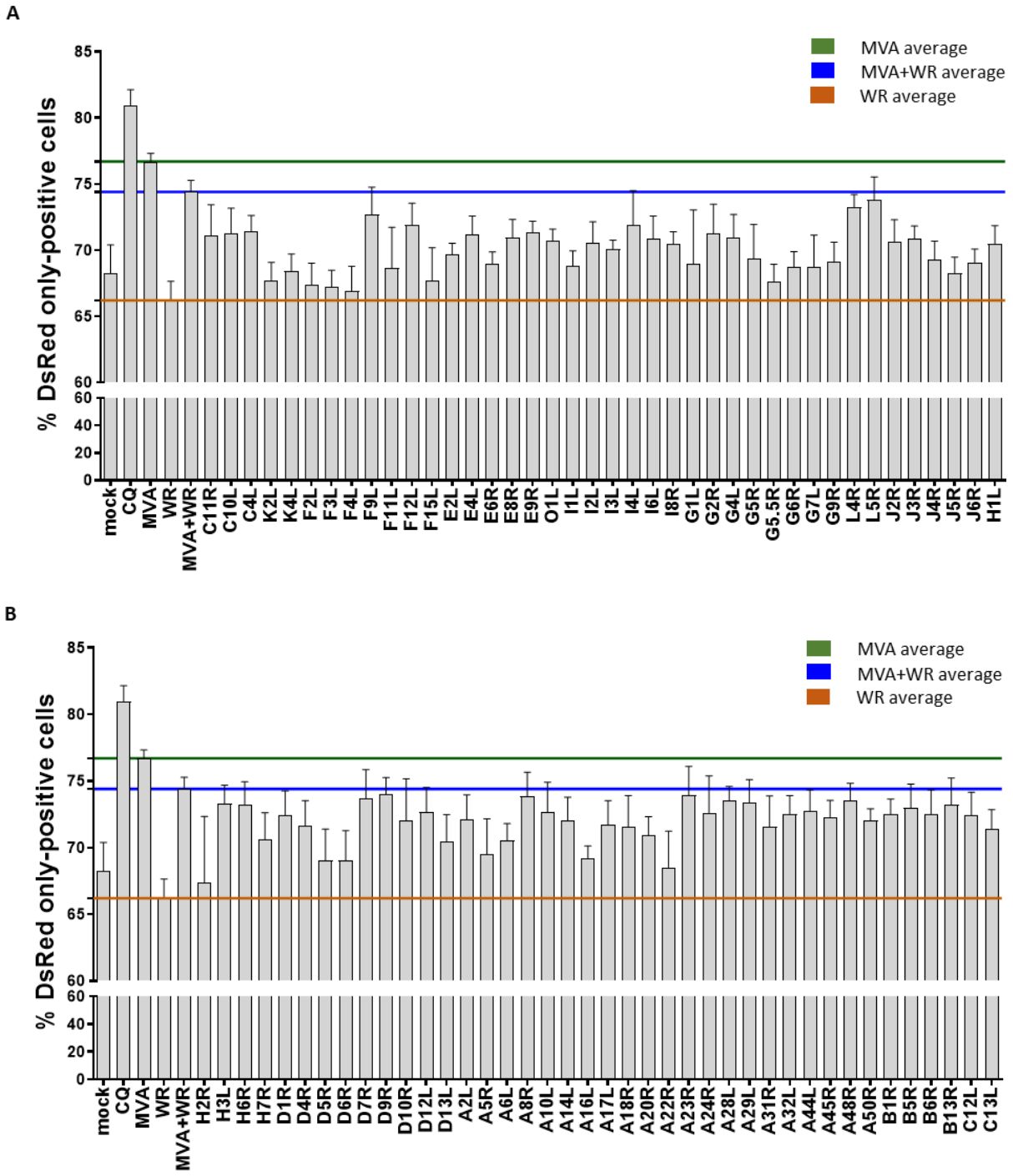

Figure 19. siRNA screen of WR genes relevant for inhibiting the induction of autophagy analysed via FACS. HeLa DsRed-LC3-eGFP (H-DLG) cells were non-infected (mock), chloroquine (CQ)-treated, MVA- or WR-infected, or MVA and WR co-infected for 6 hours. Cells were treated with siRNA 16 h prior to infection. Cells were infected with MOI 10 of MVA expressing eGFP under control of the vaccinia virus early/late promoter P7.5 (MVA) and MOI 5 of WR wild type (WR), or MOI 10 of MVA together with MOI 5 of WR (MVA+WR). For CQ treatment, 40 µM reagent was added to cells for the duration of infection. The results

depict the percentage of DsRed only-positive cells, which was calculated after pooling the results obtained for each of the three siRNA sequences specific for each gene. Scrambled siRNA (SsR)-treated control cells are excluded from the figure due to their almost identical values to similar control cells without SsR treatment. Statistics are not provided, and WR early genes are listed in increasing order from 1 to 80 according to how they were placed on the screen (n = 3).

Genes had to meet the following criteria to become a final candidate for further analysis: (1) have a similar percentage of DsRed only-positive cells as the MVA-infected cells, and (2) either be completely deleted or have major mutations at the amino-acid level in the MVA gene sequence compared with the WR sequence. Finally, five genes were selected as candidates according to the results of both, FACS and CLSM screening: A10L, A18R, B5R, B13R, and C10L. In addition, B2R was included as a final candidate due to a recent publication (140) at the time of selection, although it was not included in the screening panel.

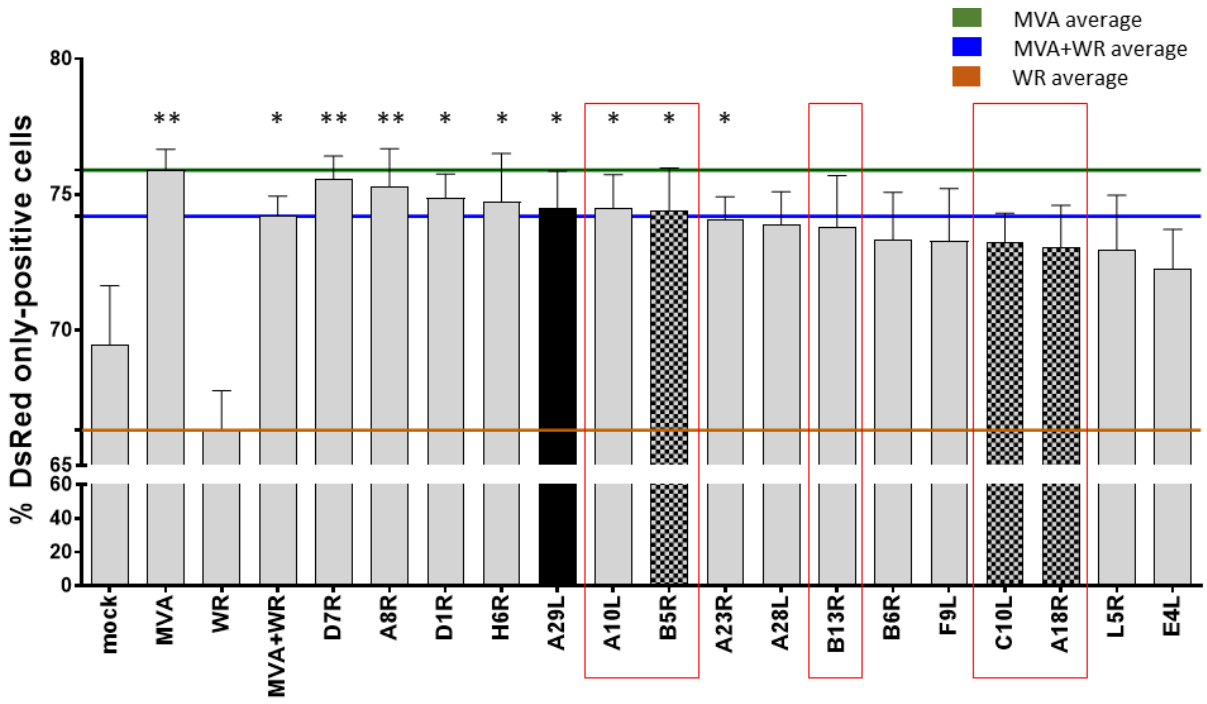

Figure 20. Top 16 candidates of the siRNA screen of WR genes relevant for inhibiting the induction of autophagy. This ranking was created based on the results of the FACS analysis (grey, with statistics) and includes four of the top seven candidates identified by high-content CLSM (black). Overlapping candidates identified by both methods are depicted by chequered columns. After comparatively analysing the DNA sequences of the respective MVA and WR candidate genes as well as sequences at the amino-acid level, the five genes marked by a red box were selected for further investigation. Data are depicted as the mean ± SD of three independent experiments. * = $p < 0.05$; ** = $p < 0.01$; ns = not significant; 1-way ANOVA test.

Interestingly, A10L, the major core protein 4a and its precursor, was described by Assarsson *et al.* as a late protein (241). However, since A10L was included in the siRNA screening panel

and the matching MVA gene 121L has modifications resulting in 12 amino-acid exchanges compared with the WR sequence, it was used for recMVA generation. Genes that appeared as top candidates for both read-outs with a high number of amino-acid changes included the DNA helicase A18R, the IL-1 receptor agonist C10L and the EEV membrane glycoprotein B5R. Serin protease inhibitor 2 B13R and the poxin B2R are both deleted from MVA, which made them excellent candidates for inhibiting autophagy during WR infection (**Supplementary table 1**).

WR gene name (Gene ID)	MVA gene name	Expression time	Function of gene product(s)	Differences compared to MVA on the amino-acid level
A10L (3707527)	121L	late	major core protein 4a precursor	12 mismatches
A18R (3707668)	129R	early/late	DNA helicase	8 mismatches
B5R (3707658)	173R	early/late for WR late for MVA	EEV membrane glycoprotein	9 mismatches
B13R (3707572)	181/182R	early	serin protease inhibitor 2	deleted from MVA
C10L (3707586)	006L	early	IL-1 receptor antagonist	5 mismatches
B2R (3707655)	168R	early	poxin	deleted from MVA

Table 1. Selected WR genes for reinsertion or replacement in MVA (recMVA generation).

While analysing the top candidates, I noticed that H3L appeared to be a possible target due to its high level of LC3 granularity compared with non-infected cells treated (or not) with scrambled sRNA in the high-content CLSM read-out in London. Interestingly, our lab already had a recMVA virus that expressed H3L fused to eGFP under the control of the early promoter PK1L; therefore, I tested this virus to observe how the WR gene product H3 affected the induction of activation of the cGAS-STING pathway for type I IFN production and for autophagy (**Supplementary figure 10**). However, the lipidation status of LC3-II as well as the phosphorylation status of P-STING, P-TBK1, and P-IRF3, during MVA-H3-eGFP infection resembled MVA-induced activation of the pathways. This finding indicated that the gene H3L expressed early is not responsible for inhibiting either pathway.

4.2.2 Process of recMVA virus generation

The protocol for generating recMVA viruses was adjusted based on previously published methods (231, 233–235, 242).

4.2.2.1 Design of candidate WR gene sequences and their insertion into pcDNA3.1D V5-His-Topo (hereinafter called ‘pcDNA3.1’) vector

Before gene synthesis, each WR gene (complete genome – GenBank: NC_006998.1) to be inserted into MVA (complete genome – GenBank: U94848.1) was embedded in a transfer sequence (hereinafter, the letter symbolising the gene's orientation is not given), which was designed as follows: first, four guanosines and the sequence of restriction enzyme *Not*I were placed at the C-terminus. This sequence was followed by a 100 – 200 base sequence that was part of the MVA genome upstream of the respective gene of interest (hereinafter 'flank 1'). Subsequently, the sequence of the genes of interest followed, including natural promoter sequences. Downstream, another 100 – 200 base long DNA stretch of the MVA genes of interest was inserted (hereinafter 'flank 2'), followed by the sequence of restriction enzyme *Age*I and four cytosines at the N-terminus in all constructs. This design enabled the synthesised genes of interest to be removed easily from the carriers provided by the company using restriction enzyme digestion and inserted with the correct orientation into the pcDNA3.1 vector. Restriction enzymes *Not*I and *Age*I were single cutters in the vector backbone and did not cut within the genes of interest (**Figure 21**). Moreover, another single cutting restriction enzyme within the WR gene sequences was selected to create an insertion point for the next step of cloning (**Figure 21A**). After the successful ligation of cut DNA and the transformation and propagation of bacterial clones on ampicillin-containing agar plates, four clones of each construct were selected and tested using colony PCR with specific primer pairs, which covered the full length of each of the genes of interest (**Figure 21B**). One clone confirmed by PCR was then sent for sequencing to Eurofins Genomics to exclude point mutations. For the C10-construct, two single cutters appeared on the gene map because, during the generation procedure, the first restriction site did not yield satisfying results; therefore, I also tried another enzyme. The reason for the smaller fragments of the B13-construct is unknown as they are not caused by repetitive primer binding.

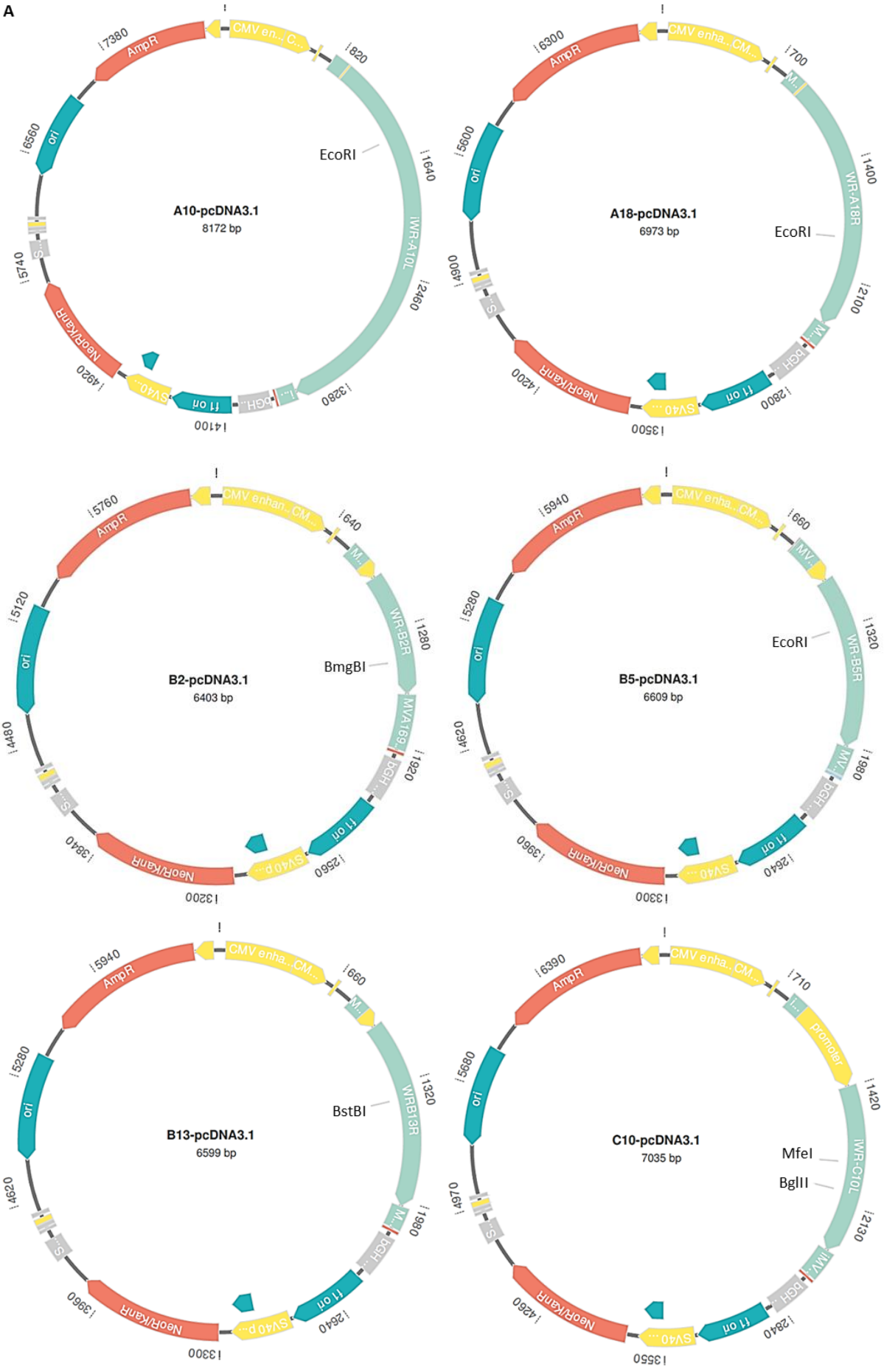
A
A10-pcDNA3.1
8172 bp
EcoRI
CMV en... C...
AmpR
ori
iWR-A10L
pGH...
f1 ori
SV40...
NeoR/KanR
A18-pcDNA3.1
6973 bp
EcoRI
CMV enha...CM...
AmpR
ori
WR-A18R
bGH...
f1 ori
SV40...
NeoR/KanR
B2-pcDNA3.1
6403 bp
BmgBI
CMV enhan...CM...
AmpR
ori
WR-B2R
MVA169...
bGH...
f1 ori
SV40 p...
NeoR/KanR
B5-pcDNA3.1
6609 bp
EcoRI
CMV enha...CM...
AmpR
ori
WR-B5R
MV...
bGH...
f1 ori
SV40...
NeoR/KanR
B13-pcDNA3.1
6599 bp
BstBI
CMV enha...CM...
AmpR
ori
WRB13R
M...
bGH...
f1 ori
SV40 p...
NeoR/KanR
C10-pcDNA3.1
7035 bp
MfeI
BglII
CMV enha...CM...
AmpR
ori
promoter
iWR-C10L
MV...
bGH...
f1 ori
SV40...
NeoR/KanR

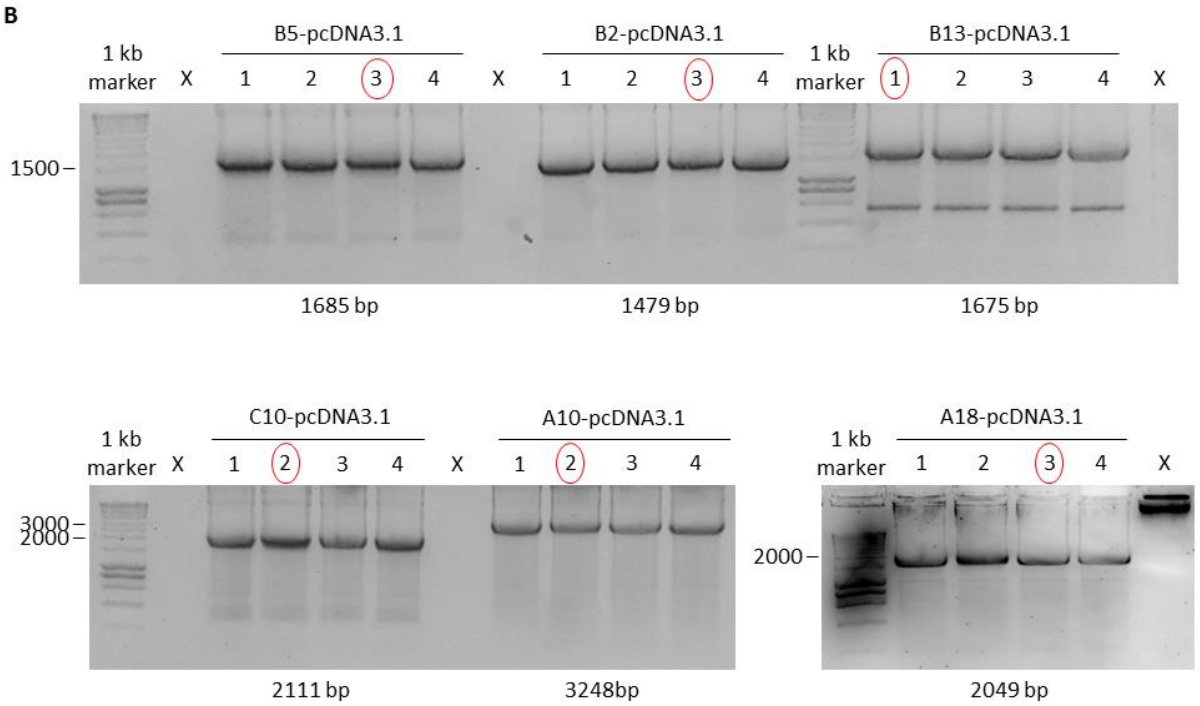

Figure 21. Plasmid maps of the six selected WR genes and their correct insertion into BAC transfer plasmid clones using colony PCR. (A) Complete plasmid maps of selected WR genes inserted into the commercial pcDNA3.1 vector as provided by the synthesising company, including selected single cutters for each gene. (B) Agarose gels containing the PCR DNA fragments for each construct demonstrating successful insert incorporation. Clone numbers marked with a red circle were sent to sequencing and, after receiving a positive result, underwent further cloning steps. X represents the primer control for each construct. Expected size for each DNA fragment is indicated below the respective construct. Marker standard is indicated on the left.

4.2.2.2 Introduction of BAC selection I-*Sce*I-kanamycin cassette (Kana) into genes of interest

Next, the constructs were prepared for *en passant* mutagenesis (233–235) by introducing an insert containing the homing endonuclease I-*Sce*I and a kanamycin resistance gene (hereinafter, this combination is referred to as 'Kana') into the genes of interest. Forward primers were designed to match the single cutters of each construct, followed by a 40 - 50 base sequence specific to each construct placed directly after a specific restriction enzyme site (Rep1 and Rep2, which later played a critical role in later eliminating the I-*Sce*I sequence). The insert was terminated by the I-*Sce*I sequence. Reverse primers were created to bind to the kanamycin resistance gene after the respective single cutter sequence. These construct-specific primer pairs were then used to amplify a Kana cassette from the pEP-MVA-dVI-pK1L (231) plasmid used as a template. This plasmid was created by Lianpan Dai, a former PhD student in Prof. Dr. Ingo Drexler's laboratory. It contains Kana because it was designed as a shuttle vector for

target genes into deletion IV of the MVA-BAC. After amplification by PCR, the product was purified by agarose gel electrophoresis and gel extraction and used as an insert, which was then ligated into the linearised (with the previously selected single cutter) pcDNA3.1 plasmid DNA containing the expression cassettes with the genes of interest (**Figure 22**). After successful ligation, transformation, and propagation of bacterial clones on ampicillin-containing and kanamycin agar plates (**Figure 22A**), clones were verified through colony PCR with specific primer pairs that covered the full length of each of the genes of interests; however, an additional primer pair was also used to confirm the orientation of Kana (**Figure 22B**). After verification, the PCR-confirmed clone was sent to Eurofins Genomics for sequencing to exclude point mutations. For the C10-construct, no clones were obtained containing the Kana insert, even after adjusting several conditions of the cloning method, including switching the single cutter. Since the reason for this failure remained unclear, the C10-construct was excluded from further cloning steps. While the reason for the smaller PCR products for the B13-construct is also unknown, they were not caused by repetitive primer binding.

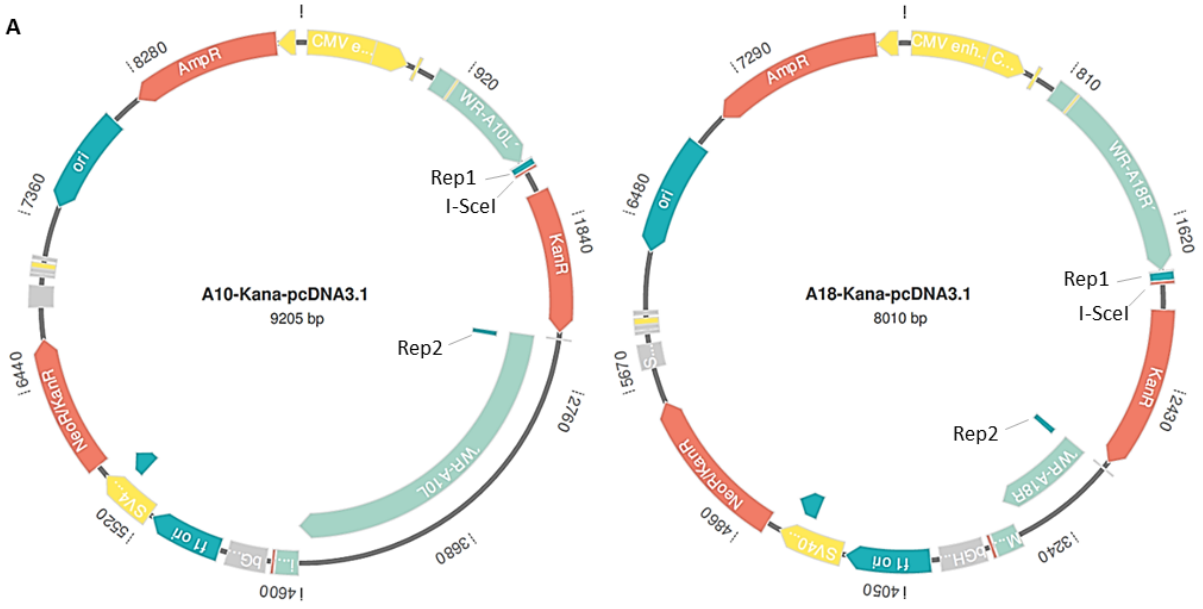

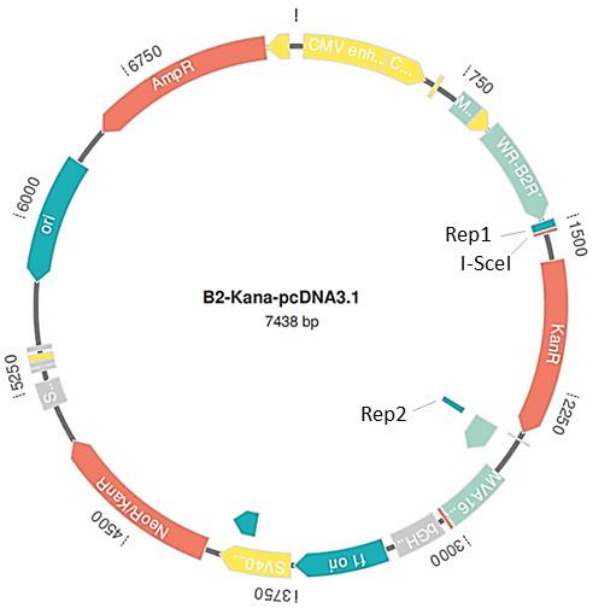
B2-Kana-pcDNA3.1
7438 bp
Rep1
I-Scel
Rep2
KanR
AmpR
ori
CMV enh... C...
WR-B2R
MVA16...
pCH...
f1 ori
SV40...
Neo(R)/KanR
S...
1
750
1500
2250
3000
3750
4500
5250
6000
6750

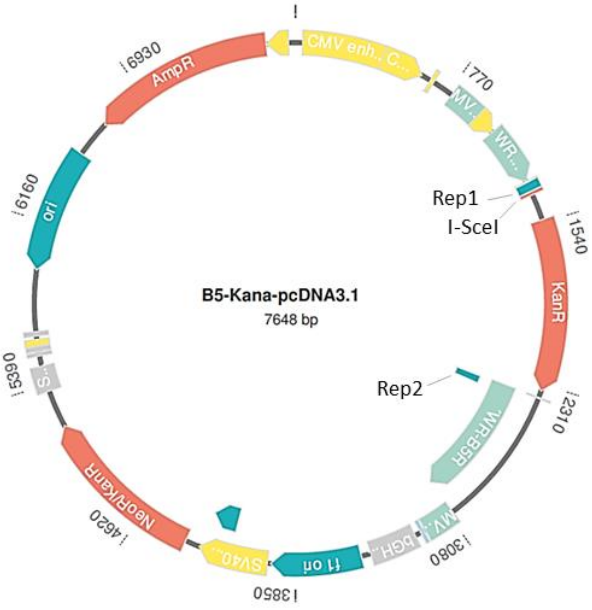
B5-Kana-pcDNA3.1
7648 bp
Rep1
I-Scel
Rep2
KanR
AmpR
ori
CMV enh... C...
MV...
WR...
WR-B5R
MV1...
pCH...
f1 ori
SV40...
Neo(R)/KanR
S...
1
770
1540
2310
3080
3850
4620
5390
6160
6930

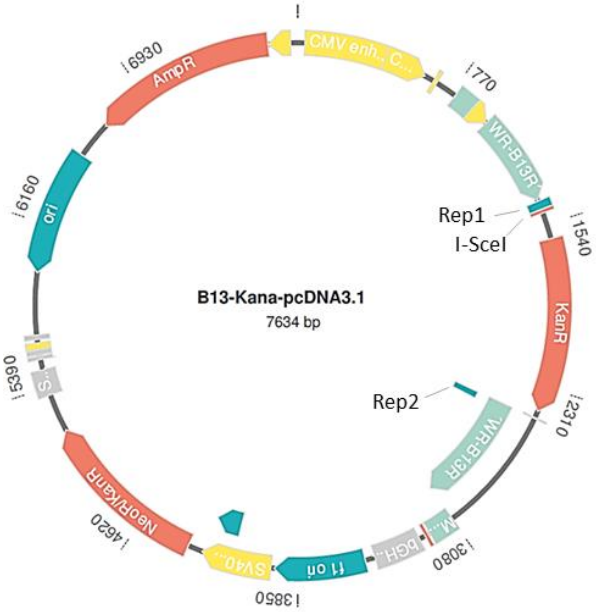
B13-Kana-pcDNA3.1
7634 bp
Rep1
I-Scel
Rep2
KanR
AmpR
ori
CMV enh... C...
WR-B13R
M...
pCH...
f1 ori
SV40...
Neo(R)/KanR
S...
1
770
1540
2310
3080
3850
4620
5390
6160
6930


C10-Kana-pcDNA3.1
8073 bp
Rep1
I-Scel
Rep2
KanR
AmpR
ori
CMV en... C...
promoter
WR-C10L
WR-C10L
M...
pCH...
f1 ori
SV40...
Neo(R)/KanR
S...
1
810
1620
2430
3240
4050
4860
5670
6480
7290

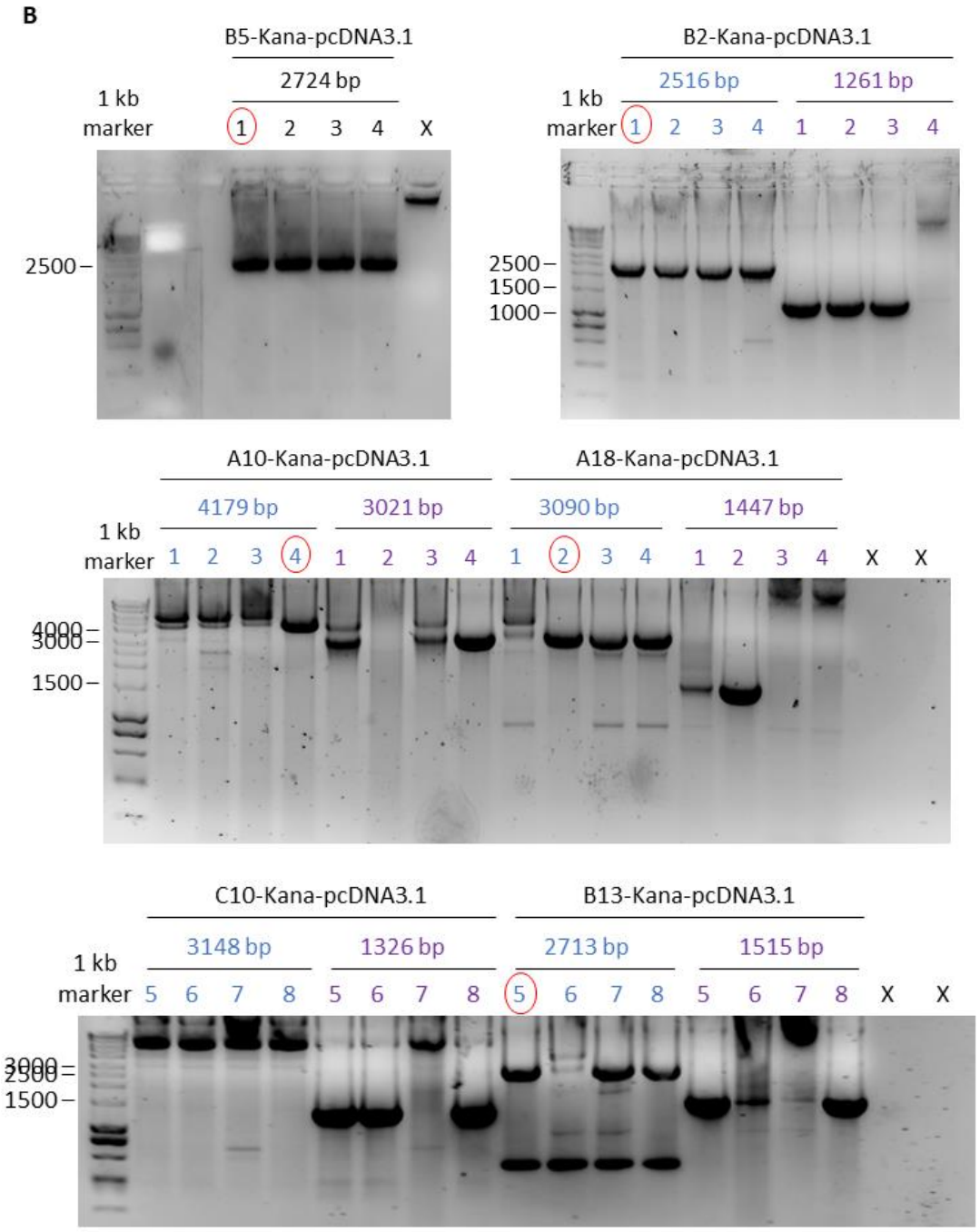

Figure 22. Integration of the kanamycin resistance cassette (Kana) into pcDNA3.1 plasmids containing the genes of interest. (A) Complete plasmid maps of Kana inserted into selected WR genes-pcDNA3.1 vector, including selected single cutters for each gene. Rep1 and Rep2 represent identical 40 – 50 base sequences following the selected single cutter of each construct. (B) Agarose gels containing the PCR DNA fragments obtained for each construct demonstrating successful integration of inserts. The fragments of a larger size represent the full-length sequences (blue), and those of a smaller size exhibit the expected lengths of products starting from Kana until the end of each construct (purple). Clone numbers marked with a red circle were sent to sequencing and, after a positive result was received, underwent further cloning steps. X represents the primer control for each construct. Expected size for each DNA fragment depending on the primer pair used for amplification is indicated below the respective construct. Marker standard is indicated on the left.

4.2.2.3 First recombination step of the two-step Red-mediated recombination system

Next, specific primer pairs were designed to amplify genes of interest including Kana with approximately 100 base flanks at the N- and C-termini (**Figure 23A-B**). PCR products were then separated by agarose gel electrophoresis, purified by gel extraction, and used as inserts for the transformation of the *E. coli* strain GS 1738 by electroporation. GS 1783 contains an MVA-BAC with a temperature-dependent expression cassette for recombination proteins and an L-arabinose-inducible I-*Sce*I gene, a chloramphenicol (CAM) resistance gene and a GFP cassette.

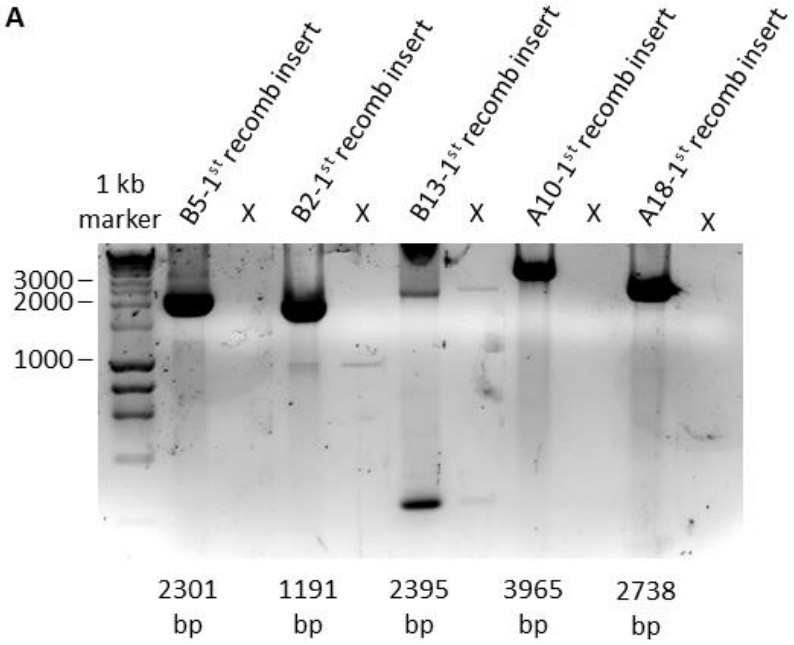

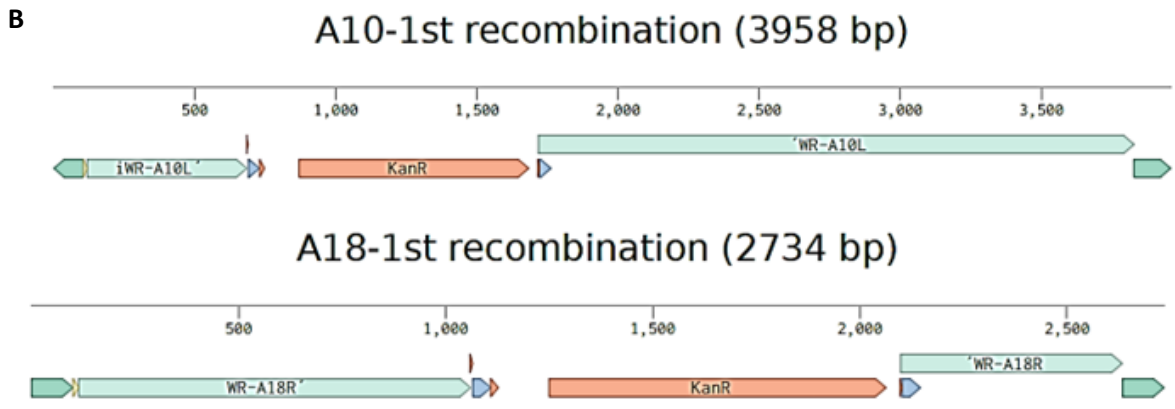

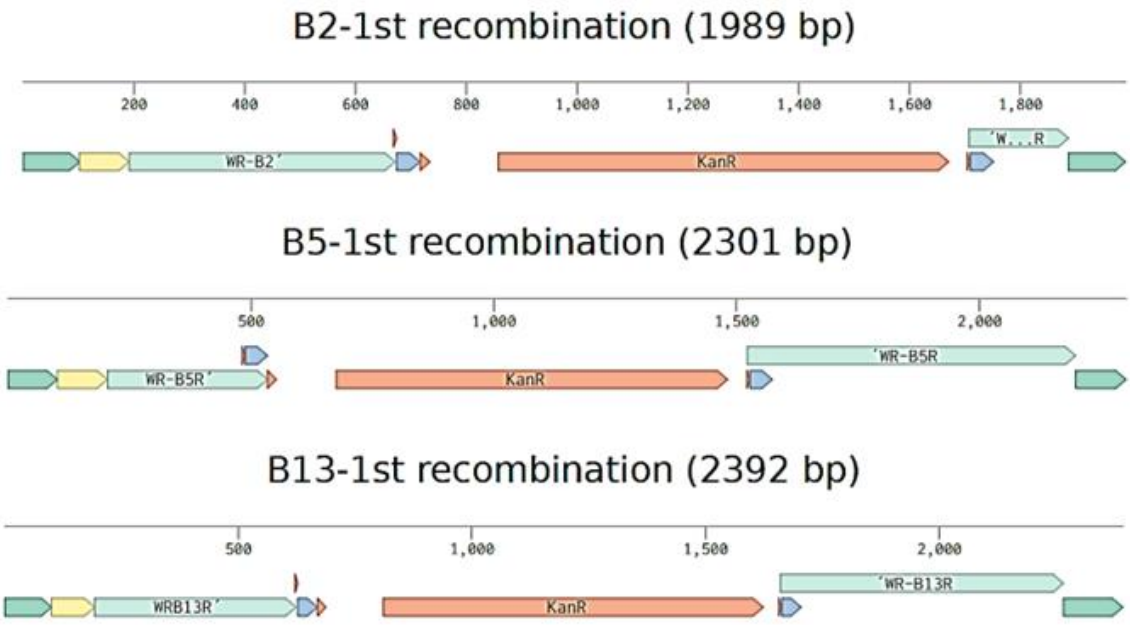
B2-1st recombination (1989 bp)
200
400
600
800
1,000
1,200
1,400
1,600
1,800
'W...R
WR-B2'
KanR
B5-1st recombination (2301 bp)
500
1,000
1,500
2,000
'WR-B5R
WR-B5R'
KanR
B13-1st recombination (2392 bp)
500
1,000
1,500
2,000
'WR-B13R
WRB13R'
KanR

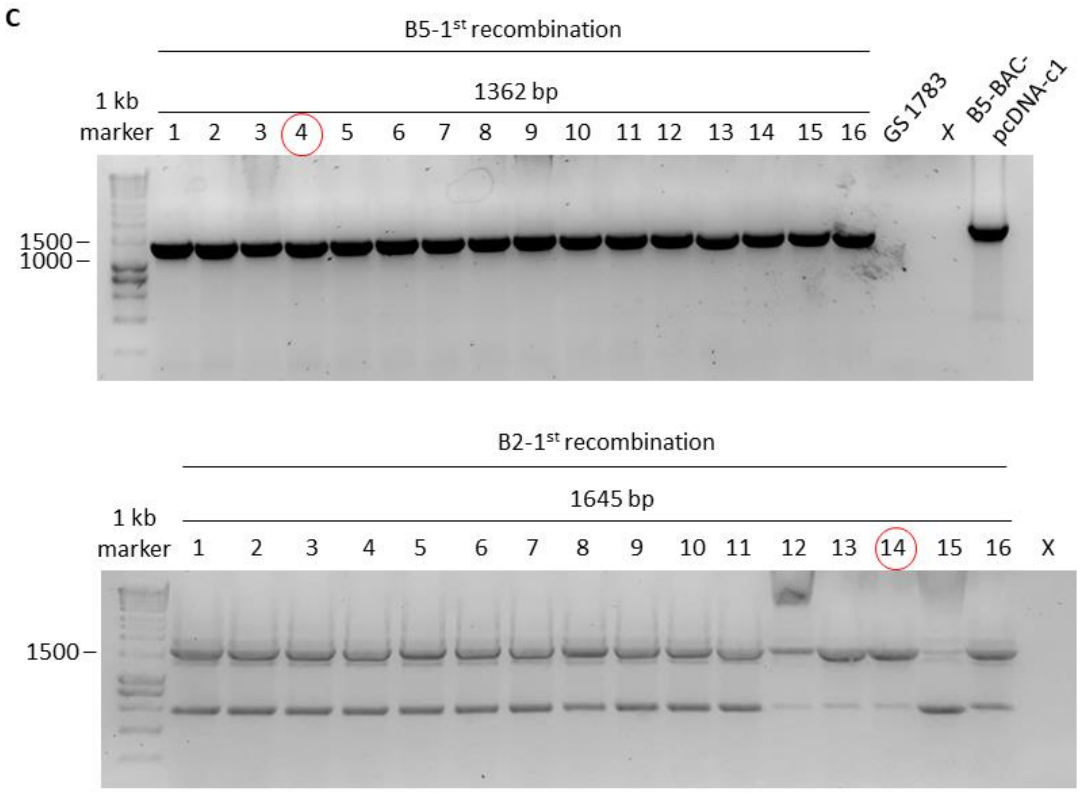
C
B5-1st recombination
1 kb
marker
1362 bp
1 2 3 4 5 6 7 8 9 10 11 12 13 14 15 16
GS1783
X
B5-BAC-pcDNA-c1
1500–
1000–
B2-1st recombination
1 kb
marker
1645 bp
1 2 3 4 5 6 7 8 9 10 11 12 13 14 15 16 X
1500–

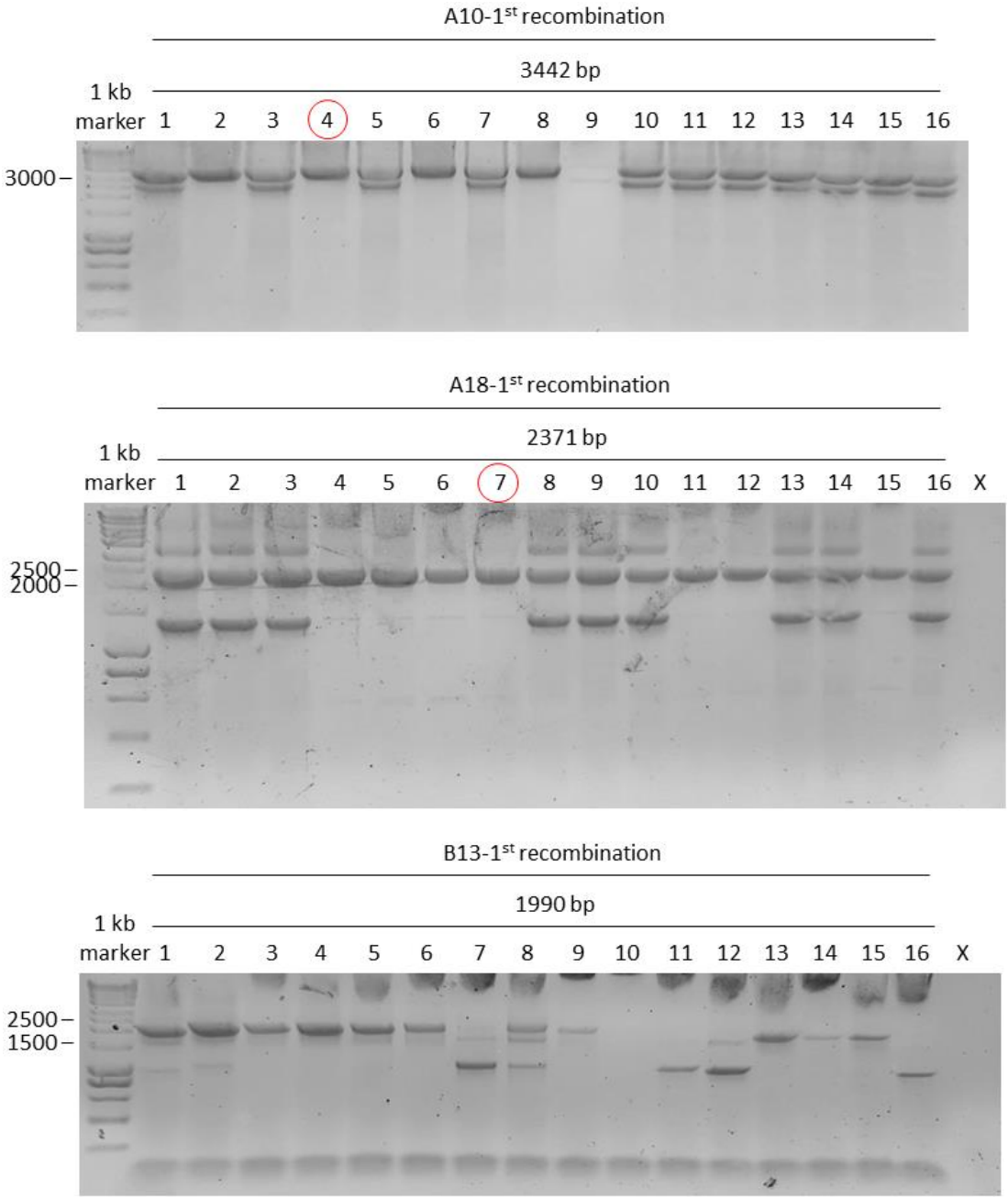

Figure 23. Integration of genes of interest containing the kanamycin resistance cassette (Kana) into an MVA-BAC inside the *E. coli* strain GS 1738. (A) Agarose gel with the PCR DNA fragments containing the expression cassettes with the indicated genes of interest used for the first recombination step. (B) Complete plasmid maps of selected genes of interest, including Kana. (C) Agarose gels with the PCR DNA fragments obtained for each construct after the first recombination step. Clone numbers marked with a red circle were sent to sequencing and, after a positive result was received, underwent further cloning steps. X represents the primer control for each. Expected size for each DNA fragment is indicated below the respective construct (A, C). Marker standard is indicated on the left.

After the successful transformation and propagation of bacterial clones on kanamycin- and CAM-containing agar plates, clones were verified using colony PCR with specific primer pairs that covered the full length of each of the genes of interests (**Figure 23C**). After verification, the PCR-confirmed clone was sent for sequencing to Eurofins Genomics to exclude point mutations. For the B13-construct, none of the clones exhibiting the expected fragment size were free of mutations, even after adjusting several cloning conditions. The reason for these constant mutations is unclear, and the B13-construct was excluded for further processing.

4.2.2.4 Second recombination step of the two-step Red-mediated recombination system

Next, selected clones were then used for the second recombination step, in which L-arabinose, added to LB medium along with CAM, induced the expression of I-*Sce*I from Kana and initiated cleavage at its position, resulting in double-stranded breaks in the DNA of the genes of interest. After incubation at 32 °C, cultures were incubated at 42 °C for 30 min to induce homologous recombination between the previously described repetitive elements (Rep1 and Rep2), thereby removing I-*Sce*I and the kanamycin cassette from the genes of interest (**Figure 24A**). After a recovery period at 32 °C, the cultures were plated on agar plates containing CAM and L-arabinose to obtain single bacterial clones. Successful clones were verified using colony PCR with specific primer pairs that cover the full length of each of the genes of interests. After verification, the PCR-confirmed clone was sent to Eurofins Genomics for sequencing to exclude point mutations (**Figure 24B**).

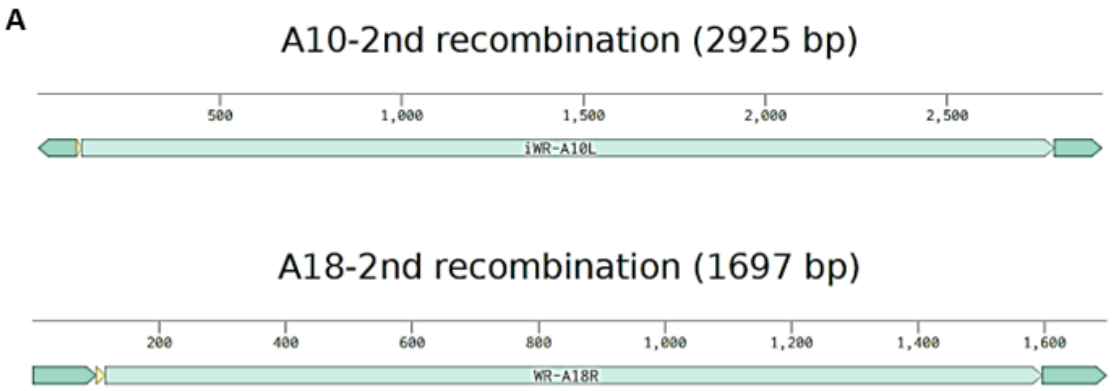

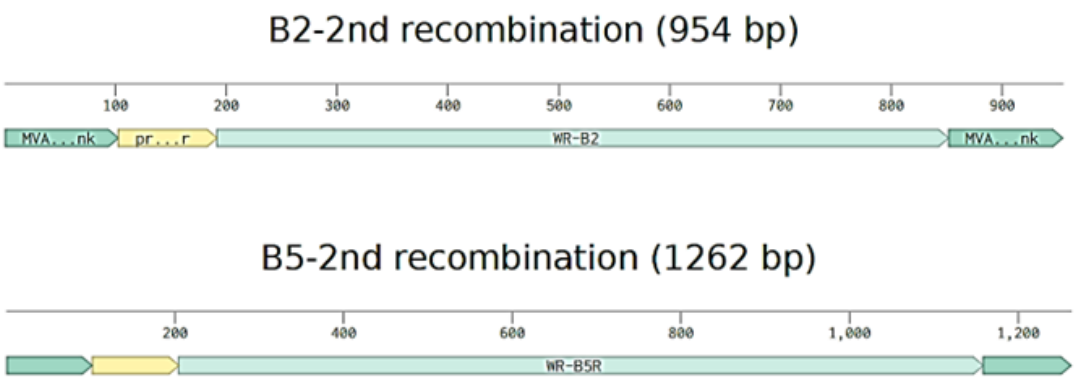
B2-2nd recombination (954 bp)
100
200
300
400
500
600
700
800
900
MVA...nk
pr...r
WR-B2
MVA...nk
B5-2nd recombination (1262 bp)
200
400
600
800
1,000
1,200
WR-B5R

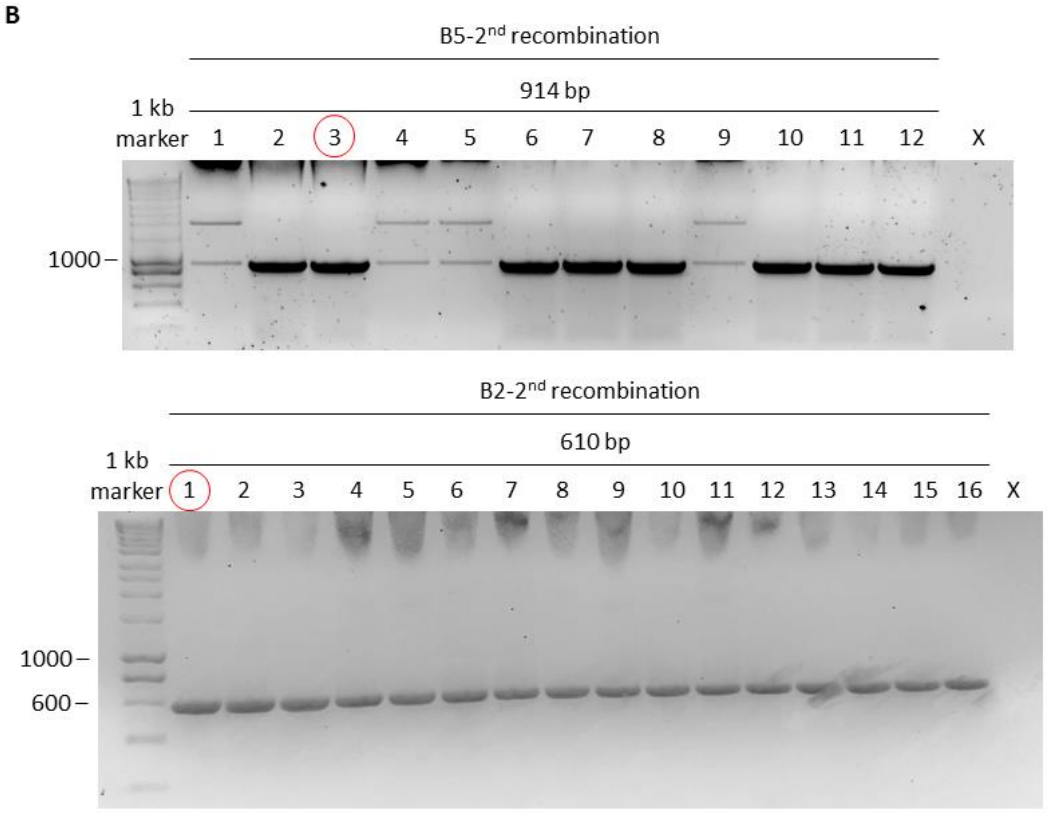
B
B5-2nd recombination
914 bp
1 kb marker
1
2
3
4
5
6
7
8
9
10
11
12
X
1000
B2-2nd recombination
610 bp
1 kb marker
1
2
3
4
5
6
7
8
9
10
11
12
13
14
15
16
X
1000
600

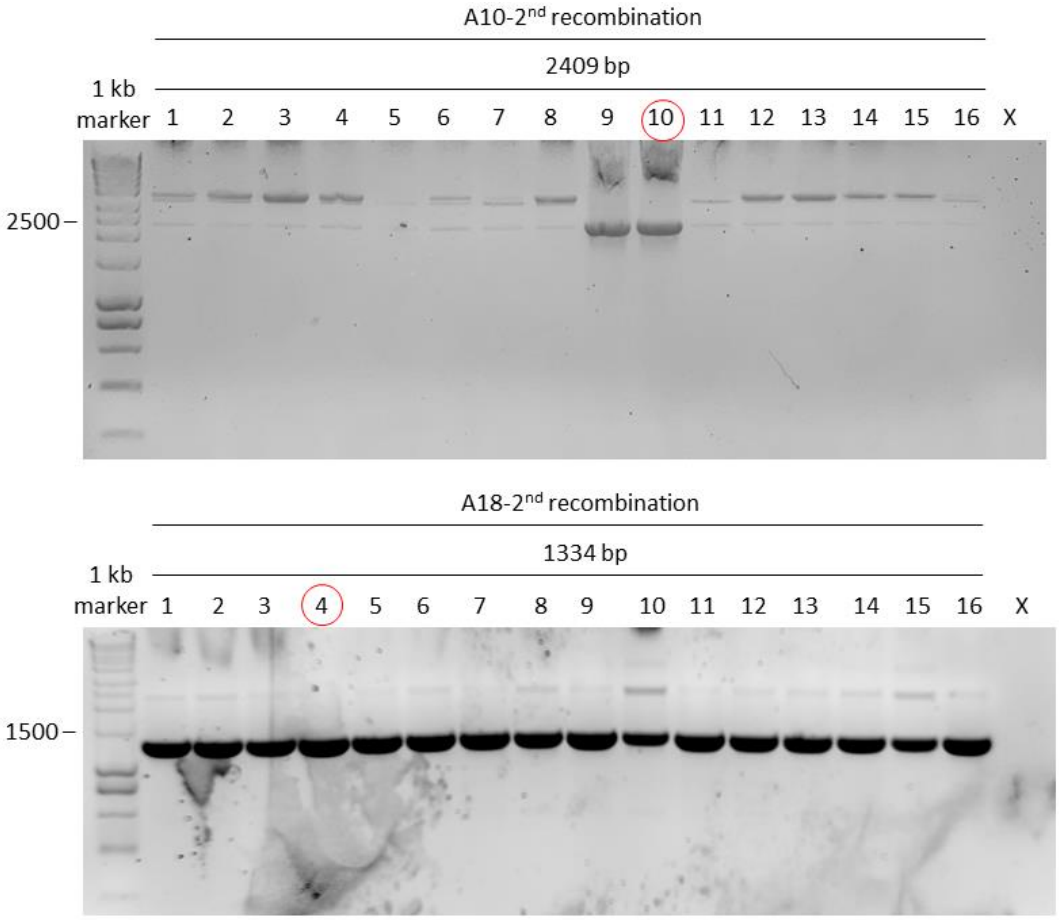

Figure 24. Removal of the kanamycin resistance cassette (Kana) during the second recombination within the genes of interest from the expression cassette of MVA-BAC inside the *E. coli* strain GS 1738. (A) Complete plasmid maps of selected genes of interest without Kana inside the MVA-BAC. (B) Agarose gels with the PCR DNA fragments obtained for each construct after the second recombination step. Clone numbers marked with a red circle were sent for sequencing and, after a positive result was received, underwent further cloning steps. X represents the primer control for each construct. Expected size for each DNA fragment is indicated below the respective construct. Marker standard is indicated on the left.

4.2.2.5 Rescue of recMVA and generation of single virus clones

The recombinant MVA-BAC clones containing the genes of interest were then used to transfect DF-1 cells which were subsequently infected with rabbit fibroma virus (RFV) as a helper virus. This induced the replication of recMVA-BAC DNA with the help of the RFV early transcription factors. Finally, following a series of sub-passages with GFP-positive clones, GFP was eliminated from recMVA due to its self-excising design (231, 233–235, 242), and only recMVA without BAC sequences remained. Subsequently, single virus clones were selected through limiting dilution and their integrity confirmed by PCR according to the size of the respective gene of interest (**Figure 25**). Additionally, clones were checked by PCR for the

presence or absence of residual GFP in the BAC sequence as well as for the presence or absence of RFV (**Supplementary figure 11**). Once the sequences of selected clones had been verified in terms of integrity, loss of GFP, and absence of helper virus, the clones were amplified on DF1 cells and purified by sucrose cushion centrifugation to be used for further experiments.

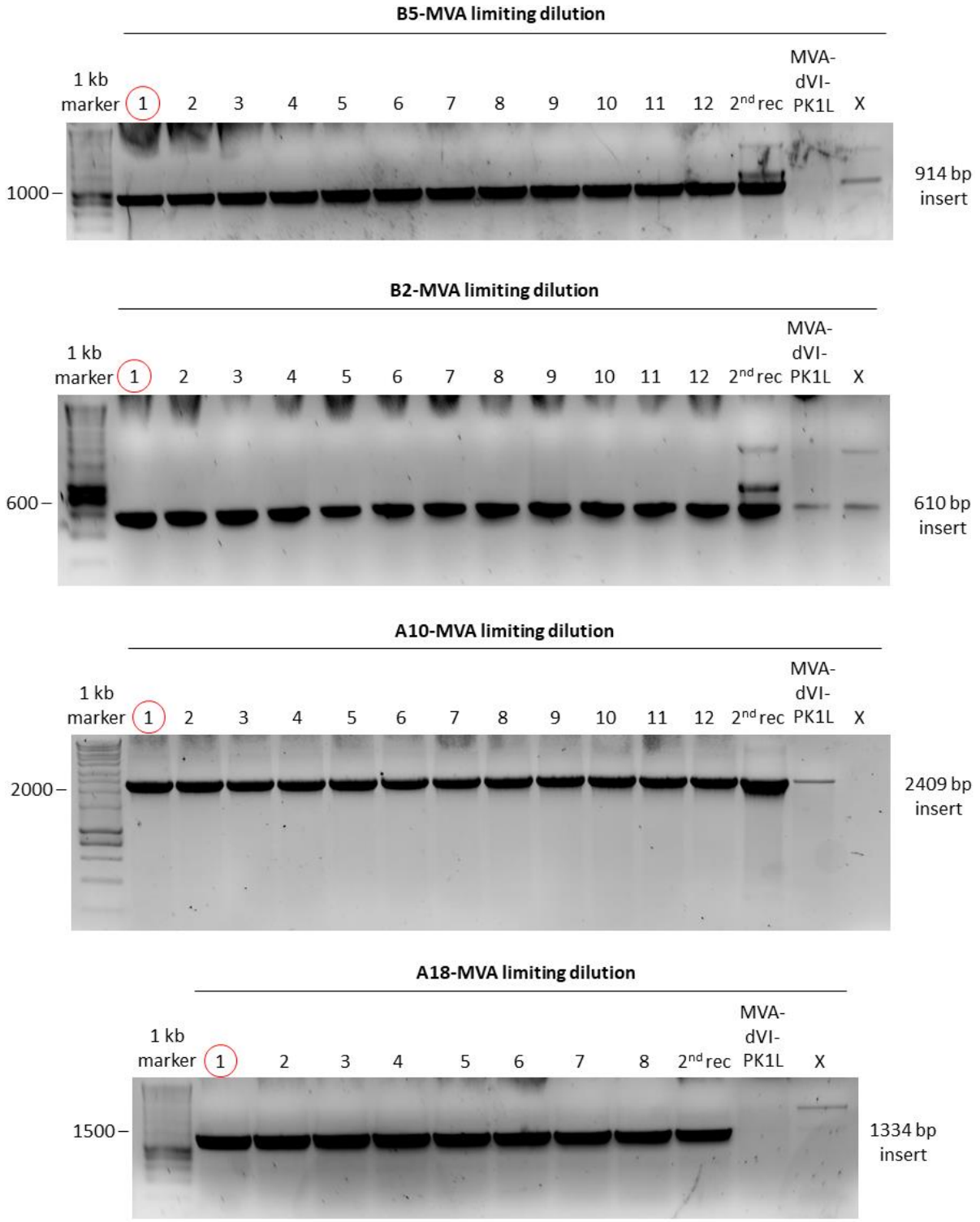

Figure 25. Recombinant MVA clones containing the WR genes of interest after rescue and limiting dilution. Agarose gels containing the PCR DNA fragments for each construct obtained after limiting dilution.

Recombinant MVA clones marked with a red circle were sent for sequencing and, after a positive result was received, underwent further amplification and purification steps. Sequenced BAC clones obtained after the second recombination (2nd rec) were used as a positive control. DNA from the plasmid pEP-MVA-dVI-PK1L (MVA-dVI-PK1L) was used as a negative control. X represents the primer control for each construct. Expected size for each DNA fragment is indicated below the respective construct. Marker standard is indicated on the left.

4.2.3 Comparative analysis of recMVA-expressing WR genes potentially involved in interfering with VACV-induced STING-dependent autophagy and/or IFN I production

Due to a lack of time, generated recMVA viruses were used only once for immunoblotting (**Figure 26**) with or without AraC treatment in a 4- or 24-h infection experiment. The latter long infection period was selected to allow for the testing of A10 which represents a late gene product in VACV.

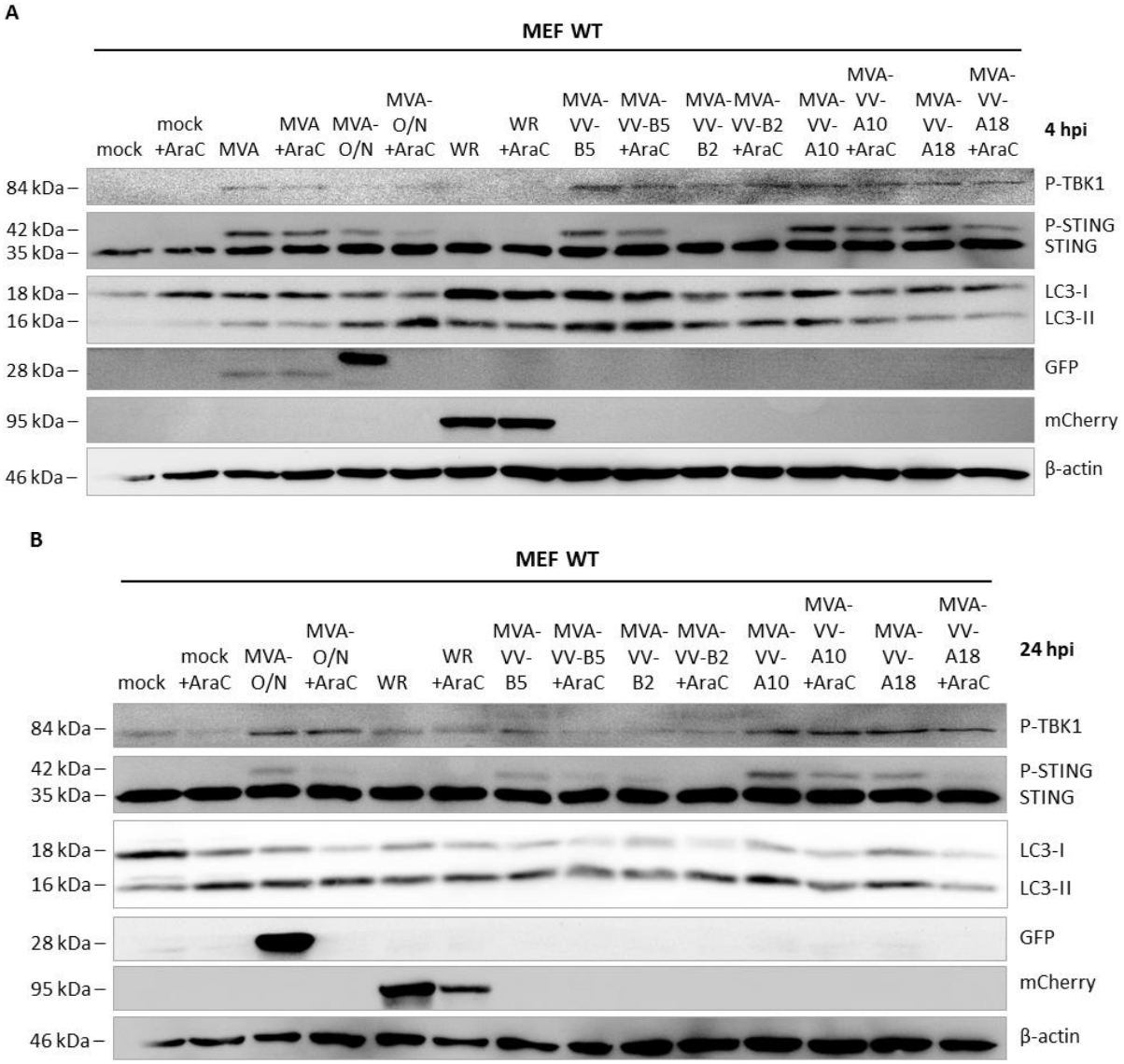

Figure 26. Comparative analysis of recombinant MVA (recMVA)-expressing WR genes potentially involved in interfering with VACV-induced STING-dependent autophagy and/or IFN I production. Induction of activation of autophagy and cGAS-STING pathway for type I IFN production was observed in wild type (WT) MEF cells with or without AraC treatment at the same time. First, 70 – 80 % confluent cells were infected for 4 h (A) or for 24 h (B). In case of (A), cells were infected with MOI 10 for MVA expressing eGFP under control of the vaccinia virus early/late promoter P7.5 (MVA-P7.5-eGFP) MOI 10 of recMVA viruses, MOI 5 of WR expressing a fusion gene coding for the influenza A nucleoprotein, ovalbumin-derived peptide SIINFEEKL and fluorescent protein mCherry under control of the vaccinia virus early/late promoter P7.5 (WR-P7.5-NP-SIIN-mCherry) or overnight with MOI 10 of MVA expressing eGFP under control of the vaccinia virus late promoter P11 (MVA-P11-eGFP). In case of (B), cells were infected with MOI 5 of WR-P7.5-NP-SIIN-mCherry, MOI 10 of MVA-P11-eGFP or MOI 10 for recMVA. After infection, cells were harvested and lysed and protein levels were determined by Western blot analysis. For AraC treatment 40 µg/ml of reagent was added to cells for the duration of the infection (n = 1).

In cells infected for 4 h (**Figure 26A**), all recMVA viruses except for MVA-VV-B2 exhibited similar levels of STING and TBK1 phosphorylation compared with control MVA-infected cells. While MVA-VV-B2 exhibited no P-STING; however, P-TBK1 was weakly detectable. Unfortunately, P-IRF3 staining did not work for this membrane. Moreover, the recMVA viruses MVA-VV-A10 and -A18 exhibited a certain level of LC3-II, although the LC3 lipidation induced by the control MVA-infected cells seemed less potent than that for the WR-infected cells. This result may suggest that during the early period of infection, the presence of B2 accelerates the degradation of P-STING and/or its activator cGAMP, leading to the impression that STING was never activated by the virus. This could also lead to weak TBK1 phosphorylation. In addition, it is possible that WR A10 and A18 gene products or their precursors are involved in autophagy inhibition, since cells infected with MVA-VV-A10 and -A18 and treated with AraC exhibited slightly less LC3-II than non-AraC-treated cells. For this hypothesis to be confirmed, this experiment must be repeated.

For cells infected for 24 h (**Figure 26B**), the mock-infected and AraC-treated cells already exhibited visible markers of stress, which likely led to the elevated level of LC3-II. Interestingly, all samples exhibited a certain level of P-TBK1, which was probably also due to the stress of the mock infections. In the WR-infected cells, since P-IRF3 staining was unsuccessful, it was not possible to discern whether, despite the phosphorylated state of TBK1, type I IFN expression was prevented, as indicated by ELISA data obtained from supernatants from samples taken after a similar WR infection period (**Supplementary figure 2**). Interestingly, not all cells infected by recMVA viruses displayed STING phosphorylation. Cells infected with MVA-VV-B2 again exhibited no P-STING and only a low amount of P-

TBK1. The other recMVA-infected and AraC-treated cells exhibited some decrease in P-STING compared with non-treated cells, while the differences for MVA-VV-A10 and -A18 seemed quite strong. The same outcome described for P-STING was also recognisable for LC3 lipidation. Samples with less P-STING also seemed to have slightly less LC3-II compared with the cells without AraC treatment. The results indicate that particularly B2 plays a crucial role not only during the early phase of infection but also at a later point. To be able to determine the role of the other WR gene products, the experiments must be repeated.

In summary, recombinant MVA viruses expressing fully functional WR A10L, A18R, B2R, and B5R genes were generated. In addition, MVA-VV-B2 seemed to be able to interfere with STING phosphorylation during the initial part of infection, a finding that is in line with a previous publication (140). Moreover, MVA-VV-A18 exhibited lower levels of P-STING during the early and late phases of infection when treated with AraC, which is understandable since A18R is thought to be an early/late gene.

5 Discussion

MVA is considered a highly promising vaccine vector due to its high immunogenicity and ability to express several recombinant antigens at a time (243–245). It has been demonstrated to induce strong type I IFN expression through the cGAS-STING pathway and to activate autophagy upon infection without the ability to fully replicate within the infected cells (92, 94). Several studies have described links between these two pathways; for example, TBK1 attenuated the cGAS-STING pathway for type I IFN production through p62-dependent autophagy (197), or that STING in a predatory marine invertebrate induced the activation of autophagy but failed to initiate an IFN response upon cGAMP treatment (148). A study also witnessed that STING can induce LC3B lipidation onto single-membrane vesicles mediated through ATG16L1 upon cGAMP treatment (225). However, whether these links are relevant during VACV infection has not been investigated thoroughly yet. VACV was observed to be able to interfere with autophagosome formation through the conjugation of ATG12 and ATG3, which led to a high LC3-II level of 24 hp; however, the viral gene behind this process was not addressed (222). Furthermore, Krause *et al.* demonstrated that the VACV-encoded kinases B1 (early gene product) and F10 (late gene product) drive p62 phosphorylation and translocation into the nucleus to prevent them being target by ubiquitination in HeLa cells; unfortunately, their effect on the STING-dependent but p62-independent autophagy was unclear (224). Therefore, this PhD thesis aimed to understand the interaction between the cGAS-STING pathway for type I IFN production and the activation of a potentially non-canonical autophagy during VACV infection. Additionally, VACV genes that could be responsible for the inhibitory phenotype of virulent-strain WR were investigated.

5.1 STING is essential for MVA-induced activation of autophagy

To understand how the cGAS-STING pathway for type I IFN production affects autophagy during VACV infection cell type independently (**Figure 4**) (92, 94, 138, 227, 246), MEF cGAS-KO and STING-KO along with WT cells were infected with MVA or WR or treated with cGAMP or rapamycin (**Figure 7**). The lack of cGAS inhibited the activation of both pathways during MVA infection; however, treating cGAS-KO cells with cGAMP-induced LC3 lipidation and the phosphorylation of STING, TBK1, and IRF3. In STING-KO cells, neither infection with VACV nor treatment with cGAMP or rapamycin induced the cGAS-STING pathway for type I IFN production, and rapamycin treatment was the only condition that enhanced the level of LC3-II and triggered the phosphorylation of TBK1 simultaneously.

The effect of introducing cGAMP to activate STING and the other downstream proteins is understandable since it is the natural activator of STING, even if it is supplied exogenously (101–103). Moreover, cGAS was necessary for both the activation of the cGAS-STING pathway for type I IFN production and autophagy upon MVA infection, suggesting that dsDNA plays a crucial role in the activation of both pathways upon MVA infection. The ability of rapamycin to trigger TBK1 phosphorylation has already been described; however, P-TBK1 has previously been observed upon rapamycin treatment together with poly(I:C) or LPS. Moreover, rapamycin inhibits mTORC1, which leads to the suppression of TLR3-induced IFN-β production by interfering with the translocation of IRF3 from the cytoplasm to the nucleus (202). Thus can also regulate TLR3-mediated cytokine production through the inhibition of phosphorylation of the mTOR pathway (247). Some studies have used mice that contain a missense mutant allele of *Sting*, also called *Goldenticket* mice, in which STING is unable to function and type I IFN expression cannot be induced upon stimulation (92, 248). Considering the finding that treating STING-KO cells with cGAMP did not restore the activation of the autophagy and cGAS-STING pathways from my experiments, and also those of Dai *et al.* and Yamashiro *et al.* regarding non-functional STING, the presence of a 'mobile' STING is likely to be essential for the induction of these mechanisms during MVA infection. This hypothesis was further supported by the outcome of GCA treatment of MEF WT cells during VACV infection (**Figure 15**). GCA is a reagent that interferes with cellular trafficking between the ER and the ERGIC by disassembling the Golgi and trans-Golgi network. MVA-infected cells treated with GCA were unable to activate the cGAS-STING pathway for type I IFN production or autophagy. This result is in line with previous findings, where blocking STING trafficking from the ER to the ERGIC also resulted in the impaired activation of the cGAS-STING pathway for type I IFN production and autophagy upon various types of dsDNA treatment (148, 249). Moreover, Gui *et al.* observed that STING could directly interact with LC3 through the LIR domain at the ERGIC (148), while the ERGIC was already recognised as a key source for phagophore upon autophagosome formation (177). According to these observations, it is highly possible that the ERGIC is the origin of the autophagosome during MVA-induced, STING-dependent, non-canonical autophagy activation. Furthermore, the varying levels of cGAS in STING-KO cells (**Figure 7**) could be explained by how the cells, displaying reduced levels of cGAS were treated (VACV infection or cGAMP/rapamycin treatment) and by the lack of stabilising feedback response from STING. Previous studies have demonstrated that cGAS is strongly activated upon infection and also degraded to prevent the prolonged

expression of type I IFN (250, 251), which could account for its low level during MVA infection in STING-KO cells. Additionally, WR could interfere with the stability of cGAS, as described in research on the Dengue or Chikungunya viruses, to circumvent type I IFN production (252, 253). In the case of rapamycin-treated STING-KO cells, a high possibility exists that rapamycin-induced canonical autophagy could interfere with cGAS through Beclin1 (117), which leading to the reduced cGAS level in this experiment.

In addition, TBK1-KO and IRF3-KO MEF cells were compared with WT samples determine the influence of the proteins, which are downstream of STING in the cGAS-STING pathway for type I IFN production, on the activation of autophagy upon VACV infection (**Figure 8**). In TBK1-KO cells, no P-STING was detected upon MVA infection or cGAMP treatment, although LC3 lipidation was visibly enhanced, just like upon rapamycin treatment. In IRF3-KO cells, the levels of activation for autophagy and cGAS-STING pathway for type I IFN production were comparable to WT cells, except downstream TBK1, when naturally there was no P-IRF3 upon any treatment. The finding that STING could not be phosphorylated when TBK1 was not present in the cells, supports Liu *et al.*'s results, as they experienced similar outcomes regarding the phosphorylation of STING for type I IFN production in HEK293T cells after cGAMP treatment. Crucial to mention is that HEK29T cells lack STING – unlike the parental HEK293, cells which have a high expression level for the protein, but in this study mouse STING was introduced into these human cells through a lentiviral vector (254). On the other hand, Balka *et al.* observed STING phosphorylation in immortalised murine bone marrow-derived macrophages lacking TBK1 upon cGAMP treatment (255).

The aforementioned results indicate how different mechanisms of action develop based on the functions of distinct cell types (e.g., fibroblasts vs. monocytes). Based on this statement, I propose that seemingly in MEF cells, STING cannot be phosphorylated without TBK1, or maybe P-STING is not stable, which was not the case in immortalised murine bone marrow-derived macrophages. To clarify this, different loss of function mutation of TBK1 (e.g., unable to interact with STING, immobile, or a defect on its phosphorylation/activation site) should be generated in MEF cells; then, the phosphorylation of STING upon stimuli should be monitored. Studies have demonstrated that mice with a STING mutation on serine 365/366 to alanine could no longer bind IRF3, which prevented I IFN expression. However, autophagy induction was undisrupted when agonistic stimuli were used. In addition, mice with a STING mutation at the C-terminal tail, which rendered the protein unable to bind TBK1, still exhibited evidence of autophagy activation (255, 256). Since cells lacking TBK1 or IRF3 could still produce elevated

levels of LC3-II during MVA infection, autophagy activation is independent of type I IFN expression but strongly relies on the presence of cGAS and STING. My results also suggest that STING has additional functions executed by a pathway that diverges before the phosphorylation of IRF3, or even TBK1. For example, the possibility that STING interacts directly with LC3 upon MVA infection could not be excluded during my experiments; however, it has been observed in other studies during treatment with cGAMP or poly(dA:dT) or upon HSV1 infection (147)(225). Moreover, cGAS plays a critical role beside STING, since it contributes to the activation of both autophagy and the STING pathway for type I IFN production upon MVA infection. On the other hand, a recent study described a direct interaction between cGAS and LC3 through their LIR domains to clear micronuclei upon genotoxic stress (257). To investigate whether cGAS directly interacts with LC3 upon MVA infection to activate autophagy, further experiments are necessary. Overall, MVA-induced STING-dependent autophagy can be considered a non-canonical form of autophagy activation.

5.2 MVA-induced activation the cGAS-STING pathway for type I IFN production and for non-canonical autophagy is dependent on Beclin1 and downstream proteins in contrast to cGAMP-induced activation

Autophagy is a complex process composed of clustered and sequentially interacting protein-protein complexes. All major complexes were inspected in this study to investigate which canonical autophagy-associated proteins play active roles in non-canonical autophagy during MVA infection. First, the initiation complex was examined using ATG13-KO MEF cells (**Figure 9**). MVA infection and cGAMP treatment were both able to induce the cGAS-STING pathway for type I IFN production and activation of autophagy, but cells incubated with rapamycin were unable to trigger LC3 lipidation. This finding indicates that MVA- and cGAMP-induced autophagy activation is independent of ATG13. It is unclear why ATG13-KO cells displayed decreased STING levels, since no study has investigated this effect. It is possible that ATG13, in addition to its well-known functions during canonical autophagy (258), has a previously unknown stabilising ability on STING by anchoring it into the ER, but this hypothesis must be further investigated in future studies. I attempted to use ULK1/2-KO MEF cells to thoroughly investigate this complex (**Supplementary figure 3**), but since we could not find any explanation for why rapamycin-treated ULK1/2-KO cells could activate LC3 lipidation, this direction was not pursued further. Nevertheless, other studies have

described ULK1/2 as dispensable for STING-dependent autophagy activation (147, 148) or even as a negative regulator of the cGAS-STING pathway (124), but they have found ATG13 to be indispensable for canonical autophagy initiation and to be able to act independently of ULK1/2 (239). The outcomes observed in my study after MVA infection in ATG13-KO cells suggest a non-canonical autophagy pathway that is independent of ATG13, an essential member of canonical autophagy activation.

For the investigation of the nucleation complex, Beclin1-KO MEF cells were compared with WT cells (**Figure 10**). Since the baseline level of LC3-II was already high in mock-infected cells, MVA infection could not induce strong LC3 lipidation, nor surprisingly the phosphorylation of STING, TBK1 or IRF3 in Beclin1-KO cells. On the other hand, cGAMP treatment led to P- STING, P-TBK1 and P-IRF3, while rapamycin treatment triggered an increase in LC3 lipidation in Beclin1-KO cells compared with similarly treated WT cells. Some studies have found that Beclin1 is not necessary for STING-dependent autophagy activation, as is VPS34 (147, 148), or that it negatively regulates cGAS to prevent prolonged type I IFN expression (117). However, the high baseline level of LC3-II observed in mock-infected Beclin1-KO MEF cells has not been seen before. Moreover, the lack of enhanced LC3 lipidation and the absence of phosphorylated members of the cGAS-STING pathway during MVA infection compared with cGAMP treatment suggests that the activation of both mechanisms during MVA infection is dependent on Beclin1, which is contrary to the findings of the aforementioned studies (e.g., decrease of Beclin1 leads to enhanced cGAS activity). Noteworthily, when MEF WT cells were treated with 3MA (a reagent that inhibits the nucleation complex and canonical autophagy) during MVA infection, MVA-induced activation of the cGAS-STING pathway for type I IFN production and for autophagy was still successful (**Figure 15**). This finding was rather unexpected because our laboratory previously indicated that using 3MA on MVA-infected BMDCs significantly reduced CD4+ T cell activation through MHC-II presentation (94). One explanation could be that the previously observed MVA-induced STING-dependent activations of type I IFN production and autophagy are dependent on the presence of only Beclin1 from the nucleation complex, while all other members of the complex are expandable in this case. Beclin1 is a scaffold protein (163) that was proven to interfere with cGAS activation to halt type I IFN production (117); however, its presence might be essential for stabilising cGAS to ensure its DNA-binding ability or NTase enzymatic activity (cGAMP synthesis) upon MVA infection in a way that remains unclear. To uncover the truth regarding this possible interaction between Beclin1 and cGAS, the generation

of KOs for other members of the nucleation complex, as well as loss of function mutants for Beclin1 infected with VACV, will be necessary in the future. As an additional finding, rapamycin seemed to induce a type of autophagy that was only dependent on the initiation complex (**Supplementary figure 4**), while the nucleation complex was not necessary in MEF cells. Li *et al.* used murine macrophage cells to demonstrate that rapamycin induced the LC3-associated phagocytosis (LAP) of *Bukholderia pseudomallei* independently of Beclin1. However, when the process was induced by starvation, the presence of this protein was necessary (259). This finding could indicate that the MVA-induced autophagy pathway is fundamentally different from rapamycin- or even cGAMP-induced autophagy activations.

For the expansion and elongation complex, ATG12-KO MEF cells were compared with WT samples **(Figure 11**). Based on the observed lack of P-STING, P-TBK1, P-IRF3, and enhanced LC3-II in MVA-infected ATG12-KO cells, MVA-induced activation of the cGAS-STING pathway for type I IFN production and for autophagy is heavily dependent on the presence of ATG12; however, this was not the case for cells treated with cGAMP (adjusted according to the information sheet from the manufacturer) or rapamycin. Research demonstrated that to activate STING-dependent autophagy, ATG5 is necessary after transfection with Flag-STING (147) or upon HSV infection (148). Moreover, since ATG12 forms a conjugate with ATG5 upon stimuli by poly(dA:dT) or cGAMP, the results of the present study are in line with the observations of the aforementioned work groups of Liu and Gui. Significantly, this result once again demonstrates the differences between MVA infection and cGAMP treatment for activating the cGAS-STING pathway for type I IFN production and autophagy, as also indicated in Beclin1-KO MEF cells. Vital to note is that Fischer *et al.* presented evidence of the formation of a STING-induced single-membrane vesicle, which includes LC3B via ATG16L1, a protein that forms a complex with the ATG12-ATG5 conjugate upon activation (225). To determine whether the formed autophagosomal vesicles in this study are similar to those observed by Fischer *et al.,* the autophagosomes formed during MVA-induced STING- and Beclin1-dependent autophagy activation must be investigated further through, for example, electron microscopy. For rapamycin-treated ATG12-KO MEF cells, the observed phenotype was the opposite of what Rangaraju *et al.* observed *in vivo* in neuropathic mice (260), which again suggests the relevance of the choice of cell types for the experimental outcome.

To investigate the last stage before autophagosomal membrane sealing, ATG7-KO and ATG3-KO MEF cells were compared with WT samples (**Figure 12**). Since both ATG7 and ATG3 are essential for the conjugation of PE to LC3, the cGAS-STING pathway for type I IFN

production was activated in KO cells in a similar manner to that seen in WT cells upon MVA infection and cGAMP treatment. Interestingly, the total level of STING seemed to be reduced in ATG3-KO cells; however, the phosphorylated forms of STING, TBK1, and IRF3 were not influenced. In one study, the researchers observed no impact on STING degradation when ATG3 was silenced with siRNA and stimulated with DMXAA (261), whereas another group reported that MEF cells lacking ATG3 displayed delayed STING degradation upon DNA stimulation (197). The present study did not examine the level of STING for more than 4 h upon VACV infection in ATG3-KO MEF cells. Since the total level of STING decreased but the amount of P-STING was unchanged in these cells, investigating the relationship between ATG3 and STING further is critical. On the other hand, LC3 lipidation was completely absent due to the lack of either of these two indispensable proteins for autophagy in the respective KO cells. This finding is in line with a study that treated ATG3-KO THP-1 cells with dsDNA and also observed the lack of LC3 lipidation and undisturbed phosphorylation of TBK1, although P-TBK1 remained stable longer. This was most probably due to the fact that autophagy was disrupted in ATG3-KO cells, which otherwise would have removed this activated protein from the cells (197). Moreover, according to a recent review that focused on all of the known binding features and functions of ATG3 (262), the lack of ATG3 may quite possibly have an impact on the stability of the ATG7 protein.

To confirm how the selective autophagy receptor p62 influences the cGAS-STING pathway for type I IFN production and for autophagy activation during VACV infection, p62-KO MEF cells were compared with MEF WT cells (**Figure 13, Supplementary figure 6**). MVA-infected p62-KO cells exhibited a massive increase in protein levels for LC3-II, P-STING, P-TBK1 and P-IRF3 after 4-h infections, but also for cells infected overnight. This result indicates that without p62, these proteins were either increasingly produced and/or accumulated and were not properly removed from infected cells which could lead to extensive and harmful type I IFN expression in the end. This finding is in line with previous studies that have described p62 as an inessential protein for STING-dependent autophagy and type I IFN expression but an important regulator of the cGAS-STING pathway (147, 148, 197). In addition, a recent publication suggested that virulent VACV can evade autophagy activation by targeting selective autophagy receptors, such as p62, NDP52 and Tax1Bp1 (224).

5.3 WR inhibits a non-canonical, STING-dependent autophagy pathway upstream of STING

Since none of the CRISPR-Cas9-generated KO cell lines had the ability to interfere or reverse the WR-inhibited cGAS-STING pathway for type I IFN production and for autophagy, MEF WT cells were treated with various reagents that affect canonical autophagy and the cGAS-STING pathway for type I IFN production during VACV infection. Treatment with the canonical autophagy inducers rapamycin and CQ seemed to reduce the activation of the cGAS-STING pathway for type I IFN production upon MVA infection (**Figure 14**), which is in line with a previous study. Said study described rapamycin as being able to enhance the phosphorylation of TBK1, although this elevated level was unable to induce the phosphorylation of IRF3 (247). A different study described that rapamycin treatment for inhibiting mTOR led to the reduced expression of STING, P-TBK1, and IRF3, as well as IFN-α production in lupus monocytes (263). Moreover, during a screening of antimalaria drugs, CQ was found to diminish IFN-β production by interfering with cGAS-dsDNA interactions (264). On the other hand, both of these reagents were barely able to increase LC3 lipidation during MVA infection compared with reagents-treated but mock-infected cells. This finding could suggest that the combination of rapamycin or CQ and the applied MOI 10 of MVA, which was determined before through increasing amounts of MVA (with an MOI of 1 to 20) (**Figure 5**), might activate both canonical and non-canonical autophagy simultaneously; however, MVA-induced activation non-canonical autophagy is highly efficient without the need for the activation of canonical autophagy. In fact, without further investigation, I cannot exclude the possibility that MVA-induced non-canonical autophagy activation represses canonical autophagy to, for example, avoid interference with the cGAS-STING signalling. This statement also applies to the MVA-induced activation of the cGAS-STING pathway for type I IFN production, since cGAMP or DMXAA treatments failed to raise the level of LC3-II or P-STING, P-TBK1, and P-IRF3 higher (**Figure 14**). Treatment with reagent to stop proteasomal degradation (epoxomicin) upon MVA infection led to similar levels of LC3 lipidation and phosphorylation of STING, TBK1, and IRF3 as those seen in MVA-infected only cells (**Figure 15**). This suggests that proteasomal degradation during the early period of MVA infection is not necessary for the activation of the cGAS-STING pathway for type I IFN production and autophagy activation. By contrast, it plays a crucial role in the processing and presentation of late viral antigens (229).

In addition, although WR infection was found to inhibit autophagy, both rapamycin and CQ induced significant LC3 lipidation when applied to cells infected with WR (**Figure 14**). Rapamycin targets mTOR and has an effect on the autophagy initiation complex, while CQ prevents the acidification and destruction of the cargo in autophagolysosomes. Thus, these two reagents activate canonical autophagy, whereas WR inhibits the activation of non-canonical autophagy and is unable to interfere with the canonical pathway. This also means that WR does not enhance mTORC1 activity or interfere with the acidification of autophagolysosomes. Moreover, WR infection almost completely blocked the phosphorylation of STING and other proteins involved in downstream signalling upon cGAMP treatment but was unable to do so when cells were treated with DMXAA. This result is in line with the findings of Eaglesham *et al.*, who identified poxins as a family (including the gene B2R) that is able to destroy 2′,3′-cGAMP, the natural second messenger of STING (140). Although poxins enable WR to disrupt cGAS-STING signalling by destroying cGAMP, it seems that these early expressed genes are essential for the WR-mediated inhibition of the cGAS-STING pathway for type I IFN production and autophagy; however, other genes might also contribute to this task, since there were slight increases in LC3-II, P-STING, P-TBK1, and P-IRF3. Nevertheless, the possibility that the amount of exogenous cGAMP applied during treatment, which is certainly higher than what is physiologically produced by cGAS upon viral infection, was more than what B2R could destroy, cannot be excluded without further investigation. In addition, the observation that WR was unable to inhibit the effect of DMXAA treatment could stem from the fact that this compound is an artificially manufactured antitumor drug (265), meaning that WR never had the opportunity to develop a countermeasure against it, as the virus did against cGAMP. By combining the results of the autophagy and cGAS-STING pathway activators, it seems that WR does not inhibit the canonical autophagy pathway, but rather interferes with a STING-dependent route due to the existence of poxins.

5.4 The induction (MVA) or inhibition (WR) of the cGAS-STING pathway for type I IFN production and autophagy originate from viral gene(s) already expressed during entry or latest at early gene expression

To understand the mechanisms of MVA-induced and WR-inhibited activation of cGAS-STING signalling for type I IFN production and non-canonical autophagy, it was essential to confirm that no late-expressed gene plays a role in the process. Using confocal microscopy,

specific autophagy-reporter cells (HeLa-DLG) were infected with MVA or WR and then monitored over time for the production of LC3-II-related signals (**Figure 6**). The results demonstrated that LC3 lipidation started at the same time as MVA-expressed GFP was detected in infected cells at 1 hpi. Moreover, non-infected bystander cells close to infected ones exhibited elevated LC3-II signals. On the other hand, cells infected with WR only displayed the first DsRed-LC3-II markers of autophagy activation after 6 hpi without influencing bystander cells. Studies have described DC maturation in bystander cells during MVA infection (95) and demonstrated that WR can affect and block DC maturation in bystander cells (266). This type of horizontal communication between infected and bystander cells has also been documented after studies have tracked the distribution of the second messenger cGAMP in the cGAS-STING pathway at the cellular level (104, 267). Moreover, in regard to autophagy, studies have reported its induction in bystander cells upon radiation (268, 269) but not after viral infection. Based on the aforementioned research, it is possible that during MVA infection, the trigger that induces cGAS-STING signalling for type I IFN production and for non-canonical autophagy activation is primarily available or expressed early in the infected cells, and that this substance (or part of it) can be transferred to bystander cells in close proximity, such as dsDNA.

To ensure that no late-expressed genes play a role in the MVA-induced and WR-inhibited activation of the cGAS-STING pathway for type I IFN production and non-canonical autophagy, WT MEF cells were treated with AraC during VACV infection (**Figure 16**) to block viral replication and late gene expression. AraC treatment did not influence the effects of MVA-induced or WR-inhibited activation of cGAS-STING signalling for type I IFN production or non-canonical autophagy. This result is in line with those of previous studies that have only investigated the cGAS-STING pathway for type I IFN production (227, 246). It also means that viral replication or late gene expression has no role in the MVA-induced or WR-inhibited activation of cGAS-STING signalling for type I IFN production or non-canonical autophagy.

Since neither MVA nor WR rely on viral DNA replication or late gene expression to achieve said activation/inhibition, as determined by the AraC experiment, PUVA treatment was applied to block the viral replication cycle already at the stage of early gene expression (**Figure 17**). Cells infected with MVA were not affected by the PUVA treatment, while WR was unable to inhibit the cGAS-STING pathway for type I IFN production or non-canonical autophagy. This finding indicated the requirement of early gene products to block cGAS-STING signalling for

type I IFN production and non-canonical autophagy. Similar results have been documented for PUVA treatment during VACV infection, but again, only the cGAS-STING pathway for type I IFN production has been examined (227, 246). Moreover, Waibler *et al.* observed a higher level of IFN-β expression *in vivo* when MVA was irradiated with UV light; however, according to the phosphorylated protein levels of members of the cGAS-STING pathway for type I IFN production, this outcome did not occur with an *in vitro* setup in the present study. These findings again suggest how different circumstances can alter the outcome of similar experiments. Moreover, WR seems to rely on early gene products to interfere with the activation of cGAS-STING signalling for type I IFN production and non-canonical autophagy.

Another approach for interfering with the viral entry and early gene expression of VACV was the use of high temperatures (42 °C and 56 °C for 1 h) to inactivate the viruses (**Figure 18**). By incubating VACV at 56 °C for 1 hour prior to infection, the secondary structures of viral proteins are denaturated (240), which leads to impaired initiation of cell entry, as well as to limited or no viral early gene expression. At 40 – 42 °C, viruses lose infectivity but they are still viable (270). Incubation at 42 °C had no effect on the viruses according to the LC3-II, P-STING, P-TBK1, and P-IRF3 proteins, though inactivation at 56 °C resulted in a major change in LC3 lipidation and phosphorylation of STING, TBK1, and IRF3 for both MVA and WR. MVA inactivated at this temperature was unable to induce the activation of the cGAS-STING pathway for type I IFN production and for non-canonical autophagy, while infection with inactivated WR was closer to the untreated MVA-infected cells. The result for MVA is both surprising and controversial: in an earlier study, Dai *et al.* demonstrated that after MVA was inactivated at 55 °C for 1 h, it produced an even higher level of type I IFN expression through the cGAS-STING pathway, in addition to producing other proinflammatory cytokines and chemokines (271). These opposing outcomes could have resulted from the different cell types used (the previous study used B16-F10 melanoma cells, while the current study used MEF cells). In regard to the infection with WR inactivated at 56 °C, studies have demonstrated that heat-inactivated virulent VACV induces high levels of TNF and type I IFN through the cGAS-STING pathway (272, 273). Interestingly, Cao *et al.* confirmed that infection with heat-inactivated WR results in high expressions of TNF and IFN-α, but treatment with increasing amounts of PI3K and Akt inhibitors reversed this effect. These results also support the theory that WR is able to inhibit a non-canonical, STING-dependent autophagy pathway that is dependent on the nucleation complex as well as other downstream members of the canonical autophagy pathway. However, the most likely possibility is that the genes responsible for

inhibition by WR had to already be expressed during viral entry and were then deformed due to heat, rendering them unfunctional, or these genes must be expressed by early genes during the uncoating process. The other possibility, based on the faint VACV protein, is that these genes are expressed as early genes immediately after entry.

5.5 WR B2R, A10L, and A18R gene products might be responsible for WR-inhibited activation of the cGAS-STING pathway for type I IFN production and non-canonical autophagy during the early-phase of WR infection

After confirming that the WR genes essential for inhibiting the non-canonical, STING-dependent autophagy pathway had been expressed early, the next step was to focus on the identification of the responsible gene(s). A previously published siRNA silencing screen with 80 conserved WR genes (232) was used in the following two ways: high-content CLSM (**Supplementary figure 9**) was used in London and FACS screening (**Figure 19**) was performed in our lab. After comparing the top candidates from both screening methods (**Figure 20**) and reviewing literature (140), six genes (A10L, A18R, B5R, B13R, C10L, and B2R) were selected (**Table 1**) because they were either missing from the MVA genome or they had five or more mismatches at the protein level between the MVA and WR genome sequences. The reason for MVA-WR-co-infected cells displaying strong autophagy activation through DsRed signals during FACS analysis may stem from the differences in methodologies and sensitivities differences of the approaches used (immunoblotting, FACS, and high-content CLSM). In the field of biology, there are constant debates regarding the question of which techniques should be trusted to achieve decisive outcomes (274–276) as well as attempts to improve already existing ones (277).

After selecting the most promising gene candidates, recombinant MVA viruses were generated, in which the selected WR genes with their promoter-like upstream DNA sequences were introduced to their orthotopic position within the MVA sequence. The protocol for generating recMVAs was optimised according to already published methods (231, 233, 234, 242). During the course of recMVA generation, when the I-*Sce*I-kanamycin cassette (Kana) was introduced into the target genes, C10-pcDNA3.1 was unable to fully ligate with the previously amplified, digested, and purified insert containing the cassette (**Figure 22**). All restriction enzymes were specifically selected for each gene of interest, amplified sequences with Kana were confirmed

on agarose gel prior to purification, and the ratio of insert:vector was adjusted according to the succession rate after each attempted ligation. Since there was no clear reason for why C10-pcDNA3.1 was unable to ligate with Kana, the decision was made that C10L should be cloned into deletion VI of MVA instead of its natural locus. A similar compromise was made after multiple failures during the first recombination of the B13-construct (**Figure 23**). From the beginning of the cloning process, a smaller second band always appeared when the B13 sequence was amplified (**Figure 21**). Initially, the primers were suspected of repeatedly binding to the target, but this possibility was ruled out after checking the sequences. Unfortunately, there was no clear explanation for why these two constructs failed during the cloning process; therefore, this must be investigated further.

After amplifying the recMVA virus stocks (the final names are MVA-VV-A10, MVA-VV-A18, MVA-VV-B2, and MVA-VV-B5), due to a lack of time, viruses were used only once to infect WT MEF cells for 4 h (**Figure 25**) or 24 h (**Figure 26**) with or without AraC treatment. Unfortunately, when immunoblotting the proteins from cells derived from the 4-h infection experiment, LC3-II for the control MVA-infected cells was less prominent than before (**Figure 26A**). This result could be due to insufficient blotting. Furthermore, cells infected with the recMVA virus expressing the WR B5R gene (MVA-VV-B5) displayed similar levels of LC3-II, P-STING and P-TBK1 compared with those previously seen during the control MVA infection. On the other hand, MVA-VV-B2 was able to inhibit STING phosphorylation regardless of the presence of AraC during infection, which is an outcome similar to that described by Eaglesham *et al.*, namely that VACV poxin degraded 2′3′-cGAMP and blocked interaction with STING (140). Unfortunately, P-IRF3 staining did not work, so it is unclear whether the cGAS-STING pathway is activated until type I IFN expression occurs; however, TBK1 seemed to have been successfully phosphorylated. To confirm that the activation of cGAS-STING signalling leads to type I IFN production upon infection with recMVA viruses, further investigations are necessary, such as ELISA analyses of infected cells. IFN-independent STING signalling was documented during HSV-1 infection in mice harbouring a mutation in STING in which serine 365 is changed to alanine in the C-terminal tail. This mutation led to the loss of type I IFN production through the cGAS-STING pathway, although it surprisingly made these mice resistant to HSV-1 infection (248). Since MVA-induced non-canonical, STING-dependent autophagy, the fact that MVA-VV-B2 was able to stop the phosphorylation of STING but not that of TBK1 and decreased LC3 lipidation compared with MVA WT demonstrates that B2 is necessary for WR to interfere with the activation of the cGAS-STING

pathway for type I IFN production and non-canonical autophagy, but possibly in cooperation with an as yet unknown gene product. It is also possible that the B2R gene product accelerates the degradation of P-STING, which would explain how TBK1 was phosphorylated without visible P-STING. In addition to the recMVA virus expressing WR B2R (MVA-VV-B2), MVA-VV-A10 and -A18 exhibited markers of decreased autophagy activation. Until now, studies using VACV containing mutations in the A18R gene have demonstrated that this gene acts as a negative transcription elongation factor (278–280) while revealing nothing about its effect on the cGAS-STING pathway for the type I IFN production and activation of non-canonical autophagy. As in the case of A18, only its interaction between the core proteins A3, A10, and L4 have been investigated (281) without examining any possible effects on LC3 lipidation or type I IFN expression. Furthermore, A10L has been identified as a late gene, and therefore, it is possible that an early expressed precursor form of A10 could affect autophagy (63, 241). Crucial to mention is that these experiments were only conducted once due to a lack of time, and thus, no definitive conclusions can be drawn based on this result. This experiment should be repeated and the recMVAs further investigated to confirm the aforementioned statements.

Regarding the 24-h-infected cells, it is understandable that mock-infected AraC-treated cells exhibited a certain upregulation of LC3 lipidation since the reagent affected not only viral but also cellular DNA replication and late gene expression (**Figure 26B**). My results confirmed that after 6 hpi, cells started to exhibit LC3 lipidation when infected with WR (**Figure 6**). Given this finding, it was unsurprising to observe that 24 hpi cells infected with WR had similar levels of LC3-II to the MVA-infected cells. In addition to WR, MVA-VV-B5 infected cells were similar to the MVA WT-infected cells for the activation of the cGAS-STING pathway for type I IFN production and for non-canonical autophagy independently of the presence of AraC. Moreover, MVA-VV-B2 infected cells again exhibited no P-STING and revealed a reduced level of P-TBK1 compared with the MVA WT-infected cells, regardless of AraC treatment. This result could indicate that P-TBK1, as seen during the 4-h infection, is degraded to prevent further stress on the infected cells. One study described suppressor of cytokine signalling 3 (SOCS3) as an endogenous negative regulator of TBK1 by promoting the proteasomal degradation of the protein (282). Another explanation could be that the B2 gene has another – as yet unknown – function and could thus interfere with TBK1 activation. The LC3-II in cells infected with MVA-VV-B2 were similar to WR-infected cells, which indicated that the inhibition of the non-canonical, STING-dependent autophagy pathway was no longer present at 24 hpi. Interestingly, cells infected with MVA-VV-A10 and -A18 exhibited a clear decrease

in P-STING and LC3-II upon AraC treatment. Given the reduced phosphorylated STING and LC3 lipidation in the presence of AraC both A10 and A18 seemed to be more noticeably affected by the activation of the cGAS-STING pathway for type I IFN production and for non-canonical autophagy at 24 hpi; however, I am unable to exclude the possibility that LC3-II and P-STING were reduced due to the accumulation of proteins or the toxicity of AraC, leading to the exhaustion of the activated forms of LC3 and STING. Since A18 is described as an early/late gene, while A10 is a late gene, these are the exact opposite effects, which were expected based on the screening results after these WR genes were silenced. On the other hand, strong P-TBK1 was detected for cells infected with the recMVA viruses, which were as robust as the similarly infected and treated cells infected for 4 h. This could mean that type I IFN production was still triggered or that TBK1 was activated through a STING-independent pathway. Viral RNA can activate TBK1 STING-independently through TLR3-TRIF or RIG-I-MAVS signalling, which could lead to the activation of the NF-κB pathway and pro-inflammation, or type I IFN production through IRF3 (254, 283). Different from my expectations, A10 and A18 – as late and early/late genes, respectively – appeared to contribute to the activation of both mechanisms during the later period of WR infection. Since WR lost its ability to inhibit autophagy at 6 hpi (**Figure 6**), the idea that these two genes could play a role in this process must be further investigated.

5.6 Conclusion

In conclusion, the results of this study suggest that MVA-induced STING-dependent but ULK1- and PI3K-III complex-independent non-canonical autophagy activation is different from cGAMP-induced type I IFN production and autophagy activation. My data indicated no activation of the cGAS-STING pathway for type I IFN production or for non-canonical autophagy activation in the absence of Beclin1 or cGAS, which raises the possibility of an unidentified stabilising interaction between cGAS and Beclin1 during MVA infection. In addition, when cellular trafficking was chemically blocked and STING was unable to travel from the ER towards the ERGIC, ATG12- and ATG7-dependent LC3 lipidation was also affected. This supports the idea that STING, through the ERGIC, may provide the phagosome source for autophagosome formation upon MVA infection (**Figure 27**).

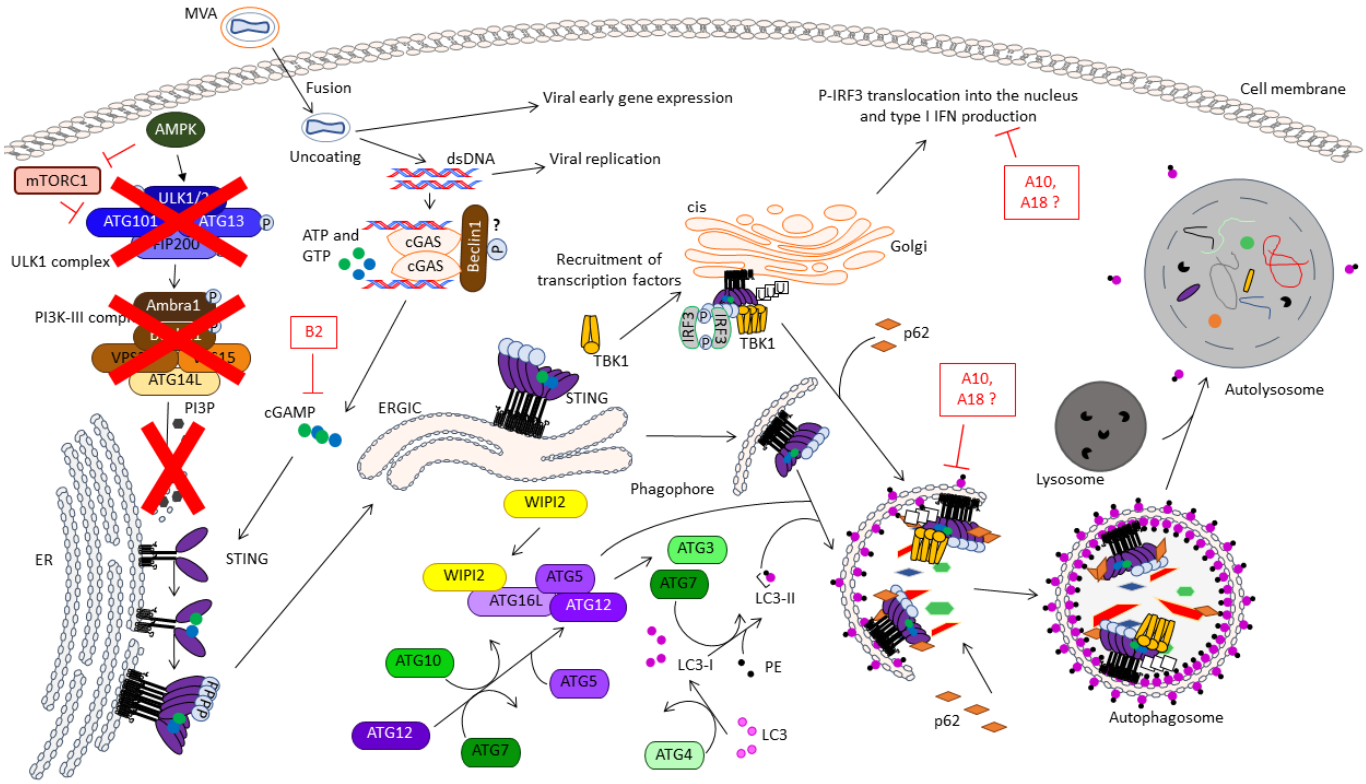

Figure 27. Model of MVA-induced STING-dependent but ULK1- and PI3K-III complex-independent non-canonical autophagy activation according to this study's findings. P = phosphorylation, U = ubiquitination. B2, A10 and A18 are WR gene products.

Moreover, my data indicate no phosphorylation of STING but elevated LC3 lipidation in TBK1-KO MEF cells, which suggests that P-STING is only stable for a short period in the absence of TBK1 in MEF cells. I also observed that p62 was not essential for MVA-induced, STING-dependent, non-canonical autophagy activation, but it played a critical role in removing the activated P-STING:P-TBK1 complex through autophagy to prevent prolonged type I IFN expression. On the other hand, I observed WR-induced inhibition of cGAS-STING signalling for type IFN production and for non-canonical autophagy to be managed through early gene products or through early genes already expressed during the uncoating process witnessed upon PUVA treatment and heat inactivation. I observed the most prominent inhibition after infection for recombinant MVA expressing B2R, but perhaps A10L and A18R also play a role in inhibiting the activation of non-canonical autophagy beside B2R – but only during the early phase of the WR infection. Although the findings for the generated recombinant MVA expressing WR A10 and A18 genes were not entirely in line with my original expectations, they demonstrated the importance of investigating the possibility that viral genes that are fully expressed during the late phase of infection could affect cellular mechanisms in their early

expressed precursor form at the early period of infection. The findings also open up more possibilities for future research to determine how viruses influence infected cells.

6 Appendix

6.1 Supplementary information for the generation of CRISPR-Cas9 KO cells

6.1.1 Supplementary materials for CRISPR-Cas9 KO cell generation

6.1.1.1 Guide RNAs (gRNAs)

The gRNAs were designed by Cornelia Barnowski, a former PhD student in the lab.

Name	Sequence
ATG7_1	GAAGTTGAACGAGTACCGCC TGG
ATG7_2	AACTCCAACGTCAAGCGGGT GGG
WIPI2_1	GAACAGCAGCTGGCCGGCGC CGG
WIPI2_2	CTAGCTGTTGGTAGTAAGTC CGG
Becn1_1	CCTGGATGGTGACCCGGTCC AGG
Becn1_2	GCCATTTATTGAAACTCGCC AGG
Atg12_1	TGCAGTTTCGCCCGGAACGG AGG
Atg12_2	AATGGGCTGTGGAGCGAACC CGG
vps34_1	GCTCCGAGCTGTCATGGGGG AGG
vps34_2	TCTTGTACTAAACGCCTTGT AGG
TBK1_1	AGACATTTGCAGTGGCCCCC TGG
TBK1_2	GAGGAGCCGTCCAATGCGTA TGG
IRF3_1	GGGCAAAATCCGCGGTTTCG GGG
IRF3_2	GGCCATCAAATAACTTCGGT AGG

6.1.1.2 Cells

Name	Description	Source/Reference
HEK293T	Human embryonal kidney epithelial cells, expresses a mutant version of the SV40 large T antigen	Prof. Dr. Veit Hornung

MEF ULK1/2-KO	MEF CRISPR-Cas9 knocked out for ULK1/2	Dr. Björn Storck

6.1.1.3 Plasmids

Name	Description	Source/Reference
pMD2.G	VSV-G envelope expressing plasmid	Addgene
psPAX2	Packaging plasmid	Addgene
RP-472/-557/-648	Trasnfer plasmid for gRNAs	Prof. Dr. Emmanuel Wiertz

6.1.1.4 Primary antibodies

Antigen	Species	Application	Source/reference
PI3 kinase class III (VPS34) (D4E2)	Rabbit	WB	Cell Signaling
WIPI2 (#8567)	Rabbit	WB	Cell Signaling

6.1.1.5 Reagents

Name	Description	Concentration	Source/reference
Torin1	mTOR inhibitor	3 µM	Invivogen

6.1.2 Supplementary methods for CRISPR-Cas9 KO cell generation

The following methods were performed by Cornelia Barnowski.

6.1.2.1 Production of lentivirus

For transfection, 3.8 x 10^6 HEK293T cells were seeded in a 10 cm petri-dish with 10 ml DMEM supplemented with 10 % FBS the day prior to transfection. The next day 500 µl pure DMEM was mixed with 5 µg pMD2.G, 5 µg psPAX2 and 10 µg RP-557 plasmid containing the gRNA sequence of interest. Then 60 µl PEI (1 mg/ml) was added to the 20 µg DNA mixture, briefly vortexed and incubated for 15 min at RT. Medium of seeded cells was exchanged to serum free medium and after the incubation period, DNA-PEI mixture was added dropwise to the cells.

Transfected HEK293T cells were incubated for 7 h at 37 °C with 5 % CO_2 and then medium was exchanged to DMEM supplemented with 10 % FBS. Cells were further cultivated for 48h at 37 °C until harvest.

To increase viral yield, transfection for each gRNA was performed in duplicate from which harvested supernatants were pooled and centrifuged as described in section 6.1.2.2.

6.1.2.2 Virus isolation

Supernatant of transfected HEK293T cells was filtered (0.45 µm) and either used immediately for transduction or to enrich virus further processed by ultracentrifugation. First, 5 ml 30 % saccharose was filled in polyallomer centrifuge tubes and supernatant was added on top. Tubes were then filled up to their maximum capacity with medium. Ultracentrifugation was performed at 16000 rpm (A621) at 4 °C for 3 h. Then, supernatant was decanted and virus containing pellet was dissolved in 230 µl PBS.

6.1.2.3 Transduction

MEF cells were seeded into a 12-well-plate one day prior to obtain 60 – 70 % confluency on the day of transduction. Either 50 µl of lentivirus enriched by ultracentrifugation and resuspended in fresh medium or the non-ultracentrifuged supernatant with 8 µg/ml polybrene were added per well. The 12-well-plate was centrifuged at 2000 rpm (ST 16R) at 37 °C for 1 h. After spinfection, cells were incubated overnight at 37 °C. The following day, 2 ml of culturing medium was added to diluted polybrene, and cells were further incubated at 37 °C for three days. Afterwards, puromycin selection was started to amplify transfected cells.

This protocol continues in Methods section 3.1.4.

6.1.3 Supplementary results for CRISPR-Cas9 KO cell generation

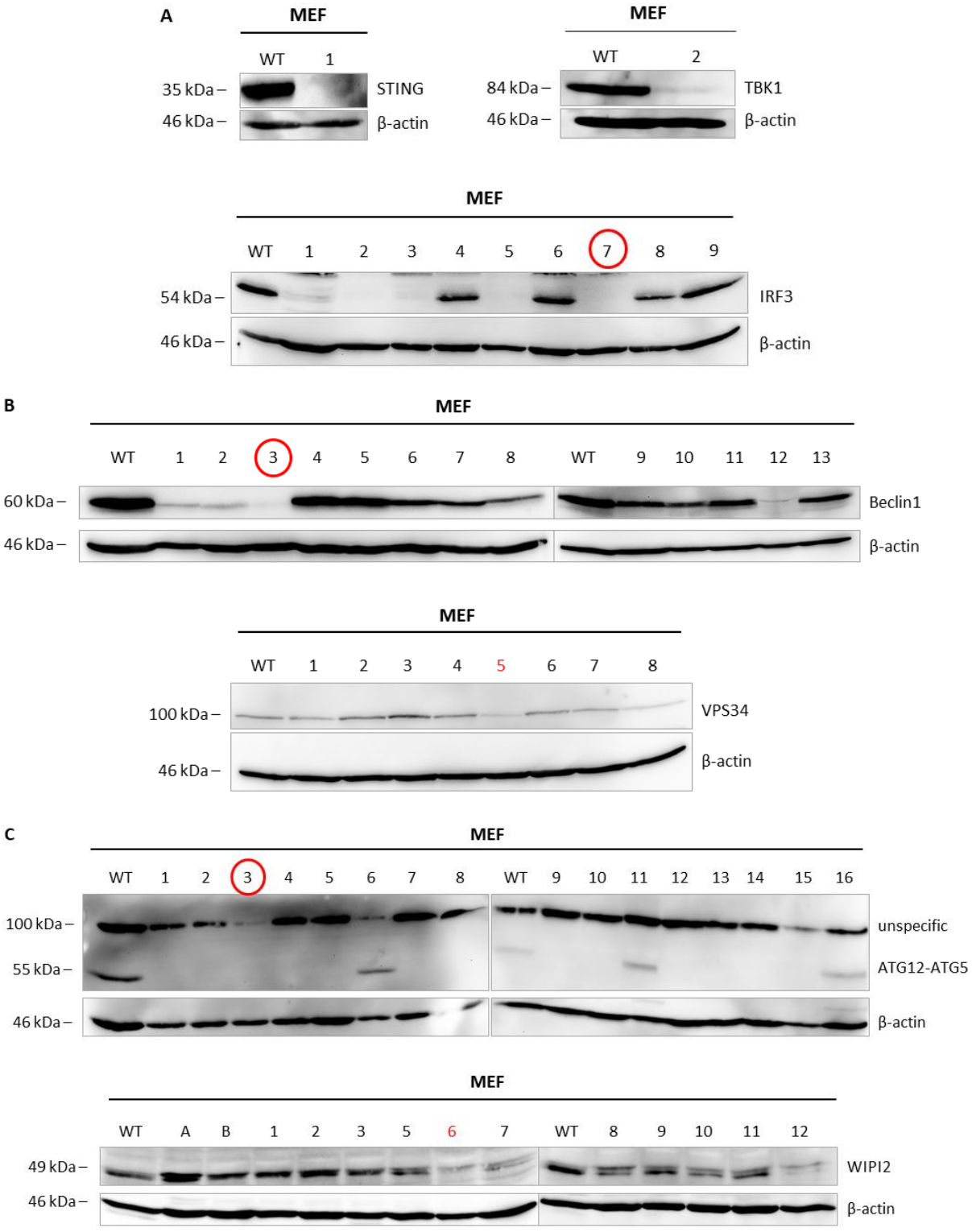

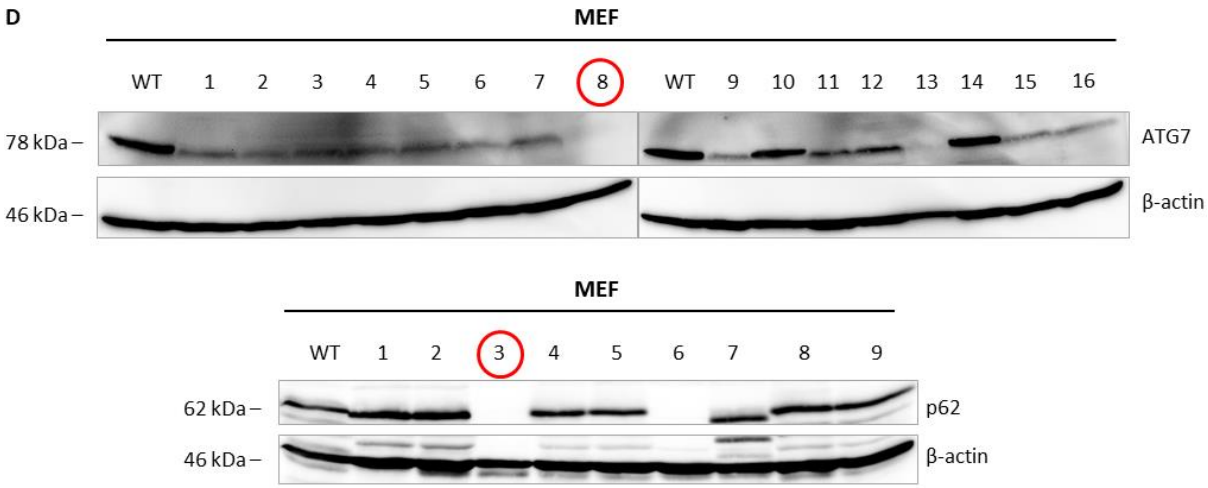

Supplementary figure 1. Generation of MEF-KO cell lines using the CRISPR-Cas9 system and selected clones for expansion and experimental usage. (A) MEF-KO cells for the cGAS-STING pathway for type I IFN production. For STING-KO cells, the bulk population was tested, revealing a complete lack of STING protein. For TBK1-KO cells, only single-cell clone (SSC) 2 survived puromycin selection after transfection and proved to be a KO. For IRF3-KO cells, SSC 3 was selected from all successful SSCs for further use. (B) MEF-KO cells for the nucleation complex of autophagy. For Beclin1-KO cells, only SSC 3 was truly lacking Beclin1 protein. For VPS34-KO cells, SSC 5 was selected originally, but during the experiments this clone reverted to WT VPS34 protein level expression, and therefore, the experimental data of this cell line were excluded from the Results chapter. (C) MEF-KO cells for the ATG12- and WIPI2-complexes. For ATG12-KO cells, SSC3 was selected. After checking SSC for a lack of ATG12 (the information sheet of the used antibody described the 55 kDa protein marker as a complex of ATG12 and ATG5; free ATG12 is rarely visible and would appear around 16 kDa; however, nothing was detected at this small size on the membrane, so this region was cropped off from the picture), SSC 3 was selected based on the phenotype where even the non-allocable – most likely unspecific – protein marker at 100 kDa seemed to be knocked out. For WIPI2-KO cells, SSC 6 was chosen, but just like the VPS34-KO clone it reverted to WT WIPI2 protein level expression; therefore, the data were also excluded from the Results chapter. (D) MEF-KO cells for the lipidation of the ATG8-complex and specific autophagy receptors. For ATG7-KO cells, SSC 8 was selected as one of the two clones that proved to be a KO for the target protein. For p62-KO cells, SSC 3 was chosen for the same reason as described above.

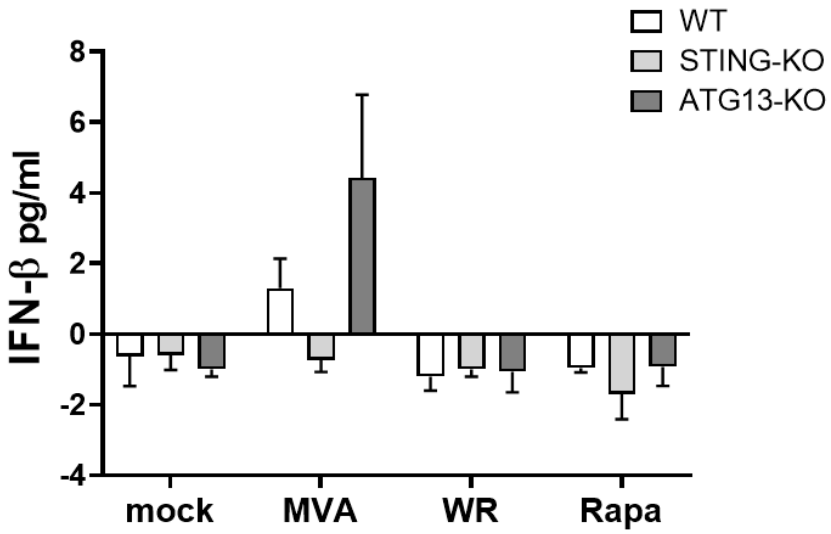

Supplementary figure 2. Seemingly lower protein level of STING observed in Figure 9 has no impact on type I IFN expression in ATG13-KO cells. ELISA for IFN-β in wild type (WT), STING-KO, and ATG13-KO MEF cells under non-infected (mock), MVA- or WR-infected, or rapamycin (Rapa)-treated conditions. Cells were infected for 22 h with MOI 10 for MVA expressing eGFP under control of the vaccinia virus early/late protomer P7.5 (MVA) and MOI 5 for WR expressing a fusion gene coding for the influenza A nucleoprotein, ovalbumin-derived peptide SIINFEEKL and fluorescent protein mCherry under control of the vaccinia virus early/late promoter P7.5 (WR). After infection, supernatants were harvested and filtered through a 0.2 µm filter and IFN-β levels were determined by ELISA. For Rapa treatment, 30 µg/ml of reagent was added to cells for the duration of infection. The difference between the expression of WT and ATG13-KO MVA-infected cells was not significant (n = 3). Data are depicted as the mean ± SD of three independent experiments. no significance; two-tailed Student´s t-test.

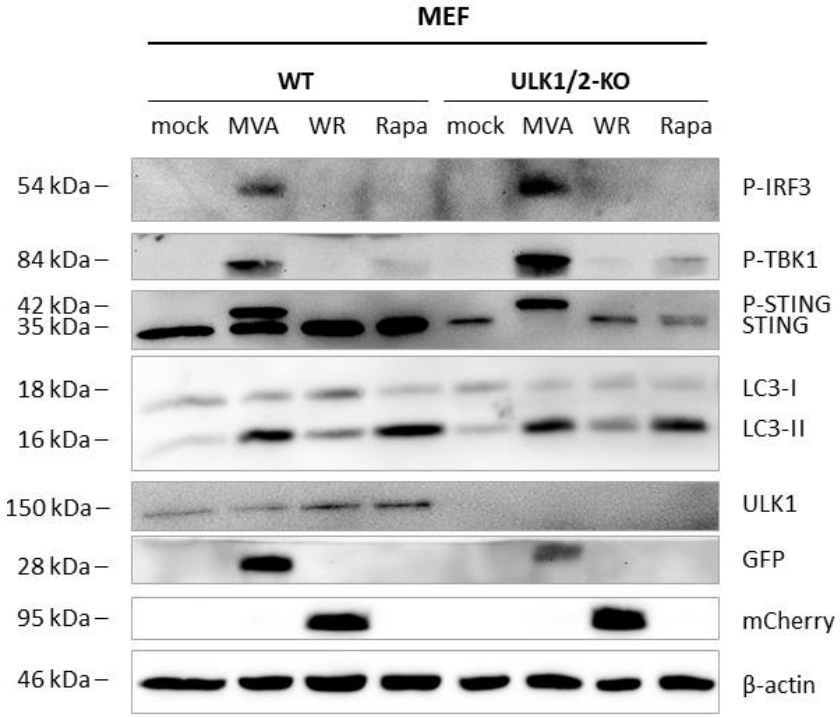

Supplementary figure 3. MVA infection as well as Rapamycin treatment induces LC3 lipidation in ULK1/2-KO MEF cells. Comparison of MEF wild type (WT) and ULK1/2-KO cells under non-infected (mock), MVA- or WR-infected, or rapamycin (Rapa)-treated conditions. First, 70 – 80 % confluent cells were infected for 4 h with MOI 10 for MVA expressing eGFP under control of the vaccinia virus early/late promoter P7.5 (MVA) and MOI 5 for WR expressing a fusion gene coding for the influenza A nucleoprotein, ovalbumin-derived peptide SIINFEEKL and fluorescent protein mCherry under control of the vaccinia virus early/late promoter P7.5 (WR). After infection, cells were harvested and lysed and protein levels were determined by Western blot analysis. For Rapa treatment, 30 µg/ml of reagent was added to cells for the duration of infection (n = 1).

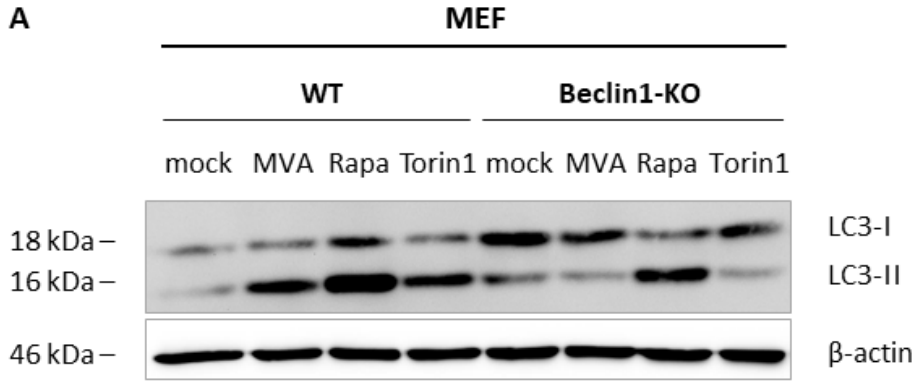

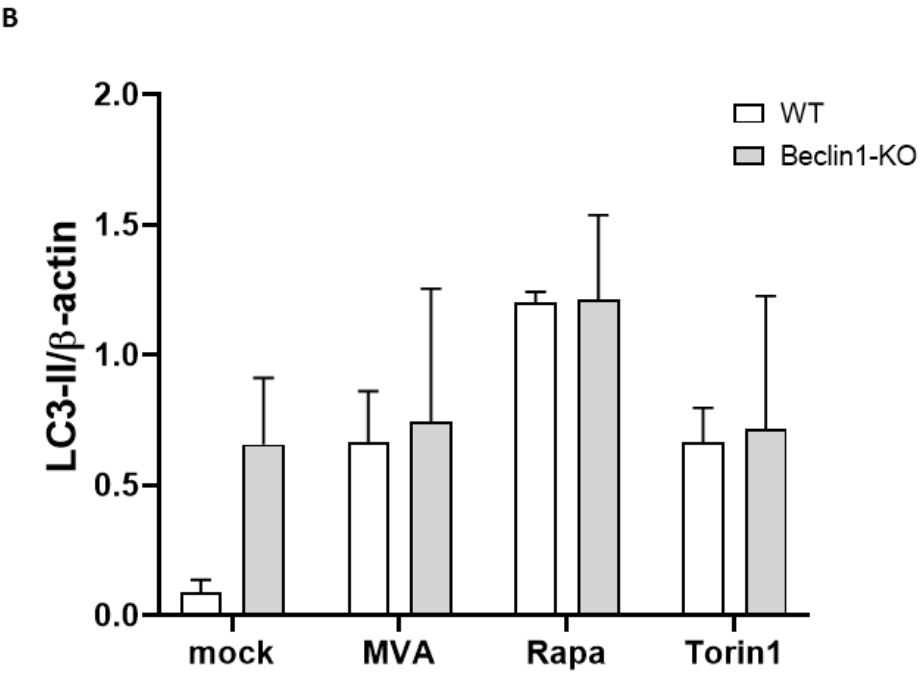

Supplementary figure 4. Effect of rapamycin and Torin1 treatment in Beclin1-KO and WT MEF. (A) LC3 lipidation was observed in MEF wild type (WT) and Beclin1-KO cells under non-infected (mock), MVA-infected, rapamycin (Rapa)- or Torin1-treated conditions. First, 70 – 80 % confluent cells were infected for 4 h with MOI 10 of MVA expressing eGFP under control of the vaccinia virus early/late promoter P7.5 (MVA).

After infection, cells were harvested and lysed and protein levels were determined by Western blot analysis. For Rapa treatment 30 µg/ml of reagent was added, for Torin1 treatment 3 µM was added to cells for the duration of infection. (B) Quantification of LC3-II protein levels normalised to β-actin in MEF WT and Beclin1-KO cells (n = 2).

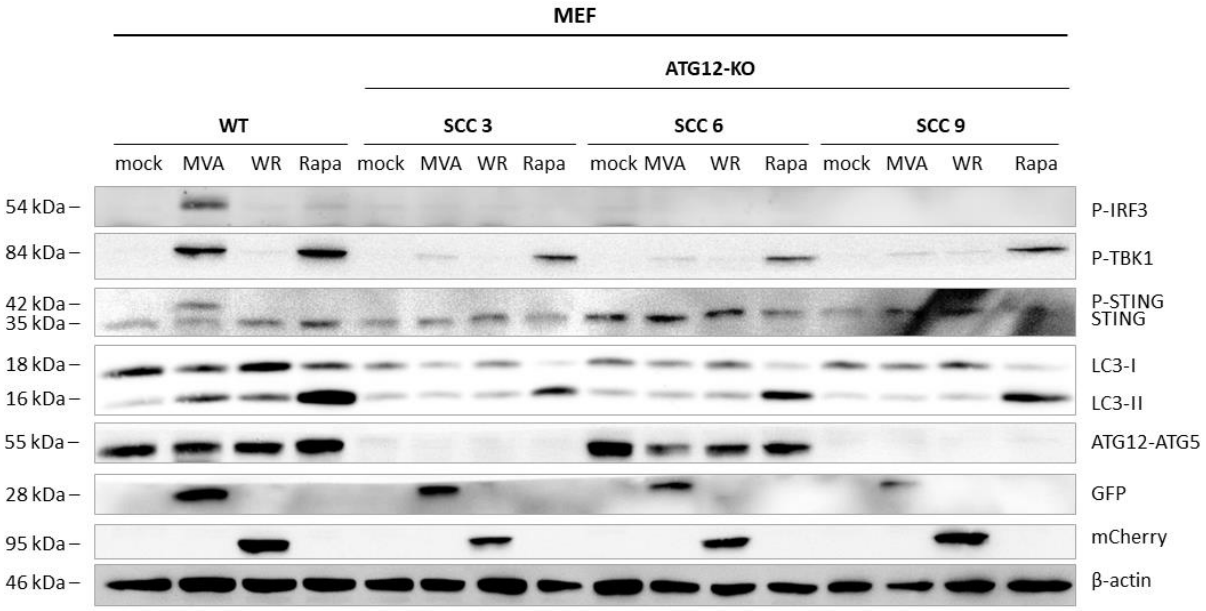

Supplementary figure 5. Investigation of possible effects of unidentified, unspecific ATG12-associated protein marker during VACV infection on the autophagy and cGAS-STING pathway for type I IFN production. Comparison of MEF wild type (WT) and single cell clone (SCC) 3, SCC 6, and SCC 9 of ATG12-KO cells under non-infected (mock), MVA- or WR-infected, or rapamycin (Rapa)-treated conditions. First, 70 – 80 % confluent cells were infected for 4 h with MOI 10 for MVA expressing eGFP under control of the vaccinia virus early/late promoter P7.5 (MVA) and MOI 5 for WR expressing a fusion gene coding for the influenza A nucleoprotein, ovalbumin-derived peptide SIINFEEKL and fluorescent protein mCherry under control of the vaccinia virus early/later promoter P7.5 (WR-P7.5-NP-SIIN-mCherry). After infection, cells were harvested and lysed and protein levels were determined by Western blot analysis. For Rapa treatment, 30 µg/ml of reagent was added to cells for the duration of infection (n = 1).

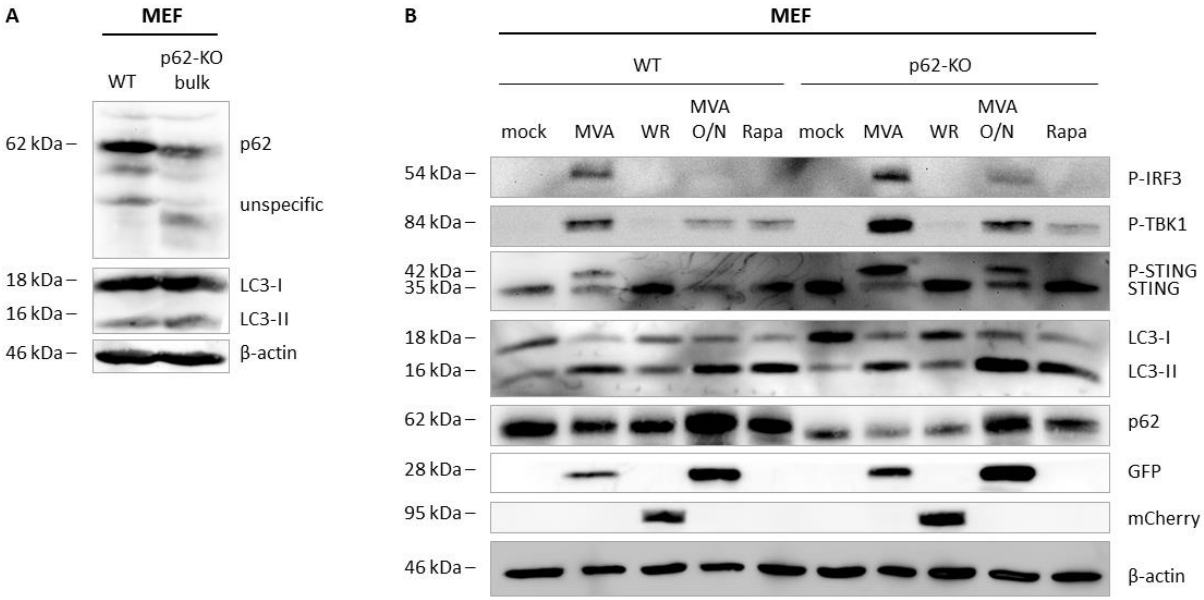

Supplementary figure 6. Confirmation of the functional properties of bulk population of p62-KO MEF cells. (A) Confirmation of p62 gene knock out and a lack of p62 protein synthesis in MEF cells after using the CRISPR-Cas9 method. Western blot analysis displayed proteins with an aberrant size for p62 in the bulk population of p62-KO cells. (B) Cells from the p62-KO bulk population were tested for any loss of function compared with wild type (WT) cells. These cells were tested under non-infected (mock), MVA-, MVA overnight- (O/N), WR-infected, or rapamycin (Rapa)-treated conditions. First, 70 – 80 % confluent cells were infected for 4 h or overnight (circa 20 h) with MOI 10 for MVA expressing eGFP under control of the vaccinia virus early/late promoter P7.5 (MVA or MVA O/N) and MOI 5 for WR expressing a fusion gene coding for the influenza A nucleoprotein, ovalbumin-derived peptide SIINFEEKL and fluorescent protein mCherry under control of the vaccinia virus early/late promoter P7.5 (WR). After infection, cells were harvested and lysed and protein levels were determined by Western blot analysis. For Rapa treatment, 30 µg/ml of reagent was added to cells for the duration of infection (n = 1).

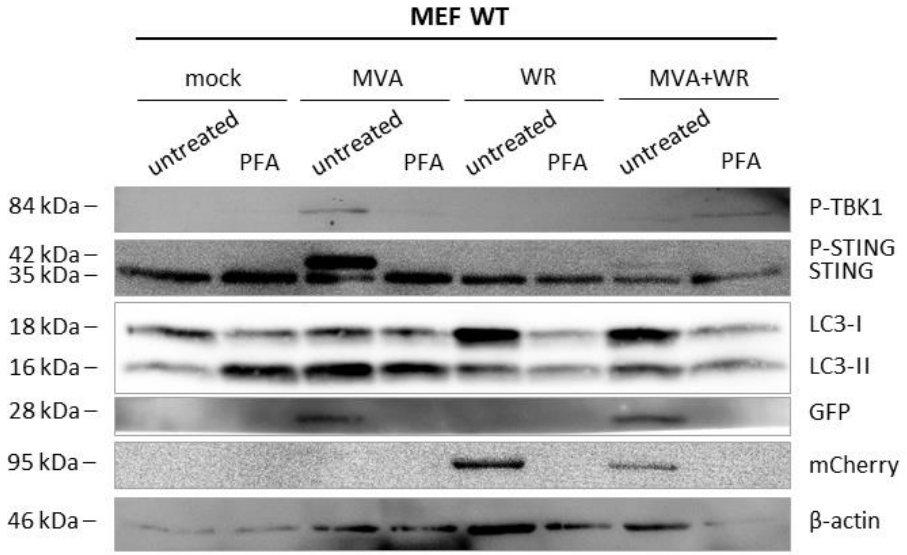

Supplementary figure 7. PFA activates autophagy in the absence of MVA infection. Induction of activation of the autophagy and cGAS-STING pathway for type I IFN production was observed in wild type (WT) MEF cells under non-infected (mock), MVA-, WR-infected or MVA-WR co-infected conditions with or without PFA treatment at the same time. First, 70 – 80 % confluent cells were infected for 4 h with MOI 10 for MVA expressing eGFP under control of the vaccinia virus early/late promoter P7.5 (MVA) and MOI 5 of WR expressing a fusion gene coding for the influenza A nucleoprotein, ovalbumin-derived peptide SIINFEEKL and fluorescent protein mCherry under control of the vaccinia virus early/late promoter P7.5 (WR), or MOI 10 of MVA together with MOI 5 of WR (MVA+WR). After infection, cells were harvested and lysed and protein levels were determined by western blot analysis. For PFA treatment, 0.85 µl of 2 % PFA was added to 10 µl of control or virus-containing medium and incubated for 1 h at 37 °C prior to infection to reach complete inactivation. This mixture was added to respective cells for the duration of infection (n = 2).

6.2 Supplementary information regarding recMVA generation

6.2.1 Supplementary materials for recMVA generation

6.2.1.1 Viruses

Name	Description	Source/Reference
MVA-pK1L-H3-eGFP	Recombinant MVA (recMVA) virus expressing VACV gene H3L (usually expressed late) fused to eGFP under control of the early promoter PK1L	Ronny Tao

6.2.1.2 siRNAs library

Antiviral siRNAs library is shown according to the original publication by Kilcher *et al.* (232).

Gene Name (VACV WR)	**Gene Name (VACV COP)**	**All sequences have 3´ dTdT overhangs**		
		siRNA Oligo1 (sense)	siRNA Oligo2 (sense)	siRNA Oligo3 (sense)
VACV-WR-009	C11R	UAUUGUAGAUGCUCUCAUG	UGUAGAUGCUCUCAUGGUU	CGGUAUUAUGCUUGUAUUA
VACV-WR-010	C10L	GUUCUAAUUGGGUACCCUU	CGUUAAAGAUAAACGUAUA	CGGAUAAGGAUAUUAUGUU
VACV-WR-024	C4L	GUUCUAUAUCUUUGACAUA	CUCUUAACUUUAGAUUCGA	GAAUGUAAAGCGCGACUAU
VACV-WR-033	K2L	CGUAGAUCCGGUAUGUCUA	CAAUCUUAAACUCCCUAAA	CCAGAUAAUGCGUCGUUUA
VACV-WR-035	K4L	CGUAUAUAGGUACCUCAAA	CUCAAAUUGGACAGGAAAU	GAGUUGAAGUACGAUACAU
VACV-WR-041	F2L	GGUCUGGUCUGUCCCUAAA	UAGGUCUGGUCUGUCCCUA	CUAGGUCUGGUCUGUCCCU
VACV-WR-042	F3L	GGAAUAUUGUGUCGAGUGU	GAGUGUUACAUGAUGGGUA	GUCAAUUUAUUACGUGCUU
VACV-WR-043	F4L	GCUAGAUGUUUCUACGGAU	GAUUUCGCAUGUUUGAUGU	GAAUGAAUUGUGAAAUGAU
VACV-WR-048	F9L	AGCUAUCGCUGAAGAAAUA	CCCGGUCAACAUAUGCUUU	AAGAGCUAUCGCUGAAGAA
VACV-WR-050	F11L	GUAGAAACAGGAUUCGUCA	GUCAUAGUUCCUGACAUCA	GUGAUGAUUAUGAACUUAA
VACV-WR-051	F12L	GUACCUACUAACGACCAUA	GACUUGAACGCAGUUACAA	GACCAUAUUCCCGUAGUUU
VACV-WR-054	F15L	CAGUUCUAAUAUCAUCAGA	GUUUAAGCAUUAAUCUAUU	CAGAAUACGGAAUCAUGAU
VACV-WR-058	E2L	CAAUGAUGAUGAAACGGUU	GUUAGUAAUGGUUAUGUGU	GAAUUAUGUCCAGAAGCUA
VACV-WR-060	E4L	GCUAUCUCUUAUUCGGUAU	CACUAUGUGAUAUGAUUUAA	CCGUCUAUUGCCACAAAUU
VACV-WR-062	E6R	GUGGUUAAACGAAAGUAUA	CGUUUAACGAGGACUUAUU	GAAUACAAUACAUACCUGU

VACV-WR-064	E8R	GUUUCUCAUGUCUCUAUAU	GUUCGAGUUUCUCAUGUCU	CUAUACAGAUAAUGCCAAA
VACV-WR-065	E9R	GUAUAAGGAUUAUAAUCUA	CUGUAUUCAUGAUGCUUGU	CCAAUACUACGUUUCACGU
VACV-WR-068	O1L	CCAAUUACUGAUUCUCUUU	GUUUAGACGUCCCAUGUCA	GAAAUUGCUGUCUGUAAUU
VACV-WR-070	I1L	GUAUGUAUGUCAUUCCCGA	GUCAAUCUAUGUGAUUCUA	CAUACAUAUCAUCUGGAAA
VACV-WR-071	I2L	CAGACUUUAUAGAAAUUGU	CGCCGCUAUAUUUGGUGUA	UCCGGAAGAUGAUUUGACA
VACV-WR-072	I3L	GAACGCAUUCCAAAUUCUU	GUCUUUCGGUGGAAACUAU	CACAAGGAACGCAUUCCAA
VACV-WR-073	I4L	GGAACUAGUCGUCACCAAA	GAACAUACGGUCUUAGAAA	GGAGUUAUGGCCAUAUACU
VACV-WR-075	I6L	CAAGUCUCAAGUUAUAGAA	GUUCAAUGUUCCGGAUUCU	CAAUGUUCCGGAUUCUAUA
VACV-WR-077	I8R	GUUACACACAUUUAUGAUA	CUAUAGGUGUACUAGGGAA	GGUACUAGAUGGAUCUCCU
VACV-WR-078	G1L	CCAGUAAGUACAAACGGUA	CGUGAUAUGCUGGUAAAUA	GCAAUUAUGGAAUCUGAUU
VACV-WR-080	G2R	GGAAUAUUUAUAUUAGGGA	GUGUAUACGGCCGUGUUAU	CGUGUUAUAAAUUAGGAGA
VACV-WR-081	G4L	GCGCGGAACCCUAAUAGGA	CUAACUACAUCGUUUCCAU	CAAAUACAAUCCACAGACA
VACV-WR-082	G5R	GGAGAAUGGCCGUUGAUAA	CCAAUUAAUGUAUGCGUUA	CUGAUAAUCAUCCUAAGAU
VACV-WR-083	G5.5R	GAACCUCAACGUAACUUAA	GAUGUACUCGUCAGUGUAA	CUCUACGUGCGGCAAAGAU
VACV-WR-084	G6R	CAUGUUAGAGAAUAUUCAA	CAGCUGAUACGUCAUUAAC	GCAGCUGAUACGUCAUUAA
VACV-WR-085	G7L	CUCAAGAACUAGCAGAAUU	GUCUCAAGAACUAGCAGAA	CACUUUGAUAACCCUGAUU
VACV-WR-087	G9R	GAAGAAGGAUGGAAAGAUA	CAUUGUUAAGACAAUCGUA	CCCAAUUGCUGUCGCACUU
VACV-WR-091	L4R	GAAUCCGCGUCGACUGAGU	CUAAAUAUGCGGGAAUUAA	CAUCACCUAUCUUGUGUAU
VACV-WR-092	L5R	GUUUAUAGAGCCCACGUUU	CCAUGGAUGACAACUCAAA	GAUCUGAAUUAAAUAUGUU

VACV-WR-094	J2R	GAGCGUAUGGCAAACGAAG	CUCCGUGAUAGGUAUCGAU	GUUCUUUCCAGACAUUGUU
VACV-WR-095	J3R	CAAAUCAGACGCUGUAAAU	CUAGUACGGCGGAUUUACU	CUGACUCGAGUUACCAAAU
VACV-WR-096	J4R	UGUGGUAAUAUCUGACUUA	GUCAUAACAAGUUUCCUGU	UGACUUAUUUCCUAGCUUU
VACV-WR-097	J5L	CGCUAUCUGAAUCAGGAAA	CCAUUACAGAUAGUAAAUU	CAAAUGGCUUCCGAUUGGA
VACV-WR-098	J6R	GUCAUUGGCUGGACUCUUA	CGGAAUUGCCAACUCUCAA	GAUAUGGUGGUCGACGGAU
VACV-WR-099	H1L	GUUGGUAGAUGAUACAACU	CUACCGAUAUUAGUAAAUA	ACCGAUAUUAGUAAAUAUU
VACV-WR-100	H2R	AAGUGAUAGAGGUAGACUU	GUGAUAGAGGUAGACUUCU	UACGGUUAACGAUUGGAAA
VACV-WR-101	H3L	CACAUAUACAGGAGGGUAU	GCCCUAUGGGAUUCUAAUU	CAUGCCAUAUUCACAUAUA
VACV-WR-104	H6R	CUAAGUGAACGAAAGGUAU	GUCCAUAUCUCCUCUUCCA	GUACAGAAUCGCAACGCUA
VACV-WR-105	H7R	UCCGAUAUCUGGAGAUGAA	CUCCGAUAUCUGGAGAUGA	GAGAUGAAUGCAAGACUCA
VACV-WR-106	D1R	CAGUUUGCUAUCCAUUAUU	GUUUAUAGCAGAAUUCUUA	GAAAUGAAAGAUACAACAA
VACV-WR-109	D4R	GUUACUGCUGCAGCAUAUA	GUCACGCGAUCUACUGGGA	CAAGUUACUGCUGCAGCAU
VACV-WR-110	D5R	GAAACCAUGCGACAAUCAU	CGUAACACCUUGUGCAUUA	CCAGAAAUGGAAGAGUUAA
VACV-WR-111	D6R	CUGAAAGAGGUAAGGCAUA	CCUAAUACUCUGGGUCAUA	GUGAAUGUACUUAAGGAUU
VACV-WR-112	D7R	UGUGUAAUAACCUACGCGU	CAUUAAACAUCGAAGAUGA	CUACGCGUAUUAUCACGUU
VACV-WR-114	D9R	GGAAAGUGAUGAACGUAUA	GAACUAAGAGAAAUCUUUA	AUUCGGAAAUGUAAUUCUA
VACV-WR-115	D10R	CAGCUACUGCUGAUAAUGA	GUAAUCUUCUUUGUCGGAA	CUACUGCUGAUAAUGAUAG
VACV-WR-117	D12L	GACCUCAGCGCACGCAAUA	CUAUACAUUAGCGAUUAUA	GAUGCUAUUAAAUCUAAUA
VACV-WR-118	D13L	CUAGUCAACGUAACGUCUA	CGAAUCAAAGGCCAAGGAU	CAACCAACGGCGACUGUAA

VACV-WR-120	A2L	AUGAGAAACUGAAUCUGAG	AUAAGUUAGUCUUUGAAAU	AGGCUAACGAGAGAAUAAA
VACV-WR-124	A5R	GACGCUAUACUAGACGUAU	AGCAGAAAGCUAUAACCUUG	CGACGCUAUACUAGACGUA
VACV-WR-125	A6L	CUCUAAACUAAUUUCUGAA	CUCUCUUAACUCUAUGUAU	CAUUUGAGAGCGUCGACUA
VACV-WR-127	A8R	UGUAAUUAAUCAAAUGGUA	AGUACGGGCGCUGUAAUUA	AAGUUCAUUAUCUGAAAUA
VACV-WR-129	A10L	CAAUUAACAUUAGUUCGGA	CUCAAUGGAUGUUCUAGCA	GACUUGAGGCAAUCAUCGU
VACV-WR-133	A14L	GCUAAUCGCUGGAAUCAUU	CAGAGUUAGCGGAGUCAUU	GAGUUAGCGGAGUCAUUCA
VACV-WR-136	A16L	CCGAUAUUUGCUCCAAACA	GAUAUUGUUCUGAGUUUAU	GAAAUUGUUGGUGCGCGAA
VACV-WR-137	A17L	GCAAUCAAUGUAUUUACGA	GAAUGUCUAUUGUGUGUAU	CUAUUGCUUAGUAACUCAA
VACV-WR-138	A18R	CGUCAUUUGCGUACCCAAU	GUCGUAUCUGAAGUAGUUU	CUAUUAGAUAGGACGGUAU
VACV-WR.141	A20R	CAUUAUUUGACGACGAGUU	GUUAAUAUAUUUAAACUAG	GUGAGUACGGAUUAAACAU
VACV-WR-142	A22R	CUGCCAAAGUUAUUUGCGU	ACACUACAGUUCUUCUAGA	GAAGGUCGCCGUAUGUUAA
VACV-WR-143	A23R	GUUGUCAUUAUUUCGACAU	GAAUACGUAUCCGGUAUUU	CGUACUUACGGCUACGGCA
VACV-WR-144	A24R	CUGCUAAGCCGUACAACAA	GGCUAAUUGCUUCGGCCAA	CAGAUUAGACGACAUGACA
VACV-WR-151	A28L	GGCAUUAGAUAGGAGAGUU	GCAGAGUGUCAGUUUCUAA	CUCAUGCAGCAUUCGAAUA
VACV-WR-152	A29L	CCAAUCUGAACGCGAUAAU	GUAUUUAGAUCUCCAUUUA	GUAUAUUCGUGGUUUGAUU
VACV-WR-154	A31R	GGGAAUGUCAUUUGUAUUU	GUAACAAUUAAUAAUCUAA	CGAUUCAAUAACUAAAGAA
VACV-WR-155	A32L	CUUAAACUUUGGAAGGCAU	CUAUUAUUCUACUAUGCCA	CCAAUAAUCGAUUGGCUAU
VACV-WR-170	A44L	CAGUAUCCGGGAUCUGAGA	GUAAUCAUGAAUGGAGCAA	CUAGUAGCAUGGAAGCAAU
VACV-WR-171	A45R	CCACGAUAAUAUCAGAGGA	GUGUGGAGUUAUUGGUAUU	GGAUGUGAUUCCAUAGGCA

VACV-WR-174	A48R	GAUGAUAGAUGACUAUCUA	GACUCUCAGUAAGAGUUAU	GGAAUCUGGUAGCAAAGAA
VACV-WR-176	A50R	GUGAAAGAGUACAAGUUCA	CAAGUGUUCAGGACACGAU	GCUAUUAGUCCUAAUGCCU
VACV-WR-183	B1R	GGUAUCUUGCCAUGGACUA	GAUGUUGAUCGGAAUCGAA	GUGGAUUACGGAUUGGUUU
VACV-WR-187	B5R	GGAAUGUCAACCUCUUCAA	GUUAUACAUCUUAGUUGUA	GAAUGUUAUUCCAUCAUGU
VACV-WR-188	B6R	GGAUACACUUAAUGGUAUA	GAAUGAACGCGAUGUUUCU	GUUGGCACCGGAAUACUAU
VACV-WR-195	B13R	CACUGAUUGUCGCACUAUA	GUCUAUGUACGGCAAGGCA	GGCAUUUAAUCACGCAUCU
VACV-WR-205	C12L	CUAAUCAACGAAUGGGUUA	ACUAGUCCGCUAUCCAUUA	GCUAUCCAUUAAUACUCGU
VACV-WR-206	C13L	CACACCUGAUGGUUUGGAU	UCGUGCAUUGUUCAAAUCA	ACUUAUUGGUCACGGUUUA

6.2.2 Supplementary methods for recMVA generation

6.2.2.1 Granularity calculation of high-content confocal microscopy images of VACV infected H-DLG cells

After the quantification of DsRed-positive VACV infected H-DLG cells by Dr. János Kriston-Vizi, all computational analysis of processed images was done by Dr. Artur Yakimovich.

LC3-granularity (based on the amount of DsRed-LC3-II in autophagosomes) of VACV-infected H-DLG cells were compared to mock-infected cells, while a shape fitting procedure (based on the shape of the DsRed-LC3-II positive organelles) was used to measure the size variations of granules, also previously adjusted according to MVA-infected reference-cells. The size of LC3 granules was calculated for each single cell and final granularity was calculated for each imaged well of specific plates.

6.2.3 Supplementary results of recMVA generation

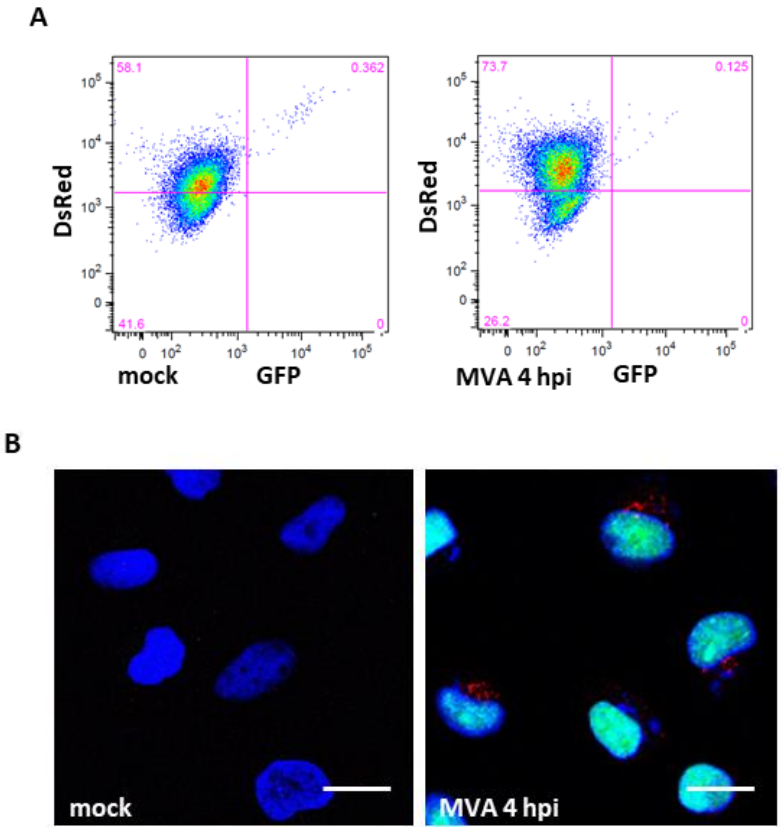

Supplementary figure 8. Confirmation of autophagosome formation upon MVA infection by FACS or CLSM imaging. HeLa DsRed-LC3-eGFP (H-DLG) cells were infected for the time indicated (n = 3). (A) MOI 10 of MVA expressing eGFP under the control of the vaccinia virus early/late promoter P7.5 (MVA) was used to infect cells as described in Section 3.3.3, and the shift of DsRed-positive only H-DLG cells was monitored using FACS analysis. (B) MOI 10 of MVA expressing a fusion gene coding for the influenza A nucleoprotein, ovalbumin-derived peptide SIINFEEKL and fluorescent protein eGFP under control of the vaccinia early/late promoter P7.5 (MVA) was used to infect cells as described in Section 3.3.2, while autophagosome formation was determined using CLSM. Scale bars represent 10 µm.

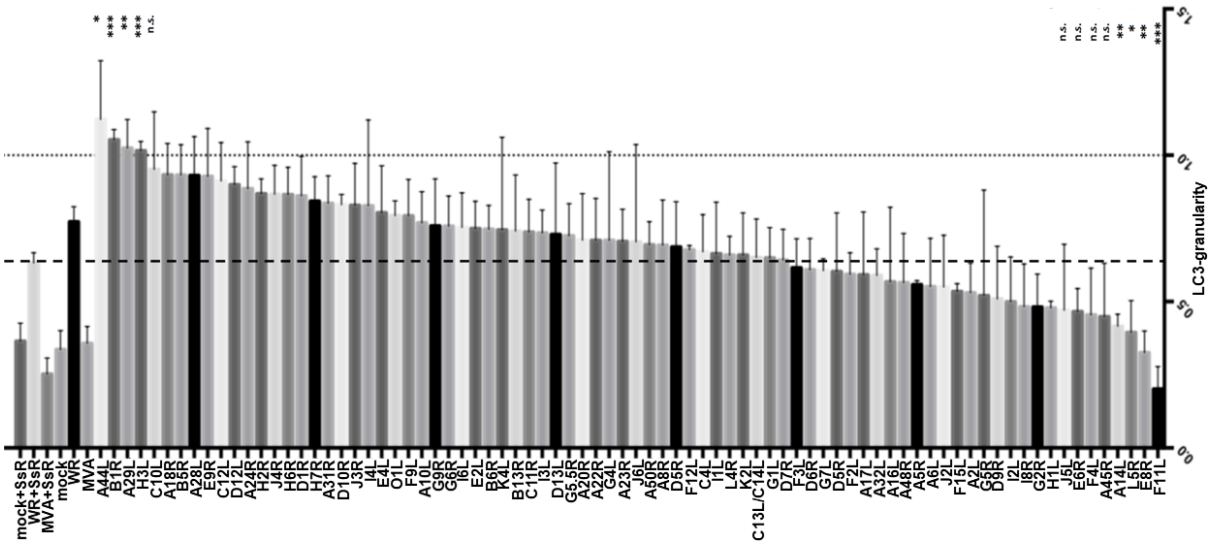

Supplementary figure 9. siRNA screen of 80 conserved WR genes potentially interfering with autophagosome formation upon WR infection analysed using high-content CLSM. HeLa DsRed-LC3-eGFP (H-DLG) cells were mock-, MVA-, or WR-infected with or without scrambled siRNA (SsR) treatment. Cells were treated with siRNA 16 h prior to infection. MOI 10 of MVA expressing eGFP under control of the vaccinia virus early/late promoter P7.5 (MVA) or MOI 10 of WR WT were used to infect the cells. The results depict the percentage of dsRed only-positive cells calculated after pooling the results obtained for each of the three siRNA sequences specific to a single gene. The dashed line represents the average of the results of WR-infected and SsR-treated cells, whereas the dotted line represents the threshold for a statistically significant difference compared with dashed line (n = 3). Data are depicted as the mean ± SD of three independent experiments. * = $p < 0.05$; ** = $p < 0.01$; *** = $p < 0.001$; ns = not significant; two-tailed Student´s t-test.

WR gene name	MVA gene name	Expression time	Read-out	Differences compared to MVA on the amino-acid level
A8R	119R	early	FACS	none
A23R	134R	early/late	FACS	1 mismatch
A28L	139L	late	FACS	none
A29L	140L	early	high-content confocal microscopy + FACS	1 mismatch
A44L	157L	early	high-content confocal microscopy	3 mismatches
B1R	167R	early	high-content confocal microscopy	1 mismatch
B6R	174R	early	FACS	none
D1R	098R	early/late	FACS	4 mismatches
D7R	104R	early/late	FACS	none
E4L	051L	early/late	FACS	2 mismatches
F9L	038L	late	FACS	2 mismatches
H3L	093L	early/late	high-content confocal microscopy	4 mismatches
H6R	096R	late	FACS	none
L5R	084R	late	FACS	1 mismatch

Supplementary table 1. Selection of 14 potential viral gene candidates for autophagy interference following the results of FACS and high-content CLSM read-outs of siRNA screening. The VACV genes listed here exhibited significant increases in LC3 lipidation compared with non-infected untreated or non-infected treated cells with scrambled siRNA, after siRNA during WR infection monitored by FACS and high-content CLSM, as described in Section 3.2.1. Due to the low levels of difference for these genes between MVA and WR, the VACV genes in this table were not selected for further investigation regarding their ability to induce the inhibition of autophagy.

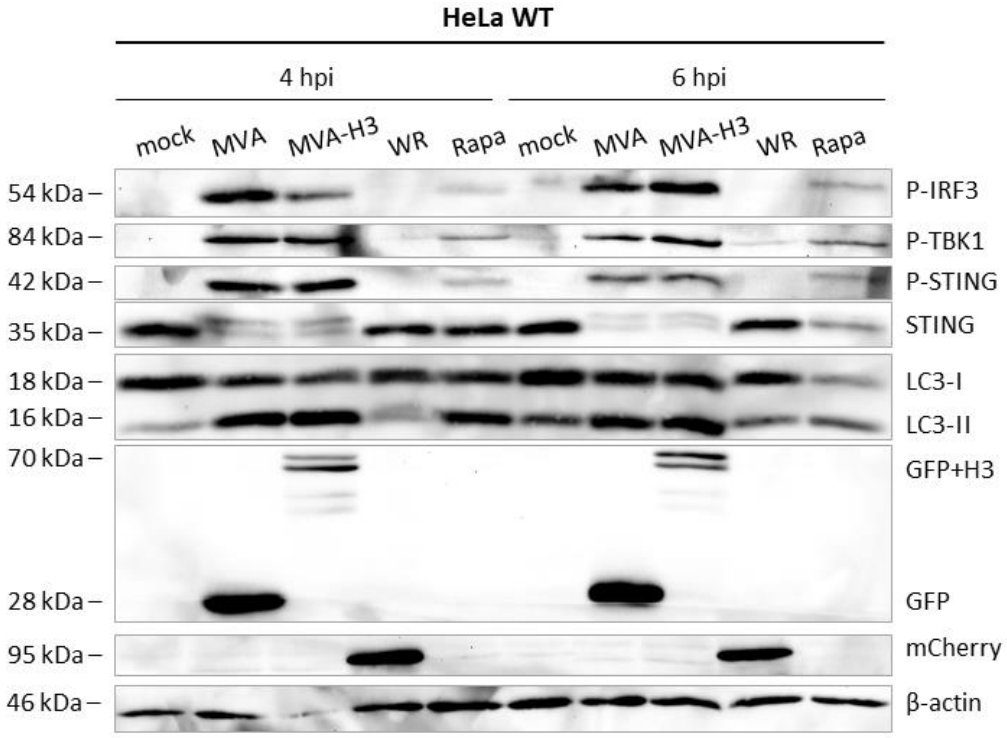

Supplementary figure 10. VACV H3L gene product is not interfering with autophagy or type I IFN production. Induction of activation of the autophagy and cGAS-STING pathway for type I IFN production was observed in HeLa wild type (WT) cells under non-infected (mock), MVA-, MVA-H3-, or WR-infected, or rapamycin (Rapa)-treated conditions. First, 70 – 80 % confluent cells were infected for 4 or 6 h with MOI 10 for MVA expressing eGFP under control of the vaccinia virus early/late promoter P7.5 (MVA), MOI 10 for MVA expressing vaccinia virus gene H3L (usually expressed late) fused to eGFP under control of the early promoter PK1L (MVA-H3) and MOI 5 for WR expressing a fusion gene coding for the influenza A nucleoprotein, ovalbumin-derived peptide SIINFEEKL and fluorescent protein mCherry under control of the vaccinia virus early/late promoter P7.5 (WR). After infection, cells were harvested and lysed and protein levels were determined by Western blot analysis. For Rapa treatment, 30 µg/ml of reagent was added to cells for the duration of infection (n = 1).

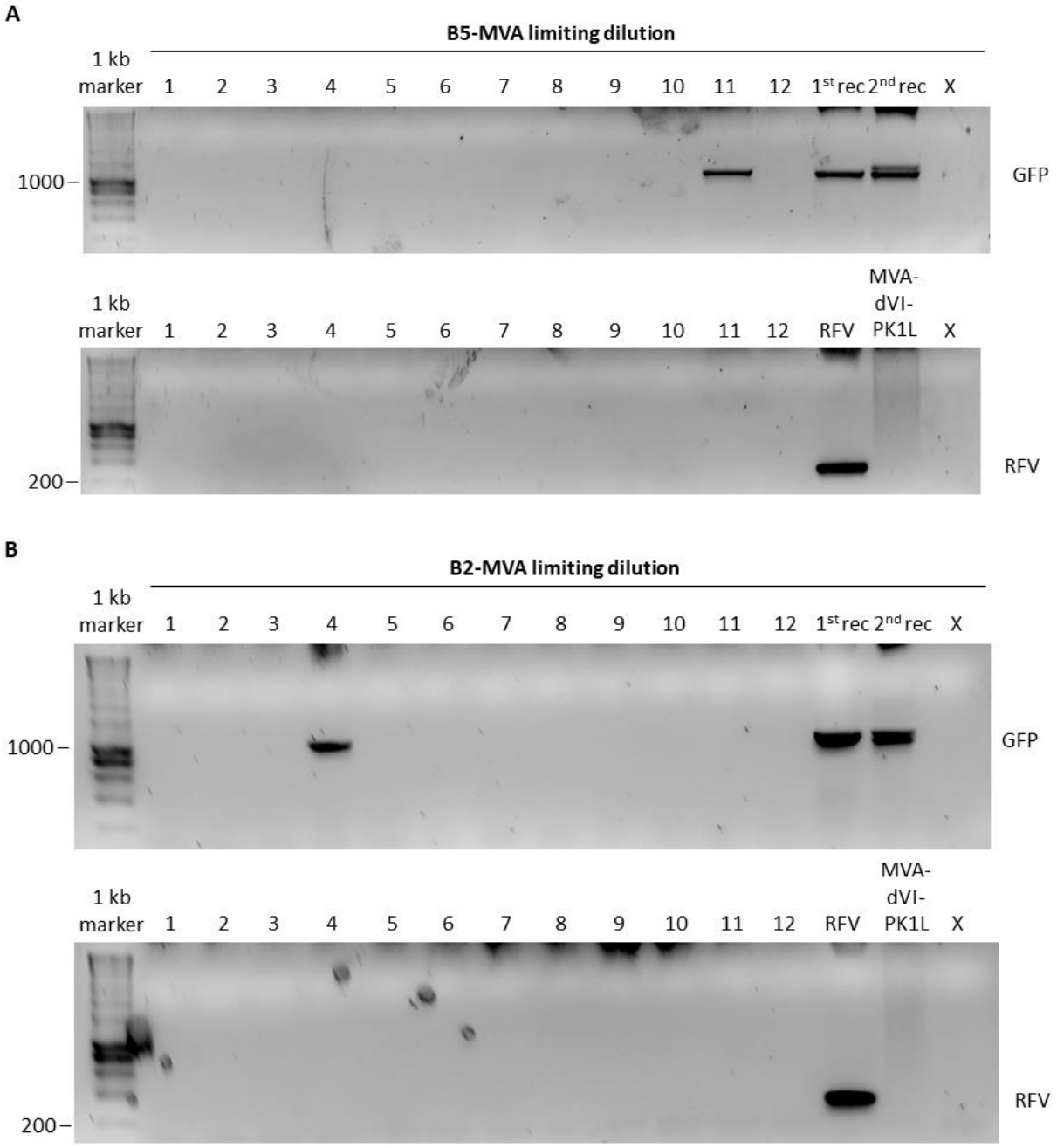
A
B5-MVA limiting dilution
1 kb marker
1 2 3 4 5 6 7 8 9 10 11 12 1st rec 2nd rec X
1000 –
GFP
1 kb marker
1 2 3 4 5 6 7 8 9 10 11 12 RFV MVA-dVI-PK1L X
200 –
RFV
B
B2-MVA limiting dilution
1 kb marker
1 2 3 4 5 6 7 8 9 10 11 12 1st rec 2nd rec X
1000 –
GFP
1 kb marker
1 2 3 4 5 6 7 8 9 10 11 12 RFV MVA-dVI-PK1L X
200 –
RFV

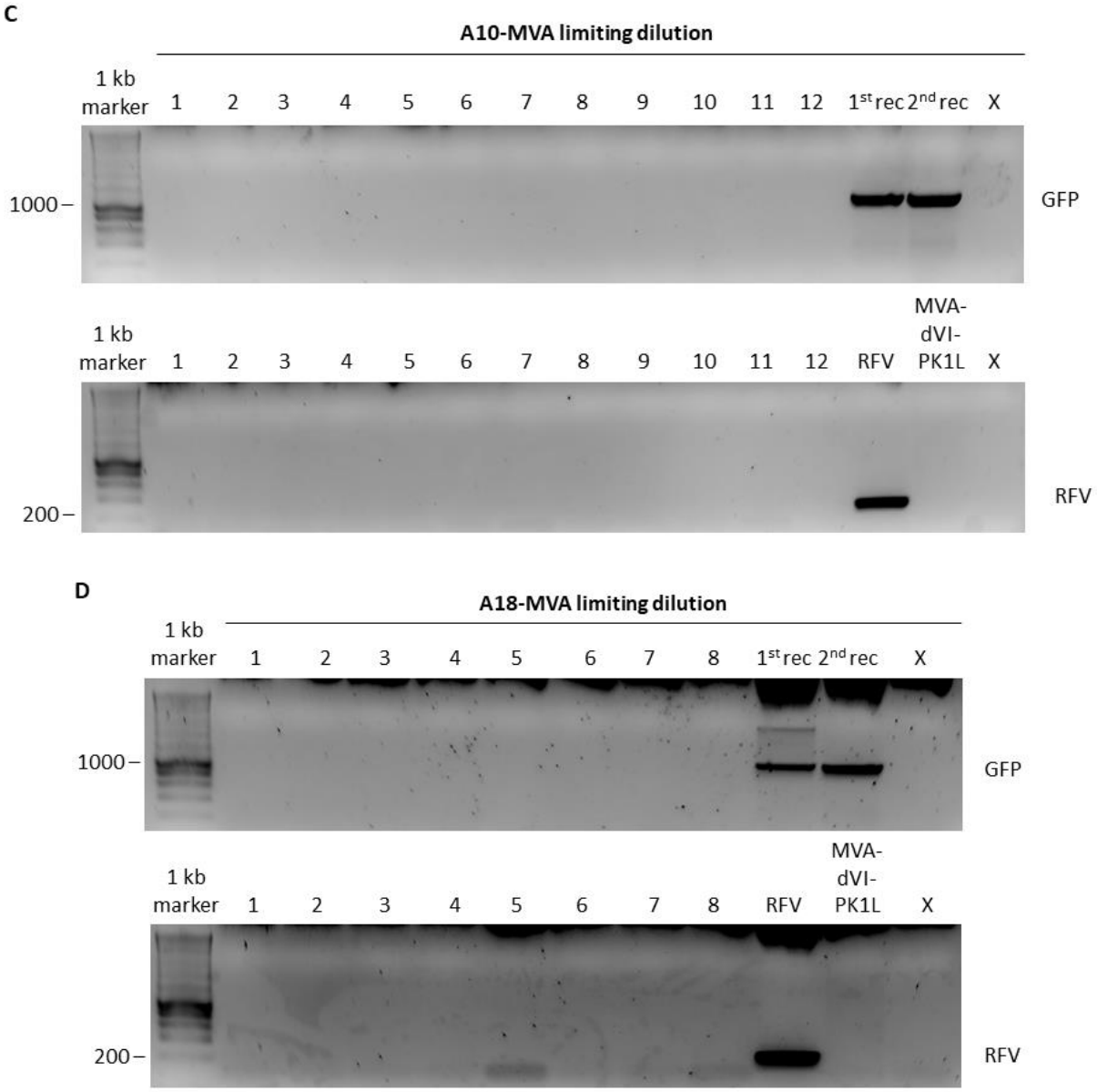

Supplementary figure 11. Loss of helper virus and BAC cassette in single recombinant MVA virus clones expressing genes of interest after limiting dilution. Agarose gels with the PCR DNA fragments for each construct allowing the evaluation of the presence or absence of GFP or rabbit fibroma virus (RFV) in selected viral clones (numbers 1 – 8 or 1 – 12). DNA from previously sequenced bacterial clones from the 1st and 2nd recombination (1st rec and 2nd rec) were used for GFP monitoring, and DNA from RFV was used as a positive control. DNA from plasmid pEP-MVA-dVI-PK1L (MVA-dVI-PK1L) was used as a negative control. X represents the primer control for each construct. B5 in (A), B2 in (B), A10 in (C), and A18 in (D). Marker standard corresponding to the expected size of each DNA fragment is indicated on the left.

6.3 Acknowledgement

This study has been performed at the Institute of Virology in the group of Prof. Dr. Ingo Drexler and was supported by the Manchot Graduate School 'Molecules of Infection' that is sponsored by the Jürgen Manchot foundation.

First of all, I am deeply grateful to my supervisor, Prof. Dr. Ingo Drexler for accepting me as his PhD student and providing me the opportunity to investigate this exciting topic in his research group. Thank you for your guidance, your time, and the extended discussions whenever I felt lost looking at my results.

I would also like to express my gratitude to Prof. Dr. Dieter Willbold for accepting to be my mentor and giving me important pointers during our meetings, even though his time schedule was never in our favour.

Special thanks to Cornelia, who always represented the 'perfect PhD student' for me by just being herself. Thank you for the amazing time in Sardinia and Beijing, for all the scientific and non-scientific discussions and simply being in the same lab with me! It was a great pleasure to work with you!

I want to thank Sara and Ylenia for all the fun and joy that we had together, and I wish them all the best for finishing their PhDs.

Thanks to my fellow lab members: Giuseppe, Sha, and Ronny.

I am also indebted to Dr. Stephanie Spelberg and the MOI III graduate school, as well as the other PhD candidates for all their help and support.

This thesis could have never been finished without the support of my husband, Márton Bán, who is for me the embodiment of patience, support, and common sense. He is my sole reason to push forward during times when I want to give up. I also want to say thank you to my family for their support.

6.4 Statement

I declare under oath that I have produced my thesis independently and without any undue assistance by third parties under consideration of the Principles for the Safeguarding of Good Scientific Practice at Heinrich Heine University Düsseldorf.

Noémi Vágó Leverkusen, 17.03.2023

7 References

1. M. A. Ruffer, A. Ferguson, Note on an eruption resembling that of variola in the skin of a mummy of the twentieth dynasty (1200-1100 BC), *The Journal of Pathology and Bacteriology* **15**, 1–3 (1911).

2. M. A. Ruffer, *Studies in the Palaeopathology of Egypt* (University of Chicago Press, 1921).

3. D. Hopkins, The Greatest Killer. Smallpox in History, Chicago 1983, (1983).

4. F. Fenner *et al.*, *Smallpox and its eradication* (World Health Organization Geneva, 1988).

5. J. C. Moore, *The history of the small pox* (Longman, Hurst, Rees, Orme, and Brown, 1815).

6. R. J. Littman, The plague of Athens: epidemiology and paleopathology, *Mount Sinai Journal of Medicine: A Journal of Translational and Personalized Medicine: A Journal of Translational and Personalized Medicine* **76**, 456–467 (2009).

7. W. P. MacArthur, The Athenian plague: a medical note, *The Classical Quarterly* **4**, 171–174 (1954).

8. R. J. Littman, M. L. Littman, Galen and the Antonine plague., *Am J Philol* **94**, 243–55 (1973).

9. J. Needham, *Science and Civilisation in China: Volume 6, Biology and Biological Technology, Part 6, Medicine* (Cambridge University Press, 1976).

10. E. Timonius, V. An account, or history, of the procuring the smallpox by incision, or inoculation; as it has for some time been practised at Constantinople, *Philosophical Transactions of the Royal Society of London* **29**, 72–82 (1714).

11. M. W. Montague, *Letters from the Right Honourable Lady Mary Wortley Montague Written During Her Travels in Europe, Asia and Africa...* (J. Smith, 1811).

12. M. Maty, XVII. A short account of the manner of inoculating the small pox, on the coast of Barbary, and at Bengal, in the East Indies, extracted from a memoir written in Dutch, by the Reverend Mr. Chais, at the Hague: by M. Maty, MDSR S, *Philosophical Transactions of the Royal Society of London* , 128–131 (1768).

13. C. P. Gross, K. A. Sepkowitz, The myth of the medical breakthrough: smallpox, vaccination, and Jenner reconsidered, *International journal of infectious diseases* **3**, 54–60 (1998).

14. A. Boylston, The origins of inoculation, *Journal of the Royal Society of Medicine* **105**, 309–313 (2012).

15. O. T. Beall, Cotton Mather, the first significant figure in American medicine, *Bulletin of the History of Medicine* **26**, 103–116 (1952).

16. E. Jenner, *An Inquiry Into the Causes and Effects of the Variolæ Vaccinæ, a Disease Discovered in Some of the Western Counties of England... and Known by the Name of the Cow Pox. By Edward Jenner, MDFRS \& C* (Printed, for the author, by Sampson Low: and sold by Law; and Murray and Highley, 1798).

17. N. Willis, Edward Jenner and the eradication of smallpox, *Scottish medical journal* **42**, 118–121 (1997).

18. S. Riedel, in *Baylor University Medical Center Proceedings*, (2005), vol. 18, pp. 21–25.

19. E. Jenner, On the origin of the vaccine inoculation, *The Medical and physical journal* **5**, 505 (1801).

20. WHO, others, *The global eradication of smallpox: final report of the Global Commission for the Certification of Smallpox Eradication, Geneva, December 1979* (World Health Organization, 1980).

21. A. Downie, others, A study of the lesions produced experimentally by cowpox virus., *Journal of Pathology and Bacteriology* **48**, 361–79 (1939).

22. A. Downie, The immunological relationship of the virus of spontaneous cowpox to vaccinia virus, *British Journal of Experimental Pathology* **20**, 158 (1939).

23. F. Fenner, The biological characters of several strains of vaccinia, cowpox and rabbitpox viruses, *Virology* **5**, 502–529 (1958).

24. H. Stickl *et al.*, MVA-stufenimpfung gegen Pocken, *DMW-Deutsche Medizinische Wochenschrift* **99**, 2386–2392 (1974).

25. A. Mayr, H. Stickl, H. Müller, K. Danner, H. Singer, The smallpox vaccination strain MVA: marker, genetic structure, experience gained with the parenteral vaccination and behavior in organisms with a debilitated defence mechanism (author's transl), *Zentralblatt fur Bakteriologie, Parasitenkunde, Infektionskrankheiten und Hygiene. Erste Abteilung Originale. Reihe B: Hygiene, Betriebshygiene, praventive Medizin* **167**, 375–390 (1978).

26. P. J. Walker *et al.*, Changes to virus taxonomy and the Statutes ratified by the International Committee on Taxonomy of Viruses (2020), (2020).

27. B. Moss, in *Seminars in cell \& developmental biology*, (2016), vol. 60, pp. 89–96.

28. B. Moss, Regulation of vaccinia virus transcription, *Annual review of biochemistry* **59**, 661–688 (1990).

29. G. C. Carter, M. Law, M. Hollinshead, G. L. Smith, Entry of the vaccinia virus intracellular mature virion and its interactions with glycosaminoglycans., *J. Gen. Virol.* **86**, 1279–90 (2005).

30. A. C. Townsley, A. S. Weisberg, T. R. Wagenaar, B. Moss, Vaccinia virus entry into cells via a low-pH-dependent endosomal pathway., *J. Virol.* **80**, 8899–908 (2006).

31. Z. Bengali *et al.*, Drosophila S2 cells are non-permissive for vaccinia virus DNA replication following entry via low pH-dependent endocytosis and early transcription, *PLoS One* **6**, e17248 (2011).

32. Z. Bengali, P. Satheshkumar, B. Moss, Orthopoxvirus species and strain differences in cell entry, *Virology* **433**, 506–512 (2012).

33. J. C. Whitbeck, C.-H. Foo, M. Ponce de Leon, R. J. Eisenberg, G. H. Cohen, Vaccinia virus exhibits cell-type-dependent entry characteristics., *Virology* **385**, 383–91 (2009).

34. M. Hollinshead, A. Vanderplasschen, G. L. Smith, D. J. Vaux, Vaccinia virus intracellular mature virions contain only one lipid membrane, *Journal of virology* **73**, 1503–1517 (1999).

35. G. L. Smith, A. Vanderplasschen, M. Law, The formation and function of extracellular enveloped vaccinia virus, *Journal of General Virology* **83**, 2915–2931 (2002).

36. G. L. Smith, B. J. Murphy, M. Law, Vaccinia virus motility, *Annual Reviews in Microbiology* **57**, 323–342 (2003).

37. B. Moss, Poxvirus cell entry: how many proteins does it take?, *Viruses* **4**, 688–707 (2012).

38. C. S. Chung, J. C. Hsiao, Y. S. Chang, W. Chang, A27L protein mediates vaccinia virus interaction with cell surface heparan sulfate., *J. Virol.* **72**, 1577–85 (1998).

39. C.-L. Lin, C.-S. Chung, H. G. Heine, W. Chang, Vaccinia virus envelope H3L protein binds to cell surface heparan sulfate and is important for intracellular mature virion morphogenesis and virus infection in vitro and in vivo, *Journal of virology* **74**, 3353–3365 (2000).

40. J.-C. Hsiao, C.-S. Chung, W. Chang, Vaccinia virus envelope D8L protein binds to cell surface chondroitin sulfate and mediates the adsorption of intracellular mature virions to cells, *Journal of*

virology **73**, 8750–8761 (1999).

41. W.-L. Chiu, C.-L. Lin, M.-H. Yang, D.-L. M. Tzou, W. Chang, Vaccinia virus 4c (A26L) protein on intracellular mature virus binds to the extracellular cellular matrix laminin, *Journal of virology* **81**, 2149–2157 (2007).

42. J.-C. Hsiao, C.-S. Chung, W. Chang, Cell surface proteoglycans are necessary for A27L protein-mediated cell fusion: identification of the N-terminal region of A27L protein as the glycosaminoglycan-binding domain, *Journal of virology* **72**, 8374–8379 (1998).

43. K. L. Roberts *et al.*, Acidic residues in the membrane-proximal stalk region of vaccinia virus protein B5 are required for glycosaminoglycan-mediated disruption of the extracellular enveloped virus outer membrane, *The Journal of general virology* **90**, 1582 (2009).

44. F. I. Schmidt, C. K. E. Bleck, A. Helenius, J. Mercer, Vaccinia extracellular virions enter cells by macropinocytosis and acid-activated membrane rupture, *The EMBO journal* **30**, 3647–3661 (2011).

45. J. Mercer, A. Helenius, Vaccinia virus uses macropinocytosis and apoptotic mimicry to enter host cells, *Science* **320**, 531–535 (2008).

46. T. G. Senkevich, S. Ojeda, A. Townsley, G. E. Nelson, B. Moss, Poxvirus multiprotein entry-fusion complex., *Proc. Natl. Acad. Sci. U.S.A.* **102**, 18572–7 (2005).

47. T. G. Senkevich, B. M. Ward, B. Moss, Vaccinia virus entry into cells is dependent on a virion surface protein encoded by the A28L gene, *Journal of virology* **78**, 2357–2366 (2004).

48. A. C. Townsley, T. G. Senkevich, B. Moss, Vaccinia virus A21 virion membrane protein is required for cell entry and fusion., *J. Virol.* **79**, 9458–69 (2005).

49. E. Brown, T. G. Senkevich, B. Moss, Vaccinia virus F9 virion membrane protein is required for entry but not virus assembly, in contrast to the related L1 protein, *Journal of virology* **80**, 9455–9464 (2006).

50. S. Ojeda, T. G. Senkevich, B. Moss, Entry of vaccinia virus and cell-cell fusion require a highly conserved cysteine-rich membrane protein encoded by the A16L gene., *J. Virol.* **80**, 51–61 (2006).

51. S. Ojeda, A. Domi, B. Moss, Vaccinia virus G9 protein is an essential component of the poxvirus entry-fusion complex, *Journal of virology* **80**, 9822–9830 (2006).

52. C. L. Wolfe, B. Moss, Interaction between the G3 and L5 proteins of the vaccinia virus entry-fusion complex., *Virology* **412**, 278–83 (2011).

53. A. C. Townsley, T. G. Senkevich, B. Moss, The product of the vaccinia virus L5R gene is a fourth membrane protein encoded by all poxviruses that is required for cell entry and cell-cell fusion, *Journal of virology* **79**, 10988–10998 (2005).

54. T. G. Senkevich, B. Moss, Vaccinia virus H2 protein is an essential component of a complex involved in virus entry and cell-cell fusion, *Journal of virology* **79**, 4744–4754 (2005).

55. H. Bisht, A. S. Weisberg, B. Moss, Vaccinia virus l1 protein is required for cell entry and membrane fusion., *J. Virol.* **82**, 8687–94 (2008).

56. P. S. Satheshkumar, J. Chavre, B. Moss, Role of the vaccinia virus O3 protein in cell entry can be fulfilled by its Sequence flexible transmembrane domain., *Virology* **444**, 148–57 (2013).

57. W. H. Munyon, S. Kit, Induction of cytoplasmic ribonucleic acid (RNA) synthesis in vaccinia-infected LM cells during inhibition of protein synthesis, *Virology* **29**, 303–309 (1966).

58. B. Moss, Poxviridae: The viruses and their replication., *Fields virology* **5** (2007).

59. I. Sarov, W. K. Joklik, Isolation and characterization of intermediates in vaccinia virus morphogenesis, *Virology* **52**, 223–233 (1973).

60. V. Zaslavsky, Uncoating of vaccinia virus., *J. Virol.* **55**, 352–6 (1985).

61. N. Tolonen, L. Doglio, S. Schleich, J. Krijnse Locker, Vaccinia virus DNA replication occurs in endoplasmic reticulum-enclosed cytoplasmic mini-nuclei., *Mol. Biol. Cell* **12**, 2031–46 (2001).

62. K.-I. Oda, W. K. Joklik, Hybridization and sedimentation studies on "early" and "late" vaccinia messenger RNA, *Journal of molecular biology* **27**, 395–419 (1967).

63. Z. Yang *et al.*, Expression profiling of the intermediate and late stages of poxvirus replication, *Journal of virology* **85**, 9899–9908 (2011).

64. J. Cairns, The initiation of vaccinia infection, *Virology* **11**, 603–623 (1960).

65. C. Morgan, S. A. Ellison, H. M. Rose, D. H. Moore, Structure and development of viruses as observed in the electron microscope: I. Herpes simplex virus, *The Journal of experimental medicine* **100**, 195–202 (1954).

66. J. Heuser, Deep-etch EM reveals that the early poxvirus envelope is a single membrane bilayer stabilized by a geodetic "honeycomb" surface coat, *The Journal of cell biology* **169**, 269–283 (2005).

67. J. Mercer, P. Traktman, Investigation of structural and functional motifs within the vaccinia virus A14 phosphoprotein, an essential component of the virion membrane, *Journal of virology* **77**, 8857–8871 (2003).

68. D. Rodriguez, J. Rodriguez, M. Esteban, The vaccinia virus 14-kilodalton fusion protein forms a stable complex with the processed protein encoded by the vaccinia virus A17L gene., *Journal of Virology* **67**, 3435–3440 (1993).

69. X. Meng, A. Embry, D. Sochia, Y. Xiang, Vaccinia virus A6L encodes a virion core protein required for formation of mature virion., *J. Virol.* **81**, 1433–43 (2007).

70. W. Resch, A. S. Weisberg, B. Moss, Vaccinia virus nonstructural protein encoded by the A11R gene is required for formation of the virion membrane, *Journal of virology* **79**, 6598–6609 (2005).

71. P. Szajner, A. S. Weisberg, B. Moss, Evidence for an essential catalytic role of the F10 protein kinase in vaccinia virus morphogenesis, *Journal of virology* **78**, 257–265 (2004).

72. P. Satheshkumar, A. Weisberg, B. Moss, Vaccinia virus H7 protein contributes to the formation of crescent membrane precursors of immature virions, *Journal of virology* **83**, 8439–8450 (2009).

73. L. Maruri-Avidal, A. Domi, A. S. Weisberg, B. Moss, Participation of vaccinia virus L2 protein in the formation of crescent membranes and immature virions, *Journal of virology* **85**, 2504–2511 (2011).

74. L. Maruri-Avidal, A. S. Weisberg, B. Moss, Direct formation of vaccinia virus membranes from the endoplasmic reticulum in the absence of the newly characterized L2-interacting protein A30. 5, *Journal of virology* **87**, 12313–12326 (2013).

75. M. Schmelz *et al.*, Assembly of vaccinia virus: the second wrapping cisterna is derived from the trans Golgi network., *J. Virol.* **68**, 130–47 (1994).

76. B. Sodeik *et al.*, Assembly of vaccinia virus: role of the intermediate compartment between the endoplasmic reticulum and the Golgi stacks., *The Journal of Cell Biology* **121**, 521–541 (1993).

77. A. R. Howard, T. G. Senkevich, B. Moss, Vaccinia virus A26 and A27 proteins form a stable complex tethered to mature virions by association with the A17 transmembrane protein, *Journal of virology* **82**, 12384–12391 (2008).

78. A. K. Earley, W. M. Chan, B. M. Ward, The vaccinia virus B5 protein requires A34 for efficient intracellular trafficking from the endoplasmic reticulum to the site of wrapping and incorporation into progeny virions, *Journal of virology* **82**, 2161–2169 (2008).

79. E. J. Wolffe, S. Isaacs, B. Moss, Deletion of the vaccinia virus B5R gene encoding a 42-kilodalton membrane glycoprotein inhibits extracellular virus envelope formation and dissemination., *Journal of virology* **67**, 4732–4741 (1993).

80. C. Schmutz, L. G. Payne, J. Gubser, R. Wittek, A mutation in the gene encoding the vaccinia virus 37,000-M (r) protein confers resistance to an inhibitor of virus envelopment and release., *Journal of Virology* **65**, 3435–3442 (1991).

81. B. M. Ward, B. Moss, Vaccinia virus intracellular movement is associated with microtubules and independent of actin tails, *Journal of virology* **75**, 11651–11663 (2001).

82. S. R. Bidgood, J. Mercer, Cloak and Dagger: Alternative Immune Evasion and Modulation Strategies of Poxviruses., *Viruses* **7**, 4800–25 (2015).

83. L. Liu, T. Cooper, P. M. Howley, J. D. Hayball, From crescent to mature virion: vaccinia virus assembly and maturation, *Viruses* **6**, 3787–3808 (2014).

84. G. Antoine, F. Scheiflinger, F. Dorner, F. G. Falkner, The complete genomic sequence of the modified vaccinia Ankara strain: comparison with other orthopoxviruses., *Virology* **244**, 365–96 (1998).

85. T. J. Blanchard, A. Alcami, P. Andrea, G. L. Smith, Modified vaccinia virus Ankara undergoes limited replication in human cells and lacks several immunomodulatory proteins: implications for use as a human vaccine., *Journal of General Virology* **79**, 1159–1167 (1998).

86. H. Meyer, G. Sutter, A. Mayr, Mapping of deletions in the genome of the highly attenuated vaccinia virus MVA and their influence on virulence., *J. Gen. Virol.* **72 (Pt 5)**, 1031–8 (1991).

87. G. Sutter, B. Moss, Nonreplicating vaccinia vector efficiently expresses recombinant genes., *Proc. Natl. Acad. Sci. U.S.A.* **89**, 10847–51 (1992).

88. I. Drexler, K. Heller, B. Wahren, V. Erfle, G. Sutter, Highly attenuated modified vaccinia virus Ankara replicates in baby hamster kidney cells, a potential host for virus propagation, but not in various human transformed and primary cells., *Journal of General Virology* **79**, 347–352 (1998).

89. M. W. Carroll, B. Moss, Host range and cytopathogenicity of the highly attenuated MVA strain of vaccinia virus: propagation and generation of recombinant viruses in a nonhuman mammalian cell line, *Virology* **238**, 198–211 (1997).

90. O. Kaynarcalidan, S. Moreno Mascaraque, I. Drexler, Vaccinia Virus: From Crude Smallpox Vaccines to Elaborate Viral Vector Vaccine Design, *Biomedicines* **9**, 1780 (2021).

91. Z. Waibler *et al.*, Modified vaccinia virus Ankara induces Toll-like receptor-independent type I interferon responses., *J. Virol.* **81**, 12102–10 (2007).

92. P. Dai *et al.*, Modified vaccinia virus Ankara triggers type I IFN production in murine conventional dendritic cells via a cGAS/STING-mediated cytosolic DNA-sensing pathway, *PLoS Pathog* **10**, e1003989 (2014).

93. B. A. Blok *et al.*, Opposite effects of Vaccinia and modified Vaccinia Ankara on trained immunity, *European Journal of Clinical Microbiology \& Infectious Diseases* **38**, 449–456 (2019).

94. F. Thiele *et al.*, Modified vaccinia virus Ankara-infected dendritic cells present CD4+ T-cell epitopes by endogenous major histocompatibility complex class II presentation pathways., *J. Virol.* **89**, 2698–709 (2015).

95. C. Barnowski *et al.*, Efficient Induction of Cytotoxic T Cells by Viral Vector Vaccination Requires STING-Dependent DC Functions, *Frontiers in immunology* **11**, 1458 (2020).

96. R. Medzhitov, C. A. Janeway Jr, Innate immunity: impact on the adaptive immune response, *Current opinion in immunology* **9**, 4–9 (1997).

97. M. R. Thompson, J. J. Kaminski, E. A. Kurt-Jones, K. A. Fitzgerald, Pattern recognition receptors and the innate immune response to viral infection, *Viruses* **3**, 920–940 (2011).

98. D. Goubau, S. Deddouche, C. R. e Sousa, Cytosolic sensing of viruses, *Immunity* **38**, 855–869 (2013).

99. L. Sun, J. Wu, F. Du, X. Chen, Z. J. Chen, Cyclic GMP-AMP synthase is a cytosolic DNA sensor that activates the type I interferon pathway., *Science* **339**, 786–91 (2013).

100. F. Civril *et al.*, Structural mechanism of cytosolic DNA sensing by cGAS, *Nature* **498**, 332–337 (2013).

101. X. Zhang *et al.*, Cyclic GMP-AMP containing mixed phosphodiester linkages is an endogenous high-affinity ligand for STING., *Mol. Cell* **51**, 226–35 (2013).

102. E. J. Diner *et al.*, The innate immune DNA sensor cGAS produces a non-canonical cyclic dinucleotide that activates human STING., *Cell Rep* **3**, 1355–61 (2013).

103. P. Gao *et al.*, Cyclic [G (2′, 5′) pA (3′, 5′) p] is the metazoan second messenger produced by DNA-activated cyclic GMP-AMP synthase, *Cell* **153**, 1094–1107 (2013).

104. A. Ablasser *et al.*, Cell intrinsic immunity spreads to bystander cells via the intercellular transfer of cGAMP., *Nature* **503**, 530–4 (2013).

105. L. Jin *et al.*, MPYS, a novel membrane tetraspanner, is associated with major histocompatibility complex class II and mediates transduction of apoptotic signals, *Molecular and cellular biology* **28**, 5014–5026 (2008).

106. W. Sun *et al.*, ERIS, an endoplasmic reticulum IFN stimulator, activates innate immune signaling through dimerization., *Proc. Natl. Acad. Sci. U.S.A.* **106**, 8653–8 (2009).

107. B. Zhong *et al.*, The adaptor protein MITA links virus-sensing receptors to IRF3 transcription factor activation., *Immunity* **29**, 538–50 (2008).

108. H. Ishikawa, G. N. Barber, STING is an endoplasmic reticulum adaptor that facilitates innate immune signalling., *Nature* **455**, 674–8 (2008).

109. D. L. Burdette *et al.*, STING is a direct innate immune sensor of cyclic di-GMP., *Nature* **478**, 515–8 (2011).

110. X. Wu *et al.*, Molecular evolutionary and structural analysis of the cytosolic DNA sensor cGAS and STING., *Nucleic Acids Res.* **42**, 8243–57 (2014).

111. S. Ouyang *et al.*, Structural analysis of the STING adaptor protein reveals a hydrophobic dimer interface and mode of cyclic di-GMP binding, *Immunity* **36**, 1073–1086 (2012).

112. Y. Tanaka, Z. J. Chen, STING specifies IRF3 phosphorylation by TBK1 in the cytosolic DNA signaling pathway., *Sci Signal* **5**, ra20 (2012).

113. E. Ogawa, K. Mukai, K. Saito, H. Arai, T. Taguchi, The binding of TBK1 to STING requires exocytic membrane traffic from the ER, *Biochemical and biophysical research communications* **503**, 138–145 (2018).

114. C. Zhang *et al.*, Structural basis of STING binding with and phosphorylation by TBK1., *Nature* **567**, 394–398 (2019).

115. Q. Chen, L. Sun, Z. J. Chen, Regulation and function of the cGAS-STING pathway of cytosolic DNA sensing, *Nature immunology* **17**, 1142–1149 (2016).

116. D. Ori, M. Murase, T. Kawai, Cytosolic nucleic acid sensors and innate immune regulation, *International reviews of immunology* **36**, 74–88 (2017).

117. Q. Liang *et al.*, Crosstalk between the cGAS DNA sensor and Beclin-1 autophagy protein shapes innate antimicrobial immune responses., *Cell Host Microbe* **15**, 228–38 (2014).

118. L. Li *et al.*, Hydrolysis of 2′ 3′-cGAMP by ENPP1 and design of nonhydrolyzable analogs, *Nature chemical biology* **10**, 1043–1048 (2014).

119. K. Kato *et al.*, Structural insights into cGAMP degradation by Ecto-nucleotide pyrophosphatase phosphodiesterase 1, *Nature communications* **9**, 1–8 (2018).

120. J. Zhang, M.-M. Hu, Y.-Y. Wang, H.-B. Shu, TRIM32 protein modulates type I interferon induction and cellular antiviral response by targeting MITA/STING protein for K63-linked ubiquitination, *Journal of Biological Chemistry* **287**, 28646–28655 (2012).

121. T. Tsuchida *et al.*, The ubiquitin ligase TRIM56 regulates innate immune responses to intracellular double-stranded DNA., *Immunity* **33**, 765–76 (2010).

122. G. J. Seo *et al.*, TRIM56-mediated monoubiquitination of cGAS for cytosolic DNA sensing, *Nature communications* **9**, 1–13 (2018).

123. Y. Wang *et al.*, TRIM30α is a negative-feedback regulator of the intracellular DNA and DNA virus-triggered response by targeting STING, *PLoS pathogens* **11**, e1005012 (2015).

124. H. Konno, K. Konno, G. N. Barber, Cyclic dinucleotides trigger ULK1 (ATG1) phosphorylation of STING to prevent sustained innate immune signaling., *Cell* **155**, 688–98 (2013).

125. X. Yu *et al.*, The STING phase-separator suppresses innate immune signalling, *Nature Cell Biology* **23**, 330–340 (2021).

126. L. Gao *et al.*, ABIN1 protein cooperates with TAX1BP1 and A20 proteins to inhibit antiviral signaling., *J. Biol. Chem.* **286**, 36592–602 (2011).

127. R. Higgs *et al.*, The E3 ubiquitin ligase Ro52 negatively regulates IFN-β production post-pathogen recognition by polyubiquitin-mediated degradation of IRF3, *The Journal of Immunology* **181**, 1780–1786 (2008).

128. H. Ishikawa, Z. Ma, G. N. Barber, STING regulates intracellular DNA-mediated, type I interferon-dependent innate immunity., *Nature* **461**, 788–92 (2009).

129. A. K. Mankan *et al.*, Cytosolic RNA: DNA hybrids activate the cGAS-STING axis, *The EMBO journal* **33**, 2937–2946 (2014).

130. J. Ahn, S. Son, S. C. Oliveira, G. N. Barber, STING-dependent signaling underlies IL-10 controlled inflammatory colitis, *Cell reports* **21**, 3873–3884 (2017).

131. W. Wang *et al.*, STING promotes NLRP3 localization in ER and facilitates NLRP3 deubiquitination to activate the inflammasome upon HSV-1 infection, *PLoS pathogens* **16**, e1008335 (2020).

132. T. Abe, G. N. Barber, Cytosolic-DNA-mediated, STING-dependent proinflammatory gene induction necessitates canonical NF-kappaB activation through TBK1, *Journal of virology* **88**, 5328–5341 (2014).

133. Z. Li *et al.*, When STING meets viruses: Sensing, trafficking and response, *Frontiers in immunology* **11** (2020).

134. J. Huang *et al.*, Herpes simplex virus 1 tegument protein VP22 abrogates cGAS/STING-mediated antiviral innate immunity, *Journal of virology* **92**, e00841–18 (2018).

135. J. Wu *et al.*, Inhibition of cGAS DNA sensing by a herpesvirus virion protein, *Cell host \& microbe* **18**, 333–344 (2015).

136. H. jin Choi *et al.*, Human cytomegalovirus-encoded US9 targets MAVS and STING signaling to evade type I interferon immune responses, *Nature communications* **9**, 1–16 (2018).

137. H.-R. Kang *et al.*, Murine gammaherpesvirus 68 encoding open reading frame 11 targets TANK binding kinase 1 to negatively regulate the host type I interferon response, *Journal of virology* **88**, 6832–6846 (2014).

138. I. Georgana, R. P. Sumner, G. J. Towers, C. Maluquer de Motes, Virulent poxviruses inhibit DNA sensing by preventing STING activation, *Journal of Virology* **92**, e02145–17 (2018).

139. N. Meade, M. King, J. Munger, D. Walsh, mTOR dysregulation by vaccinia virus F17 controls multiple processes with varying roles in infection, *Journal of virology* **93** (2019).

140. J. B. Eaglesham, Y. Pan, T. S. Kupper, P. J. Kranzusch, Publisher Correction: Viral and metazoan poxins are cGAMP-specific nucleases that restrict cGAS-STING signalling., *Nature* **569**, E12 (2019).

141. L. Unterholzner *et al.*, Vaccinia virus protein C6 is a virulence factor that binds TBK-1 adaptor proteins and inhibits activation of IRF3 and IRF7, *PLoS Pathog* **7**, e1002247 (2011).

142. C. T. Benfield, H. Ren, S. J. Lucas, B. Bahsoun, G. L. Smith, Vaccinia virus protein K7 is a virulence factor that alters the acute immune response to infection, *The Journal of general virology* **94**, 1647 (2013).

143. B. J. Ferguson *et al.*, Vaccinia virus protein N2 is a nuclear IRF3 inhibitor that promotes virulence, *The Journal of general virology* **94**, 2070 (2013).

144. L. Han *et al.*, SARS-CoV-2 ORF9b antagonizes type I and III interferons by targeting multiple components of RIG-I/MDA-5-MAVS, TLR3-TRIF, and cGAS-STING signaling pathways, *bioRxiv* (2020).

145. F. Humphries *et al.*, A diamidobenzimidazole STING agonist protects against SARS-CoV-2 infection, *Science Immunology* **6** (2021).

146. W. Liu *et al.*, Activation of STING signaling pathway effectively blocks human coronavirus infection, *Journal of Virology* **95**, e00490–21 (2021).

147. D. Liu *et al.*, STING directly activates autophagy to tune the innate immune response., *Cell Death Differ.* **26**, 1735–1749 (2019).

148. X. Gui *et al.*, Autophagy induction via STING trafficking is a primordial function of the cGAS pathway, *Nature* **567**, 262–266 (2019).

149. K.-P. Hopfner, V. Hornung, Molecular mechanisms and cellular functions of cGAS-STING signalling, *Nature Reviews Molecular Cell Biology* , 1–21 (2020).

150. K. Takeshige, M. Baba, S. Tsuboi, T. Noda, Y. Ohsumi, Autophagy in yeast demonstrated with proteinase-deficient mutants and conditions for its induction., *J. Cell Biol.* **119**, 301–11 (1992).

151. T. E. Rusten *et al.*, Programmed autophagy in the Drosophila fat body is induced by ecdysone through regulation of the PI3K pathway., *Dev. Cell* **7**, 179–92 (2004).

152. C. M. Schworer, G. E. Mortimore, Glucagon-induced autophagy and proteolysis in rat liver: mediation by selective deprivation of intracellular amino acids., *Proc. Natl. Acad. Sci. U.S.A.* **76**, 3169–73 (1979).

153. K. Suzuki, Y. Kubota, T. Sekito, Y. Ohsumi, Hierarchy of Atg proteins in pre-autophagosomal structure organization., *Genes Cells* **12**, 209–18 (2007).

154. E. Itakura, N. Mizushima, Characterization of autophagosome formation site by a hierarchical analysis of mammalian Atg proteins., *Autophagy* **6**, 764–76 (2010).

155. Y. J. Jin *et al.*, Molecular cloning of a membrane-associated human FK506- and rapamycin-binding protein, FKBP-13., *Proc. Natl. Acad. Sci. U.S.A.* **88**, 6677–81 (1991).

156. H. Erdjument-Bromage, M. Lui, P. Tempst, D. M. Sabatini, S. H. Snyder, High-Sensitivity sequencing of large proteins: Partial structure of the rapamycin-fkbp12 target, *Protein Science* **3**, 2435–2446 (1994).

157. C. J. Sabers *et al.*, Isolation of a protein target of the FKBP12-rapamycin complex in mammalian cells, *Journal of Biological Chemistry* **270**, 815–822 (1995).

158. I. G. Ganley *et al.*, ULK1-ATG13-FIP200 complex mediates mTOR signaling and is essential for autophagy, *Journal of Biological Chemistry* **284**, 12297–12305 (2009).

159. E. Y. Chan, S. Kir, S. A. Tooze, siRNA screening of the kinome identifies ULK1 as a multidomain modulator of autophagy, *Journal of Biological Chemistry* **282**, 25464–25474 (2007).

160. T. Hara *et al.*, FIP200, a ULK-interacting protein, is required for autophagosome formation in mammalian cells, *The Journal of cell biology* **181**, 497–510 (2008).

161. C. H. Jung *et al.*, ULK-Atg13-FIP200 complexes mediate mTOR signaling to the autophagy machinery., *Mol. Biol. Cell* **20**, 1992–2003 (2009).

162. N. Hosokawa *et al.*, Atg101, a novel mammalian autophagy protein interacting with Atg13., *Autophagy* **5**, 973–9 (2009).

163. X. H. Liang *et al.*, Induction of autophagy and inhibition of tumorigenesis by beclin 1, *Nature* **402**, 672–676 (1999).

164. A. Petiot, E. Ogier-Denis, E. F. Blommaart, A. J. Meijer, P. Codogno, Distinct classes of phosphatidylinositol 3′-kinases are involved in signaling pathways that control macroautophagy in HT-29 cells, *Journal of Biological Chemistry* **275**, 992–998 (2000).

165. A. Kihara, Y. Kabeya, Y. Ohsumi, T. Yoshimori, Beclin-phosphatidylinositol 3-kinase complex functions at the trans-Golgi network, *EMBO reports* **2**, 330–335 (2001).

166. K. Lindmo *et al.*, The PI 3-kinase regulator Vps15 is required for autophagic clearance of protein aggregates., *Autophagy* **4**, 500–6 (2008).

167. E. Itakura, C. Kishi, K. Inoue, N. Mizushima, Beclin 1 forms two distinct phosphatidylinositol 3-kinase complexes with mammalian Atg14 and UVRAG., *Mol. Biol. Cell* **19**, 5360–72 (2008).

168. Y. Zhong *et al.*, Distinct regulation of autophagic activity by Atg14L and Rubicon associated with Beclin 1-phosphatidylinositol-3-kinase complex, *Nature cell biology* **11**, 468–476 (2009).

169. K. Matsunaga *et al.*, Two Beclin 1-binding proteins, Atg14L and Rubicon, reciprocally regulate autophagy at different stages, *Nature cell biology* **11**, 385–396 (2009).

170. K. Matsunaga *et al.*, Autophagy requires endoplasmic reticulum targeting of the PI3-kinase complex via Atg14L, *Journal of Cell Biology* **190**, 511–521 (2010).

171. G. M. Fimia *et al.*, Ambra1 regulates autophagy and development of the nervous system, *Nature* **447**, 1121–1125 (2007).

172. A. Kihara, T. Noda, N. Ishihara, Y. Ohsumi, Two Distinct Vps34 Phosphatidylinositol 3-Kinase complexes function in autophagy and carboxypeptidase Y Sorting inSaccharomyces cerevisiae, *Journal*

of Cell Biology **152**, 519–530 (2001).

173. J. Cheng *et al.*, Yeast and mammalian autophagosomes exhibit distinct phosphatidylinositol 3-phosphate asymmetries, *Nature communications* **5**, 1–12 (2014).

174. E. L. Axe *et al.*, Autophagosome formation from membrane compartments enriched in phosphatidylinositol 3-phosphate and dynamically connected to the endoplasmic reticulum, *The Journal of cell biology* **182**, 685–701 (2008).

175. M. Hamasaki *et al.*, Autophagosomes form at ER-mitochondria contact sites, *Nature* **495**, 389–393 (2013).

176. D. W. Hailey *et al.*, Mitochondria supply membranes for autophagosome biogenesis during starvation, *Cell* **141**, 656–667 (2010).

177. L. Ge, D. Melville, M. Zhang, R. Schekman, The ER-Golgi intermediate compartment is a key membrane source for the LC3 lipidation step of autophagosome biogenesis, *Elife* **2**, e00947 (2013).

178. H. E. J. Polson *et al.*, Mammalian Atg18 (WIPI2) localizes to omegasome-anchored phagophores and positively regulates LC3 lipidation., *Autophagy* **6**, 506–22 (2010).

179. H. C. Dooley *et al.*, WIPI2 links LC3 conjugation with PI3P, autophagosome formation, and pathogen clearance by recruiting Atg12-5-16L1., *Mol. Cell* **55**, 238–52 (2014).

180. D. Fracchiolla, C. Chang, J. H. Hurley, S. Martens, A PI3K-WIPI2 positive feedback loop allosterically activates LC3 lipidation in autophagy, *Journal of Cell Biology* **219** (2020).

181. A. Kuma, N. Mizushima, N. Ishihara, Y. Ohsumi, Formation of the~ 350-kDa Apg12-Apg5\textperiodcentered Apg16 multimeric complex, mediated by Apg16 oligomerization, is essential for autophagy in yeast, *Journal of Biological Chemistry* **277**, 18619–18625 (2002).

182. A. K. G. Velikkakath, T. Nishimura, E. Oita, N. Ishihara, N. Mizushima, Mammalian Atg2 proteins are essential for autophagosome formation and important for regulation of size and distribution of lipid droplets, *Molecular biology of the cell* **23**, 896–909 (2012).

183. A. Orsi *et al.*, Dynamic and transient interactions of Atg9 with autophagosomes, but not membrane integration, are required for autophagy., *Mol. Biol. Cell* **23**, 1860–73 (2012).

184. S. Jia *et al.*, Mammalian Atg9 contributes to the post-Golgi transport of lysosomal hydrolases by interacting with adaptor protein-1, *FEBS letters* **591**, 4027–4038 (2017).

185. S. E. Kaiser *et al.*, Non-canonical E2 recruitment by the autophagy E1 revealed by Atg7-Atg3 and Atg7-Atg10 structures, *Nature structural \& molecular biology* **19**, 1242 (2012).

186. T. Shpilka, H. Weidberg, S. Pietrokovski, Z. Elazar, Atg8: an autophagy-related ubiquitin-like protein family, *Genome biology* **12**, 1–11 (2011).

187. A. Stolz, A. Ernst, I. Dikic, Cargo recognition and trafficking in selective autophagy, *Nature cell biology* **16**, 495–501 (2014).

188. S. Pankiv *et al.*, p62/SQSTM1 binds directly to Atg8/LC3 to facilitate degradation of ubiquitinated protein aggregates by autophagy, *Journal of biological chemistry* **282**, 24131–24145 (2007).

189. L. Jahreiss, F. M. Menzies, D. C. Rubinsztein, The itinerary of autophagosomes: from peripheral formation to kiss-and-run fusion with lysosomes, *Traffic* **9**, 574–587 (2008).

190. L. Yu, Y. Chen, S. A. Tooze, Autophagy pathway: cellular and molecular mechanisms, *Autophagy* **14**, 207–215 (2018).

191. J. D. Lane, R. Roberts, N. T. Ktistakis, Omegasomes: PI3P platforms that manufacture autophagosomes, *Essays in biochemistry* **55**, 17–27 (2013).

192. A. Abada, Z. Elazar, Getting ready for building: signaling and autophagosome biogenesis, *EMBO reports* **15**, 839–852 (2014).

193. I. Dikic, Z. Elazar, Mechanism and medical implications of mammalian autophagy, *Nature reviews Molecular cell biology* **19**, 349–364 (2018).

194. T. Ichimiya *et al.*, Autophagy and Autophagy-Related Diseases: A Review, *International Journal of Molecular Sciences* **21**, 8974 (2020).

195. Y. Du *et al.*, LRRC25 inhibits type I IFN signaling by targeting ISG15-associated RIG-I for autophagic degradation, *The EMBO journal* **37**, 351–366 (2018).

196. H. K. Lee, J. M. Lund, B. Ramanathan, N. Mizushima, A. Iwasaki, Autophagy-dependent viral recognition by plasmacytoid dendritic cells, *Science* **315**, 1398–1401 (2007).

197. T. Prabakaran *et al.*, Attenuation of cGAS-STING signaling is mediated by a p62/SQSTM1-dependent autophagy pathway activated by TBK1., *EMBO J.* **37** (2018), doi:10.15252/embj.201797858.

198. T. Saitoh *et al.*, Loss of the autophagy protein Atg16L1 enhances endotoxin-induced IL-1β production, *Nature* **456**, 264–268 (2008).

199. C. Gerada, K. M. Ryan, Autophagy, the innate immune response and cancer, *Molecular Oncology* **14**, 1913–1929 (2020).

200. T. Saitoh *et al.*, Atg9a controls dsDNA-driven dynamic translocation of STING and the innate immune response., *Proc. Natl. Acad. Sci. U.S.A.* **106**, 20842–6 (2009).

201. M. Pilli *et al.*, TBK-1 promotes autophagy-mediated antimicrobial defense by controlling autophagosome maturation, *Immunity* **37**, 223–234 (2012).

202. C. Bodur *et al.*, The IKK-related kinase TBK1 activates mTORC1 directly in response to growth factors and innate immune agonists, *The EMBO journal* **37**, 19–38 (2018).

203. R. J. Antonia *et al.*, TBK1 limits mTORC1 by promoting phosphorylation of raptor Ser877, *Scientific reports* **9**, 1–10 (2019).

204. A. S. Tooley, D. Kazyken, C. Bodur, I. E. Gonzalez, D. C. Fingar, The innate immune kinase TBK1 directly increases mTORC2 activity and downstream signaling to Akt, *bioRxiv* (2021).

205. L. Ahmad, S. Mostowy, V. Sancho-Shimizu, Autophagy-Virus Interplay: From Cell Biology to Human Disease., *Front Cell Dev Biol* **6**, 155 (2018).

206. A. Orvedahl *et al.*, Image-based genome-wide siRNA screen identifies selective autophagy factors, *Nature* **480**, 113–117 (2011).

207. A. Orvedahl *et al.*, Autophagy protects against Sindbis virus infection of the central nervous system., *Cell Host Microbe* **7**, 115–27 (2010).

208. B. Yordy, N. Iijima, A. Huttner, D. Leib, A. Iwasaki, A neuron-specific role for autophagy in antiviral defense against herpes simplex virus, *Cell host \& microbe* **12**, 334–345 (2012).

209. G. B. Kyei *et al.*, Autophagy pathway intersects with HIV-1 biosynthesis and regulates viral yields in macrophages, *Journal of Cell Biology* **186**, 255–268 (2009).

210. S. Sagnier *et al.*, Autophagy restricts HIV-1 infection by selectively degrading Tat in CD4+ T lymphocytes, *Journal of virology* **89**, 615–625 (2015).

211. Y. Choi, J. W. Bowman, J. U. Jung, Autophagy during viral infection—a double-edged sword, *Nature reviews microbiology* **16**, 341–354 (2018).

212. H. Yin *et al.*, Interactions between autophagy and DNA viruses, *Viruses* **11**, 776 (2019).

213. J. Mao *et al.*, Autophagy and viral infection, *Autophagy Regulation of Innate Immunity* , 55–78 (2019).

214. C. Guévin *et al.*, Autophagy protein ATG5 interacts transiently with the hepatitis C virus RNA polymerase (NS5B) early during infection, *Virology* **405**, 1–7 (2010).

215. L. Wang, Y. Tian, J. J. Ou, HCV induces the expression of Rubicon and UVRAG to temporally regulate the maturation of autophagosomes and viral replication, *PLoS Pathog* **11**, e1004764 (2015).

216. X. Hui *et al.*, SARS-CoV-2 promote autophagy to suppress type I interferon response, *Signal transduction and targeted therapy* **6**, 1–3 (2021).

217. Y. Zhang *et al.*, The SARS-CoV-2 protein ORF3a inhibits fusion of autophagosomes with lysosomes, *Cell discovery* **7**, 1–12 (2021).

218. A. Orvedahl *et al.*, HSV-1 ICP34. 5 confers neurovirulence by targeting the Beclin 1 autophagy protein, *Cell host \& microbe* **1**, 23–35 (2007).

219. X. Liu, R. Matrenec, M. U. Gack, B. He, Disassembly of the TRIM23-TBK1 complex by the Us11 protein of herpes simplex virus 1 impairs autophagy, *Journal of virology* **93**, e00497–19 (2019).

220. M. Granato *et al.*, Epstein-barr virus blocks the autophagic flux and appropriates the autophagic machinery to enhance viral replication, *Journal of virology* **88**, 12715–12726 (2014).

221. H. Zhang *et al.*, Cellular autophagy machinery is not required for vaccinia virus replication and maturation, *Autophagy* **2**, 91–95 (2006).

222. J. G. Moloughney *et al.*, Vaccinia virus leads to ATG12–ATG3 conjugation and deficiency in autophagosome formation., *Autophagy* **7**, 1434–47 (2011).

223. M. Mauthe *et al.*, An siRNA screen for ATG protein depletion reveals the extent of the unconventional functions of the autophagy proteome in virus replicationUnconventional functions of ATG proteins, *The Journal of cell biology* **214**, 619–635 (2016).

224. M. Krause, A. Yakimovich, J. Kriston-Vizi, M. Huttunen, J. Mercer, Vaccinia virus subverts xenophagy through phosphorylation and nuclear targeting of p62, *bioRxiv* (2021).

225. T. D. Fischer, C. Wang, B. S. Padman, M. Lazarou, R. J. Youle, STING induces LC3B lipidation onto single-membrane vesicles via the V-ATPase and ATG16L1-WD40 domain, *Journal of Cell Biology* **219** (2020).

226. R. Fang *et al.*, NEMO-IKK\beta are essential for IRF3 and NF-\kappaB activation in the cGAS-STING pathway, *The Journal of Immunology* **199**, 3222–3233 (2017).

227. H. Khatif, thesis, (2017).

228. C. Staib, I. Drexler, G. Sutter, in *Vaccinia Virus and Poxvirology*, (Springer, 2004), pp. 77–99.

229. S. Tao *et al.*, Sequestration of late antigens within viral factories impairs MVA vector-induced protective memory CTL responses, *Frontiers in immunology* **10**, 2850 (2019).

230. B. Samreen, S. Tao, K. Tischer, H. Adler, I. Drexler, ORF6 and ORF61 expressing MVA vaccines impair early but not late latency in murine gammaherpesvirus MHV-68 infection, *Frontiers in immunology* **10**, 2984 (2019).

231. L. Dai, thesis, (2014).

232. S. Kilcher *et al.*, siRNA screen of early poxvirus genes identifies the AAA+ ATPase D5 as the virus genome-uncoating factor, *Cell host \& microbe* **15**, 103–112 (2014).

233. B. Karsten Tischer, J. von Einem, B. Kaufer, N. Osterrieder, Two-step red-mediated recombination for versatile high-efficiency markerless DNA manipulation in Escherichia coli, *Biotechniques* **40**, 191–197 (2006).

234. B. K. Tischer, G. A. Smith, N. Osterrieder, in *In vitro mutagenesis protocols*, (Springer, 2010), pp. 421–430.

235. M. G. Cottingham, S. C. Gilbert, Rapid generation of markerless recombinant MVA vaccines by en passant recombineering of a self-excising bacterial artificial chromosome, *Journal of virological methods* **168**, 233–236 (2010).

236. U. K. Laemmli, Cleavage of structural proteins during the assembly of the head of bacteriophage T4, *nature* **227**, 680–685 (1970).

237. C. Martin, S. Kilcher, in *Vaccinia Virus*, (Springer, 2019), pp. 119–130.

238. M. E. S. Krause, thesis, (2020).

239. S. Alers *et al.*, Atg13 and FIP200 act independently of Ulk1 and Ulk2 in autophagy induction, *Autophagy* **7**, 1424–1433 (2011).

240. J. Harper, M. Parsonage, H. Pelham, G. Darby, Heat inactivation of vaccinia virus particle-associated functions: properties of heated particles in vivo and in vitro, *Journal of Virology* **26**, 646–659 (1978).

241. E. Assarsson *et al.*, Kinetic analysis of a complete poxvirus transcriptome reveals an immediate-early class of genes, *Proceedings of the National Academy of Sciences* **105**, 2140–2145 (2008).

242. F. Kugler, I. Drexler, U. Protzer, D. Hoffmann, H. Moeini, Generation of recombinant MVA-norovirus: a comparison study of bacterial artificial chromosome-and marker-based systems, *Virology journal* **16**, 100 (2019).

243. L. Priyamvada *et al.*, Serological responses to the MVA-based JYNNEOS monkeypox vaccine in a cohort of participants from the Democratic Republic of Congo, *Vaccine* (2022).

244. A. Vardeu *et al.*, Intravenous administration of viral vectors expressing prostate cancer antigens enhances the magnitude and functionality of CD8+ T cell responses, *Journal for ImmunoTherapy of Cancer* **10**, e005398 (2022).

245. C. M. Zu Natrup *et al.*, Stabilized recombinant SARS-CoV-2 spike antigen enhances vaccine immunogenicity and protective capacity, *The Journal of Clinical Investigation* (2022).

246. Z. Waibler *et al.*, Vaccinia virus-mediated inhibition of type I interferon responses is a multifactorial process involving the soluble type I interferon receptor B18 and intracellular components, *Journal of virology* **83**, 1563–1571 (2009).

247. J. Zhao *et al.*, Mammalian target of rapamycin (mTOR) regulates TLR3 induced cytokines in human oral keratinocytes, *Molecular immunology* **48**, 294–304 (2010).

248. L. H. Yamashiro *et al.*, Interferon-independent STING signaling promotes resistance to HSV-1 in vivo, *Nature communications* **11**, 1–11 (2020).

249. B. L. Uhlorn, E. R. Gamez, S. Li, S. K. Campos, Attenuation of cGAS/STING activity during mitosis, *Life science alliance* **3** (2020).

250. M.-M. Hu *et al.*, Sumoylation Promotes the Stability of the DNA Sensor cGAS and the Adaptor STING to Regulate the Kinetics of Response to DNA Virus., *Immunity* **45**, 555–569 (2016).

251. M. Chen *et al.*, TRIM14 inhibits cGAS degradation mediated by selective autophagy receptor p62 to promote innate immune responses, *Molecular cell* **64**, 105–119 (2016).

252. S. Aguirre *et al.*, Dengue virus NS2B protein targets cGAS for degradation and prevents mitochondrial DNA sensing during infection., *Nat Microbiol* **2**, 17037 (2017).

253. L. Webb *et al.*, Chikungunya virus antagonizes cGAS-STING mediated type-I interferon responses by degrading cGAS, *PLoS pathogens* **16**, e1008999 (2020).

254. S. Liu *et al.*, Phosphorylation of innate immune adaptor proteins MAVS, STING, and TRIF induces IRF3 activation, *Science* **347** (2015).

255. K. R. Balka *et al.*, TBK1 and IKKepsilon Act Redundantly to Mediate STING-Induced NF-kappaB Responses in Myeloid Cells, *Cell Reports* **31**, 107492 (2020).

256. S. Yum, M. Li, Y. Fang, Z. J. Chen, TBK1 recruitment to STING activates both IRF3 and NF-κB that mediate immune defense against tumors and viral infections, *Proceedings of the National Academy of Sciences* **118** (2021).

257. M. Zhao *et al.*, CGAS is a micronucleophagy receptor for the clearance of micronuclei, *Autophagy* **17**, 3976–3991 (2021).

258. H. Popelka, D. J. Klionsky, The molecular mechanism of Atg13 function in autophagy induction: What is hidden behind the data?, *Autophagy* **13**, 449–451 (2017).

259. X. Li, M. Prescott, B. Adler, J. D. Boyce, R. J. Devenish, Beclin 1 is required for starvation-enhanced, but not rapamycin-enhanced, LC3-associated phagocytosis of Burkholderia pseudomallei in RAW 264.7 cells, *Infection and immunity* **81**, 271–277 (2013).

260. S. Rangaraju *et al.*, Rapamycin activates autophagy and improves myelination in explant cultures from neuropathic mice, *Journal of Neuroscience* **30**, 11388–11397 (2010).

261. V. K. Gonugunta *et al.*, Trafficking-mediated STING degradation requires sorting to acidified endolysosomes and can be targeted to enhance anti-tumor response, *Cell reports* **21**, 3234–3242 (2017).

262. D. Fang, H. Xie, T. Hu, H. Shan, M. Li, Binding features and functions of ATG3, *Frontiers in Cell and Developmental Biology* **9** (2021).

263. G. Murayama *et al.*, Inhibition of mTOR suppresses IFNalpha production and the STING pathway in monocytes from systemic lupus erythematosus patients, *Rheumatology* **59**, 2992–3002 (2020).

264. J. An, J. J. Woodward, T. Sasaki, M. Minie, K. B. Elkon, Cutting edge: antimalarial drugs inhibit IFN-β production through blockade of cyclic GMP-AMP synthase-DNA interaction, *The Journal of Immunology* **194**, 4089–4093 (2015).

265. A. S. Jassar *et al.*, Activation of tumor-associated macrophages by the vascular disrupting agent 5, 6-dimethylxanthenone-4-acetic acid induces an effective CD8+ T-cell-mediated antitumor immune response in murine models of lung cancer and mesothelioma, *Cancer research* **65**, 11752–11761 (2005).

266. S. Greiner *et al.*, The highly attenuated vaccinia virus strain modified virus Ankara induces apoptosis in melanoma cells and allows bystander dendritic cells to generate a potent anti-tumoral immunity, *Clinical \& Experimental Immunology* **146**, 344–353 (2006).

267. C. Zhou *et al.*, Transfer of cGAMP into bystander cells via LRRC8 volume-regulated anion channels augments STING-mediated interferon responses and anti-viral immunity, *Immunity* (2020).

268. E. Y. Kong, S. H. Cheng, K. N. Yu, Induction of autophagy and interleukin 6 secretion in bystander cells: metabolic cooperation for radiation-induced rescue effect?, *Journal of radiation research* **59**, 129–140 (2018).

269. M. Song *et al.*, Bystander autophagy mediated by radiation-induced exosomal miR-7-5p in non-targeted human bronchial epithelial cells, *Scientific reports* **6**, 1–12 (2016).

270. S. Riddell, S. Goldie, A. Hill, D. Eagles, T. W. Drew, The effect of temperature on persistence of SARS-CoV-2 on common surfaces, *Virology journal* **17**, 1–7 (2020).

271. P. Dai *et al.*, Intratumoral delivery of inactivated modified vaccinia virus Ankara (iMVA) induces systemic antitumor immunity via STING and Batf3-dependent dendritic cells, *Science immunology* **2** (2017).

272. H. Cao *et al.*, Innate immune response of human plasmacytoid dendritic cells to poxvirus infection is subverted by vaccinia E3 via its Z-DNA/RNA binding domain, *PLoS One* **7**, e36823 (2012).

273. W. Wang *et al.*, Elucidating Mechanisms of Antitumor Immunity Mediated by Live Oncolytic Vaccinia and Heat-Inactivated Vaccinia, *bioRxiv* (2021).

274. L. He, M. H. Fox, Comparison of flow cytometry and western blotting to measure Hsp70., *Cytometry* **25**, 280–6 (1996).

275. R. Revelen *et al.*, Comparison of cell-ELISA, flow cytometry and Western blotting for the detection of antiendothelial cell antibodies, *Clinical and experimental rheumatology* **20**, 19–26 (2002).

276. I. Orhon, F. Reggiori, Assays to monitor autophagy progression in cell cultures, *Cells* **6**, 20 (2017).

277. L. Koepke *et al.*, An improved method for high-throughput quantification of autophagy in mammalian cells, *Scientific reports* **10**, 1–20 (2020).

278. D. R. Latner, Y. Xiang, J. I. Lewis, J. Condit, R. C. Condit, The vaccinia virus bifunctional gene J3 (nucleoside-2′-O-)-methyltransferase and poly (A) polymerase stimulatory factor is implicated as a positive transcription elongation factor by two genetic approaches, *Virology* **269**, 345–355 (2000).

279. C. A. Lackner, R. C. Condit, Vaccinia virus gene A18R DNA helicase is a transcript release factor, *Journal of Biological Chemistry* **275**, 1485–1494 (2000).

280. D. A. Simpson, R. C. Condit, The vaccinia virus A18R protein plays a role in viral transcription during both the early and the late phases of infection., *J. Virol.* **68**, 3642–9 (1994).

281. D. M. Jesus *et al.*, Vaccinia virus protein A3 is required for the production of normal immature virions and for the encapsidation of the nucleocapsid protein L4, *Virology* **481**, 1–12 (2015).

282. D. Liu *et al.*, SOCS3 drives proteasomal degradation of TBK1 and negatively regulates antiviral innate immunity, *Molecular and cellular biology* **35**, 2400–2413 (2015).

283. H. Abe *et al.*, Priming phosphorylation of TANK-binding kinase 1 by IκB kinase β is essential in toll-like receptor 3/4 signaling, *Molecular and Cellular Biology* **40**, e00509–19 (2020).